

**Homolytic Aromatic Substitution, Conformational Dynamics of Dihydrophenanthridines,  
and High-Throughput Synthesis of Amides with Fluorous Technology: Methodologies in  
Reaction, Analysis, and Separation**

by

Adam I. Keller

B.S. Chemistry, The Ohio State University, 2002

Submitted to the Graduate Faculty of  
The University of Pittsburgh in partial fulfillment  
of the requirements for the degree of  
Doctor of Philosophy

University of Pittsburgh

2007

UNIVERSITY OF PITTSBURGH  
COLLEGE OF ARTS AND SCIENCES

This dissertation was presented

by

Adam I. Keller

It was defended on

March 2<sup>nd</sup>, 2007

and approved by

Craig Wilcox, Professor, Chemistry

Paul Floreancig, Associate Professor, Chemistry

Billy Day, Professor, Pharmaceutical Science

Dissertation Advisor: Dennis P. Curran, Professor, Chemistry

Copyright © by Adam I. Keller

2007

**Homolytic Aromatic Substitution, Conformational Dynamics of  
Dihydrophenanthridines, and High-Throughput Synthesis of Amides with Fluorous  
Technology: Methodologies in Reaction, Analysis, and Separation**

Adam I. Keller, PhD

Homolytic aromatic substitution encompasses a wide range of synthetic transformations based on inter- and intramolecular additions of radicals to arenes. Additions of radicals derived from aryl iodides to arenes are promoted by tris(trimethylsilyl)silane and occur under exceptionally mild conditions in non-degassed benzene. Experimental observations led to a proposed mechanism involving reaction of the intermediate cyclohexadienyl radical with dioxygen to generate the aromatic product and the hydroperoxy radical. This methodology was extended to the synthesis of biaryl and heterocyclic compounds.

*N*-Acetyldihydrophenanthridines exhibit remarkable conformational dynamics that are observable on the NMR timescale. Semiempirical calculations were performed to understand their conformational preferences. The predictions derived from the calculated structures were verified by x-ray crystallography, two-dimensional exchange and variable temperature NMR spectroscopy. The rate constants for conformational switching were calculated by a matrix-based routine with data extracted from the two-dimensional exchange spectra.

A fluororous equivalent of diisopropylcarbodiimide (FDIC) was synthesized to overcome the separation problems encountered when conducting solution-phase, carbodiimide mediated acyl couplings. The reactivity of the fluororous analog was not greatly affected by the presence of a fluororous domain, and was equally as effective as diisopropylcarbodiimide in facilitating amide bond formation. Coupled with a reverse F-SPE strategy, FDIC mediated couplings were conducted to provide the target amides in high-purities (95-99%). A small library of amides was prepared in a high-throughput fashion to demonstrate the utility of this approach.

## TABLE OF CONTENTS

<b>LIST OF ABBREVIATIONS .....</b>	<b>XIV</b>
<b>1.0 HOMOLYTIC AROMATIC SUBSTITUTION IN ORGANIC SYNTHESIS .....</b>	<b>1</b>
1.1 Biaryl synthesis .....	1
1.2 Heterocycle syntheses.....	3
1.3 The mechanism of HAS and the role of AIBN.....	4
1.4 Other fates of cyclohexadienyl radicals.....	8
1.5 Tris(trimethylsilyl)silane (TTMSS) as an alternative to Bu <sub>3</sub> SnH.....	9
<b>2.0 INVESTIGATION INTO THE USE OF OXIDANTS IN HOMOLYTIC AROMATIC SUBSTITUTION.....</b>	<b>12</b>
2.1 Aim of project .....	12
2.2 Reaction of an Aryl Halide with Bu <sub>3</sub> SnH/AIBN in Benzene – Control Experiments .....	12
2.3 Diazo Compound Screening .....	16
2.4 Use of other oxidants.....	19
2.5 Experimentation with TTMSS.....	24
2.6 Utility of TTMSS without AIBN or TEMPO .....	26
2.7 The importance of dioxygen .....	30
2.8 Application of TTMSS/pyridine protocol to intramolecular HAS.....	31
2.9 Proposed role of oxygen .....	34
2.10 <sup>29</sup> Si NMR experiments: attempts to identify silicon containing byproducts .....	36
2.11 Summary .....	39

2.12	Experimental .....	40
<b>3.0</b>	<b>APPLICATION OF NMR TO THE STUDY OF CONFORMATIONAL DYNAMICS .....</b>	<b>49</b>
3.1	Introduction.....	49
3.2	Two dimensional exchange spectroscopy (2D EXSY) .....	49
3.3	Choosing an appropriate mixing time .....	51
3.4	Example of 2D EXSY applied to the study of conformational exchange .....	52
<b>4.0</b>	<b>INVESTIGATION OF THE CONFORMATIONAL DYNAMICS OF <i>ORTHO</i>-SUBSTITUTED <i>N</i>-ACYL-DIHYDROPHENANTHRIDINES .....</b>	<b>55</b>
4.1	Aim of project .....	55
4.2	Molecular modeling of silylated benzazapine <b>60</b> .....	56
4.3	Crystal structure of silylated dihydrophenanthridine <b>60</b> .....	58
4.4	2D EXSY NMR of silylated hydrophenanthridine <b>60</b> .....	61
4.5	<sup>1</sup> H NMR of dihydrophenanthridine <b>60</b> at elevated temperatures.....	66
4.6	Conformational dynamics of hydrophenanthridine <b>59</b> .....	68
4.7	Attempted synthesis of <i>N</i> -alkyl analogs .....	74
4.8	HPLC experiments .....	76
4.9	Summary.....	77
4.10	Experimental .....	78
<b>5.0</b>	<b>APPLICATION OF FLUOROUS TECHNOLOGY TO AMIDE BOND SYNTHESIS</b>	<b>81</b>
5.1	Introduction.....	81
5.1.1	Carbodiimide-mediated amide bond synthesis .....	81
5.1.2	Light-fluorous reagents.....	83
5.2	Discovery and synthesis of a fluorinated carbodiimide.....	84
5.3	Model studies with FDIC.....	87

5.4	Optimization of a high-throughput purification strategy .....	90
5.5	FDIC-mediated synthesis of a small amide library .....	93
5.6	Conclusion .....	97
5.7	Experimental .....	98
<b>APPENDIX A</b>	.....	<b>107</b>
<b>APPENDIX B</b>	.....	<b>115</b>
<b>APPENDIX C</b>	.....	<b>125</b>
<b>BIBLIOGRAPHY</b>	.....	<b>156</b>

## LIST OF TABLES

Table 1. Selected examples and yields of aryl radical addition to benzene .....	2
Table 2. Radical addition of halobenzoates <b>35</b> to benzene .....	13
Table 3. Model reaction in the presence of diazo compounds <b>40a-e</b> .....	17
Table 4. Model reaction in the presence of TEMPO of Galvinoxyl.....	21
Table 5. Preliminary experiments with TTMSS.....	26
Table 6. HAS of benzene with iodobenzene analogs <b>47a-e</b> in the presence of TTMSS and pyridine.....	28
Table 7. Standard silica gel TLC retention factors for amide <b>102</b> and fluorous urea <b>95</b> .....	91
Table 8. 3x5 amide coupling reactions mediated by FDIC .....	95

## LIST OF FIGURES

Figure 1. GC chromatogram of entry 4, Table 2 after 3 h.....	14
Figure 2. Proposed structure of the $m/z$ 250 ion in GC-MS analysis of side products from the control reaction (left) and proposed structure of the side products (right).....	15
Figure 3. GC chromatogram of entry 6, Table 3 after 20 h.....	18
Figure 4. GC chromatogram of entry 1, Table 4 after 18 h.....	23
Figure 5. GC chromatogram of entry 2, Table 5 after 14 h.....	24
Figure 6. GC chromatogram of mixture obtained from reaction of <b>35b</b> , TTMSS and pyridine after 3 h at room temperature.....	27
Figure 7. nOe enhancements of cyclic silyl ether <b>61</b> confirming the exocyclic alkene geometry ( <i>E</i> ).....	34
Figure 8. $^{29}\text{Si}$ NMR (60 MHz) in benzene- $d_6$ of the crude reaction mixture obtained from reaction of aryl iodide <b>35b</b> and TTMSS after 40% conversion.....	38
Figure 9. Pulse sequence employed in a 2D EXSY NMR experiment.....	50
Figure 10. Conformational interconversion amongst four diastereomeric atropisomers of tricyclic pyridone <b>71</b> .....	52
Figure 11. $^1\text{H}$ NMR 2D EXSY spectrum of tricyclic pyridone <b>71</b> in $d_6$ -DMSO at 300 K (left) and 340 K (right) (taken from reference 92).....	53

Figure 12. 500 MHz $^1\text{H}$ NMR spectrum from 3.5 to 6.0 ppm of dihydrophenanthridine <b>60</b> in $\text{CDCl}_3$ .....	56
Figure 13. AM1-calculated minimum energy structures of <b>60</b> .....	57
Figure 14. X-ray crystal structure (right) and AM1 calculated structure (left) of <b>60</b> .....	59
Figure 15. 300 MHz $^1\text{H}$ NMR spectrum of <b>60</b> from 225 K to room temperature in $\text{CD}_2\text{Cl}_2$ .....	60
Figure 16. Key NOE enhancements from the 2D NOESY spectrum of dihydrophenanthridine <b>60</b> in $\text{CDCl}_3$ .....	61
Figure 17. Proton assignments accompanying 2DEXSY spectra of dihydrophenanthridines .....	62
Figure 18. 500 MHz 2D EXSY spectrum of <b>60</b> in $\text{CDCl}_3$ (4.8 to 6.2 ppm) with a mixing time of 0.35 s .....	63
Figure 19. Model of conformational interconversion of dihydrophenanthridine <b>60</b> based on 2D EXSY $^1\text{H}$ NMR at 295 K .....	65
Figure 20. $^1\text{H}$ NMR of hydrophenanthridine <b>60</b> from 3.75-4.75 ppm in $d_6$ -DMSO at elevated temperatures.....	67
Figure 21. 500 MHz $^1\text{H}$ NMR spectrum of dihydrophenanthridine <b>59</b> in $\text{CDCl}_3$ .....	68
Figure 22. AM1-calculated minimum energy structures of <b>59</b> .....	69
Figure 23. 500 MHz 2D EXSY spectrum of <b>59</b> (3.3 to 6.2 ppm) in $\text{CDCl}_3$ with a mixing time of 0.35 s .....	70
Figure 24. Model of conformational interconversion of <b>59</b> based on 2D EXSY $^1\text{H}$ NMR at 295 K .....	72
Figure 25. $^1\text{H}$ NMR of dihydrophenanthridine <b>59</b> from 3.75-4.75 ppm in $d_6$ -DMSO at elevated temperatures.....	73
Figure 26. Dihydrophenanthridine analogs <b>72</b> and <b>73</b> .....	74

Figure 27. Dihydrophenanthridine analog lacking an <i>ortho</i> substituent.....	75
Figure 28. 300 MHz <sup>1</sup> H NMR spectrum of dihydrophenanthridine <b>78</b> in CDCl <sub>3</sub> .....	77
Figure 29. Dicyclohexylcarbodiimide ( <b>79</b> ) and diisopropylcarbodiimide ( <b>80</b> ).....	81
Figure 30. Pictorial representation of reverse F-SPE over standard silica gel .....	83
Figure 31. First and second generation fluororous carbodiimides.....	85
Figure 32. Fluorous DIC analog (FDIC).....	85
Figure 33. Model amide employed for F-SPE optimization experiments.....	91
Figure 34. Weight of fluororous urea <b>95</b> per fraction collected from SPE over standard silica gel.....	92
Figure 35. Carboxylic acids and amines used for 3x5 matrix of amide syntheses .....	93
Figure 36. Amide products from 3x5 matrix of coupling reactions .....	96
Figure 37. <sup>1</sup> H NMR of fluorobenzyl amide <b>105ab</b> .....	97
Figure 38. <sup>19</sup> F NMR of fluorobenzyl amide <b>105ab</b> .....	97

## LIST OF SCHEMES

Scheme 1. Aryl radical addition to benzene .....	2
Scheme 2. Mechanism of aryl radical addition to benzene .....	3
Scheme 3. Bowman's synthesis of phenanthridone <b>6</b> via HAS.....	3
Scheme 4. Tandem radical annulation en route to the methyl ester of Danishefsky's tetracycle ..	4
Scheme 5. Synthesis of oxindole <b>10</b> via HAS .....	5
Scheme 6. Proposed oxidative role of AIBN in the conversion of aryl bromide <b>9a</b> into oxindole <b>10a</b> .....	6
Scheme 7. Oxidation of benzhydryl radicals by azoalkanes .....	7
Scheme 8. Evidence of $\pi$ -radical disproportionation during the cyclization of deuterated anilide <b>11</b> .....	8
Scheme 9. Proposed mechanism for the autooxidation of tris(trimethylsilyl)silane .....	10
Scheme 10. Autooxidation of Bu <sub>3</sub> SnH in the presence of molecular oxygen.....	11
Scheme 11. Model reaction for radical addition to an arene .....	13
Scheme 12. Hypothesized participation of TEMPO in intermolecular HAS.....	20
Scheme 13. Decomposition of TEMPOH.....	25
Scheme 14. Synthesis of iodoanilide cyclization precursors <b>49</b> and <b>50</b> .....	32
Scheme 15. Cyclization of precursors <b>49-52</b> using TTMSS/pyridine at room temp.....	33
Scheme 16. Proposed mechanism for homolytic aromatic substitution mediated by TTMSS/O <sub>2</sub>	35

Scheme 17. Synthesis of silyl iodide <b>68</b> and silyl alcohol <b>70</b> as authentic samples for $^{29}\text{Si}$ NMR experiments.....	37
Scheme 18. Formation of 2,4-dimethylphenanthridine <b>73</b> .....	74
Scheme 19. Synthesis of <i>N</i> -pivaloyl hydrophenanthridine analog <b>78</b> .....	76
Scheme 20. Carbodiimide mediated amide synthesis.....	82
Scheme 21. Synthesis of fluorous urea <b>95</b> .....	86
Scheme 22. Synthesis of FDIC <b>87</b> from fluorous urea <b>95</b> .....	87
Scheme 23. FDIC-mediated synthesis of amide <b>98</b> .....	88
Scheme 24. DIC-mediated synthesis of amide <b>98</b> .....	89

## LIST OF ABBREVIATIONS

AcCl = Acetylchloride

AcCN = Acetonitrile

AIBN = Azobis(isobutyronitrile)

AM1 = Austin model 1

9-BBN = 9-Borobicyclo[3.3.1]nonane

BnBr = Benzyl bromide

BTMA•ICl<sub>2</sub> = Benzyltrimethylammonium dichloroiodate

*s*-BuLi = *sec*-Butyllithium

*t*-BuLi = *tert*-Butyllithium

Bu<sub>3</sub>SnH = Tributyltin hydride

CAS = Chemical Abstracts Service

CIP = Cahn-Ingold-Prelog

CLSA = Complete line shape analysis

DCC = Dicyclohexylcarbodiimide

DCM = Dichloromethane

DDQ = 2,3-dichloro-5,6-dicyano-1,4-benzoquinone

DFT = Density functional theory

DIC = Diisopropylcarbodiimide

DMF = Dimethylformamide

DMSO = Dimethylsulfoxide

EI = Electron ionization  
Et<sub>2</sub>O = Diethyl ether  
EtOAc = Ethyl acetate  
EXSY = Exchange spectroscopy  
FC-72 = Perfluorohexanes  
FDIC = Fluorous carbodiimide  
F-SPE = Fluorous solid-phase extraction  
FTI = Fluorous Technologies, Inc.  
GC = Gas chromatography with flame ionization detection  
GC-MS = Gas chromatograph mass spectrometry  
HAS = Homolytic aromatic substitution  
HFE-7100 = Perfluorobutyl methyl ether  
HOBt = 1-Hydroxybenzotriazole  
HPLC = High pressure liquid chromatography  
HRMS = High resolution mass spectrometry  
IR = Infrared spectroscopy  
LAH = Lithium aluminum hydride  
LDA = Lithium diisopropylamide  
LRMS = Low resolution mass spectrometry  
MeOH = Methanol  
MS = Mass spectrometry  
NBS = *N*-Bromosuccinimide  
NMR = Nuclear magnetic resonance  
NOE = Nuclear overhauser effect  
PivCl = Pivaloyl chloride  
PS = Polymer supported  
pyr = Pyridine

RF = Response factor

$R_f$  = Retention factor

sisyl = Tris(trimethylsilyl)silyl

SPE = Solid phase extraction

TBDPS = *tert*-Butyldiphenylsilyl

TEMPO = 2,2,6,6-tetramethylpiperidine *N*-oxide

TEMPOH = 2,2,6,6-tetramethylpiperidine *N*-hydroxide

THF = Tetrahydrofuran

TLC = Thin-layer chromatography

$T_m$  = Mixing time

TMS = Trimethylsilyl

TMSCl = Trimethylsilylchloride

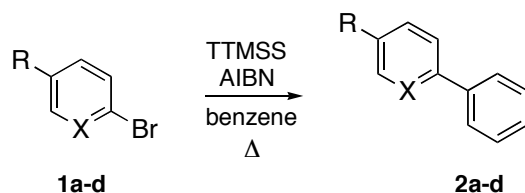
TTMSS = Tris(trimethylsilyl)silane

## 1.0 HOMOLYTIC AROMATIC SUBSTITUTION IN ORGANIC SYNTHESIS

### 1.1 Biaryl synthesis

Homolytic aromatic substitution (HAS) is the addition of a radical to an arene followed by the loss of an atom or group ( $H\cdot$  or  $R\cdot$ ) to generate a newly substituted aromatic product.<sup>1</sup> Over the past few decades, there have been numerous published reports of HAS to construct carbon-carbon bonds to generate heterocyclic compounds.<sup>2-14</sup> There are also several examples of using HAS to achieve intermolecular couplings to afford substituted arenes and bi-aryl systems.<sup>15-18</sup> Such radical transformations are commonly achieved by treatment of an organic halide with tributyltin hydride ( $Bu_3SnH$ ) and 2,2-azobisisobutyronitrile (AIBN), or tris(trimethylsilyl)silane (TTMSS) and AIBN.

An example of using HAS to assemble biaryl compounds comes from recent work by Alvarez-Builla and coworkers,<sup>15,16</sup> and is related to the research presented in Chapter 2. Their method is based on the intermolecular radical addition of aryl radicals onto aromatic solvents as demonstrated in **Scheme 1**.



**Scheme 1. Aryl radical addition to benzene**

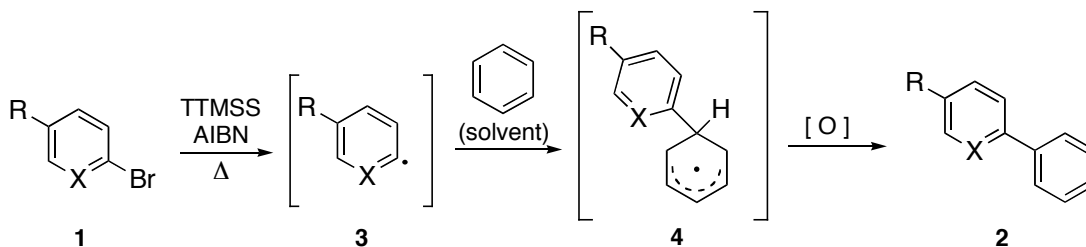
**Table 1. Selected examples and yields of aryl radical addition to benzene**

entry <sup>a</sup>	substrate	X	R	product	yield (%)
1	<b>1a</b>	N	H	<b>2a</b>	41
2	<b>1b</b>	CH	Me	<b>2b</b>	51
3	<b>1c</b>	CH	OMe	<b>2c</b>	50
4	<b>1d</b>	CH	CO <sub>2</sub> Me	<b>2d</b>	52

<sup>a</sup> rxn cond: a mixture of TTMSS (2 equiv), AIBN (2 equiv), and aryl bromide **1** in benzene was slowly added (8 h) to a refluxing solution of benzene.

The authors optimized the reaction conditions in **Scheme 1** using entry 1 of **Table 1** as a control, and found the best results were obtained by slow addition (8 h) of a mixture of TTMSS (2 equiv), AIBN (2 equiv) and aryl bromide **1** in benzene to a refluxing solution of benzene. Only 7% yield of biaryl **2a** was obtained when Bu<sub>3</sub>SnH was used, compared to 41% when TTMSS was used under otherwise analogous conditions.

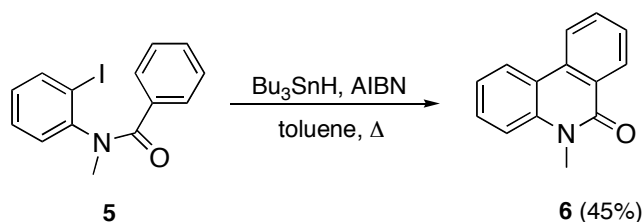
The addition of a radical species to benzene, like most HAS reactions, exhibits two unique and unusual features when compared to radical reactions as a whole. First, a stoichiometric amount of reducing agent (TTMSS or Bu<sub>3</sub>SnH) is used, but the HAS reaction is not a reduction. Second, a stoichiometric amount of initiator, such as AIBN, is required to achieve complete consumption of aryl bromide **1**. This feature is consistent with a hypothesis put forth first by Curran<sup>6,19</sup> that AIBN may be playing a role in the oxidation of cyclohexadienyl radical **4** to form the rearomatized product **2** (**Scheme 2**). The mechanistic details of HAS are discussed in the next section.



**Scheme 2. Mechanism of aryl radical addition to benzene**

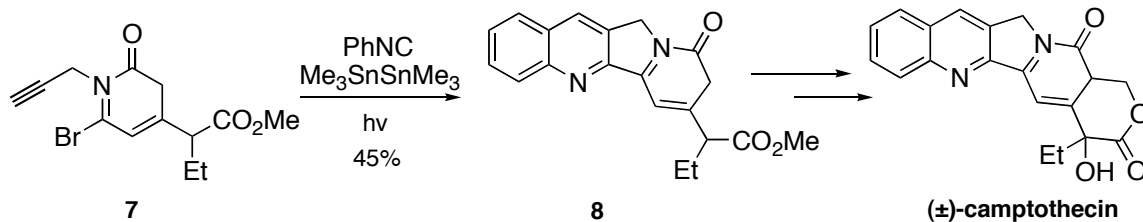
## 1.2 Heterocycle syntheses

The majority of published HAS reactions involve the intramolecular addition of a radical to an arene; a representative example published by Bowman and coworkers<sup>2</sup> is shown in **Scheme 3**. Treatment of iodoanilide **5** with  $\text{Bu}_3\text{SnH/AIBN}$  in refluxing toluene affords *N*-methylphenanthridinone **6** in 45% yield.



**Scheme 3. Bowman's synthesis of phenanthridone 6 via HAS**

Curran's synthesis of ( $\pm$ )-camptothecin included HAS as a key step in the radical annulation of bromopyridone **7** and phenylisocyanide to assemble the methyl ester analog of Danishefsky's tetracycle **8**, which was then carried on to the natural product (**Scheme 4**).<sup>6</sup> This example illustrates the power of radical chemistry and HAS to assemble complex heterocycles from relatively simple starting materials.



Scheme 4. Tandem radical annulation en route to the methyl ester of Danishefsky's tetracycline

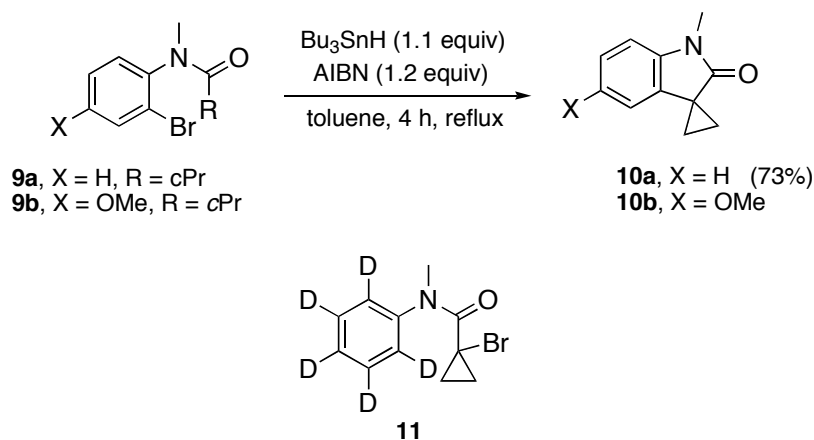
### 1.3 The mechanism of HAS and the role of AIBN

The mechanism of HAS is not well understood and is the subject of debate in the literature.<sup>20</sup> A common feature of most, but not all, HAS reactions performed with  $\text{Bu}_3\text{SnH/AIBN}$  is the need for stoichiometric amounts of AIBN, whereas only catalytic amounts of initiator are sufficient for radical additions to non-aromatic alkenes.<sup>21-23</sup>

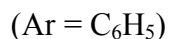
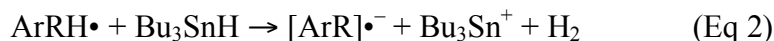
The baffling mechanistic aspect of HAS is how the cyclohexadienyl radical obtained after radical addition to an arene is oxidized to its aromatic counterpart (**Scheme 2**). Bowman has proposed a single electron transfer ( $\text{S}_{\text{RN}}1$ ) mechanism to account for this oxidation.<sup>2</sup> His proposal requires that  $\text{Bu}_3\text{SnH}$  act as a base rather than a radical carrier. This  $\text{S}_{\text{RN}}1$  mechanism is supported by a limited number of examples where HAS reactions worked with catalytic amounts of AIBN.<sup>14,24</sup> Curran later proposed that AIBN plays a role in the oxidation of cyclohexadienyl radicals by abstracting  $\text{H}\cdot$ , accounting for the stoichiometric need of AIBN in most reported cases of HAS.<sup>19,25</sup> Another possibility is a reductive pathway where the cyclohexadienyl radical abstracts  $\text{H}\cdot$  from  $\text{Bu}_3\text{SnH}$  in a chain propagating step. However, Crich and coworkers<sup>20</sup> have shown that cyclohexadienyl radicals generated by  $\text{Bu}_3\text{SnH}$  mediated HAS cyclizations can be trapped by the good  $\text{H}\cdot$  donor  $\text{PhSeH}$  to afford dihydro products. Furthermore, the reduced cyclohexadiene products do not typically rearomatize under standard reaction conditions.<sup>5</sup>

Since Bowman proposed his  $\text{S}_{\text{RN}}1$  mechanism, he has published work in collaboration with Beckwith and Storey that supports the hypothesis of an AIBN assisted oxidation

mechanism.<sup>25</sup> The authors concluded the transformation of aryl bromide **9a** to oxindole **10a** (**Scheme 5**) does not occur via a Bowman's proposed S<sub>RN</sub>1 mechanism based on the following key observations: (1) Treatment of **9a** with Bu<sub>3</sub>SnD/AIBN did not yield any detectable amount of HD in the gaseous products of the reaction; (2) Treatment of deuterated radical precursor **11** with Bu<sub>3</sub>SnH/AIBN did not yield any detectable amount of HD; (3) Reaction of an equimolar mixture of **9a** and its *p*-methoxy derivative **9b** with 0.5 equiv of Bu<sub>3</sub>SnH/AIBN resulted in the consumption of both substrates to an equal extent (the more readily reduced substrate **9b** should be consumed faster if the reaction pathway involves electron transfer according to Eqs 2-4). These observations offer convincing evidence that the reaction shown in **Scheme 5** does not involve a single electron transfer mechanism described by Eqs 1 or 2-4.

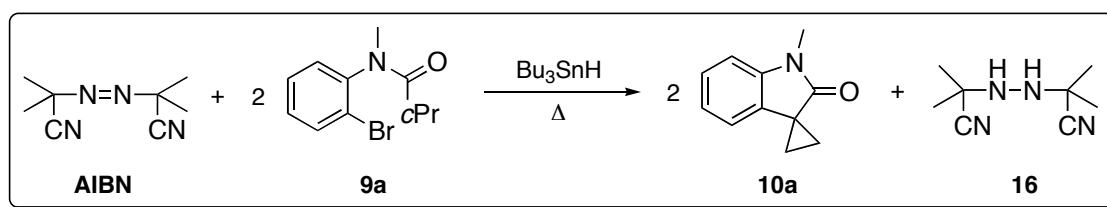


**Scheme 5. Synthesis of oxindole 10 via HAS** <sup>26</sup>

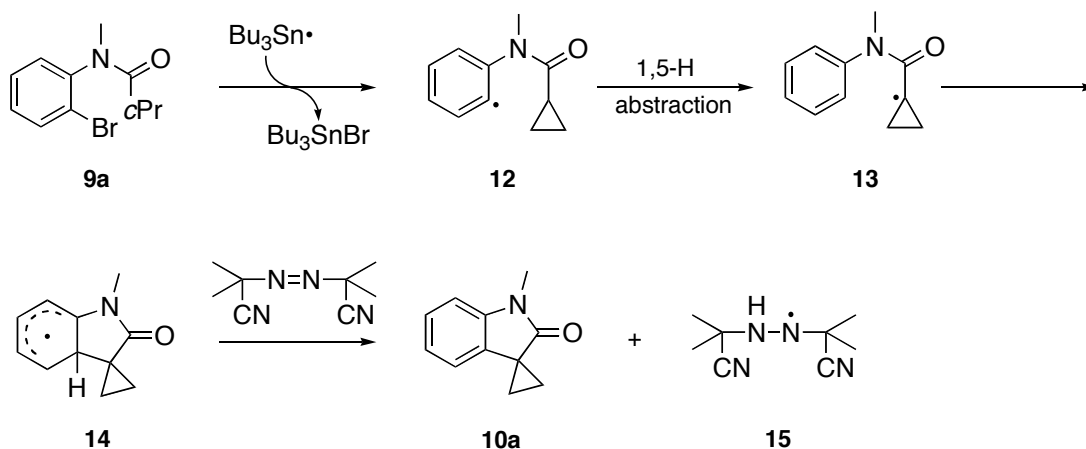


The authors presented further support for the role of AIBN as the oxidant when aryl bromide **9a** was treated under the standard conditions (110 °C, 240 min) with Bu<sub>3</sub>SnH/AIBN (1.2 equiv). GC analysis of the gaseous byproducts of the reaction mixture revealed the evolution of only 0.3 equiv of nitrogen gas, which means the remaining 0.9 equiv of AIBN was consumed by some pathway other than thermal decomposition into 2-cyano-2-propyl radicals and N<sub>2</sub>.<sup>26</sup> While the authors were unable to isolate the reduced hydrazine **16** (Scheme 6), they were able to independently synthesize it and show that it is unstable under the employed reaction conditions.<sup>4</sup>

The mechanism of the conversion of aryl bromide **9a** to oxindole **10a** with AIBN acting as an oxidant, according to Beckwith and Bowman, is shown Scheme 6. Bromine atom abstraction from aryl bromide **9a** by Bu<sub>3</sub>Sn• results in the formation of Bu<sub>3</sub>SnBr and aryl radical **12**, which undergoes a 1,5 hydrogen shift to give tertiary radical **13**. The cyclopropyl radical **13** then adds to the anilide ring to generate cyclohexadienyl radical **14**. Hydrogen atom abstraction



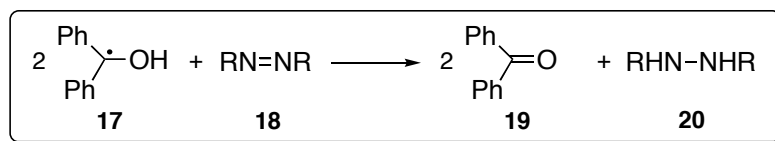
mechanism:



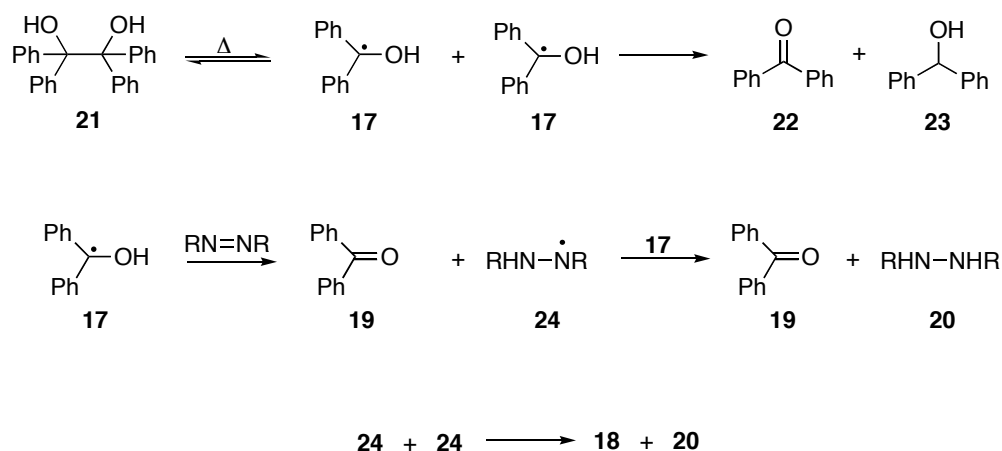
Scheme 6. Proposed oxidative role of AIBN in the conversion of aryl bromide **9a** into oxindole **10a**

from **14** by AIBN affords the desired rearomatized product **10a** and hydrazyl radical **15**. This hydrazyl radical can then proceed to oxidize a second equiv of the  $\pi$ -radical **14**. This proposed mechanism requires the stoichiometric use of AIBN where the oxidation of cyclohexadienyl radical **14** constitutes a chain-terminating step. Alternatively, 2 equiv of hydrazyl radical **15** can undergo a known disproportionation to regenerate 1 equiv of AIBN and produce the corresponding hydrazine **16** directly.<sup>27</sup>

Diazo compounds (such as AIBN) are known to oxidize benzhydryl radicals to yield the corresponding ketones by H• abstraction.<sup>28</sup> The mechanism proposed by Engel is shown in **Scheme 7**. Upon heating, benzopinacol **21** homolytically cleaves into 2 equiv of benzhydryl radical **17**, which undergoes disproportionation in the absence of other reaction pathways.



*mechanism:*



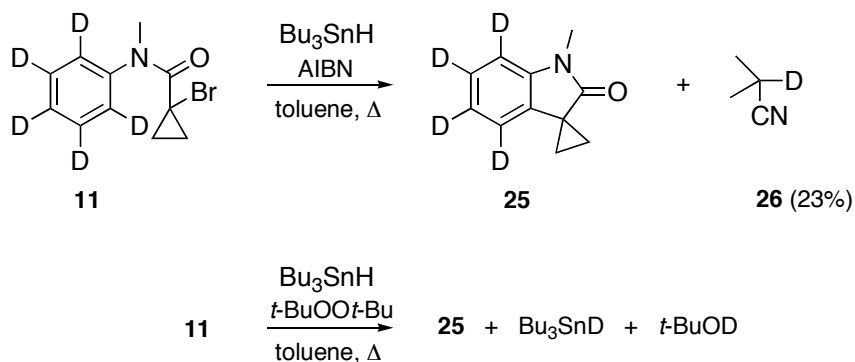
**Scheme 7. Oxidation of benzhydryl radicals by azoalkanes**

In the presence of an azoalkane, radical benzhydryl radical **17** transfers H• to the azoalkane yielding ketone **18** and the corresponding hydrazyl radical **24**. This hydrazyl radical can oxidize a second equiv of the benzhydryl radical or undergo the known disproportionation mentioned previously to yield azoalkane **18** and hydrazine **20**.

Engel's mechanism for the oxidation of benzhydryl radicals by azoalkanes offers precedent for the proposed mechanism involving AIBN oxidation of cyclohexadienyl radicals in HAS reactions.<sup>28</sup>

#### 1.4 Other fates of cyclohexadienyl radicals

Bowman and Beckwith were able to show that cyclohexadienyl radicals undergo disproportionations with initiator-derived radicals. When deuterated anilide **11** was treated with Bu<sub>3</sub>SnH/AIBN to afford tetradeutero oxindole **25**, they found Me<sub>2</sub>CDCN (**26**) was formed in 23% yield (**Scheme 8**).



**Scheme 8.** Evidence of  $\pi$ -radical diproportionation during the cyclization of deuterated anilide **11**<sup>26</sup>

When the reaction in **Scheme 8** was repeated, this time using di-*t*-butylperoxide as the initiator, the authors detected the presence of *t*-BuOD and Bu<sub>3</sub>SnD by <sup>2</sup>H NMR of the reaction mixture. The detection of deuterated initiator-derived products in HAS reactions is important

and offers further support that cyclohexadienyl radicals undergo oxidation to their rearomatized counterparts in a chain-terminating step, explaining the need for stoichiometric amounts of initiator.

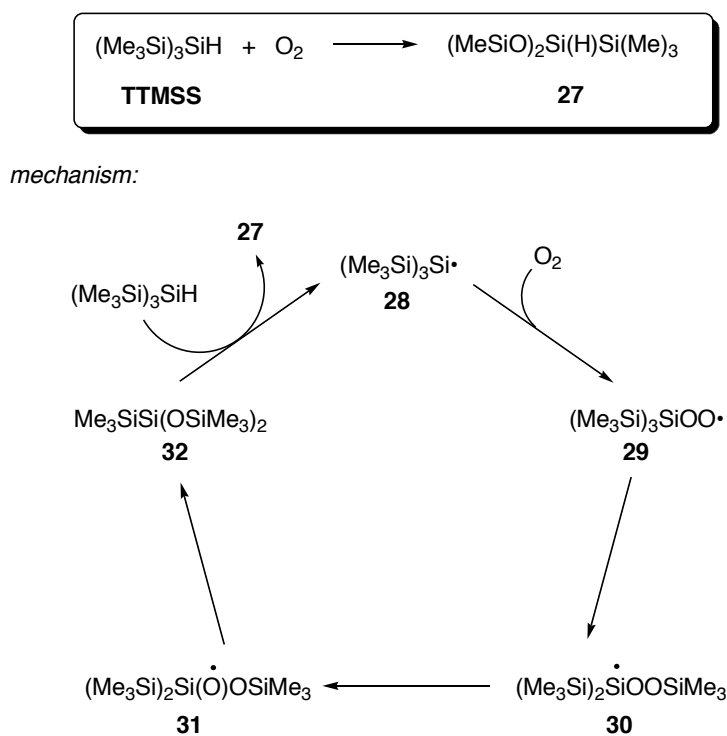
### 1.5 Tris(trimethylsilyl)silane (TTMSS) as an alternative to Bu<sub>3</sub>SnH

Two well known problems are associated with the use of organotin compounds in synthetic chemistry.<sup>29</sup> 1) Organotin compounds are highly toxic, and 2) Tin residues are difficult to separate from the desired product(s). For these reasons, TTMSS has become an attractive alternative to tin hydrides since its introduction into organic synthesis during the late 1980s.<sup>30,31</sup>

The rate of halogen abstraction from organic halides by (TMS)<sub>3</sub>Si• is comparable to that of Bu<sub>3</sub>Sn•.<sup>30</sup> For (TMS)<sub>3</sub>Si•, the rate constant for bromine abstraction from PhBr is 4.6 x 10<sup>6</sup> M<sup>-1</sup> s<sup>-1</sup> at 25 °C.<sup>32</sup> For Bu<sub>3</sub>Sn•, the approximate rate constant for bromine abstraction from 3-bromoanisole is 4.0 x 10<sup>6</sup> M<sup>-1</sup> s<sup>-1</sup> at 80 °C.<sup>33</sup> However, TTMSS is less reactive as a hydrogen donor than Bu<sub>3</sub>SnH, most likely because the Si-H bond is about 5 kcal mol<sup>-1</sup> stronger than the Sn-H bond (the bond strengths are 84.0 and 78.6 kcal mol<sup>-1</sup>, respectively).<sup>31,35</sup> Therefore, TTMSS is more attractive than Bu<sub>3</sub>SnH in radical reactions where undesired direct reduction of intermediate radicals is problematic.<sup>35</sup>

TTMSS undergoes an interesting auto-oxidation process in the presence of molecular oxygen. Chatgililoglu and co-workers have shown the auto-oxidation of TTMSS can be accomplished by bubbling air or pure oxygen through a neat sample of TTMSS, or through a solution of TTMSS, resulting silyloxy species **27**.<sup>35-37</sup> The proposed mechanism is shown in **Scheme 9**. The authors suggest a radical chain is initiated by hydrogen atom abstraction from TTMSS by molecular oxygen to produce radical **28** since no initiator was used in the reaction.<sup>36</sup> Silyl radical **28** adds to dioxygen to yield silylperoxyl radical **29** which rearranges to silyl radical **30** via a 1,3 migration of a Me<sub>3</sub>Si group. Silyl radical **30** then undergoes internal homolytic

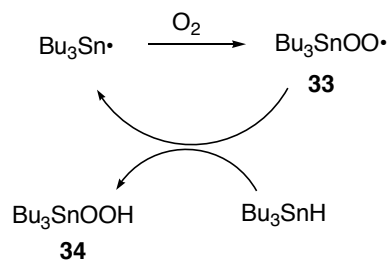
substitution to siloxy radical **31**, which further undergoes a 1,2 migration of a Me<sub>3</sub>Si group resulting in silyl radical **32**. Hydrogen atom abstraction by **32** from TTMSS generates the observed product **27** and (Me<sub>3</sub>Si)<sub>3</sub>Si•, thus completing the radical chain. The authors propose the intramolecular oxidation process depicted in **Scheme 9** over an intermolecular version based on labeling experiments and kinetic studies.<sup>36</sup> In the most recent publication on the autooxidation of TTMSS,<sup>37</sup> Chatgililoglu and coworkers conducted a computational study that suggests silylperoxy radical **29** rearranges to **31** in a single unimolecular step.



**Scheme 9.** Proposed mechanism for the autooxidation of tris(trimethylsilyl)silane<sup>38</sup>

Bu<sub>3</sub>Sn• reacts with dioxygen at a diffusion controlled rate ( $k = 7 \times 10^9 \text{ M}^{-1} \text{ s}^{-1}$ ),<sup>38</sup> albeit in a more straightforward manner than does TTMSS. Once the Bu<sub>3</sub>Sn• radical is generated from Bu<sub>3</sub>SnH via H• abstraction, either by an initiator or by oxygen itself, it quickly combines with O<sub>2</sub> to form stannylperoxy radical **33**. Bu<sub>3</sub>Sn• is regenerated by H• abstraction from Bu<sub>3</sub>SnH by stannylperoxy radical **33** to afford stannylperoxide **34** (**Scheme 10**). Bennasar and coworkers

have suggested that  $\text{Bu}_3\text{SnOO}\cdot$  is responsible for hydrogen atom abstraction from cyclohexadienyl radicals to form the corresponding aromatic products.<sup>39</sup>



**Scheme 10. Autooxidation of  $\text{Bu}_3\text{SnH}$  in the presence of molecular oxygen**

## 2.0 INVESTIGATION INTO THE USE OF OXIDANTS IN HOMOLYTIC AROMATIC SUBSTITUTION

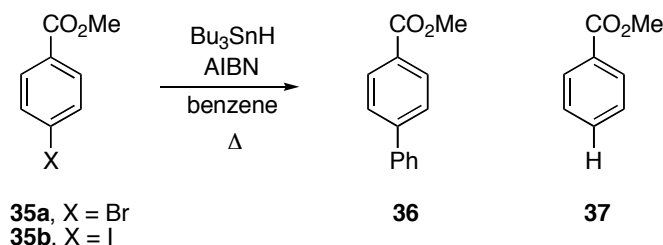
### 2.1 Aim of project

Homolytic aromatic substitutions typically require high temperatures, prolonged reaction times, and a stoichiometric amount of initiator, while providing the desired products in only modest yields. The goal of the work described herein was to better understand the mechanism of HAS and to explore reaction conditions in which it could proceed with a catalytic amount of initiator and a stoichiometric amount of co-oxidant. Based on the hypothesis that AIBN acts as an oxidant for the cyclohexadienyl radical intermediate obtained after radical addition to an arene,<sup>19,25,26</sup> it was postulated that a thermally stable diazo compound may serve as a superior oxidant relative to AIBN and perhaps allow these reactions to proceed with higher yields and shorter reaction times. Furthermore, by eliminating the need for stoichiometric initiator, the possibility of conducting these reactions on large scale becomes viable.

### 2.2 Reaction of an Aryl Halide with Bu<sub>3</sub>SnH/AIBN in Benzene – Control Experiments

A model system was chosen to observe the effect of diazo compounds in homolytic aromatic substitution (**Scheme 11**). Typical experiments were conducted by dissolving halobenzoate **35** in benzene (50 mL, 4 mM) and adding to the solution Bu<sub>3</sub>SnH (1 equiv), AIBN and octadecane as an internal standard for determination of product yields by GC. The resulting

reaction mixtures were refluxed under argon at 80 °C for 3 h. The GC detector response factors for **35**, **36** and **37** (relative to octadecane) were calculated so yields could be determined from the GC chromatogram of the reaction mixtures.<sup>40</sup>



**Scheme 11. Model reaction for radical addition to an arene**

Initial control experiments were conducted to determine how the product yields were affected by varying the amount of AIBN employed in the reaction; the results are compiled in **Table 2**. When 0.2 equiv of AIBN and 1 equiv of  $\text{Bu}_3\text{SnH}$  were used with aryl bromide **35a**, only 7% of desired biphenyl **36** was formed alongside 3% of the directly reduced product **37**,

**Table 2. Radical addition of halobenzoates **35** to benzene**

entry <sup>a</sup>	substrate	initiator (equiv)	$\text{Bu}_3\text{SnH}$ (equiv)	% <b>35</b> <sup>d</sup>	% <b>36</b> <sup>d</sup>	% <b>37</b> <sup>d</sup>
1 <sup>b</sup>	<b>35a</b>	AIBN (0.2)	1.0	76	7	3
2 <sup>b</sup>	<b>35a</b>	AIBN (1.0)	1.0	23	16	5
3 <sup>c</sup>	<b>35b</b>	AIBN (0.2)	1.0	46	27	3
4 <sup>c</sup>	<b>35b</b>	AIBN (1.0)	1.0	0	27	9
5 <sup>c,e</sup>	<b>35b</b>	Dilauryl peroxide (1.0)	1.0	10	40	-

<sup>a</sup> reaction conditions: aryl halide **35** was dissolved in benzene (50 mL, 0.004 M), along with initiator and  $\text{Bu}_3\text{SnH}$  and the mixture was refluxed under argon for 3 h. <sup>b</sup> Reported yields are the average of three runs. <sup>c</sup> Reported yields are the average of 2 runs. <sup>d</sup> Yield determined by GC with octadecane as the internal standard. <sup>e</sup>  $\text{Bu}_3\text{SnH}$  was consumed prior to complete reaction of **35b**.

leaving  $\text{Bu}_3\text{SnH}$  and 76% of the bromobenzoate unreacted (**Table 2**, entry 1). By using 1.0 equiv of AIBN under the same conditions (**Table 2**, entry 2), biaryl **36** was formed in 16% yield,

but 23% of bromide **35a** still remained unreacted after complete consumption of the tin hydride had occurred.

Due to the poor reactivity of bromobenzoate **35a**, the more reactive iodo analog **35b** was employed for the model system. Reaction of **35b** with 0.2 equiv of AIBN and 1.0 equiv of  $\text{Bu}_3\text{SnH}$  resulted in 27% yield of biphenyl **36** with 46% of the aryl iodide **35b** left unreacted (Table 2, entry 3). The reaction went to 100% conversion when **35b** was treated with stoichiometric amounts of AIBN and tin hydride at reflux in benzene, although the total mass balance was low, since only 27% yield of the desired biphenyl **36** was formed along with 9% of the directly reduced methyl benzoate **37** (Table 2.1, entry 4). These results show that the percent conversion of iodobenzoate **35b** is dependent on the amount of AIBN used, and the iodo precursor is more reactive than the bromo analog.

The GC chromatogram of the reaction mixture described in Table 2, entry 4 is shown in Figure 1, and it is representative of a typical GC chromatogram obtained from the reactions in Table 2.

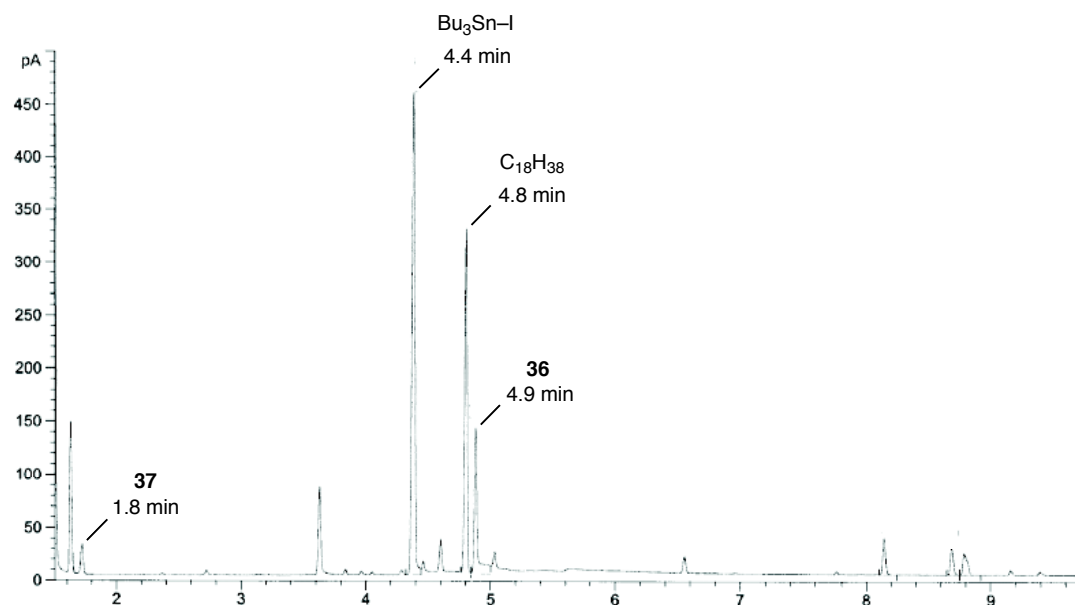
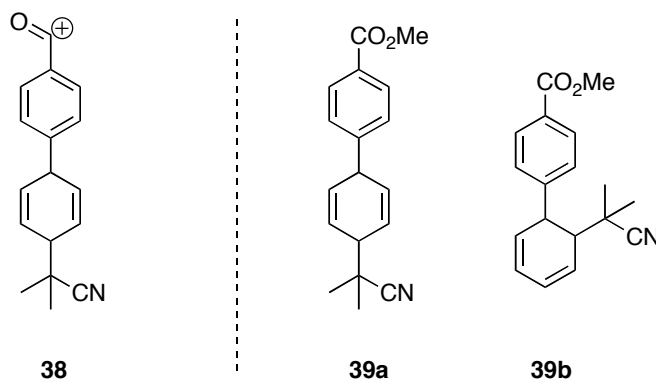


Figure 1. GC chromatogram of entry 4, Table 2 after 3 h

The major products of the reaction are  $\text{Bu}_3\text{SnI}$  ( $T_R = 4.4$  min) and phenyl benzoate **36** ( $T_R = 4.9$  min).<sup>41</sup> The reaction products observed between 8-9 min may be the result of the cyclohexadienyl radical intermediate reacting with AIBN, which may explain the fate of a portion of the “missing” starting material (recall that 66% of starting material **35b** reacted to give rise to something other than the biaryl product **36** or directly reduced product **37**). GC-MS analysis of these peaks (Appendix A) between 8–9 min gives rise to fragment ions corresponding to 2-cyanopropyl ion ( $m/z$  69), biphenyl ion ( $m/z$  154), and acyl cation **38** ( $m/z$  250, **Figure 2**). Products resulting from the addition of 2-cyano-2-propyl radicals to indolyl radicals have been isolated and shown to breakdown to give the aromatic product.<sup>39,42</sup> Conversely, addition of 2-cyano-2-propyl radicals to cyclohexadienyl radicals is known to give rise to adducts that are stable to refluxing in benzene for several days.<sup>5</sup> Based on this knowledge, and the MS data (**Appendix A.1**) the peaks between 8-9 min from Figure 2.1 probably represent isomeric 2-cyano-2-propyl trapped cyclohexadienes **39a** and **39b** shown below.

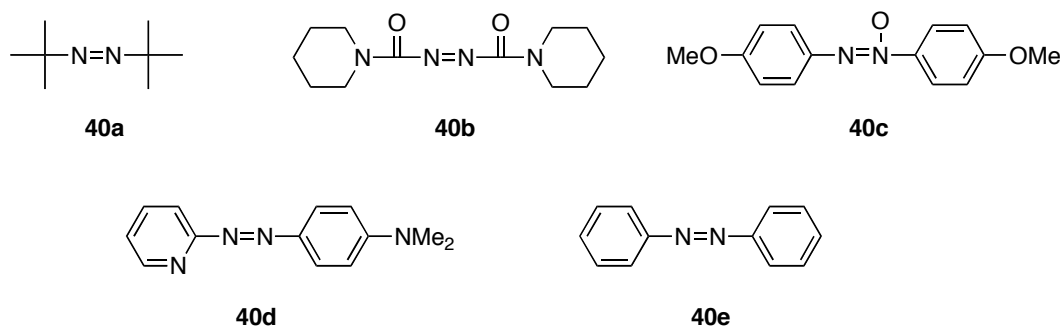


**Figure 2. Proposed structure of the  $m/z$  250 ion in GC-MS analysis of side products from the control reaction (left) and proposed structure of the side products (right)**

## 2.3 Diazo Compound Screening

Several commercially available diazo compounds were tested with the model system depicted in **Scheme 11**; the results are summarized in **Table 3**. The general procedure entailed adding diazo compound **40** (1 equiv), AIBN, Bu<sub>3</sub>SnH and octadecane as an internal standard to a solution of **35b** (0.004 M) in benzene at room temperature under an atmosphere of argon. The resulting mixtures were refluxed under an argon atmosphere and the reaction progress was monitored by GC. In all cases where 0.2 equiv of AIBN was used (**Table 3**, entries 1–5), the product yields were comparable to the yields obtained in the control reaction; much of the starting iodide was recovered (54–88%) alongside lesser amounts of substitution (10–33%) and reduction (2–5%) products with comparable total mass balances (86–99%). When 1 equiv of azobenzene was used with 0.2 equiv of AIBN, 61% of the aryl iodide **35b** remained unreacted with 33% yield of biphenyl **36** and 5% of the directly reduced product **37**, accounting for virtually all of the reacted starting material (**Table 3**, entry 5). However, when 1 equiv of AIBN was used in conjunction with a 1 equiv of azobenzene (**Table 3**, entry 6) the yield of desired biaryl product **36** improved two-fold (65%) compared to the control reaction (27%), yet a small amount of starting material still remained unreacted after complete consumption of the tin hydride. This result suggests that azobenzene inhibits the reaction to some degree, in spite of the higher yield of **36**.

The improved results obtained in entry 6 of **Table 3** can be rationalized by envisioning the reduction of the azobenzene via hydrogen atom transfer from the cyclohexadienyl intermediate, as exemplified by **Scheme 6** in Chapter 1.2.

**Table 3. Model reaction in the presence of diazo compounds 40a-e**

entry <sup>a</sup>	substrate	diazo compound	AIBN (equiv)	% <b>35</b> <sup>b</sup>	% <b>36</b> <sup>b</sup>	% <b>37</b> <sup>b</sup>
control <sup>c</sup>	<b>35b</b>	–	0.2	46	27	3
control <sup>c</sup>	<b>35b</b>	–	1.0	0	27	9
1	<b>35b</b>	<b>40a</b>	0.2	54	28	4
2	<b>35b</b>	<b>40b</b>	0.2	74	20	4
3	<b>35b</b>	<b>40c</b>	0.2	48	33	5
4	<b>35b</b>	<b>40d</b>	0.2	88	10	2
5	<b>35b</b>	<b>40e</b>	0.2	61	33	5
6 <sup>e</sup>	<b>35b</b>	<b>40e</b>	1.0	7	65 (58) <sup>d</sup>	8

<sup>a</sup> reaction conditions: aryl iodide **35b** was dissolved in benzene (50 mL, 0.004 M). Added to the solution were AIBN, Bu<sub>3</sub>SnH (1 equiv) and azo compound **40** (1 equiv). The resulting mixture was refluxed under argon for 3 h. <sup>b</sup> Yields determined by GC with octadecane as the internal standard. <sup>c</sup> From Table 2.1

<sup>d</sup> Yield in parentheses denotes isolated yield. <sup>e</sup> Reaction time of 20 h.

This hypothesis is supported by the detection of 1,2-diphenylhydrazine in the GC chromatogram ( $t_R = 4.5$  min), shown in **Figure 2.3**. Clearly azobenzene was reduced under the reaction conditions. However, injection of commercially obtained 1,2-diphenylhydrazine into the GC gave rise to two peaks: one at 3.5 min, which corresponds to azobenzene, and one at 4.5 min attributed to 1,2-diphenylhydrazine. This result suggests the hydrazo compound is unstable at the GC temperatures used and is partially converted to azobenzene. Therefore quantitation of 1,2-diphenylhydrazine by GC was not considered reliable.

The areas of the peaks between 8–9 min in the chromatogram shown in **Figure 3** were smaller than in the control reaction (**Figure 1**). The absolute amount of the side products could not be determined because they were not isolated, and therefore the GC response factor(s) could not be calculated. However, comparison of the relative area of the side product peaks from the control reaction to the reaction with azobenzene could be accomplished by dividing the area of

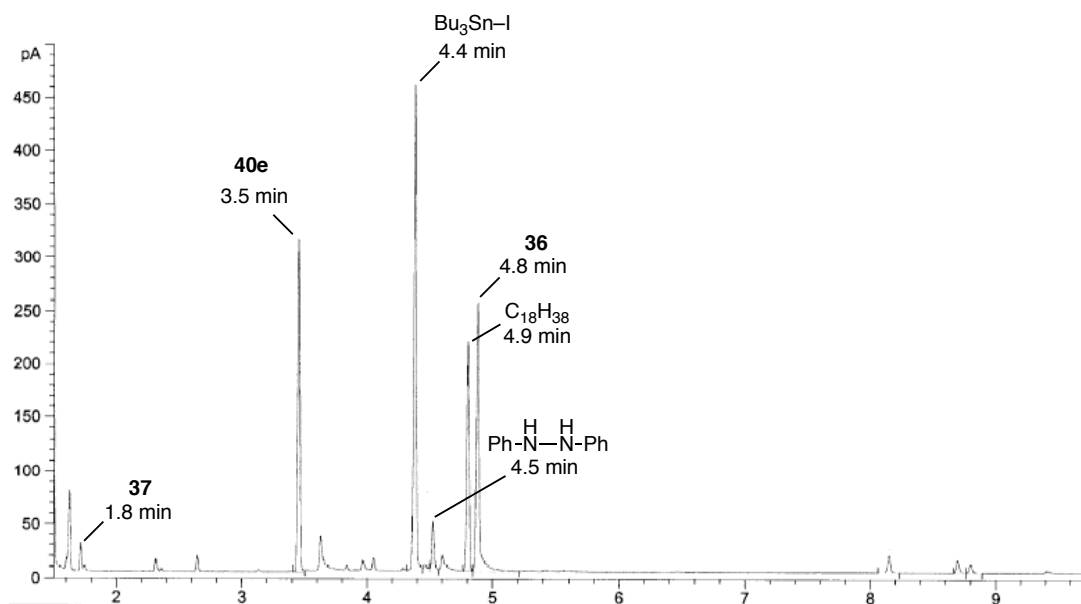


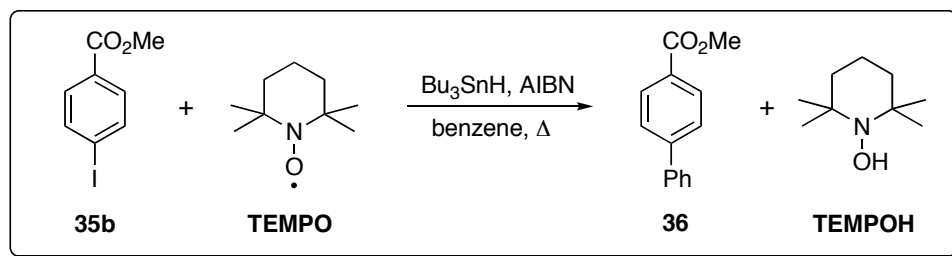
**Figure 3.** GC chromatogram of entry 6, Table 3 after 20 h

These “late” peaks by the area of the internal standard peak.<sup>46</sup> Doing so gave a value of 0.32 for the control reaction (**Figure 1**) and a value of 0.20 for the reaction with 1 equiv of azobenzene (**Figure 3**). This translates to a 38% reduction in the formation of the side products responsible for these peaks when azobenzene is incorporated into the reaction when compared to the control.

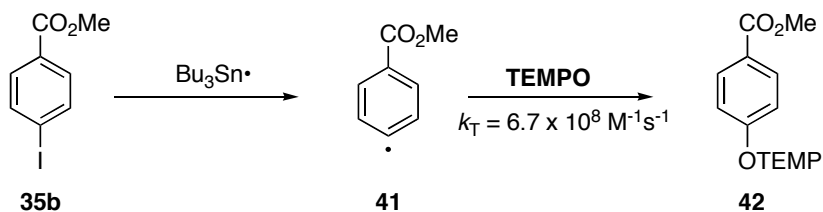
Based on these results, the presence of a thermally stable diazo compound with catalytic AIBN does not substantially improve percent conversion and yield of HAS reactions when compared to using catalytic AIBN alone. However, a two-fold increase in the yield of biphenyl **36** was observed when a stoichiometric amount of azobenzene was used alongside a stoichiometric amount of AIBN.

## 2.4 Use of other oxidants

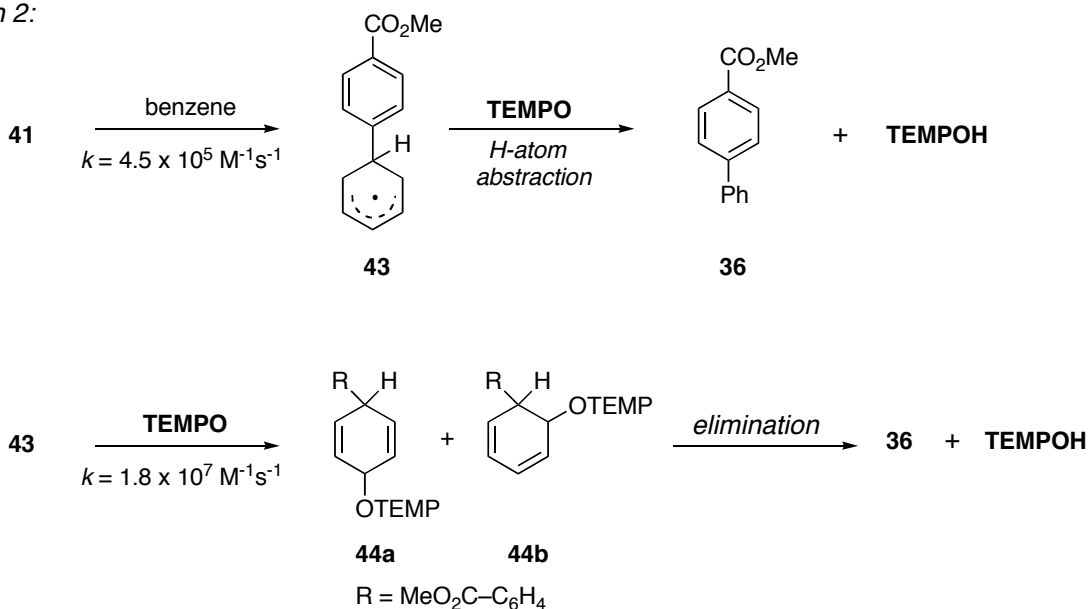
Given the lackluster results obtained with the various diazo compounds, experiments were performed under the same conditions described in Chapter 2.2, but with added oxidant. When DDQ was used, the reaction did not proceed and an insoluble white precipitate was observed. This precipitate was also formed by reaction of DDQ and the  $\text{Bu}_3\text{SnH}$  alone, suggesting these two reagents react directly with each other. Based on the use of the persistent radical TEMPO in radical cyclizations reported by Boger<sup>43</sup> and more recently by Studer,<sup>13,44-47</sup> and the known oxidizing ability of TEMPO,<sup>48,49</sup> the possible utility of TEMPO as an oxidant (i.e., a cyclohexadienyl radical trap) was investigated. The envisioned non-chain reaction pathway is outlined in **Scheme 12**.



path 1:



path 2:



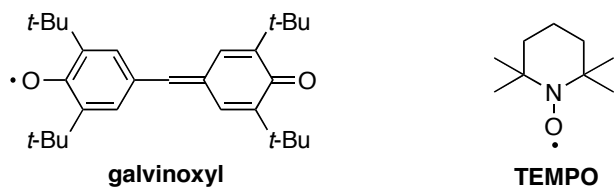
**Scheme 12. Hypothesized participation of TEMPO in intermolecular HAS**

There are two possible reaction pathways once radical **41** is generated in the presence of TEMPO. Combination of aryl radical **41** and TEMPO (path 1) can be expected to occur at a rate of about  $6.7 \times 10^8 \text{ M}^{-1} \text{ s}^{-1}$  (based on the rate of a primary nonyl radical combining with TEMPO in benzene).<sup>50</sup> Nonetheless, aryl radical **41** is expected to react with benzene (path 2) at a faster rate ( $k = 4.5 \times 10^5 \text{ M}^{-1} \text{ s}^{-1}$ )<sup>51-53</sup> given the higher concentration of the benzene solvent ( $\sim 11 \text{ M}$ ) relative to the concentration of TEMPO (equiv,  $0.004 \text{ M}$ ). Thus, addition of aryl radical **41** to

benzene would generate cyclohexadienyl radical **43**. The more stable resultant cyclohexadienyl radical **43** (relative to the initial aryl radical) could then survive long enough to combine with TEMPO to yield a mixture of alkoxyamine-substituted cyclohexadienes **44a** and **44b**. These dienes are expected to thermally eliminate into the desired product **36** and TEMPOH, an event recently proposed and reported by Studer.<sup>13,47</sup> Another possibility for generation of the desired biaryl **36** is hydrogen abstraction from intermediate **43** by TEMPO to yield biaryl product **36** and TEMPOH, resulting in the same distribution of products obtained from thermal elimination of diene **44**.

To test this hypothesis, a mixture of **35b** (0.004 M), AIBN (1 equiv), Bu<sub>3</sub>SnH (1 equiv), and TEMPO (1 equiv) in benzene was refluxed under argon for 18 h. The yield of desired biphenyl **36** was increased to 67%, although 8% of the starting iodide **35b** remained after complete consumption of the tin hydride (entry 1, **Table 4**). Summarized in **Table 4** are the

**Table 4. Model reaction in the presence of TEMPO of Galvinoxyl**



entry <sup>a</sup>	oxidant (equiv)	equiv of AIBN	equiv of Bu <sub>3</sub> SnH	% <b>35b</b> <sup>b</sup>	% <b>36</b> <sup>b</sup>	% <b>37</b> <sup>b</sup>
control		1.0	1.0	0	27	9
1	TEMPO (1.0)	1.0	1.0	8	67	10
2	TEMPO (1.0)	0.2	1.0	44	44	5
3	TEMPO (1.0)	0.5	1.0	18	64	9
4	TEMPO (0.5)	1.0	1.0	0	50	10
5	Galvinoxyl (1.0)	1.0	1.0	0	70	8

<sup>a</sup> reaction conditions: aryl iodide **35b** was dissolved in benzene (50 mL, 0.004 M), along with AIBN, Bu<sub>3</sub>SnH and oxidant. The resulting mixtures were refluxed under argon for 18 h. <sup>b</sup> yields determined by GC with octadecane as the internal standard.

results obtained from varying the relative amounts of AIBN and TEMPO under analogous reaction conditions. Decreasing the amount of AIBN in the reaction resulted in incomplete conversion of aryl iodide **35b**, and decreasing the amount of TEMPO resulted in lower yield of the desired biaryl product **36**.

Galvinoxyl was also examined as an oxidant (entry 5, **Table 4**), based on its similarity to TEMPO in its ability to trap transient radicals.<sup>54,55</sup> The yield of biphenyl **36** was 70% (GC) when galvinoxyl was used, but attempts to isolate and purify the product proved to be quite difficult. After column chromatography of the reaction with galvinoxyl (entry 5, **Table 4**) and thorough drying of biphenyl on a vacuum pump for 12 h, phenylbenzoate **36** was isolated as a yellow solid, and in 85% yield by weight. This indicated that the isolated product contained at least 15% impurity by weight, since the calculated yield by GC was only 70%. In all subsequent attempts to use galvinoxyl, the same difficulty in purification was encountered, and thus any further investigations into its utility as a synthetically useful reagent were abandoned.

The GC chromatogram of the reaction mixture obtained from refluxing 1 equiv of aryl iodide **35b**, 1 equiv of AIBN, 1 equiv of Bu<sub>3</sub>SnH and 1 equiv of TEMPO in benzene for 18 h (entry 1, **Table 4**) is shown in **Figure 4**. The ratio of the sum of the peak areas between 8-9 minutes divided by the internal standard peak area is 0.007, compared to a value of 0.32 for the control reaction (**Figure 1**). The presence of TEMPO reduced the amount of side products obtained by four-fold, presumably because cyclohexadienyl radical **43** is trapped by TEMPO before it can undergo combination with 2-cyano-2-propyl radicals or other side reactions to a significant extent.

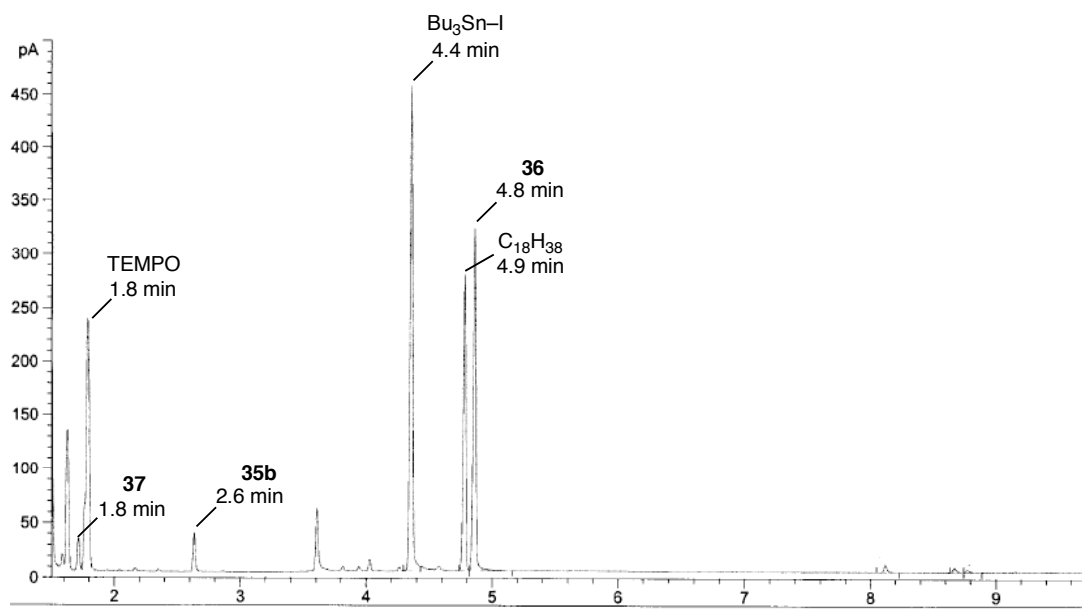


**Figure 4. GC chromatogram of entry 1, Table 4 after 18 h**

Across the examples in **Tables 1–3**, there is a clear correlation between the yield of the desired product **36** and the intensity of the peaks at 8–9 min: the higher the intensity of the “late” peaks, the lower the yield of biphenyl **36**.

In light of the improved yield of biphenyl **36** offered by the use of TEMPO, it remains that AIBN must be used in stoichiometric quantities to achieve complete consumption of the starting aryl iodide employed. Thus efforts were shifted towards improving the reaction results and requirements by other means.

## 2.5 Experimentation with TTMSS

Alvarez-Builla and coworkers<sup>15,16</sup> have found tris(trimethylsilyl)silane (TTMSS) gives better yields in their reported synthesis of biaryl compounds than does  $\text{Bu}_3\text{SnH}$  (Chapter 1.1). We found that this was the case in the reaction performed here as well. When iodide **35b**, TTMSS (1 equiv), and AIBN (1 equiv) were dissolved in benzene and the resulting mixture was refluxed under argon, the desired biaryl product **36** was formed in 68% yield after 14 h with complete consumption of the starting aryl iodide (entry 1, **Table 5**). An analogous reaction was performed in the presence of TEMPO (1 equiv), resulting in 90% yield of desired compound **36** (entry 2, **Table 5**). The GC chromatogram of this reaction is shown in **Figure 5** below.

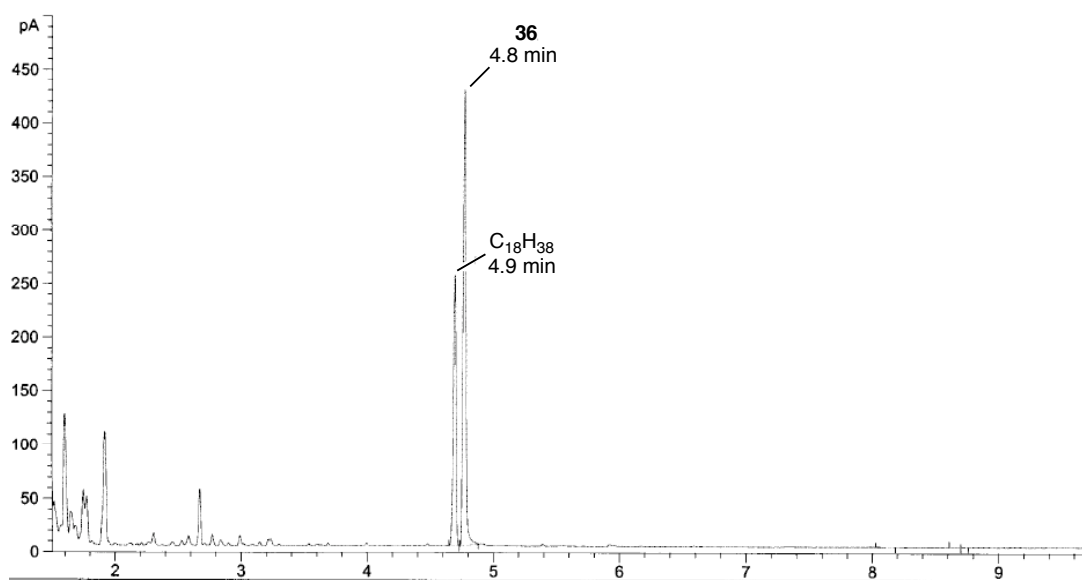
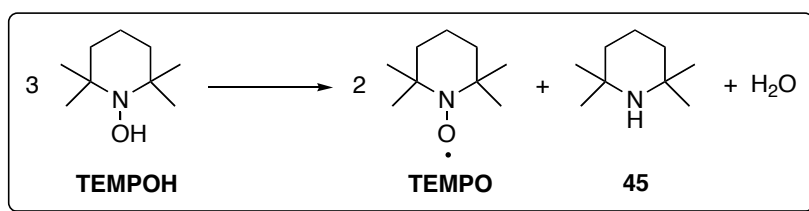


**Figure 5.** GC chromatogram of entry 2, **Table 5** after 14 h

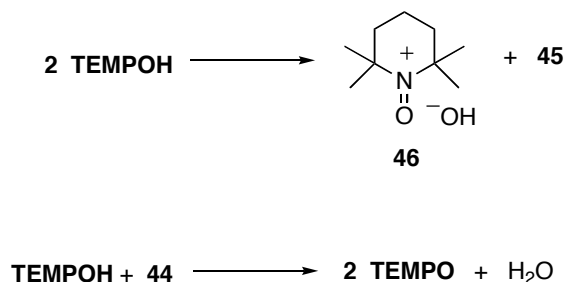
Apparent from the GC chromatogram above, the side product peaks between 8–9 min were extremely small. This confirms the conclusion that a higher yield of biaryl product **36** correlates to the decreased area of side product peaks between 8–9 min.

Not only was the yield of phenyl benzoate **36** improved, but also the use of the TTMSS/AIBN/TEMPO system provided insight into the mechanism of the TEMPO-assisted

oxidation. Once the reaction described in entry 2, **Table 5** was complete, as gauged by GC analysis, the reaction mixture was filtered and tetramethylpiperidinium iodide (27%) was isolated as a white solid (confirmed by  $^1\text{H}$ ,  $^{13}\text{C}$  NMR spectroscopy and MS). TEMPOH is an unstable compound, and 3 equiv of TEMPOH readily disproportionates into 2 equiv of TEMPO, 1 equiv of water and 1 equiv of tetramethylpiperidine (**Scheme 13**).<sup>56</sup> It is therefore hypothesized that the water generated hydrolyzes the silyl iodide, liberating HI in the process, which is neutralized by the tetramethylpiperidine.

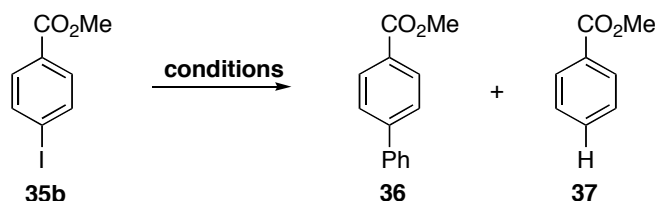


*mechanism:*



**Scheme 13. Decomposition of TEMPOH**<sup>60</sup>

Nitrosonium hydroxide **45** is an excellent  $1\text{-e}^-$  oxidizing agent,<sup>48,49,56</sup> so it is likely that it too can oxidize cyclohexadienyl intermediate **43**, resulting in the generation of biphenyl **36**, TEMPO and water. Since the formation of TEMPOH must occur before nitrosonium hydroxide **45** can be formed, it is concluded that the oxidation of cyclohexadienyl radical **43** proceeds as depicted in **Scheme 12** and, regardless of whether nitrosonium **45** reacts with TEMPOH or  $\pi$  radical **43**, tetramethylpiperidine and water are ultimately formed in a one-to-one ratio.

**Table 5. Preliminary experiments with TTMSS**

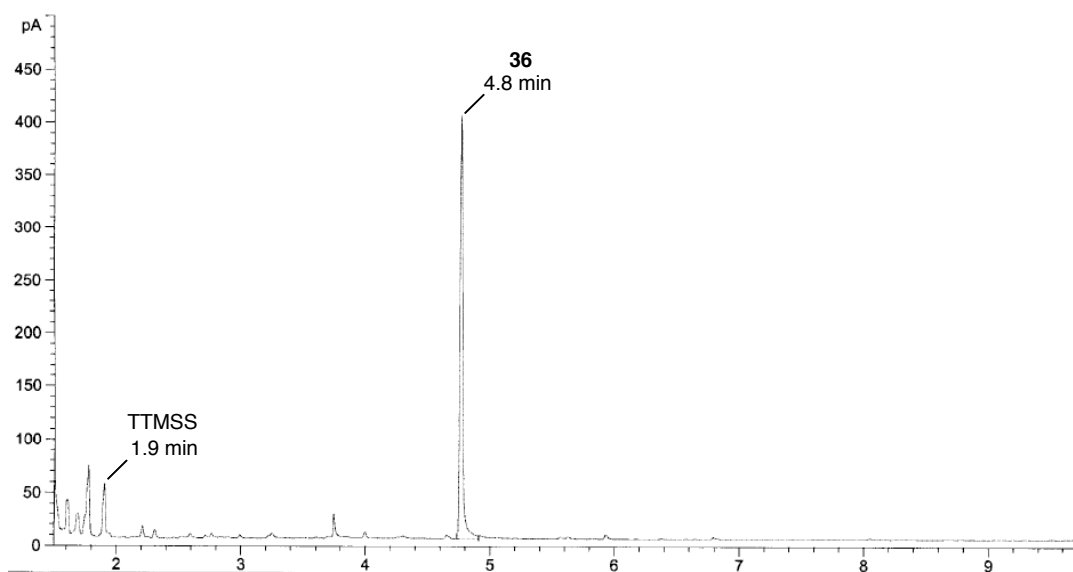
entry	conditions <sup>a</sup>	% <b>35b</b>	% <b>36</b>	% <b>37</b>
control	Bu <sub>3</sub> SnH (1.0 equiv), AIBN (1 equiv), benzene, reflux, 3 h	0	27 <sup>b</sup>	9 <sup>b</sup>
1	TTMSS (1.2 equiv), AIBN (1 equiv), benzene, reflux, 14 h	0	68 <sup>b</sup>	6 <sup>b</sup>
2	TTMSS (1.2 equiv), AIBN (1 equiv), TEMPO (1 equiv), benzene, reflux	0	90 <sup>b</sup>	-
3	TTMSS (1.2 equiv), benzene, rt	0	87 <sup>c</sup>	-

<sup>a</sup>All reactions were conducted under argon atmosphere unless stated otherwise. <sup>b</sup>yield determined by GC with octadecane as an internal standard. <sup>c</sup>Denotes isolated yield.

## 2.6 Utility of TTMSS without AIBN or TEMPO

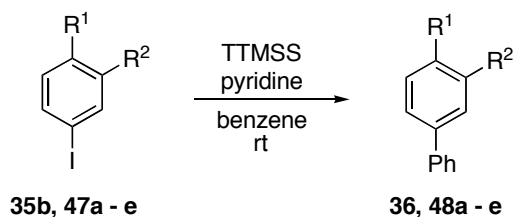
During the course of running various control experiments, it was discovered that TTMSS alone was sufficient to facilitate complete reaction of aryl iodide **35b** at room temperature. TTMSS (1.2 equiv) was added to a solution of iodide **35b** in benzene (0.004 M) under argon and the resulting colorless mixture was allowed to stir at room temperature (entry 3, **Table 5**). After 3 h, the following observations were made: (i) the GC chromatogram (**Figure 6**) of the mixture did not contain the side peaks between 8-9 min observed under refluxing conditions with AIBN; (ii) the reaction mixture eventually became brilliant purple in color, analogous to the color of I<sub>2</sub> in benzene; and (iii) the reaction mixture was acidic (pH approx. 1-3 based on litmus paper), presumably due to the presence of HI. The desired biphenyl **36** was isolated in 87% yield by concentration of the reaction mixture and column chromatography. In light of the acidic reaction

medium, the reaction was repeated several times in the presence of base. No reaction occurred in the presence of triethylamine (5 equiv), which may be due to reaction of Et<sub>3</sub>N with molecular iodine in the reaction mixture.<sup>57</sup> When a mixture of aryl iodide **35b**, TTMSS (1.2 equiv) and pyridine (5 equiv) in benzene was stirred at room temperature, the reaction proceeded smoothly with the generation of a white precipitate with properties consistent with pyridinium hydroiodide (<sup>1</sup>H NMR, <sup>13</sup>C NMR). The precipitate was isolated by filtration, although it was observed to be partially soluble in benzene, in 62% yield.



**Figure 6. GC chromatogram of mixture obtained from reaction of **35b**, TTMSS and pyridine after 3 h at room temperature**

The GC chromatogram of the mixture resulting from reaction of aryl iodide **35b** with TTMSS and pyridine (entry 1, **Table 6**) is shown in **Figure 6**. This is the only GC chromatogram presented in which the side product peaks between 8–9 minutes were completely absent, and this is the only reaction where AIBN was excluded. This is taken to mean that AIBN is directly responsible for the formation of these side products.

**Table 6. HAS of benzene with iodobenzene analogs 47a-e in the presence of TTMSS and pyridine**

entry <sup>a</sup>	aryl iodide	R <sup>1</sup>	R <sup>2</sup>	product	isolated yield (%)
1	<b>35b</b>	CO <sub>2</sub> Me	H	<b>36</b>	87
2	<b>47a</b>	H	H	<b>48a</b>	75
3	<b>47b</b>	OMe	H	<b>48b</b>	90
4	<b>47c</b>	H	CO <sub>2</sub> Et	<b>48c</b>	82
5	<b>47d</b>	<i>t</i> -butyl	H	<b>48d</b>	90
6	<b>47e</b>	H	OMe	<b>48e</b>	89

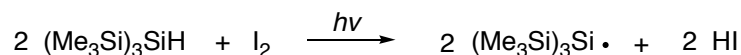
<sup>a</sup> reaction conditions: the aryl iodide was dissolved in benzene (50 mL, 4 mM) along with TTMSS (1.2 equiv) and pyridine (5 equiv). The resulting mixtures were stirred at rt for 30–60 min. When reactions were complete by TLC, the mixtures were concentrated by roto-evaporation and purified via column chromatography.

The TTMSS/pyridine protocol was extended to various iodobenzene analogs, and the results are summarized in **Table 6**. TTMSS (1.2 equiv) and pyridine (5 equiv) were added to a solution of aryl iodide **47** in benzene (50 mL, 4 mM) and the resulting mixtures were placed under argon and stirred at room temperature. All reactions were typically complete within 1 h, and the isolated yields of the desired biphenyl products **48a-e** ranged from 75–90% after column chromatography.

In light of the outstanding results reported in **Table 6**, experiments were conducted to verify that these reactions were taking place via a radical mechanism rather than via an ionic pathway. To this end, iodobenzene was reacted with chlorobenzene and toluene at room temperature, with all other conditions being the same as those used in **Table 6**. The o/m/p distributions of the products were measured by GC (assuming the isomeric products all have the same GC-FID detector response factor) and were compared to those reported in the literature for the addition of a phenyl radical to each of the aforementioned solvents. In the case of chlorobenzene, the o/m/p distribution of the chlorobiphenyl products was 65:17:18 in 79%

overall isolated yield, in good agreement with previously reported results of 74:13:12 at room temperature.<sup>18</sup> In the case of toluene, the o/m/p ratio was 11:5:4 in 64% overall yield, also in good agreement with the previously reported distribution of 42:39:19 at room temperature.<sup>18</sup>

Given that an initiator is not added to any of the reactions conducted with the new protocol, how is the reaction initiating? Since all of the starting materials **35b** and **47a-e** were obtained from commercially available sources, it is speculated these starting materials contained trace amounts of iodine (based on their yellowish color). The iodine contaminant cleaves homolytically in ambient light and may serve as an initiator according to the following equation:



To test this hypothesis, two side-by-side reactions were conducted. TTMSS (1.2 equiv), pyridine (5 equiv) and crystalline iodine (5 mol%) were added to a solution of iodoanisole **47b** in benzene (0.004 M) under argon. This control reaction was complete after 10 minutes (as gauged by GC analysis). In the other reaction, hexabutylditin (10 mol%) was added to a solution of iodoanisole **47b** in benzene with TTMSS (1.2 equiv) and pyridine (5 equiv). No reaction occurred after 3 h. Subsequent addition of iodine (10 mol%) did not facilitate any observable reaction after 1 h, but when an additional 5 mol% of iodine was added, aryl iodide **47b** was completely consumed after 25 min. Hexabutylditin readily reacts with iodine molecules and iodine radicals,<sup>58,59</sup> thus in the presence of the ditin no reaction occurred. But when an excess of iodine (relative to the ditin) was added, the ditin was consumed and the reaction proceeded. This supports the hypothesis that iodine is initiating the reaction, although it does not rule out the possibility that molecular oxygen may be acting as the initiator, because oxygen was not rigorously excluded from any of the solvents before use in the reactions discussed thus far.<sup>36</sup>

## 2.7 The importance of dioxygen

An initially perplexing result occurred when the TTMSS-mediated reaction of iodobenzoate **35b** with benzene was attempted at large scale (40 mM). When a solution of **35b** in non-degassed benzene (50 mL, 40 mM) was treated with TTMSS (1.2 equiv) and pyridine (5 equiv) under argon, about 50% of the starting iodide and TTMSS was left unreacted after 18 h. This result led to the hypothesis that the residual oxygen in the benzene solvent may be playing a role in the reaction; when this reaction was performed on a 4 mM scale (**Table 6**), the starting iodide and TTMSS fully reacted.

Control experiments verified that molecular oxygen is necessary for the reaction of an aryl iodide with TTMSS/pyridine to occur (**Table 6**). The reaction in entry 3, **Table 5** was repeated, but this time the benzene was deoxygenated by vigorously bubbling argon through it before use, and 0% conversion of iodobenzoate **35b** was observed (by GC) after 4 h. Non-degassed benzene is approx. 0.002 M in oxygen;<sup>60</sup> therefore, when this reaction was conducted the first time (without deoxygenating the solvent), there was approx. 0.5 equiv of oxygen present relative to aryl iodide **35b**.

The molar ratio of aryl iodide to oxygen can be varied in a facile way by varying the concentration of the aryl iodide in non-degassed benzene. When the reaction described in entry 3, **Table 5** was conducted at a concentration of 18 mM in iodide **35b** in 50 mL of non-degassed benzene (roughly a 9:1 ratio of starting material to oxygen) under argon, 15% of aryl iodide **35b** and 26% of the TTMSS remained unreacted after 4 h, with 60% yield of biphenyl **36**. Performing the same reaction under an atmosphere of oxygen (excess) resulted in 11% of iodide **35b** left unreacted with total consumption of the TTMSS. After an additional 20 mol% of TTMSS was added, the reaction proceeded to 100% conversion and in 65% yield of biphenyl **36**. Clearly, a sufficient amount of oxygen must be present to facilitate a complete reaction. However, the presence of oxygen in large excess results in the premature consumption of the

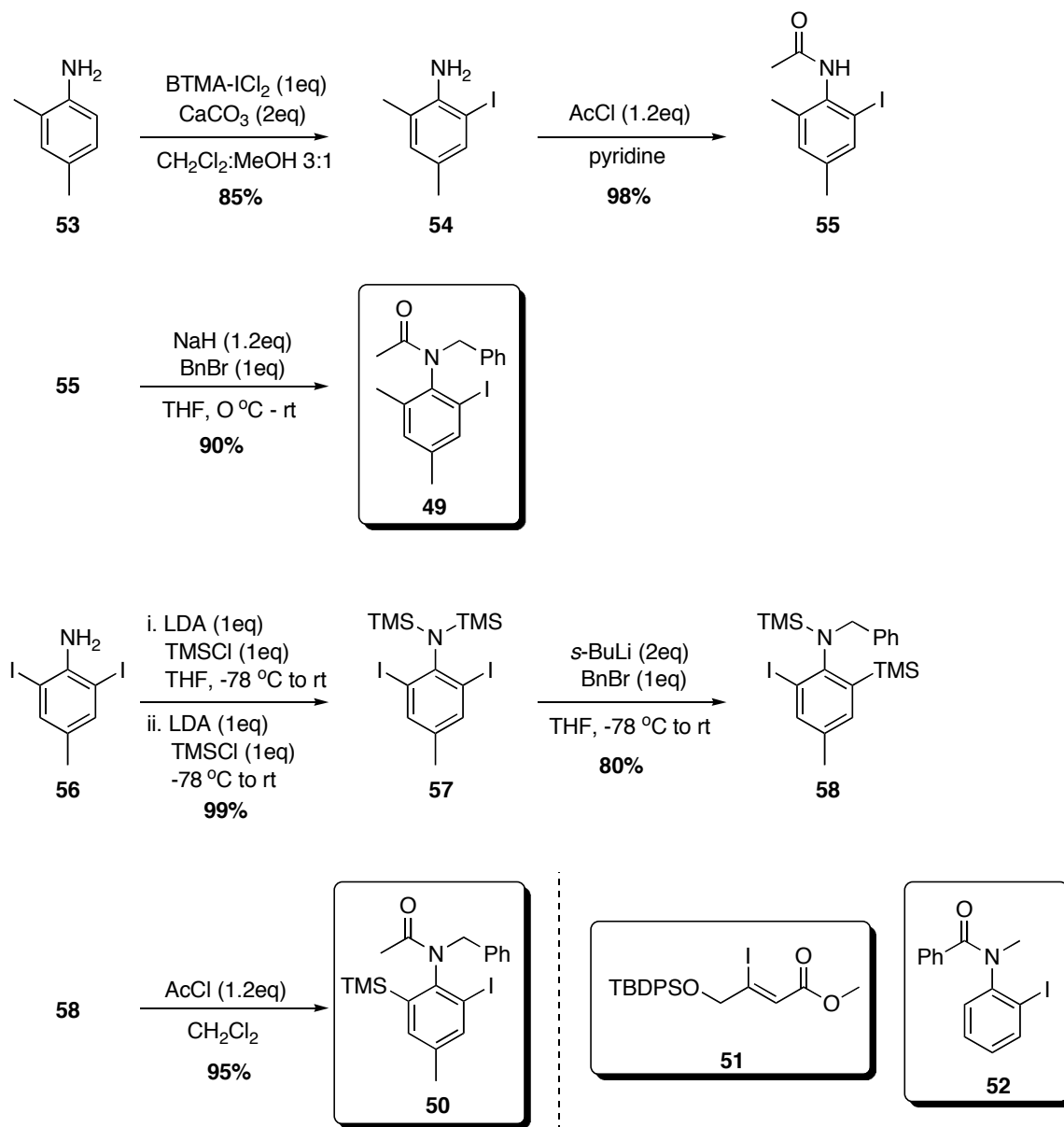
TTMSS (before all of the aryl iodide can react), likely due to the oxidation process described by Chatgililoglu (see Chapter 1.4).<sup>37,38</sup>

To further test the necessity of oxygen, aryl iodide **35b** (0.24 g, 0.92 mmol), pyridine (0.3 mL, 5 equiv) and iodine (1 mol%) were dissolved in benzene (50 mL, 18 mM) and the resulting faint yellow solution was degassed by bubbling a stream of dry argon through it for 45 min, at which point 1 equiv of TTMSS was added in one portion. After 12 h, a trace amount of precipitate had formed, the reaction was colorless, and had proceeded to only 3% yield of biaryl **36** (GC). At this point, 10 mL of non-degassed benzene (containing 2 mol% of O<sub>2</sub>) was added to the reaction. The mixture briefly turned yellow before returning to colorless. After 1 h, desired biaryl **36** was formed in only 8% yield, while 81% of the initial iodide **35b** remained unreacted. The mixture was then exposed to the ambient atmosphere and, after 1 h, aryl iodide **35b** and the TTMSS were completely consumed, giving a 77% yield of biaryl **36**. These results confirm the percent conversion and product yield are dependent on the oxygen concentration, and suggest the optimum conditions require an ambient atmosphere rather than an inert atmosphere.

## 2.8 Application of TTMSS/pyridine protocol to intramolecular HAS

This methodology was further applied to intramolecular cyclizations of radicals onto phenyl rings. Novel cyclization precursors **49** and **50** were synthesized in a straightforward manner starting from the appropriate commercially available aniline (**Scheme 14**). Iodoanilide **49** was constructed starting with dimethylaniline **62**, which was iodinated with BTMA-ICl<sub>2</sub> in 85% yield to give iodoaniline **54**. Acetylation of **54** followed by benzylation provided the desired cyclization precursor **49** in 88% yield over the two steps. To obtain precursor **50**, diiodoaniline **56** was silylated to give *N,N*-bis(trimethylsilyl)aniline **57** in 99% yield. Stepwise treatment of **57** with *s*-BuLi, followed by BnBr in a one-pot procedure, afforded *N*-benzylaniline **58** in 80% yield. Subsequent acetylation provided the desired cyclization precursor **50**. Vinyl

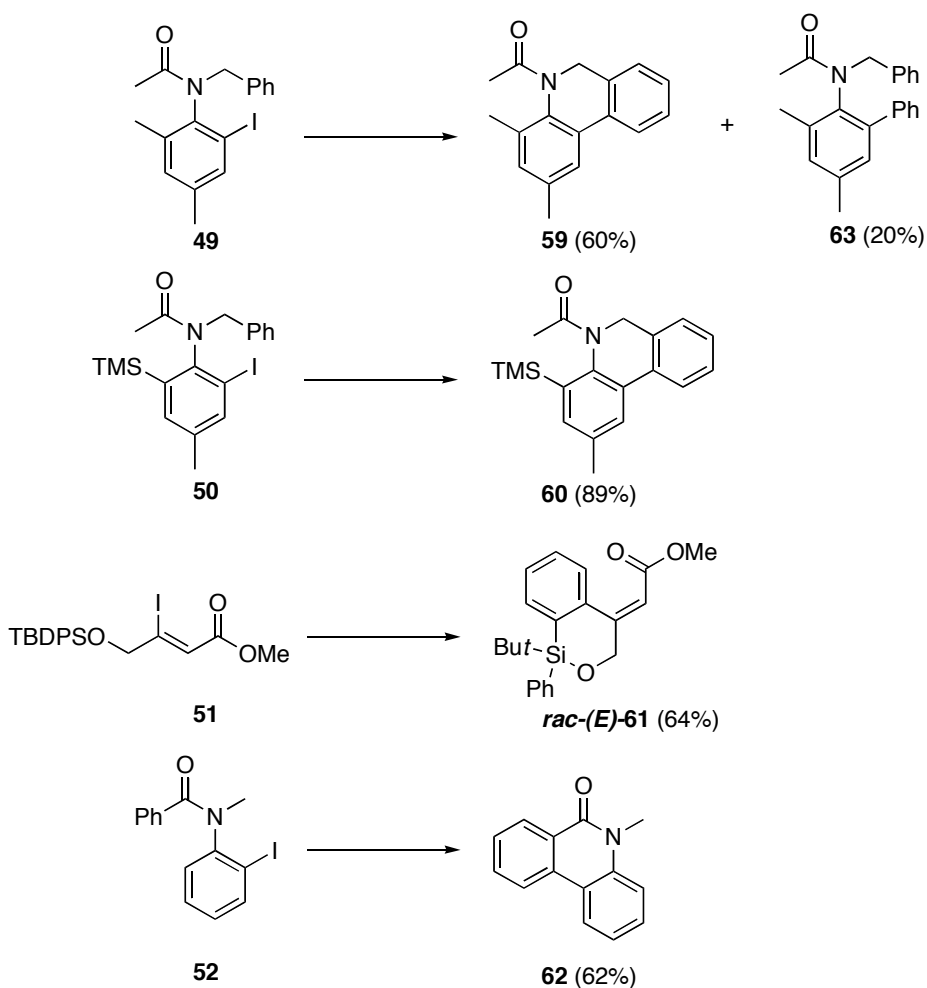
iodide **51** was obtained from a co-worker in our laboratories and known compound **52** was easily obtained from benzylation and methylation of commercially available 2-iodoaniline.



Scheme 14. Synthesis of iodoanilide cyclization precursors **49** and **50**

Precursors **49–52** were smoothly converted to the corresponding heterocycles **59–62** using the standard TTMSS/pyridine procedure (Scheme 15). The substrate was dissolved in non-degassed benzene (10 mM), TTMSS (1.2 equiv) and pyridine (5 equiv) were added, and the

reaction mixture was left open to the air. An accelerated rate of reaction was observed when the mixture was exposed to air when compared to conducting the reaction under argon. A catalytic amount of iodine (2 mol%) was necessary to initiate the cyclizations, otherwise induction periods of >1 h were observed. After the cyclizations were complete, as determined by TLC analysis (usually 3 h), the resulting mixtures were concentrated and the resulting crude mixtures were separated and purified by silica gel column chromatography.



**Scheme 15.** Cyclization of precursors 49-52 using TTMSS/pyridine at room temp

Cyclization of **49** in benzene resulted in 60% isolated yield of *N*-acetyldihydrophenanthridine **59**, along with 20% of the less polar phenylated product **63**

(characterized by  $^1\text{H}$  NMR spectroscopy and HRMS). Cyclization of the TMS analog **50** resulted in 89% yield of only the silylated dihydrophenanthridine **60**. Both **59** and **60** exhibit interesting conformational dynamics, which are discussed in detail in Chapter 4.

The TTMSS/pyridine methodology was also successful in generating a vinyl radical from vinyl iodide **51**. It was initially expected that this vinyl radical would react with benzene to give a styrene type product; instead, cyclization onto a phenyl ring of the TBDPS group occurred to afford silacycle (*E*)-**61** as the sole product in 64% yield. The geometry of the exocyclic alkene was confirmed by a 1D nOe experiment. Irradiation of the vinyl proton resonance led to nOe enhancements in both allylic proton resonances as well as the methyl ester resonance (**Figure 7**).

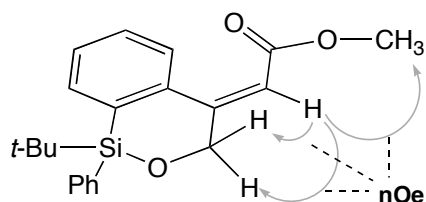
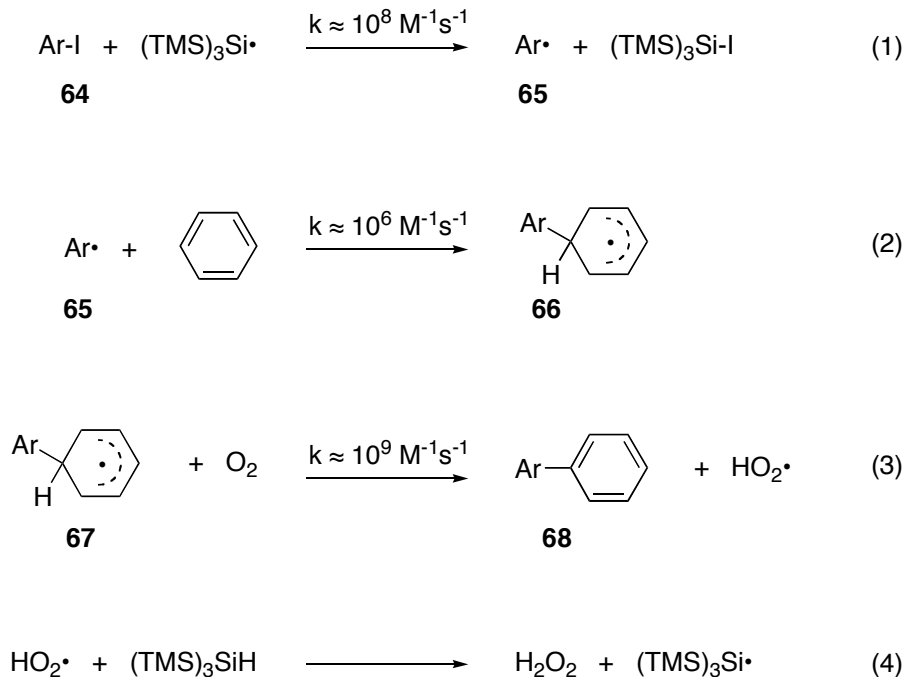


**Figure 7.** nOe enhancements of cyclic silyl ether **61** confirming the exocyclic alkene geometry (*E*)

## 2.9 Proposed role of oxygen

A mechanistic pathway for the intermolecular addition of a radical to benzene under oxygen promoted conditions is proposed in **Scheme 16**. Aryl iodide **64** undergoes iodide abstraction by the  $(\text{TMS})_3\text{Si}\cdot$  to provide the aryl radical **65**, which subsequently adds to benzene to provide the cyclohexadienyl radical **66** (steps 1 and 2).<sup>52</sup> The cyclohexadienyl radical does not abstract a hydrogen atom from TTMSS to propagate a chain, but does react with dioxygen at a near-diffusion controlled rate to afford the aromatized product and a hydroperoxyl radical (step 3).<sup>38</sup> Dioxygen also reacts quickly with aryl radicals as well as the  $(\text{TMS})_3\text{Si}$  radical, but these side reactions should not occur to any significant extent if the concentration of oxygen is low.



**Scheme 16. Proposed mechanism for homolytic aromatic substitution mediated by TTMSS/O<sub>2</sub>**

It is proposed that the reaction of cyclohexadienyl radical **66** and dioxygen to form a hydroperoxyl radical is formally a disproportionation, as opposed to recombination to form an intermediate organoperoxy species. Scaiano and Ingold suggest disproportionation based on product studies because the reaction of a cyclohexadienyl radical and oxygen produces benzene.<sup>38</sup> Hendry and Schuetzle also favor the disproportionation pathway based on calculated bond strengths.<sup>61</sup> The strength of the sp<sup>3</sup> C-H bond in the cyclohexadienyl radical has been calculated to be 24 kcal/mol.<sup>62a</sup> Since the strength of the O-H bond formed after H atom abstraction by dioxygen is 47 kcal/mol,<sup>62b</sup> the disproportionation reaction is exothermic by 23 kcal/mol.

It also seems reasonable to consider the reaction of a cyclohexadienyl radical and oxygen as a combination, resulting in an organoperoxy species, which in turn undergoes cleavage to produce benzene and a hydroperoxyl radical. Hendry and Schuetzle concluded the combination of dioxygen and cyclohexadienyl radical is an equilibrium reaction where  $K_{\text{eq}} \leq 0.1$ ,

and thus not the favored pathway. However, Mulder and others argue that the expected enthalpy of reaction for the disproportionation is -56 kcal/mol, while the experimental value they measured is only -16 kcal/mol.<sup>63</sup> They conclude the reaction of cyclohexadienyl radical and oxygen in water exclusively results in recombination to yield a mixture of 1,3- and 1,4-cyclohexadienylperoxy species, which is consistent with DFT calculations.<sup>63b</sup>

In either case, the cyclohexadienyl radical **66** is oxidized by dioxygen, producing the aromatized product **68** and the hydroperoxy radical in the process. It seems reasonable that the hydroperoxyl radical can propagate the chain by abstracting hydrogen from TTMSS, although the rate at which this abstraction occurs is unknown. A cumylperoxy radical abstracts hydrogen from TTMSS with a rate constant of only  $66 \text{ M}^{-1}\text{s}^{-1}$ , but tertiary peroxy radicals tend to be much less reactive than the hydroperoxy radical.<sup>61,64</sup> Hydrogen abstraction from TTMSS forms hydrogen peroxide (step 4), which in turn may be capable of oxidizing another cyclohexadienyl radical. Oxidation of  $\pi$ -radical intermediates by hydroperoxy radicals formed *in situ* by reduction of dioxygen has also been suggested.<sup>65</sup>

## 2.10 <sup>29</sup>Si NMR experiments: attempts to identify silicon containing byproducts

In the reaction of an aryl iodide with  $(\text{Me}_3\text{Si})_3\text{Si}\cdot$ , an aryl radical and  $(\text{Me}_3\text{Si})_3\text{SiI}$  are the expected products.

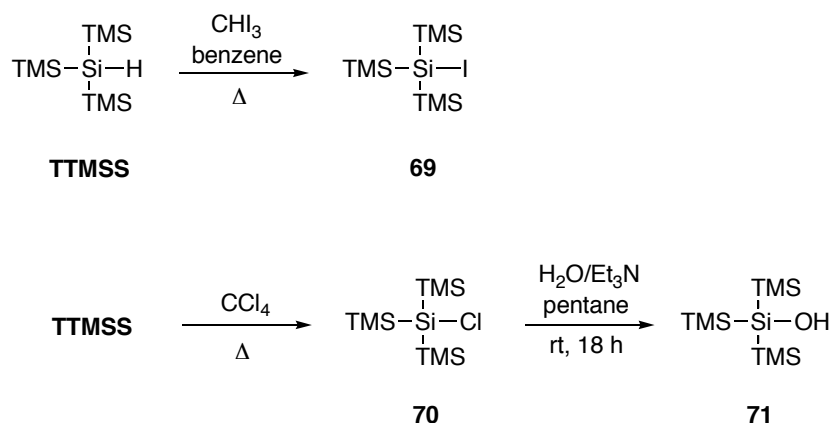


In the experiments with the TTMSS/pyridine/O<sub>2</sub> (**Tables 5, 6** and **Scheme 15**), there was no indication by GC analysis of these reactions that the stoichiometric formation of  $(\text{Me}_3\text{Si})_3\text{SiI}$  (as compared to the formation of  $\text{Bu}_3\text{SnI}$  in **Figure 1**) occurred. However, HI was proven to be formed in nearly quantitative proportions, based on the isolation of pyridinium iodide. These

observations suggest that  $(\text{Me}_3\text{Si})_3\text{SiI}$  is merely a transient species, and that it undergoes further reaction, giving rise to other silyl byproducts and ultimately forming HI as a byproduct.

$^{29}\text{Si}$  NMR was used to analyze the mixture obtained from the reaction of an aryl iodide with TTMSS in the presence of pyridine and  $\text{O}_2$  at room temperature. To this end, authentic samples of  $(\text{Me}_3\text{Si})_3\text{SiI}$  and  $(\text{Me}_3\text{Si})_3\text{SiOH}$  were synthesized so that their respective  $^{29}\text{Si}$  NMR spectra could be compared to that of the mixture obtained from reaction of TTMSS/pyridine with an aryl iodide.

Silyl iodide **69** was obtained by refluxing TTMSS with iodoform in benzene for 4 h according to a previously described procedure.<sup>66</sup> The silanol **71** was synthesized via the silyl chloride **70** as depicted in **Scheme 17**.<sup>67,68</sup>



**Scheme 17.** Synthesis of silyl iodide **68** and silyl alcohol **70** as authentic samples for  $^{29}\text{Si}$  NMR experiments

The  $^{29}\text{Si}$  NMR of TTMSS, **68** and **70** were recorded in benzene- $d_6$  at 60 MHz (300 MHz,  $^1\text{H}$ ). The  $\delta$  values for each compound were measured relative to tetramethylsilane. The  $^{29}\text{Si}$  NMR decoupled spectrum of TTMSS showed two signals, one at  $-11$  ppm (3 Si) and one at  $-115$  ppm (1 Si). The  $^{29}\text{Si}$  NMR of silyl iodide **69** showed singlets at  $-14$  ppm (3 Si) and  $-58$  ppm (1 Si), and for the silyl alcohol **70** the  $^{29}\text{Si}$  resonances appeared at  $-16$  ppm (3 Si) and  $-2$  ppm (1 Si).

The reaction of iodobenzoate **35b** with TTMSS and pyridine was performed in benzene- $d_6$  and the  $^{29}\text{Si}$  NMR spectrum of the resulting crude mixture was obtained for comparison to the spectra of the authentic silyl compounds. TTMSS (1.2 equiv) was added to a solution of aryl iodide **35b** (2 mmol) and pyridine (5 equiv) in non-degassed benzene- $d_6$  (50 mL, 40 mM) and the resulting mixture was stirred under argon for 12 h at room temperature. As expected, the reaction only went to about 40% conversion of iodide **35b** since a sufficient amount of oxygen was not introduced into the reaction mixture. Thus, remaining in the mixture was unreacted TTMSS, plus the resulting silyl biproduct. The reaction mixture was concentrated on a rotary evaporator, and the crude product was taken up in benzene- $d_6$ . Four distinct silyl peaks are evident in the  $^{29}\text{Si}$  NMR spectrum shown in **Figure 8**: TTMSS (-11, -115 ppm) and silyl alcohol **70** (-2, -16 ppm). This supports the hypothesis that silyl iodide **68** is unstable under the reaction conditions, and supports the assertion that it is ultimately converted to  $\text{TMS}_3\text{SiOH}$ .

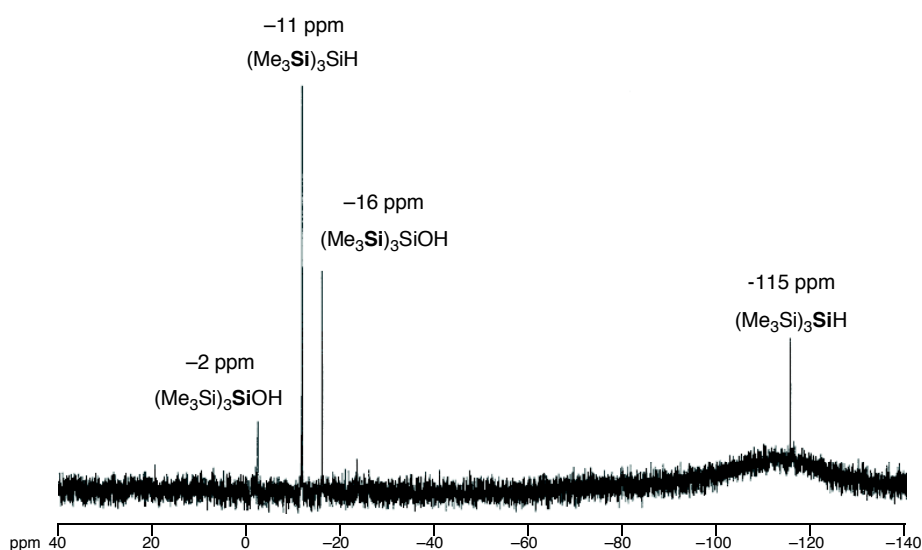


**Figure 8.**  $^{29}\text{Si}$  NMR (60 MHz) in benzene- $d_6$  of the crude reaction mixture obtained from reaction of aryl iodide **35b** and TTMSS after 40% conversion

Attempts at isolating silanol **70** from a reaction failed. In the reaction of iodobenzene with TTMSS/pyridine in chlorobenzene as solvent (described earlier in Chapter 2.5), a clear

waxy solid was isolated by column chromatography of the crude mixture (eluting with hexanes/ethyl acetate 15:1,  $R_f = 0.4$ ). The  $^{13}\text{C}$  NMR spectrum of this waxy solid confirms it is not silyl alcohol **70**, silyl iodide **68** or TTMSS, but showed four signals at  $-2.4$ ,  $-2.1$ ,  $2.0$  and  $2.2$  ppm, confirming that the only carbon atoms in this compound are bonded to Si. GC-MS of this compound showed three peaks, each possessing a fragmentation pattern containing an  $m/z$  73 ion as the most abundant fragment (characteristic of  $\text{TMS}^+$ ). This data suggests the silanol generated in the reaction mixture is converted to other unknown silyl biproduct(s) upon workup and/or column chromatography.

## 2.11 Summary

Novel conditions for achieving inter- and intramolecular homolytic substitution have been reported. Treatment of an aryl halide with TTMSS (1 to 1.5 equiv depending on the substrate) in the presence of oxygen and catalytic iodine affords the desired HAS products in comparable or better yields than reported for similar substrates under the standard  $\text{Bu}_3\text{SnH/AIBN}$  or TTMSS/AIBN conditions. The presence of pyridine is not critical, but certainly desirable since HI is formed quantitatively. Control experiments prove that oxygen is required and the extent of reaction is dependent on the oxygen concentration.

Earlier studies suggest the presence of AIBN is detrimental to the formation of homolytic aromatic substitution products, because cyclohexadienyl radical intermediates are at least partially trapped by 2-cyano-2-propyl radicals. In addition to our new TTMSS/pyridine/ $\text{O}_2$  methodology, we have shown the addition of TEMPO to HAS reactions mediated by TTMSS/AIBN or  $\text{Bu}_3\text{SnH/AIBN}$  gives a higher yield of the desired substituted product and decreased amounts of side products.

The discovery that TTMSS in the presence of oxygen achieves homolytic aromatic substitution at room temperature is an important one, and has implications for both preparatory

and mechanistic radical chemistry. The mild reaction conditions may be applicable to a wide range of functionally diverse benzenes and heteroarenes. While HAS reactions have been commonly used in organic synthesis, they typically require forcing conditions (excess initiator, high temperatures) and are usually low yielding. The use of oxygen in formal HAS reactions has not been considered. Typically, reaction mixtures are actually degassed in order to avoid the trapping of intermediate radicals with dioxygen. But if radical addition to benzene is fast enough, than the presence of oxygen should promote the oxidation and rearomatization of the intermediate cyclohexadienyl radical. Our methodology offers a high-yielding protocol for the synthesis of biaryl compounds, without the need for transition metal catalysis, and should pave the way for a new approach to formal homolytic aromatic substitution.

## 2.12 Experimental

### General

All reactions were performed under argon atmosphere unless specifically stated otherwise. Air and moisture sensitive chemicals were handled using standard syringe techniques. Benzene was used as received. Dichloromethane and THF were dried by passage through columns of activated alumina. All other chemicals and solvents were purchased from chemical companies and used without purification unless stated otherwise.  $^1\text{H}$ ,  $^{13}\text{C}$ , and  $^{29}\text{Si}$  NMR spectra were recorded on Bruker Avance DPX 300 (300 MHz), Avance 300 (300 MHz), and Avance DRX 500 (500 MHz) NMR spectrometers. Chemical shifts ( $\delta$ ) are reported in ppm relative to TMS using the residual solvent proton resonance of  $\text{CDCl}_3$  (7.27 ppm) or the  $\text{CDCl}_3$  carbon peak (77.0 ppm) for calibration. Alternatively, TMS was added to samples where calibration by residual solvent was not possible. In reporting data, the following abbreviations were employed: s = singlet, d = doublet, dd = doublet of doublets, m = multiplet, dd = doublet of doublet. IR spectra

were recorded as thin films or neat on NaCl plates on an ATI Mattson Genesis Series FT-IR spectrometer. Low and high resolution mass spectra were obtained on a Micromass Inc., Autospec with an E-B-E geometry. Gas chromatography (GC) was performed on an Agilent 19091Z-413E gas chromatograph with FID detection and equipped with an enhanced HPCHEM integrator. An HP-1 capillary methyl siloxane column of 30 m in length and 0.32 mm in diameter was used for all reported runs. The initial temperature of the program was 150 °C with a temperature ramp of 10 °C/min up to 315 °C, thereafter the temperature is maintained for 10 min. The GC detector response factors for all compounds quantitated by GC were calculated relative to octadecane as the internal standard. Standard mixtures containing 25% (1 mM), 50% (2 mM), and 100% (4 mM) theoretical yield of **35**, **36** and **37** and a fixed concentration of octadecane (0.06 mmol) were analyzed by GC to determine the response factors. The response factor for each compound did not vary when varying the concentrations and/or molar ratios of compound and internal standard. Response factors were calculated according to the following equation:

$$RF = \frac{(M_S)(A_X)}{(M_X)(A_S)}$$

RF = response factor

(A<sub>S</sub>) = area of internal standard peak

(A<sub>X</sub>) = area of compound "X" peak

(M<sub>S</sub>) = moles of internal standard

(M<sub>X</sub>) = moles of compound "X"

$$RF_{35} = 0.32$$

$$RF_{36} = 0.60$$

$$RF_{37} = 0.35$$

Thin layer chromatography (TLC) was performed on silica gel 60 F<sub>254</sub> glass-backed plates with a layer thickness of 0.25 mm manufactured by E. Merck. TLC visualization was achieved by illumination with a 254 nm UV lamp or by staining with a anisaldehyde solution and subsequent heating. Flash chromatography was performed on silica gel (230-400 mesh ASTM) purchased from Bodman or Sorbtech.

Experimental procedures and spectroscopic data for compounds **36**,<sup>69</sup> **48a**,<sup>70,71</sup> **48b**,<sup>69</sup> **48e**,<sup>72</sup> **52**,<sup>2</sup> **54**,<sup>73</sup> **55**,<sup>74</sup> **56**,<sup>73</sup> **57**,<sup>75</sup> **62**,<sup>2</sup> **69**,<sup>66</sup> **70**,<sup>68</sup> and **71**<sup>67</sup> have been reported elsewhere. All the reactions described below were deemed complete by TLC before work-up unless stated otherwise.

**General procedure for synthesis of biphenyl derivatives 36 and 48a-d: Synthesis of biphenyl 4-carboxylic acid methyl ester (36):** Aryl iodide **35b** (52 mg, 0.2 mmol) was dissolved in benzene (50 mL, 4 mmol). TTMS (0.075 mL, 1.2 equiv) and pyridine (0.08 mL, 5 equiv) were added and the resulting mixture was allowed to stir at room temperature. Upon consumption of the aryl iodide (30 min to 3 h), the reaction mixture was concentrated via rotoevaporation and the resulting crude product was purified by flash chromatography on silica gel eluting with hexanes/ethyl acetate (50:1) to provide the *title compound* as a white solid (37 mg, 87%); CAS# 720-75-2.

**Biphenyl (48a):**

Using iodobenzene **47a** (41 mg, 0.2 mmol) and eluting with hexanes/ethyl acetate (100/1) yielded the *title compound* as a white solid (23 mg, 75%); CAS# 92-52-4.

**4-Methoxybiphenyl (48b):**

Using iodoanisole **47b** (47 mg, 0.2 mmol) and eluting with hexanes/ethyl acetate (30/1) yielded the *title compound* as a white solid (33 mg, 90%); CAS# 613-37-6.

### **Biphenyl 3-carboxylic acid ethyl ester (48c):**

Using iodobenzoate **47c** (62 mg, 0.22 mmol) and eluting with hexanes/ethyl acetate (20/1) yielded the *title compound* as a colorless oil (41 mg, 82%); CAS# 19926-50-2; <sup>1</sup>H NMR (300 MHz, CDCl<sub>3</sub>) δ 1.43 (t, *J* = 7.1 Hz, 3H), 4.43 (q, *J* = 7.2 Hz, 2H), 7.39 (dddd, *J* = 6.9, 6.9, 1.3, 1.3, 1H), 7.51 (m, 3 H), 7.64 (m, 2H), 7.80 (ddd, *J* = 7.7, 1.9, 1.2 Hz, 1H), 8.05 (ddd, *J* = 7.7, 1.3, 1.3 Hz, 1H), 8.30 (dd, *J* = 1.7 Hz, 1H); <sup>13</sup>C NMR (75 MHz, CDCl<sub>3</sub>) δ 14.4, 61.0, 127.2, 127.7, 128.2, 128.3, 128.8, 128.9, 131.1, 131.4, 140.2, 141.5, 166.6.

### **4-*t*-Butylbiphenyl (48d):**

Using *t*-butyliodobenzene **47d** (70 mg, 0.27 mmol) and eluting with hexanes/ethyl acetate (40/1) yielded the *title compound* as a white solid (51 mg, 90%); CAS# 1625-92-9; <sup>1</sup>H NMR (300 MHz, CDCl<sub>3</sub>) δ 1.41 (s, 9H), 7.36 (dddd, *J* = 7.6, 7.6, 1.3, 1.3 Hz, 1H), 7.51 (m, 6H), 7.63 (ddd, *J* = 6.0, 1.4, 1.4 Hz, 2H); <sup>13</sup>C NMR (75 MHz, CDCl<sub>3</sub>) δ 31.4, 34.5, 125.7, 126.8, 126.9, 127.0, 128.7, 138.3, 141.0, 150.2.

### **3-Methoxybiphenyl (48e):**

Using iodoanisole **47e** (51 mg, 0.22 mmol) and eluting with hexanes/ethyl acetate (50/1) provided the *title compound* as a faintly yellow oil (36 mg, 89%); CAS# 2113-56-6.

### **2-Iodo-4,6-dimethylaniline (54):**

To a solution of commercial 2,4-dimethyl aniline **53** (5.13 mL, 0.041 mol) in CH<sub>2</sub>Cl<sub>2</sub> (360 mL) and MeOH (140 mL) was added CaCO<sub>3</sub> (9.01 g, 0.09 mol) followed by BTMA•ICl<sub>2</sub> (Benzyltrimethylammonium dichloroiodate) (14.36 g, 0.041 mol). The resulting mixture was stirred for 14 h. The reaction mixture was filtered and the filtrate was concentrated to yield the crude as a dark brown solid. The crude mixture was purified via column chromatography eluting with hexanes/ethyl acetate (20/1) to yield (8.67 g, 85%) of the known *title compound* as a white solid; CAS# 4102-54-9;

***N*-(2-Iodo-4,6-dimethylphenyl)acetamide (55):**

To a solution of 2-iodo-4,6-dimethylaniline **54** (3.00 g, 0.012 mol) in dry CH<sub>2</sub>Cl<sub>2</sub> (100 mL) at 0 °C under an argon atmosphere was added pyridine (6 mL, 0.076 mol) in one portion, followed by the dropwise addition of acetyl chloride (1.15 mL, 0.0144 mol). The resulting mixture warmed to room temperature, diluted with CH<sub>2</sub>Cl<sub>2</sub> (100 mL) and washed with NaHCO<sub>3</sub> (1 x 50 mL) and water (1 x 50 mL). The organic layer was collected, dried over MgSO<sub>4</sub> and concentrated to yield the crude product as an off-white solid. The crude mixture was purified via flash chromatography eluting with hexanes/ethyl acetate (4/1) to yield the *title compound* as a white solid (3.18 g, 92%); CAS# 208659-18-0.

***N*-Benzyl-*N*-(2-iodo-4,6-dimethylphenyl)acetamide (49):**

NaH (0.32 g, 13.3 mmol) was added portionwise to a solution of iodoanilide **55** (3.20 g, 11.1 mmol) in THF (75 mL) at 0 °C under an argon atmosphere. Benzyl bromide (1.58 mL, 13.3 mmol) was added dropwise via syringe and the resulting mixture was stirred for 15 minutes after warming to room temperature. The reaction mixture was diluted with H<sub>2</sub>O (50 mL) and extracted with diethyl ether (2 x 100 mL) and CH<sub>2</sub>Cl<sub>2</sub> (1 x 100 mL). The organic layer was collected, dried over MgSO<sub>4</sub> and concentrated to yield the crude product as a brown oil. The crude mixture was purified via column chromatography eluting with hexanes/ethyl acetate (15/1) to yield (3.03 g, 72% yield) of the *title compound* as a faint yellow oil; IR (neat, CHCl<sub>3</sub>, NaCl, cm<sup>-1</sup>) 3060.5, 3027.7, 2888.9, 1664.3, 1388.5, 702.0; <sup>1</sup>H NMR (300 MHz, CDCl<sub>3</sub>) δ 1.49 (s, 3H), δ 1.67 (s 3H), δ 2.18 (s, 3H), δ 3.97 (d, *J* = 13.8 Hz, 1H), δ 5.38 (d, *J* = 13.8 Hz, 1H), δ 6.82 (s, 1H), δ 7.14 (m, 5H), δ 7.52 (s, 1H); <sup>13</sup>C NMR (75 MHz, CDCl<sub>3</sub>) δ 18.7, 20.4, 22.4, 51.8, 100.7, 127.6, 128.2, 130.4, 132.1, 136.8, 138.4, 138.5, 139.8, 140.4, 170.4; HRMS (EI) calcd for C<sub>17</sub>H<sub>19</sub>INO M<sup>+</sup> 379.0431, found 379.0433; LRMS (EI) *m/z* 379 (M<sup>+</sup>, 50), 336 (87), 253 (100), 232 (95), 209 (80), 131 (97), 103 (100), 89 (97), 78 (98), 63 (93).

***N, N*-[Bis(trimethylsilyl)]-2,6-diiodo-4-methylaniline (57):**

Diiodoaniline **56** (6.52 g, 16.2 mmol) was dissolved in dry THF (200 mL) under argon and cooled to  $-78^{\circ}\text{C}$  in an acetone/dry ice bath. LDA (17.5 mmol) was added to the reaction mixture dropwise, followed by dropwise addition of trimethylsilyl chloride (1.37 mL, 17.5 mmol). The resulting mixture was warmed to room temperature and stirred for 10 min, at which point the mixture was cooled to  $-78^{\circ}\text{C}$ , followed by the dropwise addition of LDA (17.5 mmol) and the subsequent addition of trimethylsilyl chloride (1.37 mL, 17.5 mmol). The resulting mixture was again warmed to rt and the reaction was deemed complete by TLC. The mixture was diluted with diethyl ether (200 mL) and washed with aq.  $\text{NH}_4\text{Cl}$  (1 x 100 mL) and aq. brine solution (1 x 100 mL). The organic layer was collected, dried over  $\text{MgSO}_4$  and concentrated to yield the crude product as a yellow solid. The crude mixture was purified via column chromatography eluted with pentane to yield the *title compound* as a white solid (8.12 g, 99%); CAS# 768382-49-6

***N*-Benzyl-*N*-(trimethylsilyl)-2-iodo-4-methyl-6-(trimethylsilyl)aniline (58):**

A 1.4 M solution of *sec*-BuLi in hexanes (7.6 mL, 10.6 mmol) was added dropwise to a solution of **57** (2.67 g, 5.3 mmol) in dry THF (40 mL) at  $-78^{\circ}\text{C}$  under argon. The resulting solution was stirred for 10 min. Subsequently, benzyl bromide (0.71 mL, 6.0 mmol) was added dropwise and the resulting mixture was warmed to rt. The reaction mixture was diluted with water (25 mL) and extracted with diethyl ether (4 x 50 mL). The organic layer was successively washed with a sat'd aq  $\text{NH}_4\text{Cl}$  solution (50 mL) and brine (50 mL), dried over  $\text{MgSO}_4$  and concentrated to yield the crude product as a yellow solid. The crude mixture was purified via column chromatography eluting with hexanes/ether (100/1) to yield the *title compound* as a clear crystalline solid (2.30 g, 92%); mp  $64\text{--}67^{\circ}\text{C}$ ; IR (thin film,  $\text{CHCl}_3$ , NaCl,  $\text{cm}^{-1}$ ) 3062.4, 3029.6, 2950.6, 2898.5, 1419.4, 1249.7, 1078.0, 1045.2, 900.6, 848.6;  $^1\text{H}$  NMR (300 MHz,  $\text{CDCl}_3$ )  $\delta$  0.26 (s, 9H), 0.28 (s, 9H), 2.28 (s, 3H), 4.07 (d,  $J = 13.6$  Hz, 1H), 4.39 (d,  $J = 13.6$  Hz, 1H), 6.97 (dd,  $J = 7.8, 1.6$  Hz, 2H),

7.21 (m, 3H), 7.34 (app d,  $J = 1.3$  Hz, 1H), 7.73 (app d,  $J = 1.3$  Hz, 1H);  $^{13}\text{C}$  NMR (75 MHz,  $\text{CDCl}_3$ )  $\delta$  1.7, 2.6, 57.2, 107.8, 127.0, 127.9, 130.7, 135.5, 137.4, 138.8, 142.3, 142.9, 151.9; HRMS (EI) calcd for  $\text{C}_{20}\text{H}_{30}\text{INSi}_2$  467.0955, found 467.0962; LRMS (EI)  $m/z$  467 ( $\text{M}^+$ , 100), 395 (85), 326 (87), 252 (76), 185 (72), 74 (97), 59 (95).

***N*-Benzyl-*N*-(2-iodo-4-methyl-6-trimethylsilylphenyl)acetamide (50):**

Acetyl chloride (0.32 mL, 4.4 mmol) was added dropwise to a solution of **58** (1.70 g, 3.6 mmol) in dry  $\text{CH}_2\text{Cl}_2$  (30 mL) and the resulting mixture was stirred under argon at rt for 12 h. The reaction mixture was washed with sat.  $\text{NaHCO}_3$  (2 x 20 mL), dried over  $\text{MgSO}_4$  and concentrated to yield the crude product as a yellow oil. The crude mixture was purified via column chromatography eluting with hexanes/ethyl acetate (12/1) to yield the *title compound* as a clear crystalline solid (1.51 g, 96%); mp 76–79 °C; IR (thin film,  $\text{CHCl}_3$ ,  $\text{NaCl}$ ,  $\text{cm}^{-1}$ ) 3029.6, 2952.5, 2898.5, 1654.6, 1430.9, 1386.6, 1270.9, 1251.6, 1097.3, 842.7, 783.6, 700.0;  $^1\text{H}$  NMR (300 MHz,  $\text{CDCl}_3$ )  $\delta$  0.28 (s, 9H), 1.97 (s, 3H), 2.42 (s, 3H), 4.44 (d,  $J = 13.6$  Hz, 1H), 5.32 (d,  $J = 13.6$  Hz, 1H), 7.30 (m, 5H), 7.44 (app d,  $J = 1.6$  Hz, 1H), 7.79 (app d,  $J = 1.6$  Hz, 1H);  $^{13}\text{C}$  NMR (75 MHz,  $\text{CDCl}_3$ )  $\delta$  0.25, 20.4, 23.5, 53.9, 103.3, 127.7, 128.1, 131.2, 135.6, 137.2, 138.7, 141.2, 141.9, 145.7, 170.3; HRMS (EI) calcd for  $\text{C}_{19}\text{H}_{24}\text{INOSi}$  437.0670, found 437.0672; LRMS (EI)  $m/z$  437 ( $\text{M}^+$ , 20), 364 (48), 310 (100), 295 (27), 91 (47), 73 (96).

**General Procedure for cyclizations to yield heterocycles 59-62: Synthesis of *N*-acetyl-1,3-dimethyl-5(6H)-dihydrophenanthridine (59):**

TTMSS (0.11 mL, 0.36 mmol) and anhydrous pyridine (0.1 mL, 5 equiv) was added to a solution of iodoanilide **49** (114 mg, 0.3 mmol) in benzene. A crystal of iodine (1 mol%) was subsequently added and the resulting mixture was stirred open to air at rt. Once the reaction was complete, the reaction mixture was filtered and the resulting filtrate was concentrated via

rotoevaporation. The crude product was purified by column chromatography eluting with hexanes/ethyl acetate (5/1) to provide the *title compound* as a white powder (45 mg, 60%); mp 115–118 °C; IR (thin film, CHCl<sub>3</sub>, NaCl, cm<sup>-1</sup>) 2981.4, 2923.6, 2858.0, 1662.3, 1434.8, 1369.2, 1209.2, 779.1, 744.4; <sup>1</sup>H NMR (500 MHz, CDCl<sub>3</sub>, 2.7/1 mixture of amide rotamers); MAJOR ROTAMER: δ 1.92 (s, 3H), 2.38 (s, 3H), 2.45 (s, 3H), 3.97 (d, *J* = 14.8 Hz, 1H), 5.81 (d, *J* = 14.8 Hz, 1H), 7.10 (s, 1H), 7.36 (m, 3 H); MINOR ROTAMER: δ 2.31 (s, 3H), 2.34 (s, 3H), 2.43 (s, 3H), 4.42 (d, *J* = 15.4 Hz, 1H), 4.86 (d, *J* = 15.4 Hz, 1H), 7.36 (m, 4H); OVERLAPPING: δ 7.49 (s, 1H), 7.83 (d, *J* = 7.7 Hz, 1H); <sup>13</sup>C NMR (125 MHz, CDCl<sub>3</sub>) δ 18.1, 18.7, 21.1, 21.2, 22.2, 46.1, 50.3, 123.0, 123.5, 124.1, 124.8, 126.1, 127.3, 127.7, 127.8, 128.2, 130.7, 131.1, 132.4, 132.8, 135.2, 136.0, 136.3, 136.4, 168.9, 171.3; HRMS (EI) calcd for C<sub>17</sub>H<sub>17</sub>NO 251.1310, found 251.1312; LRMS (EI) *m/z* 251 (M<sup>+</sup>, 36), 208 (100), 192 (24), 165 (22).

#### ***N*-Benzyl-*N*-[2,4-dimethyl-6-(phenyl)phenyl]acetamide (63):**

In the synthesis of **69** described above, the *title compound* was isolated as an undesired biproduct as a colorless oil (19 mg, 20%); <sup>1</sup>H NMR (300 MHz, CDCl<sub>3</sub>) δ 1.57 (s, 3H), 2.02 (s, 3H), 2.32 (s, 3H), 3.30 (d, *J* = 13.8 Hz, 1H), 5.13 (d, *J* = 13.8 Hz, 1H), 6.94 (app dd, *J* = 0.7, 0.7 Hz, 1H), 7.04 (ddd, *J* = 7.7, 7.7, 1.8 Hz, 2H), 7.07 (m, 1H), 7.15 (m, 3H), 7.29 (dd, *J* = 8.1 Hz, 1.8 Hz, 2H), 7.41 (m, 3H); <sup>13</sup>C NMR (75 MHz, CDCl<sub>3</sub>) δ 17.6, 21.0, 22.2, 51.2, 127.3, 127.5, 128.0, 128.3, 128.4, 128.6, 128.9, 129.4, 130.0, 130.1, 131.1, 137.2, 137.8, 139.6, 171.0; HRMS (EI) calcd for C<sub>23</sub>H<sub>23</sub>NO 329.1781, found 329.1780; LRMS (EI) *m/z* 329 (M<sup>+</sup>, 48), 182 (57), 132 (19), 91 (100).

#### ***N*-Acetyl-1-methyl-5-trimethylsilyl-5(6*H*)phenanthridine (60):**

Using aryl iodide **59** (175 mg, 0.4 mmol) and eluting with hexanes/ethyl acetate (10/1) provided the *title compound* as a colorless crystals (110 mg, 89%); mp 134–138 °C; IR (thin film, CHCl<sub>3</sub>, NaCl, cm<sup>-1</sup>) 3043.1, 2952.5, 2921.6, 2898.5, 1668.1, 1402.0, 1249.7, 1209.2, 860.4, 842.7, 742.5; <sup>1</sup>H NMR (500 MHz, CDCl<sub>3</sub>, 2.9/1 mixture of amide rotamers) major rotamer: δ 0.35 (s, 9H),

1.82 (s, 3H), 2.47 (s, 3H), 3.98 (d,  $J = 14.8$  Hz, 1H), 5.70 (d,  $J = 14.8$  Hz, 1H); minor rotamer:  $\delta$  0.32 (s, 9H), 2.27 (s, 3H), 2.45 (s, 3H), 4.40 (d,  $J = 15.6$  Hz, 1H), 4.82 (d,  $J = 15.6$  Hz, 1H); overlapping:  $\delta$  7.34 (m, 4H), 7.62 (s, 1H), 7.82 (d,  $J = 7.7$  Hz, 1H);  $^{13}\text{C}$  NMR (125 MHz,  $\text{CDCl}_3$ )  $\delta$  -0.1, 0.3, 21.5, 22.5, 23.1, 46.8, 50.3, 109.6, 123.5, 124.2, 124.9, 125.9, 126.1, 126.4, 127.5, 127.8, 127.9, 130.7, 132.2, 135.6, 135.9, 136.5, 136.6, 137.0, 137.8, 141.5, 171.3, 172.9; HRMS (EI) calcd for  $\text{C}_{19}\text{H}_{23}\text{NOSi}$  309.1542, found 309.1549; LRMS (EI)  $m/z$  309 ( $\text{M}^+$ , 8), 295 (100), 250 (60), 220 (70), 194 (70), 178 (57), 73 (71).

**(*E*)-Methyl-2-(1-*tert*-butyl-1-phenyl-1*H*-benzo[*c*][1,2]oxasilin-4(3*H*)-ylidene)acetate (61):**

Using vinyl iodide **51** (100 mg, 0.21 mmol) and eluting with hexanes/ethyl acetate (25/1) provided the *title compound* as a colorless oil (40 mg, 54%);  $^1\text{H}$  NMR (300 MHz,  $\text{CDCl}_3$ )  $\delta$  1.03 (s, 9H), 3.78 (s, 3H), 4.54 (dd,  $J = 1.0, 13.2$  Hz, 1H), 5.74 (dd,  $J = 0.5, 13.3$  Hz, 1H), 6.27 (s, 1H), 7.56 (m, 9H);  $^{13}\text{C}$  NMR (75 MHz,  $\text{CDCl}_3$ )  $\delta$  19.2, 26.1, 51.5, 61.5, 77.2, 117.0, 126.3, 127.8, 128.8, 129.8, 130.1, 132.7, 133.7, 133.9, 134.5, 144.7, 153.6, 166.4; HRMS (EI) calcd for  $\text{C}_{21}\text{H}_{24}\text{O}_3\text{Si}$  352.1495, found 352.1492; LRMS (EI)  $m/z$  352 ( $\text{M}^+$ , 38), 295 (100), 263 (46), 217 (70), 115 (41).

***N*-Methyl-6(5*H*)-phenanthridinone (62):**

Using aryl iodide **61** (135 mg, 0.4 mmol) and eluting with hexanes/ethyl acetate (4/1) provided the *title compound* as a faintly yellow solid (52 mg, 62%); CAS# 4594-73-4;  $^{13}\text{C}$  NMR (75 MHz,  $\text{CDCl}_3$ )  $\delta$  30.0, 115.0, 119.3, 121.6, 122.4, 123.2, 125.6, 127.9, 128.9, 129.5, 132.4, 133.5, 138.0, 161.6.

### **3.0 APPLICATION OF NMR TO THE STUDY OF CONFORMATIONAL DYNAMICS**

#### **3.1 Introduction**

Nuclear magnetic resonance spectroscopy (NMR) is an indispensable tool in the study of reversible reactions and chemical exchange processes.<sup>76</sup> Popular methods for observing chemical exchange and the calculation of rate coefficients include complete line shape analysis (CLSA), saturation transfer, and 2D exchange spectroscopy (2D EXSY). The latter, first introduced by Jeener and coworkers in 1979,<sup>77</sup> has increasingly grown in popularity during the last two decades.

#### **3.2 Two dimensional exchange spectroscopy (2D EXSY)**

Two-dimensional exchange spectroscopy (EXSY) has proven useful in the observation of dynamic chemical exchange processes by allowing the detection of multiple exchange pathways simultaneously. Crosspeaks between resonances arise if the corresponding nuclei are spatially close to another (nOe) or are in chemical exchange with one another (EXSY). The pulse sequence is identical to that used for a phase sensitive 2D NOESY experiment and is illustrated in **Figure 9**.<sup>77</sup>

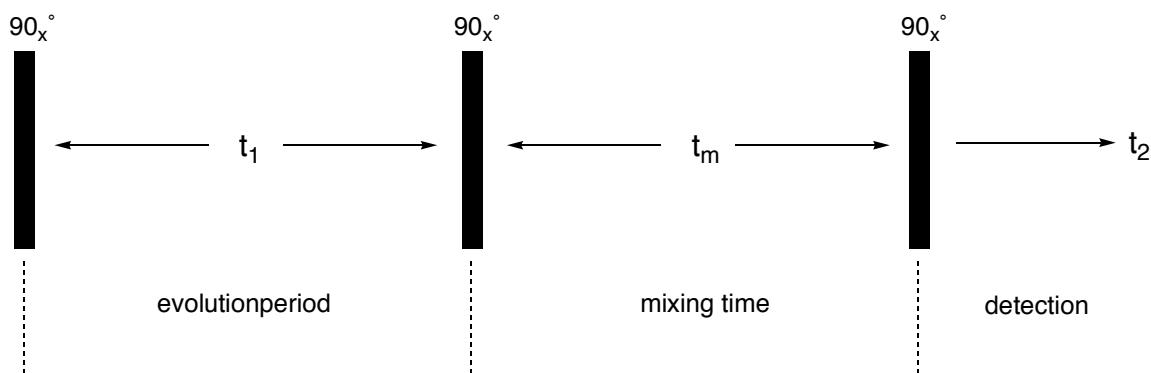


**Figure 9. Pulse sequence employed in a 2D EXSY NMR experiment**

The first  $90^\circ$  pulse causes transverse magnetization, and during the evolution period each resonance precesses according to its Larmor frequency (i.e., each resonance becomes “labeled” by their its environment). The second  $90^\circ$  pulse induces longitudinal magnetization (along the  $z$  axis), and during this mixing time ( $t_m$ ) the resonances in chemical exchange transfer magnetization between one another, which ultimately leads to crosspeaks in the 2D spectrum. After exchange, a third  $90^\circ$  pulse rotates the transverse magnetization into the  $xy$  plane for detection. The resulting 2D EXSY spectrum is essentially a graphic display of the exchange process, where the crosspeaks map out the exchange pathways by showing protons exchange chemical environments.

Besides a qualitative picture of exchange pathways, quantitative information is provided as well, provided the rate constant falls within the range observable by EXSY NMR ( $10^{-2}$ – $10^2$   $s^{-1}$ ).<sup>78</sup> The rate constants ( $k = k_{AB}$  or  $k_{BA}$ ) governing an exchange process between uncoupled frequencies  $\nu_A$  and  $\nu_B$  is a function of the crosspeak intensities ( $I_{AB}$ ,  $I_{BA}$ ), the diagonal peak intensities ( $I_{AA}$ ,  $I_{BB}$ ), mixing time ( $t_m$ ) and the mole fractions of sites A and B ( $X_A$ ,  $X_B$ ):

$$k = \frac{1}{t_m} \ln \left( \frac{r+1}{r-1} \right) \quad (\text{Eq 5})^{76}$$

where

$$r = 4X_A X_B \left( \frac{I_{AA} + I_{BB}}{I_{AB} + I_{BA}} \right) - (X_A - X_B)^2$$

This equation is only useful for approximating the rate constant as a sum of the forward and reverse rate constants for a simple two-site exchange system. In a simple case of two-site exchange, magnetization transfer or line-shape analysis is typically just as efficient as EXSY for obtaining rate information.<sup>78</sup> *The real power of 2D EXSY lies in the ability to calculate the forward and reverse rate constants independently for a multisite exchange system using matrix calculation methods.* The calculations are easily performed on a computer and software is available<sup>79</sup> where the only requirement of the user is to input the resonance crosspeak intensities, mole fractions of each resonance, and mixing time.

Care must be taken in interpreting the 2D spectrum so that NOE peaks are not confused with EXSY peaks, and vice versa. However, distinguishing between the two is simple because NOE peaks have the opposite phase as the diagonal peaks, and EXSY peaks have the same phase as the diagonal peaks.<sup>76,80</sup>

### 3.3 Choosing an appropriate mixing time

The choice of mixing time is critical for obtaining accurate kinetic data from 2D EXSY spectroscopy.<sup>81</sup> The mixing time must be long enough to allow for a detectable amount of exchange to occur between the second and third 90° pulses, but must not be so long that the intensity of the crosspeaks become insensitive to the exchange rate(s). The best procedure for obtaining precise rate parameters is iterative in nature. The rate constant must first be approximated from the 1D <sup>1</sup>H NMR spectra; from there a mixing time ( $t_m$ ) can be approximated,<sup>81</sup> and then the 2D EXSY spectrum is recorded with the approximated mixing time. From the EXSY spectrum the rate constant can be calculated, a new  $t_m$  can be estimated, and if this is much different from the first one the whole process is repeated until the  $t_m$  is constant. This process requires a substantial amount of spectrometer time. An alternative method for finding an appropriate mixing time that requires less spectrometer usage has been proposed by Vassilev and Dimitrov.<sup>81</sup>

In short, the ideal mixing time is when the uncertainty in the calculated rate constants is minimized.

### 3.4 Example of 2D EXSY applied to the study of conformational exchange

Gibson and co-workers found that heterocycle **71** gives rise to four distinct conformations which are observable on the  $^1\text{H}$  NMR timescale (**Figure 10**).<sup>82</sup> Rotation about the pyridone-tolyl bond (a) gives rise to diastereomeric conformations **71a** and **71b**. There is also a second element of asymmetry in **71** with respect to the conformation of the benzazepine ring. The “ring flipping” (b) causes interconversion between diastereomers **71a/ent-71b** and **71b/ent-71a**.

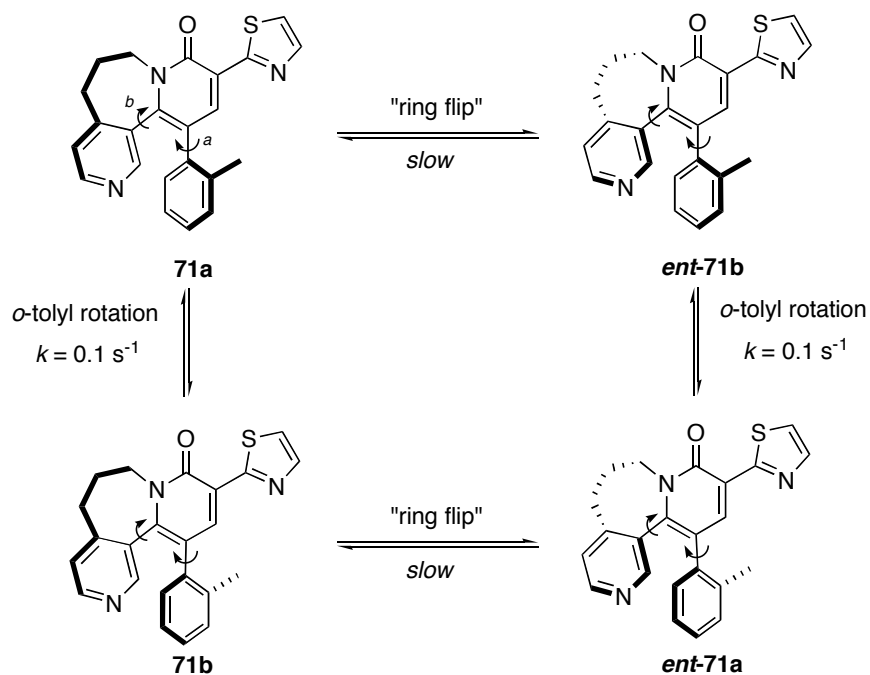


**Figure 10. Conformational interconversion amongst four diastereomeric atropisomers of tricyclic pyridone 71**

Gibson and coworkers conducted 2D EXSY NMR experiments to calculate the rate of interconversion between diastereomeric *o*-tolyl rotamers **71a** and **71b**. The  $^1\text{H}$  NMR 2D EXSY

spectrum of **71** between 7.7 and 8.2 ppm is shown in **Figure 11**, and the crosspeaks due to chemical exchange are highlighted in red boxes. The two exchanging aromatic protons represented in **Figure 11** were not assigned by the authors, but they are indeed diastereotopic based on their unequal populations, and constitute a simple case of two-site exchange where Eq 5 can be safely applied. The observed crosspeaks are EXSY peaks because they have the same phase as the diagonal peaks. Furthermore, the intensities of the crosspeaks are larger at 340 K than at 300 K, because increasing the temperature increases the rate of exchange. Therefore, the rate at which these proton resonances exchange is representative of the rate at which rotation about the *o*-tolyl bond occurs in **71**. Using Eq 5,<sup>78</sup> the authors calculated a rate constant of 0.1 s<sup>-1</sup> for *o*-tolyl bond rotation, which translates to a free energy barrier of  $\Delta G^\ddagger = 18.9 \text{ kcal mol}^{-1}$  at 300 K.

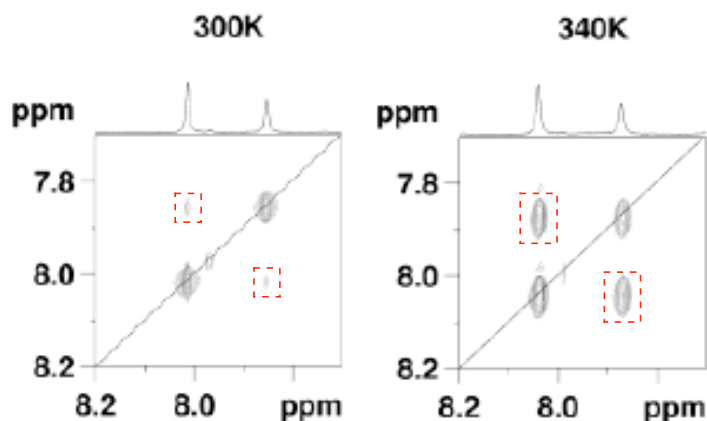


**Figure 11.** <sup>1</sup>H NMR 2D EXSY spectrum of tricyclic pyridone **71** in *d*<sub>6</sub>-DMSO at 300 K (left) and 340 K (right) (taken from reference 92)

The “ring-flipping” caused by rotation about the pyridine-pyridone bond in **71** is too slow to measure by <sup>1</sup>H EXSY. The authors were able to separate the four diastereomers into two mixtures (**71a/71b** and *ent*-**71a/ent-71b**) by chiral HPLC. By measuring the rate of racemization of each mixture they were able to calculate the rate of “ring flipping” ( $k = 2.6 \times 10^{-4}$ ,  $\Delta G^\ddagger = 21.9$

kcal mol<sup>-1</sup> at 293 K). These experiments illustrate the value of 2D EXSYNMR for measuring events that are otherwise difficult to determine.

## 4.0 INVESTIGATION OF THE CONFORMATIONAL DYNAMICS OF *ORTHO*- SUBSTITUTED *N*-ACYL-DIHYDROPHENANTHRIDINES

### 4.1 Aim of project

The peculiar  $^1\text{H}$  NMR spectra of dihydrophenanthridine analogs **59** and **60** prompted the investigation of the dynamic behavior of these molecules. The  $^1\text{H}$  NMR spectrum of silylated dihydrophenanthridine **60** is shown in **Figure 12** (spectral data for methyl analog **59** is presented and discussed later in this chapter). There are the four distinct proton doublets between 3.9 ppm and 5.8 ppm, consisting of two large coupled doublets at 3.9 and 5.8 ppm ( $J = 14.9$  Hz) and two smaller coupled doublets at 4.4 and 4.8 ppm ( $J = 15.9$  Hz). The major to minor ratio is 2.9/1. These four resonances are attributed to four non-equivalent benzylic hydrogens of **60**, based on the chemical shift and the large (geminal) coupling constants. One might assume dihydrophenanthridine **60** is an achiral molecule by inspection of the structure when drawn in the standard planar representation, considering it has only one carbon that is not  $\text{sp}^2$  hybridized. But the resonances in the NMR spectrum show that it must possess two elements of conformational asymmetry, which translates into four distinct conformational stereoisomers, interchanging at rates slower than the NMR timescale.

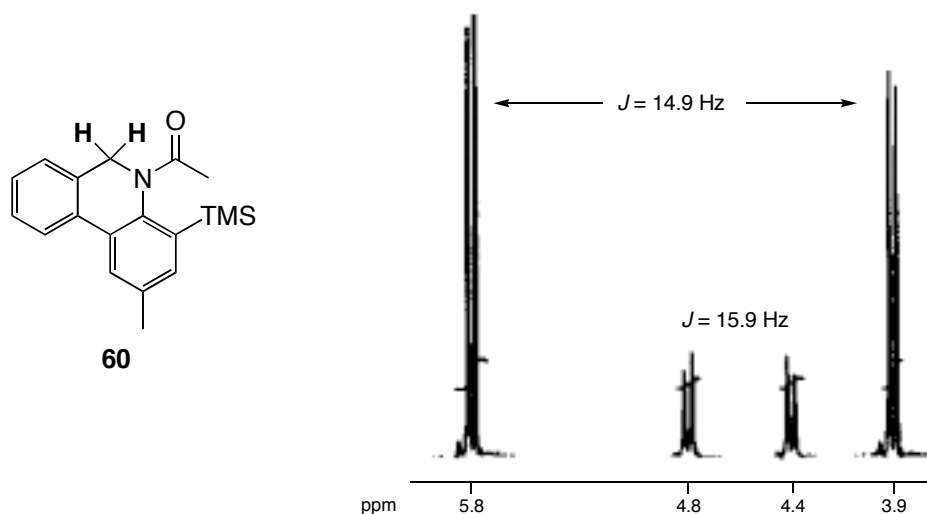


Figure 12. 500 MHz  $^1\text{H}$  NMR spectrum from 3.5 to 6.0 ppm of dihydrophenanthridine **60** in  $\text{CDCl}_3$

#### 4.2 Molecular modeling of silylated benzazapine **60**

To better understand the conformational preferences of **60**, molecular modeling studies were conducted. The energy of **60** was minimized with restricted semi-empirical calculations at the AM1 level of theory in Chem 3D Pro 5.0. All atoms were arranged in a single plane as the starting point for the calculation. The amide rotamer labeled as (*E*)-**60** (based on the CIP priority rules) was found to be the lowest energy conformation. Reiterating the calculation at  $10^\circ$  intervals about the N–CO bond revealed a second minimum energy conformation, (*Z*)-**60**. All starting point rotamers about the amide bond relaxed to either (*E*)-**60** or (*Z*)-**60** during the minimization process. Both (*E*)-**60** and (*Z*)-**60** represent diastereomeric conformations due to twisting about the N–CO bond, differing in ground-state energy by  $1.44 \text{ kcal mol}^{-1}$ , suggesting (*E*)-**60** is the major amide rotamer (Figure 13). It is typical of anilides for the *E* amide rotamer to predominate.

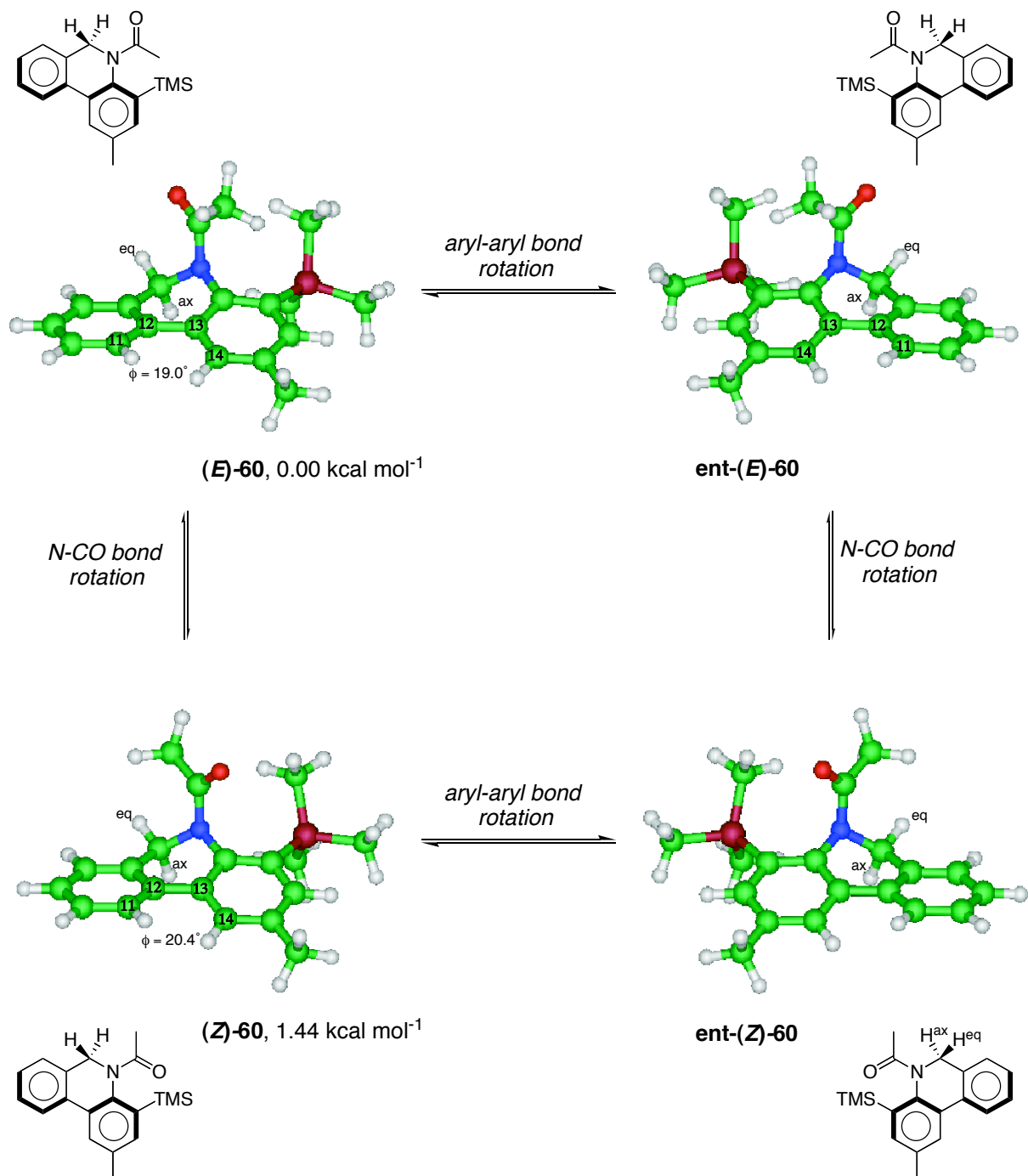


Figure 13. AM1-calculated minimum energy structures of 60

To measure the planarity about the amide nitrogen in the *E* and *Z* rotamers, the three bond angles centered on the nitrogen were summed. If the nitrogen were truly planar ( $sp^2$  hybridized), then the sum of the three angles should total  $360^\circ$ . The sums of these angles in the

calculated structures are 348.4° and 347.3° for the *E* and *Z* rotamers, respectively. If the nitrogen were truly tetrahedral (sp<sup>3</sup> hybridized), then the sum of the angles should be 3 x 109.5° = 328.5°. Assuming this bond angle comparison is meaningful, the calculation predicts the amide nitrogen is about 65% sp<sup>2</sup>-hybridized, and 35% sp<sup>3</sup>-hybridized. This information implies the barrier to rotation about the N-CO bond should be smaller than the barrier observed in a typical planar amide where the nitrogen is considered to be 100% sp<sup>2</sup> hybridized.

Each diastereomer (*E*)-**60** and (*Z*)-**60** exhibits a second element of asymmetry due to rotation about the aryl-aryl (C12-C13) bond, with a dihedral angle between C11 and C14 of 19.0° in the major (*E*) rotamer and 20.4° in the minor (*Z*) rotamer. This aryl-aryl bond “twist” puts the two hydrogens at the benzylic position in pseudo-axial and equatorial positions, rendering them chemically non-equivalent. Furthermore, rotation about the aryl-aryl bond is accompanied by a ring flip that accomplishes enantiomerization, giving rise to **ent-(E)-60** or **ent-(Z)-60**. Thus, the benzylic proton resonances in the <sup>1</sup>H NMR spectrum should appear as a pair of doublets for each diastereomer, with a large (geminal) coupling constant, provided aryl-aryl bond rotation is slow relative to the NMR timescale. This prediction is consistent with the observed <sup>1</sup>H NMR spectrum of **60** in CDCl<sub>3</sub> (**Figure 12**). Assuming the calculated ground state energies in **Figure 13** are qualitatively accurate, the proton resonances at 3.9 ppm and 5.7 ppm belong to the benzylic hydrogens of the major amide rotamer, (*E*)-**60**, and the signals at 4.4 and 4.8 ppm belong to the benzylic hydrogens of the minor amide rotamer, (*Z*)-**60**.

### 4.3 Crystal structure of silylated dihydrophenanthridine **60**

X-ray quality crystals of **60** were obtained by a slow evaporation technique. Dihydrophenanthridine **60** was dissolved in hexanes/isopropanol (9:1), and the resulting mixture was left open to the air. After two weeks a single hexagonal crystal had formed (10 mg).

The crystal structure of **60** (**Figure 14**)<sup>83</sup> confirmed the molecule prefers to exist as a twist conformation about the aryl-aryl bond with a dihedral angle of 22.6°, in good agreement with the calculated angle of 20.4°. The sum of the bond angles about the nitrogen is 351.8°, about four degrees closer to planarity than predicted by the calculated structure (347.3°). The twisting of the aromatic rings causes the amide nitrogen to pucker to one side of the molecule, forcing the amide electron pair out of conjugation with the aniline ring. If the molecule were planar in such a way to allow *N*-lone pair conjugation to the aromatic system, the acetyl group would sterically crowd the TMS substituent. It is clear by examination of both the crystal structure and the calculated structures that this steric demand outweighs the stabilization gained by *N*-lone pair donation into the aniline ring.

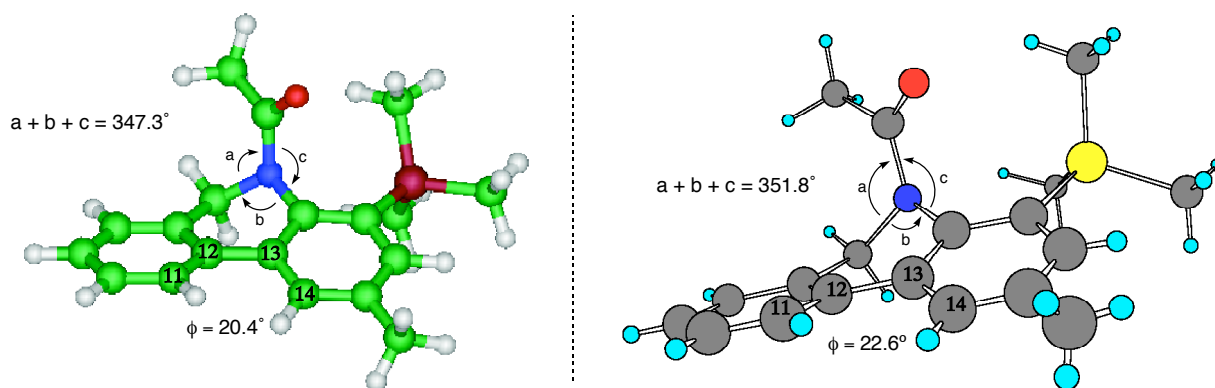


**Figure 14.** X-ray crystal structure (right) and AM1 calculated structure (left) of **60**

The crystal structure conformation of **60** most closely resembles the calculated minor conformation with respect to the orientation of the *N*-acetyl group. Thus, we hypothesized the crystal structure is representative of the minor conformer observed in CDCl<sub>3</sub>, whose benzylic hydrogens give rise to the frequencies at 4.4 and 4.8 ppm in the <sup>1</sup>H NMR spectrum.

A low temperature <sup>1</sup>H NMR experiment was conducted to test this hypothesis (**Figure 15**). A solid crystal of **60** was dissolved in CD<sub>2</sub>Cl<sub>2</sub> that was precooled to 195 K in an NMR tube. After complete solvation of the crystal at 195 K (25 min), the sample was immediately loaded

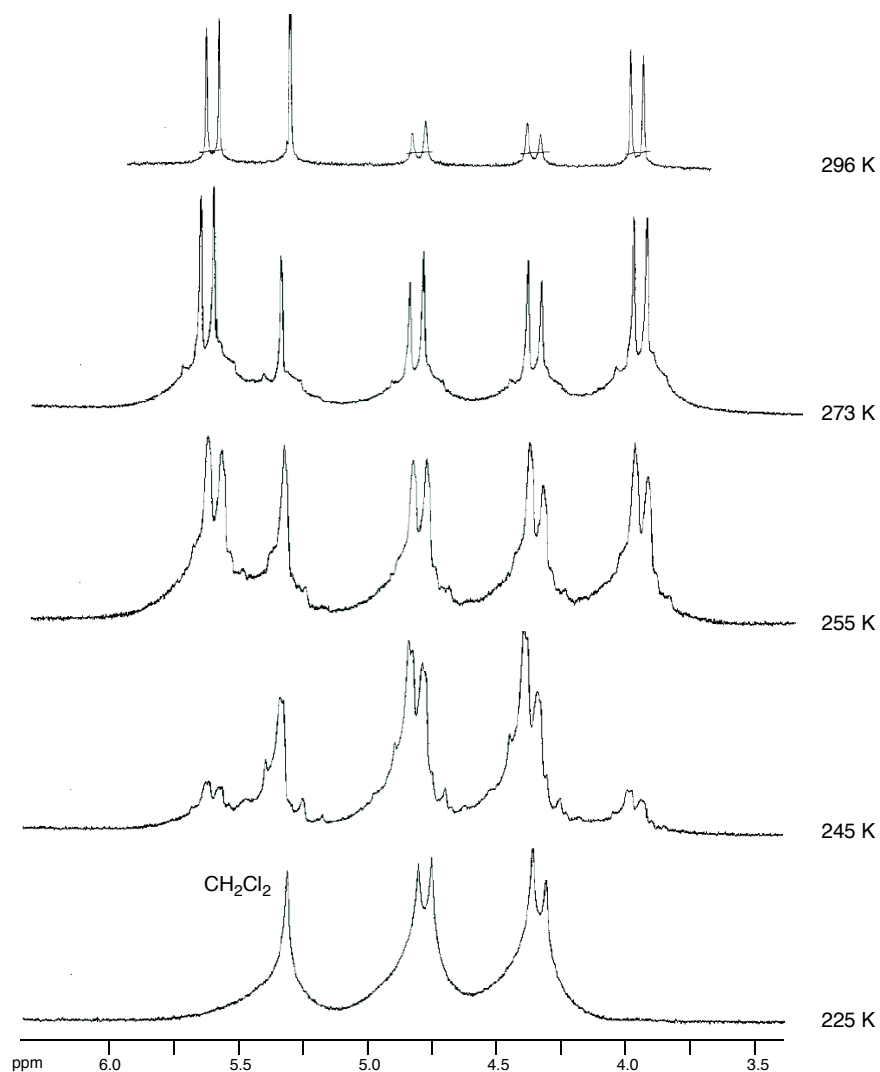


**Figure 15.** 300 MHz  $^1\text{H}$  NMR spectrum of **60** from 225 K to room temperature in  $\text{CD}_2\text{Cl}_2$

into a 300 MHz NMR spectrometer equipped with a temperature controller. The sample was then slowly warmed to room temperature and  $^1\text{H}$  NMR spectra at were recorded at the temperatures noted in **Figure 15**. Only the minor amide rotamer (**Z**)-**60** is present in solution up to 225 K, but upon warming, the resonances assigned to the major rotamer appear. This is strong evidence that the calculated structures are comparatively accurate with respect to amide bond orientation, and that the crystal structure of **60** corresponds to the minor amide rotamer observed in solution.

#### 4.4 2D EXSY NMR of silylated hydrophenanthridine 60

The direct observation of interconversion between the four possible conformations of **60** was achieved by 2D EXSY  $^1\text{H}$  NMR experiments. The spectrum of **60** was obtained in  $\text{CDCl}_3$  at 500 MHz with a mixing time of 0.35 s at room temperature.<sup>84</sup> For the purpose of this discussion, the benzylic protons have been tentatively assigned to the frequencies in the  $^1\text{H}$  NMR spectrum so that the pseudo-equatorial proton ( $\text{H}^{eq}$ ) is the more downfield frequency in both the major and minor conformations. This assignment is made because the two downfield benzylic proton resonances show an nOe correlation to an aromatic proton (**Figure 16**). There is also an nOe between the more downfield minor resonance (4.8 ppm) and the acetyl methyl group, further supporting our assignment that the more downfield resonance in each rotamer represents the pseudo-equatorial proton. In theory, the pseudo-equatorial benzylic proton should give rise to the more downfield resonance since it is positioned closer to the deshielding region of the benzene ring.

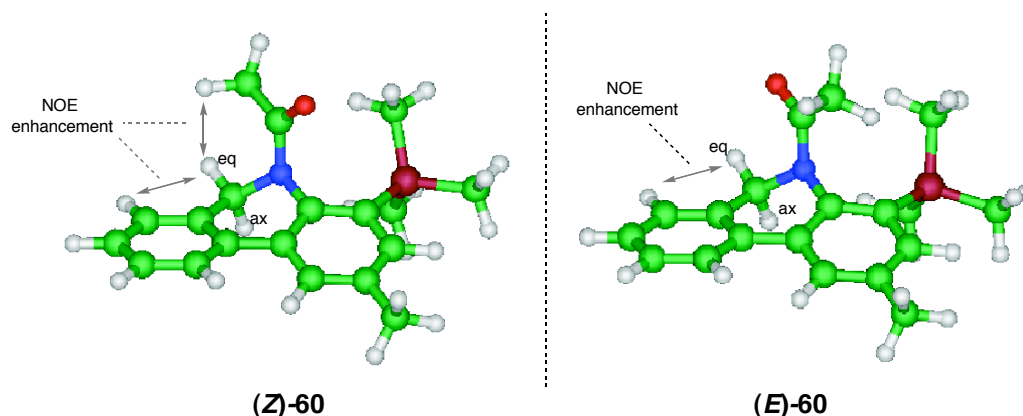


**Figure 16.** Key NOE enhancements from the 2D NOESY spectrum of dihydrophenanthridine **60** in  $\text{CDCl}_3$

**Figure 18** shows an expansion of the EXSY spectrum of dihydrophenanthridine **60**. The crosspeaks highlighted in red dotted boxes denote correlations that arise due to chemical exchange (*i.e.*, these peaks have the same phase as the diagonal peaks). The crosspeaks

highlighted in blue dotted boxes represent nOe correlations. The assignment of the benzylic protons to the resonances in the 2DEXSY spectrum is clarified in **Figure 17** below.

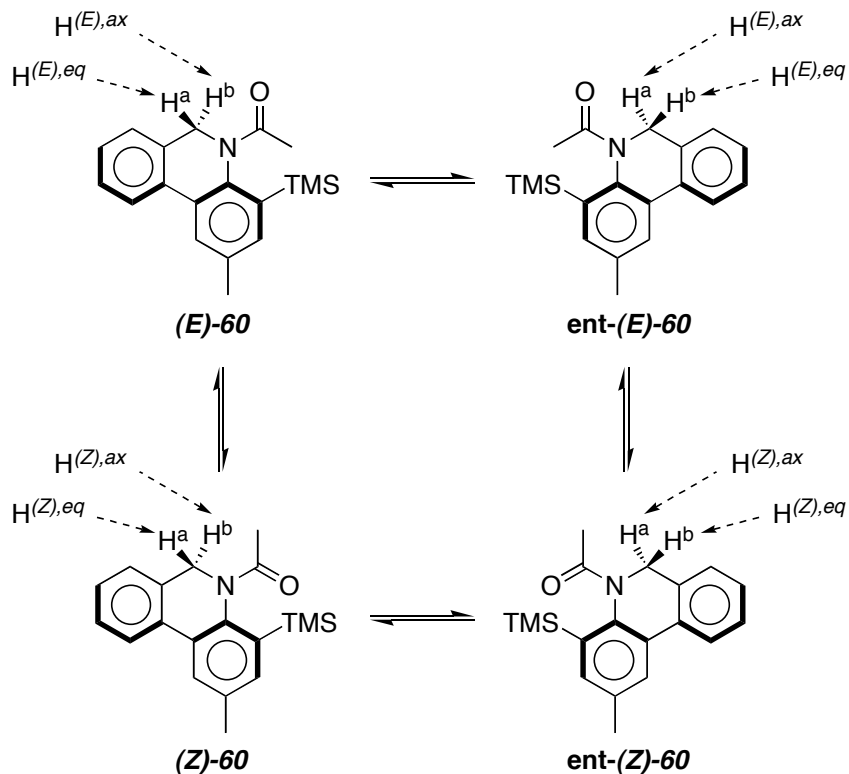


**Figure 17. Proton assignments accompanying 2DEXSY spectra of dihydrophenanthridines**

The chemical exchange between  $H^{(Z),eq} / H^{(E),eq}$  and  $H^{(Z),ax} / H^{(E),ax}$  represents amide bond rotation, responsible for the interconversion between **(E)-60** and **(Z)-60** (thus between **ent-(E)-60** and **ent-(Z)-60** as well). The observed chemical exchange between the  $H^{(Z),eq} / H^{(Z),ax}$  resonances represents that the enantiomerization of **(Z)-60** via aryl-aryl bond rotation, which occurs at a rate expressed by the rate constant  $k_Z$  (**Figure 19**). The crosspeaks between the major frequencies ( $H^{(E),eq}$  and  $H^{(Z),ax}$ ) do not arise from chemical exchange, but rather indicate a strong nOe, because the phase of the correlating crosspeaks is opposite that of the diagonal peaks. This means that **(E)-60** and **ent-(E)-60** either do not directly interconvert with one another, or interconvert at a rate much slower than the NMR timescale. We conclude the orientation of the

*N*-acetyl group in (*E*)-**60** prevents enantiomerization from occurring for steric reasons: the acetyl methyl group would have to pass through the TMS substituent upon flipping the nitrogen to the other side of the molecule. On the other hand, when dihydrophenanthridine **60** exists as (*Z*)-**60**, the carbonyl oxygen passes by the TMS group more easily: a plausible indication that there is a Si-O Lewis acid/base interaction in the (*Z*) rotamer. This potential interaction is also implied by the proximity of the Si and O atoms in the crystal structure presented earlier (**Figure 14**).

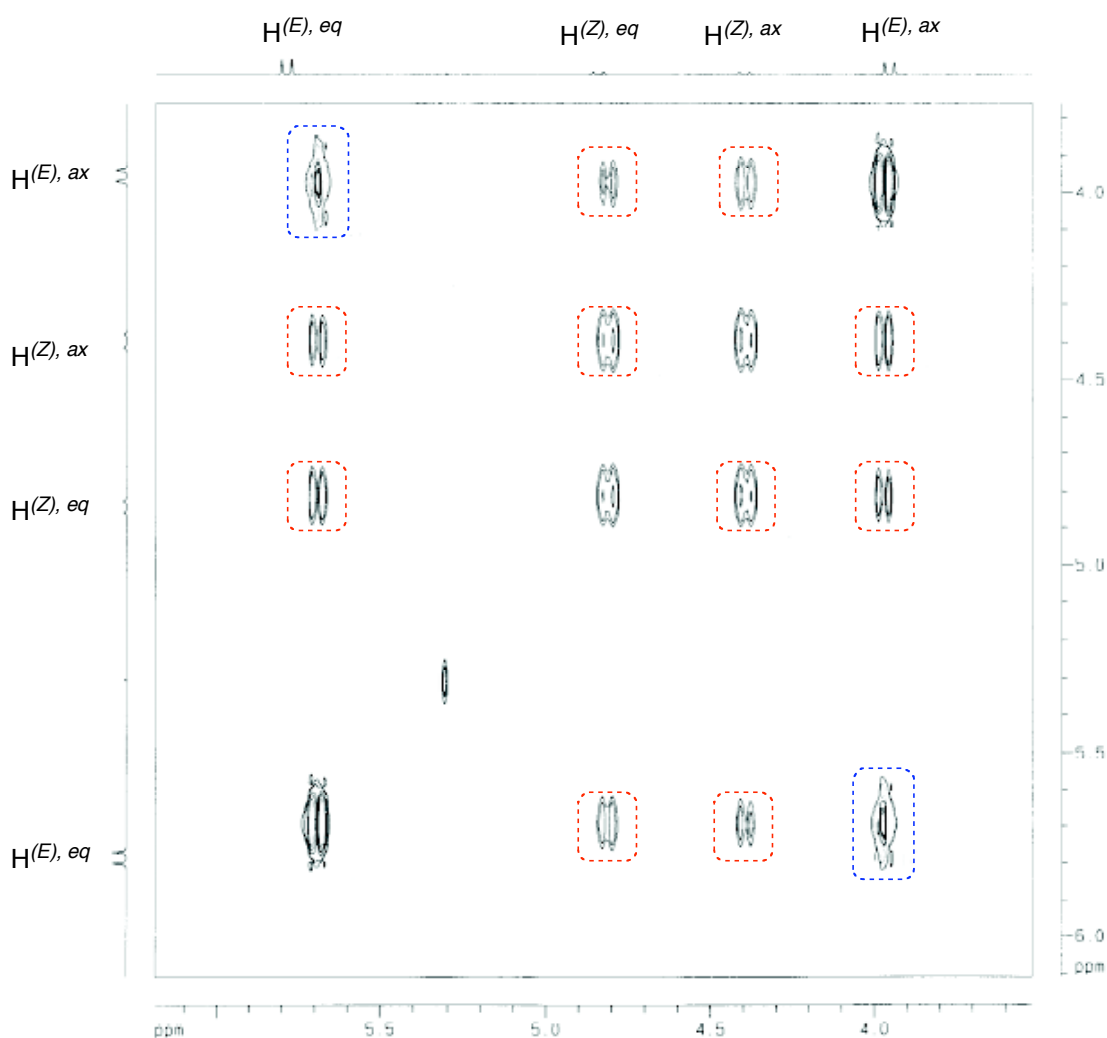
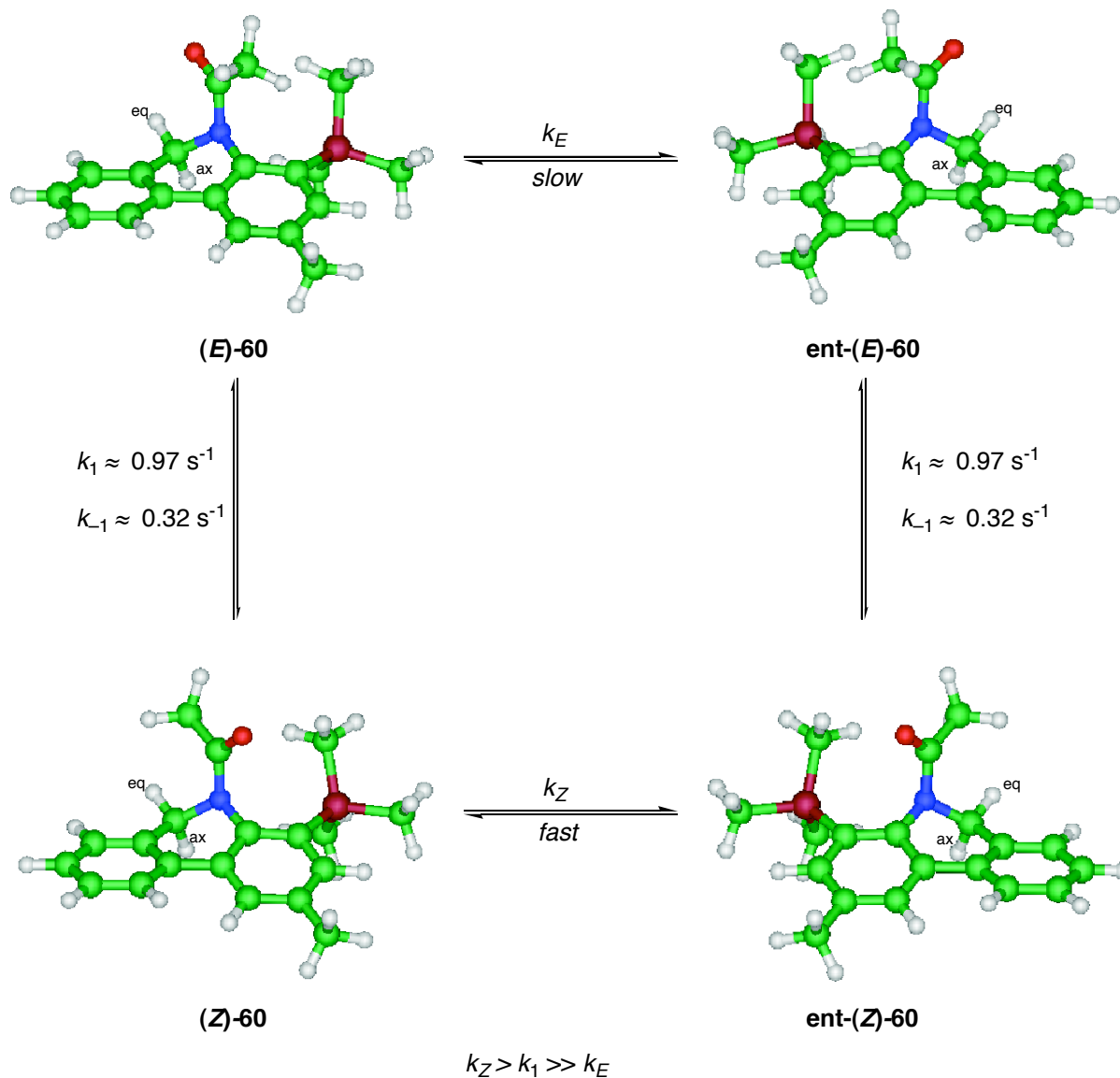


Figure 18. 500 MHz 2D EXSY spectrum of **60** in  $CDCl_3$  (4.8 to 6.2 ppm) with a mixing time of 0.35 s

The crosspeaks between  $H^{(E),ax}/H^{(Z),eq}$  and  $H^{(Z),ax}/H^{(E),ax}$  indicate interconversion between **(E)-60/ent-(Z)-60** and **ent-(E)-60/(Z)-60**. The observation of these interconversions probably arises because the combined rate of amide bond rotation followed by aryl-aryl bond rotation in the (Z) rotamer is fast enough to observe by EXSY NMR. Therefore the interconversions between **ent-(E)-60/(Z)-60** and **(E)-60/ent-(Z)-60** (and the rate at which they occur) are representative of N-CO rotation followed by aryl-aryl bond rotation in the (Z) conformer, and vice versa.

The rate constants governing the conformational interconversions of **60**, illustrated in **Figure 19**, were calculated with the D2DNMR program developed by Abel and coworkers.<sup>79</sup> The program requires the input of the crosspeak and diagonal peak intensities, the mole fractions of the exchanging resonances (measured from the <sup>1</sup>H NMR spectrum), and the mixing time. The D2DNMR program calculates the forward and reverse rate constants independently in a matrix-based routine.<sup>85</sup>



**Figure 19. Model of conformational interconversion of dihydrophenanthridine 60 based on 2D EXSY  $^1\text{H}$  NMR at 295 K**

The rate constant  $k_1$ , calculated with D2DNMR, was found to be  $0.97 \pm 0.02 \text{ s}^{-1}$  for the conversion of **(Z)-60** to **(E)-60** and  $0.32 \pm 0.02 \text{ s}^{-1}$  for the conversion **(E)-60** to **(Z)-60** ( $k_{-1}$ ). These values equate to energy barriers to amide bond rotation of 17.3 and 17.9 kcal mol $^{-1}$ , respectively.<sup>86</sup> Therefore the difference in energy between **(Z)-60** and **(E)-60** is 0.6 kcal mol $^{-1}$ . By using the equilibrium ratio of 2.9/1 with the relationship  $\Delta G = -RT (\ln K)$ , the ground state

energy difference works out to be  $0.62 \text{ kcal mol}^{-1}$ , in very close agreement with the value determined by EXSY, but less than half of the calculated energy difference of  $1.44 \text{ kcal mol}^{-1}$ .

The rate constant corresponding to aryl-aryl bond rotation in the (*Z*) rotamer,  $k_Z$ , cannot be accurately determined with the D2DNMR program due to strong spin-spin coupling between  $H^{(Z),eq}$  and  $H^{(Z),ax}$ . However, the crosspeaks between these two resonances have the same magnitude as their diagonal peaks, meaning that the rate of exchange is at the upper limit that can be measured by EXSY at the given mixing time.

The rate constant associated with the two-step conversion of (*E*)-**60** to **ent-(Z)-60** and **ent-(E)-60** to (*Z*)-**60** is  $0.60 \pm 0.02 \text{ s}^{-1}$ . The reverse rate constant  $0.21 \pm 0.02 \text{ s}^{-1}$ . Comparison of these values to  $k_{N-CO}$  ( $0.97$  and  $0.32 \text{ s}^{-1}$ ) means amide bond rotation followed by aryl-aryl bond rotation in the (*Z*) rotamer, and vice versa, is about 60% as fast as amide bond rotation alone.

#### 4.5 $^1\text{H}$ NMR of dihydrophenanthridine **60** at elevated temperatures

To corroborate the conclusions drawn from 2D EXSY spectroscopy, the  $^1\text{H}$  NMR spectrum of dihydrophenanthridine **60** was recorded at higher temperatures to obtain qualitative (and approximate quantitative) information about its conformational dynamics and energy barriers. Deuterated DMSO was used as the solvent for  $^1\text{H}$  NMR at elevated temperatures. The sample in  $\text{DMSO-}d_6$  was held at each temperature for 10 min before recording the  $^1\text{H}$  NMR spectra presented in **Figure 19**. Since the previously discussed  $^1\text{H}$  NMR spectra of dihydrophenanthridine **60** were obtained in  $\text{CDCl}_3$ , we worked under the assumption that the conformational dynamics of **60** do not differ greatly between chloroform and DMSO, for the sake of comparing the spectral data obtained in either solvent. The room temperature spectra obtained in either solvent are similar; the only difference the amide rotamer ratio in DMSO is about 1/1 (2.9 to 1 in  $\text{CDCl}_3$ ).

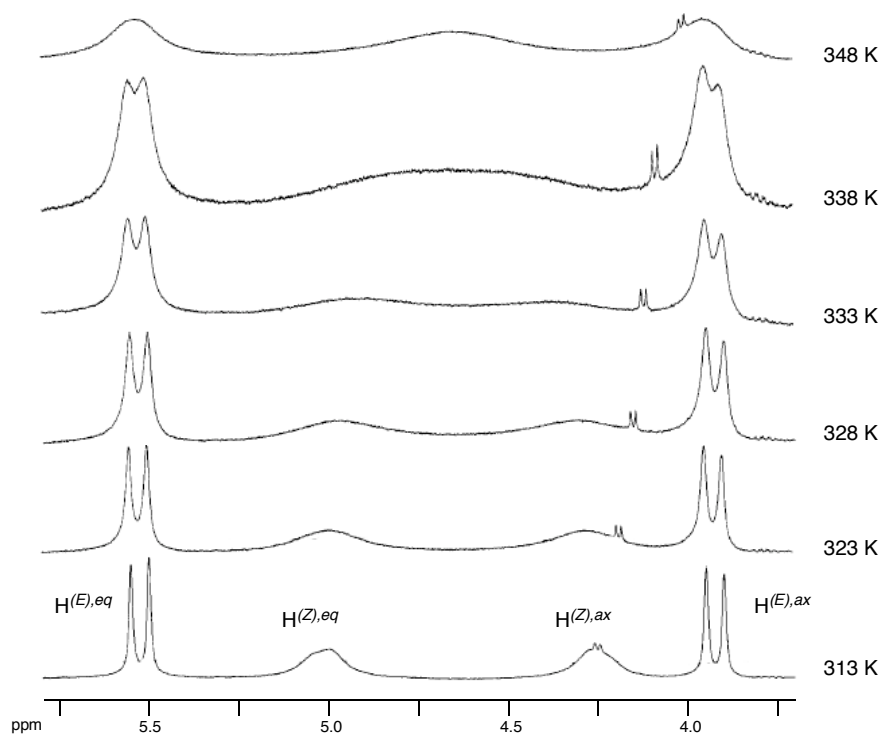


**Figure 20.**  $^1\text{H}$  NMR of hydrophenanthridine **60** from 3.75-4.75 ppm in  $d_6$ -DMSO at elevated temperatures

At approx. 338 K, the frequencies corresponding to the benzylic hydrogens of the (**Z**)-**60** (4.25 and 5.00 ppm) coalesce. Thus aryl-aryl bond rotation of (**Z**)-**60**, which causes the chemical exchange between the frequencies at 4.25 and 5.00 ppm, is faster than N-CO bond rotation; otherwise, the two downfield peaks and the two upfield peaks would coalesce first, since they are closer to one another. Coalescence of other resonances in the spectrum corresponding to the  $\text{CH}_3$  groups, the TMS group, and aromatic protons in each amide rotamer were also observed, but the overlapping of these resonances prevented the extraction of rate data.

The rate constant for aryl-aryl bond rotation in the (*Z*) rotamer,  $k_Z$ , at the coalescence temperature (338K) can be calculated from Eq 6,

$$k_{\text{coal}} = \pi \left[ (\Delta\nu)^2 + \frac{6(J_{\text{AB}})^2}{2^{1/2}} \right]^{1/2} \quad (\text{Eq 6})^{74}$$

where  $\Delta\nu$  is the difference in frequency between the coalescing peaks at lower temperatures when they are well defined,  $k_{\text{coal}}$  is the rate constant at the coalescence temperature, and  $J_{\text{AB}}$  is the coupling constant between sites A and B. Eq 6 yields a value of  $714 \text{ s}^{-1}$  for  $k_Z$  at the coalescence temperature 333 K, which translates to an energy barrier of approx.  $15 \text{ kcal mol}^{-1}$ . The barrier to rotation of *N*-aromatic amides is typically higher, around  $16\text{--}20 \text{ kcal mol}^{-1}$ .<sup>87</sup>

#### 4.6 Conformational dynamics of hydrophenanthridine **59**

The  $^1\text{H}$  NMR spectrum of dihydrophenanthridine **59** (Figure 21) is analogous to that of silylated dihydrophenanthridine **60** in the benzylic proton region. There are four peaks corresponding to the benzylic hydrogens between 4 and 6 ppm, with a major-to-minor ratio of 2.7/1.

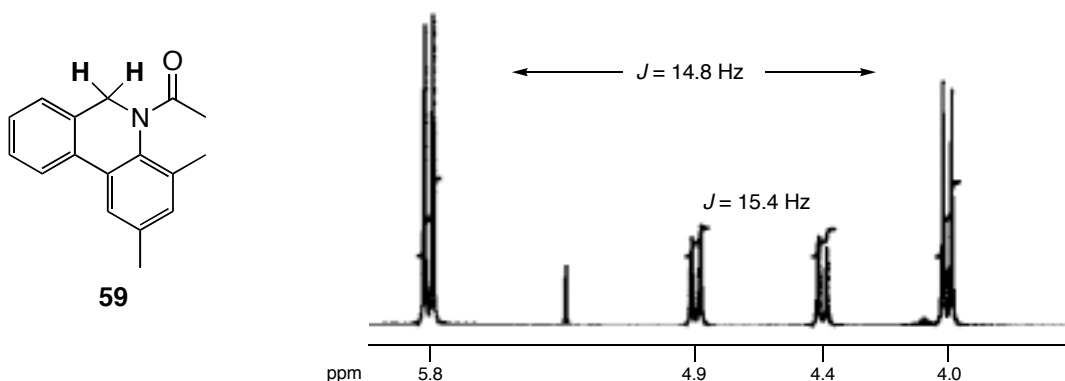


Figure 21. 500 MHz  $^1\text{H}$  NMR spectrum of dihydrophenanthridine **59** in  $\text{CDCl}_3$

We followed the same procedure in studying the conformational dynamics of dihydrophenanthridine **59** as described for the TMS analog **60**. The energy minima calculated for hydrophenanthridine **59** are qualitatively identical to those calculated for **60**, with twisting about the aryl-aryl (C12-C13) bond in each amide rotamer, and the (*E*) rotamer is the major (Figure 212). We were unable to obtain the crystal structure of hydrophenanthridine **59**, so we

assume the AM1 calculation is accurate in predicting the structure of the major and minor amide rotamers, as was the case for the TMS analog **60**.

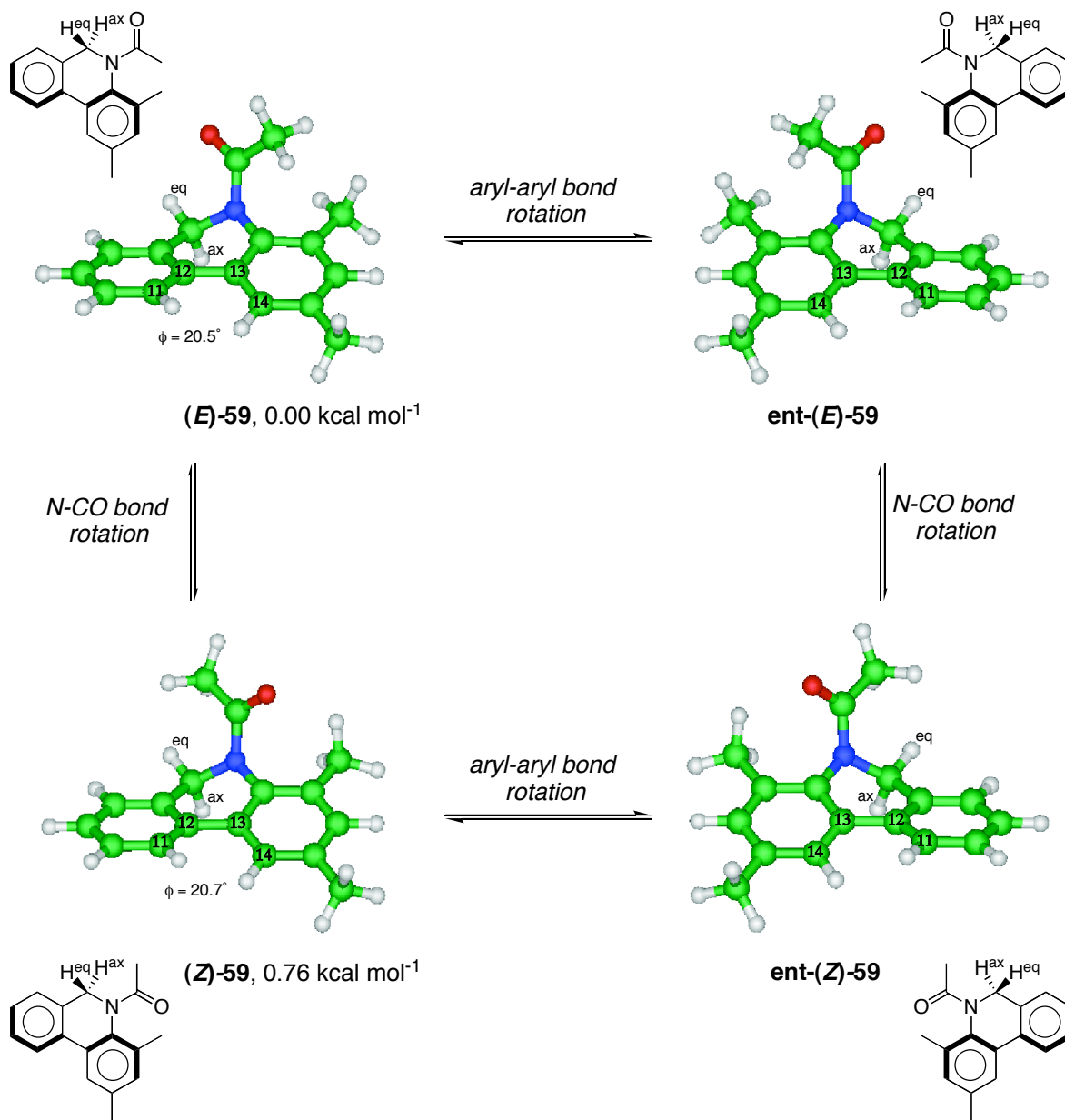
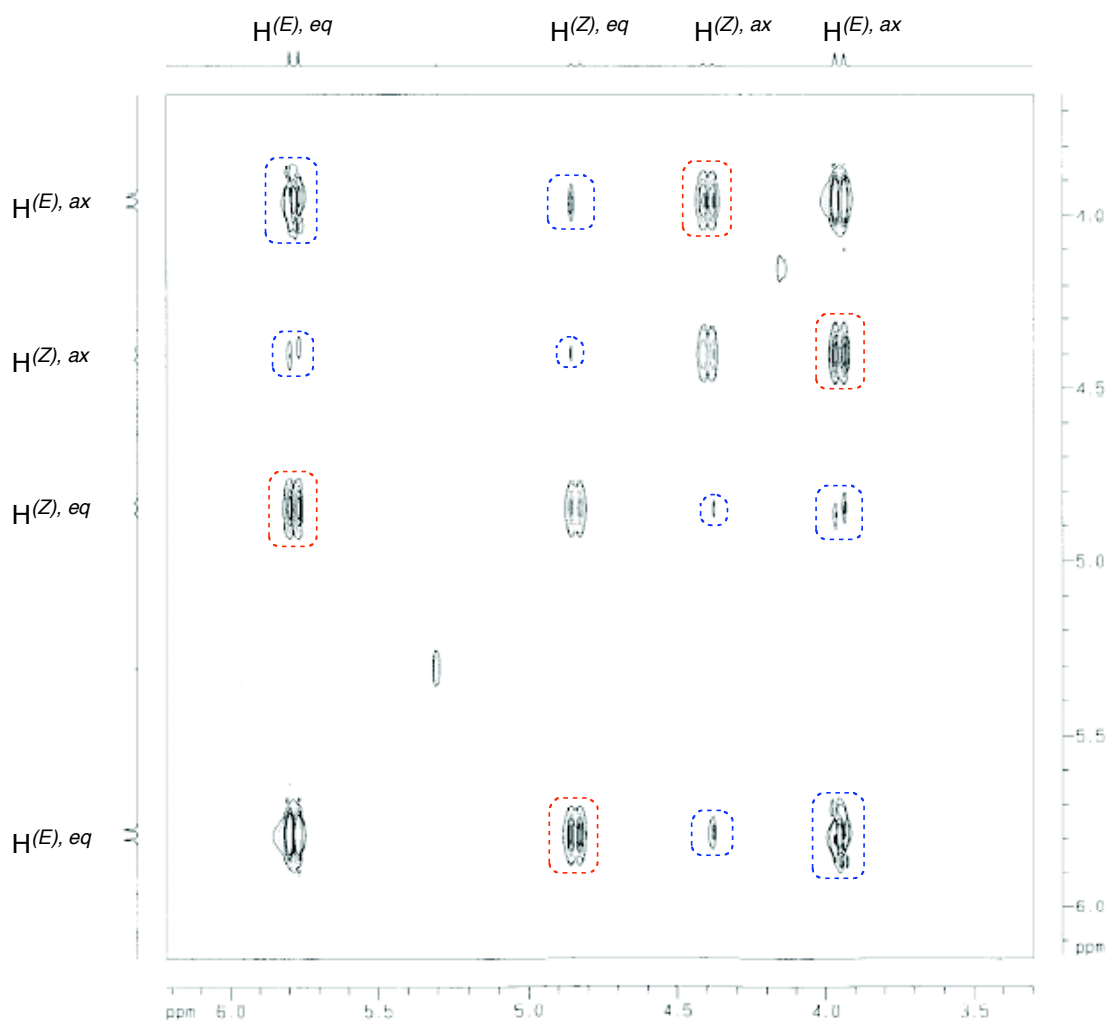


Figure 22. AM1-calculated minimum energy structures of **59**

The sum of the calculated bond angles to the amide nitrogen in **59** are 352.1° and 353.1° for (*Z*)-**59** and (*E*)-**59**, respectively. These values are about 5° higher than those calculated for TMS analog **60**, which is reasonable since the calculation probably attributes more steric

hindrance to the TMS group than it does for the CH<sub>3</sub> group. By relating the degree of planarity to *N*-hybridization, as in the previous example, the amide nitrogen in the methyl analog **59** is about 75% sp<sup>2</sup>-hybridized, and 25% sp<sup>3</sup> according to the predicted energy minima (compared to 65% sp<sup>2</sup>/35% sp<sup>3</sup> for **60**).

The 2D <sup>1</sup>H NMR EXSY spectrum (**Figure 23**) of dihydrophenanthridine **59** was obtained in the under the same conditions as described for the TMS analog **60**. The frequencies between



**Figure 23.** 500 MHz 2D EXSY spectrum of **59** (3.3 to 6.2 ppm) in CDCl<sub>3</sub> with a mixing time of 0.35 s

4 and 6 ppm are also labeled in the same manner, where the more downfield frequency of each rotamer is attributed to the pseudo-equatorial proton ( $H^{eq}$ ). The crosspeaks arising from chemical exchange are highlighted in red dotted boxes, and nOe peaks are highlighted in blue.

The only crosspeaks arising from chemical exchange in **Figure 23** are between  $H^{(Z),eq}/H^{(E),eq}$  and  $H^{(Z),ax}/H^{(Z),eq}$ , indicating N-CO bond rotation is the only process that is fast enough to observe by EXSY. Rate constants for N-CO bond rotation in **59**,  $k_{N-CO}$  and  $K \times k_{N-CO}$ , are 5.48 and  $2.01 \pm 0.04 \text{ s}^{-1}$  respectively (**Figure 24**). This translates to energy barriers of 16.3 and 16.8 kcal mol<sup>-1</sup>.<sup>86</sup> Thus, the energy difference between the major and minor amide rotamers is 0.5 kcal mol<sup>-1</sup>. Calculation of the ground state energy difference ( $\Delta G = -RT \ln K$ ) from the equilibrium ratio of 2.7/1 (measured from the <sup>1</sup>H NMR) yields a value of 0.58 kcal mol<sup>-1</sup>, in good agreement with the value determined by EXSY.

The lack of crosspeaks due to chemical exchange between  $H^{(Z),eq}/H^{(Z),ax}$  and  $H^{(E),eq}/H^{(E),ax}$  means that enantiomerization of (**Z**)-**59** and (**E**)-**59** is not occurring to a measurable extent by EXSY NMR at room temperature. This is in contrast to the silylated analog **60**, where aryl-aryl twisting in the (**Z**) rotamer is fast at room temperature. The apparent Si-O interaction (**Z**)-**60** lowers the energy barrier to “ring flipping” dramatically compared to the *o*-methyl analog **59**.

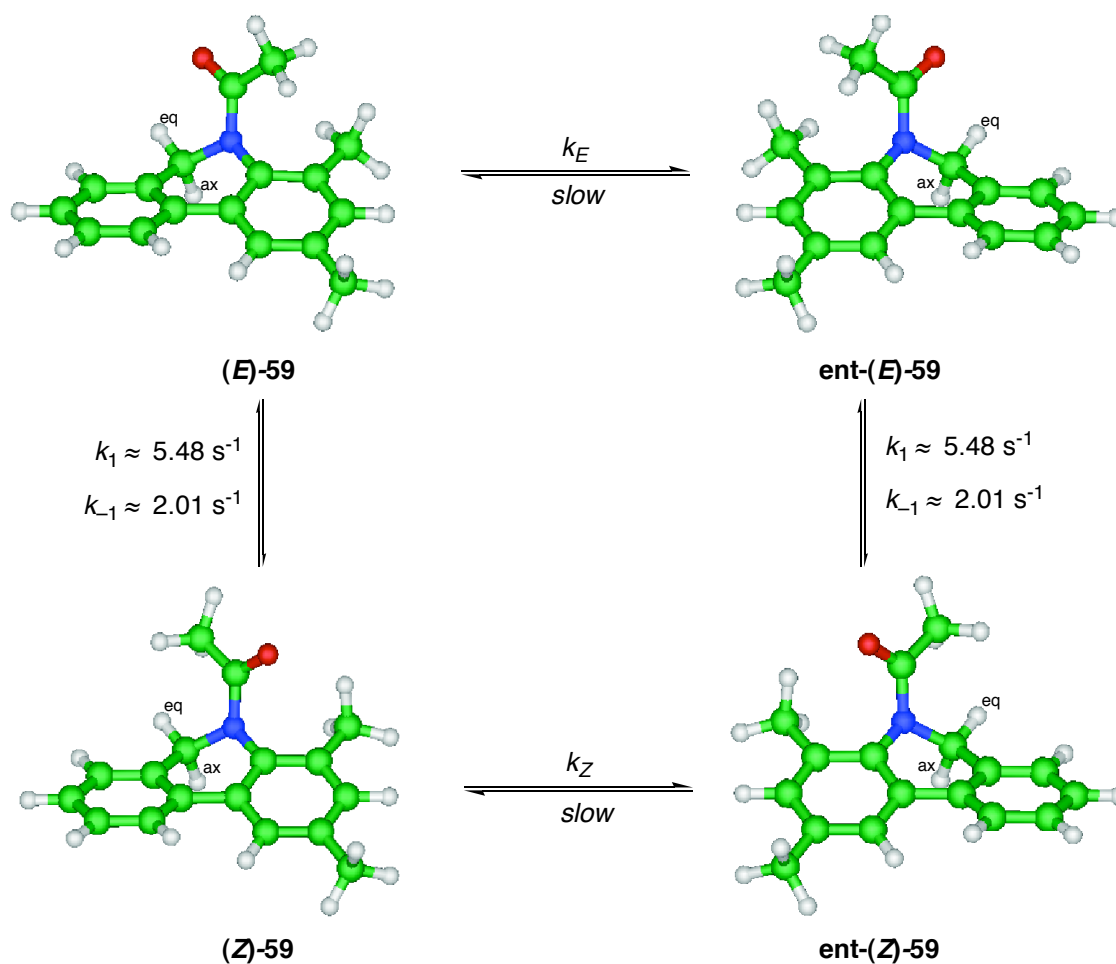


**Figure 24. Model of conformational interconversion of 59 based on 2D EXSY  $^1\text{H}$  NMR at 295 K**

The high temperature  $^1\text{H}$  NMR spectra of *o*-methyl dihydrophenanthridine **59** in  $\text{DMSO-}d_6$  are consistent with the calculated model depicted **Figure 24**. As the temperature is increased, the two downfield peaks and the two upfield peaks ( $\text{H}^{\text{eq}}$  and  $\text{H}^{\text{ax}}$  respectively) converge until the coalescence point is reached at approximately 348 K for the upfield sites<sup>88</sup> and 353 K for the downfield sites. The converging resonances are not coupled to one another, so a simpler form of Eq 6 is used to approximate the rate constant (Eq 7).

$$k_{\text{coal}} = \frac{\pi \Delta\nu}{2^{1/2}} \quad (\text{Eq 7})^{74}$$

The approximate rate constant ( $k_{N-CO}$ ) from Eq 7 and the data extracted from Figure 4.13 is  $404 \text{ s}^{-1}$  (348 K) and  $357 \text{ s}^{-1}$  (353 K), which translates to a free energy barrier of about  $\Delta G^\ddagger = 16.5 \text{ kcal mol}^{-1}$ . This value is in fairly good agreement with the forward and reverse barriers to amide bond rotation determined by the EXSY experiments of 16.3 and 16.8  $\text{kcal mol}^{-1}$ .

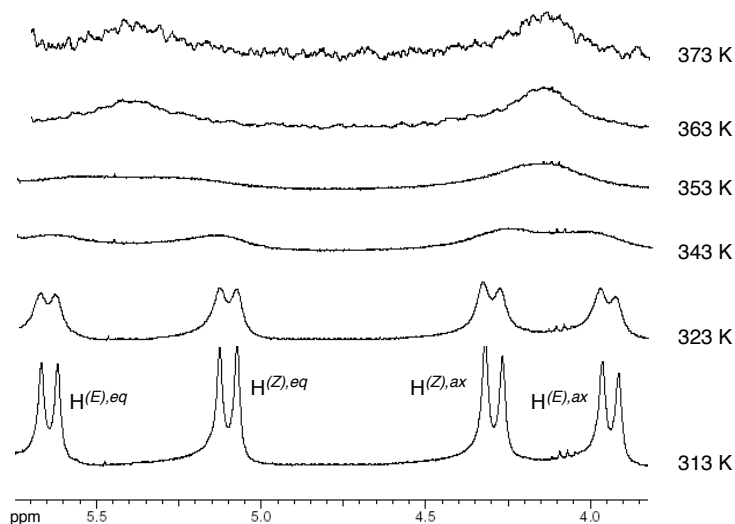


Figure 25.  $^1\text{H}$  NMR of dihydrophenanthridine **59** from 3.75–4.75 ppm in  $d_6$ -DMSO at elevated temperatures

Two broad signals still remain at 373 K for dihydrophenanthridine **59**, and the working temperature range of our spectrometer restricted us from recording spectrum at temperatures any higher than this. If we assume those signals still present at 373 K coalesce at 374 K, then on the low end (according to Eq 3) the approx. energy barrier to aryl-aryl bond twisting (i.e. ring flipping) in **59** is at least  $17 \text{ kcal mol}^{-1}$ . The barrier to aryl-aryl twisting in the silyl analog **60** was much lower. In other words, the carbonyl group can pass by TMS group more easily than it can pass by a methyl group, which is a direct result of the carbonyl oxygen sterically tolerating a silicon atom more so than a carbon atom.

#### 4.7 Attempted synthesis of *N*-alkyl analogs

For comparison to dihydrophenanthridines **59** and **60**, we wanted to study the conformational properties of an *N*-alkyl dihydrophenanthridine such as **72** or the *N*-H analog **73** (Figure 26).

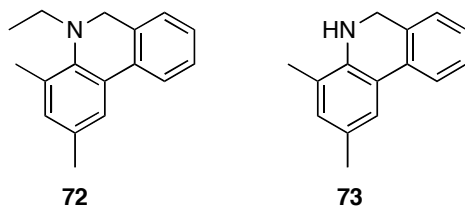
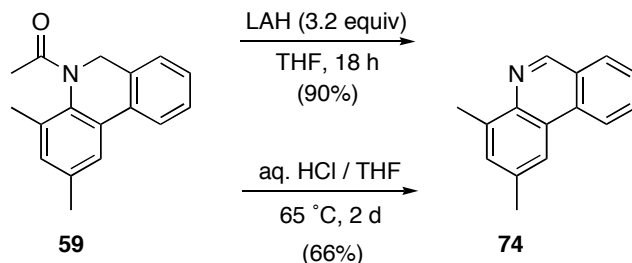


Figure 26. Dihydrophenanthridine analogs **72** and **73**

It was imagined **72** could be easily obtained from LAH reduction of *N*-acetyl dihydrophenanthridine **59**. Treatment of **59** with LAH (1.2 equiv) in THF at room temperature was very sluggish: after 2 h only starting material remained (as determined by TLC analysis). An additional 5 equiv of LAH was added to the reaction and the resulting mixture was refluxed 18 hours before complete consumption of starting material had occurred (by TLC) to give dimethyl phenanthridine **74** as the sole product in 90% isolated yield (after purification by silica gel flash chromatography). Attempted hydrolysis of **59** to yield dimethyldihydrophenanthridine **73** also failed, and instead afforded phenanthridine **74** in 66% yield (Scheme 18).



Scheme 18. Formation of 2,4-dimethylphenanthridine **73**

The dihydrophenanthridine **73** is therefore believed to be a common intermediate in both of the reactions in **Scheme 18**, and that it is simply undergoes oxidation during workup or upon exposure to air. This conclusion implies the amide in **59** behaves more like an ester in the LAH reduction, rather than forming the iminium ion intermediate expected from an amide upon hydride reduction of the carbonyl by LAH.

Although initial attempts at modifying dihydrophenanthridine **59** were unsuccessful, a molecule related to **59** and **60** was found in the literature (**Figure 27**).<sup>89</sup> Dihydrophenanthridine analog **75** is structurally similar to **59** and **60** except that it lacks an *ortho* substituent on the anilide ring. The benzylic hydrogens of **75** show up as a singlet at 2.02 ppm in the <sup>1</sup>H NMR spectrum, indicating **75** has *only one observable conformation on the NMR timescale*. Based on previous studies of *N*-aromatic amides we believe **75** exists only as the (*E*) amide rotamer, where the carbonyl oxygen and the aniline ring are antiperiplanar.<sup>74</sup>

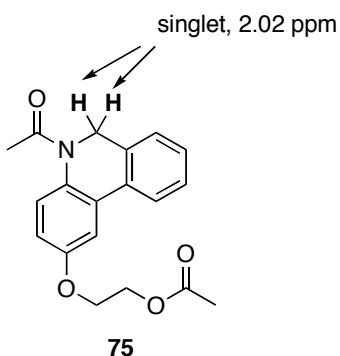


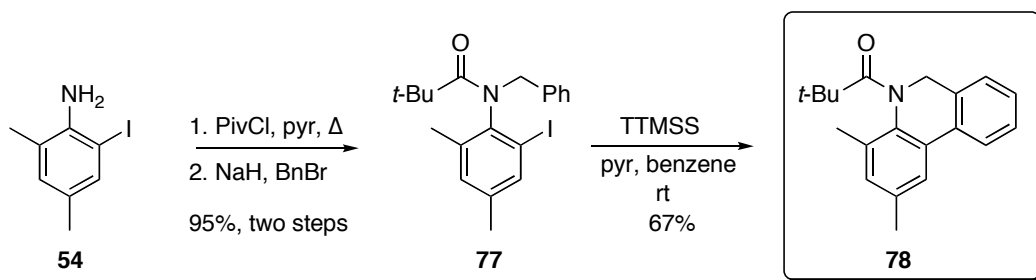
**Figure 27. Dihydrophenanthridine analog lacking an *ortho* substituent**

Dihydrophenanthridine analog **75** offers solid evidence that *N*-acyl dihydrophenanthridines *must possess an ortho substituent in order to give rise to more than one observable conformation on the NMR timescale*.

## 4.8 HPLC experiments

Attempts at separating the conformers of **59** and **60** at room temperature by chiral HPLC failed. Three different chiral columns were employed, in a variety of solvent systems, but in all cases we observed only one broad peak for **59** and **60**.

It was hypothesized the free energy barrier to ring flipping and/or amide bond rotation could be influenced by putting a bulkier alkyl group on the *N*-acyl sidechain. A compound that possesses a high enough barrier to allow for separation of atropisomers by chiral HPLC was desired.



**Scheme 19.** Synthesis of *N*-pivaloyl hydrophenanthridine analog **78**

*N*-Pivaloyl amide **78** was obtained in three steps from iodoaniline **54** in a manner analogous to the synthesis of *N*-acetyl analog **59** presented in Chapter 2 (**Scheme 19**). The  $^1\text{H}$  NMR of **78** in  $\text{CDCl}_3$  at room temperature showed the presence of only one amide rotamer, but the pair of doublets corresponding to the benzylic hydrogens indicated the molecule does possess a mode of asymmetry, presumably due to aryl-aryl bond rotation previously described. Furthermore, the pair of doublets corresponding to the benzylic hydrogens exhibited line broadening at room temperature: the rate of aryl-aryl bond rotation is actually faster than for analogs **59** and **60**. The bulky *t*-Bu group had the opposite effect than predicted. Qualitative interpretation of the  $^1\text{H}$  NMR spectrum in **Figure 28** suggests the pivaloyl amide has a lower barrier to aryl-aryl bond rotation than the two analogs discussed earlier.

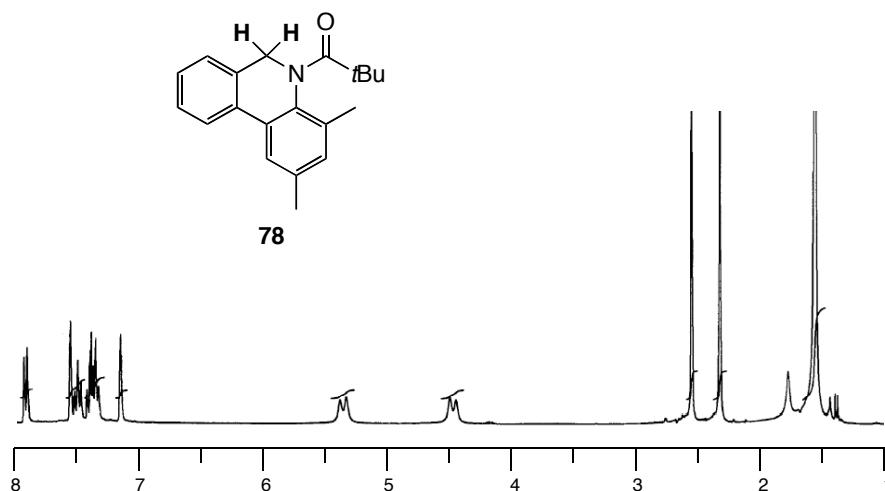


Figure 28. 300 MHz  $^1\text{H}$ NMR spectrum of dihydrophenanthridine **78** in  $\text{CDCl}_3$

#### 4.9 Summary

*N*-Acyldihydrophenanthrine analogs bearing an *ortho* substituent possess interesting conformational dynamics, giving rise to conformations that interconvert slower than the NMR time scale. Semi-empirical calculations along with 2D EXSY NMR were indispensable tools in elucidating the shapes of these compounds, observing their modes of conformational exchange, and calculating the rates at which they occur.

The size of the *N*-acyl side chain is critical in dictating the rate at which aryl-aryl bond twisting occurs and the major/minor amide rotamer ratio. A relatively small acyl substituent, such as methyl, causes aryl-aryl bond rotation to proceed more slowly than a large group, such as *t*-butyl. Increasing the size of the *N*-acyl group also increases the energy difference between (*E*) and (*Z*) amide rotamers. The lack of an *ortho* substituent in *N*-acyl-dihydrophenanthridines gives rise to only one observable conformation on the NMR timescale.

## 4.10 Experimental

### General

Refer to Chapter 2.12 for general information regarding how experiments were conducted and technical information.

### 2,4-Dimethylphenanthridine (74):

*N*-Acetyl-(5*H*)-phenanthridine **59** (41 mg, 0.16 mmol) was dissolved in dry THF (15 mL) and placed under argon atmosphere. Lithium aluminumhydride (7 mg, 0.19 mmol) was added in one portion and the resulting mixture was stirred at rt for 2 hours. An additional 2 equiv of LAH was added and the resulting mixture was followed by TLC every 90 minutes. After 10 hours the reaction was quenched with aq. sat'd tartrate solution (15 mL). The mixture was extracted with ether (3 x 25 mL), the organic layer was dried over MgSO<sub>4</sub> and concentrated to yield a crude yellow tar. Purification by flash chromatography eluting with hexanes/EtOAc (7/1) afforded the *title compound* as a yellow crystalline solid (31 mg, 90%); mp 76-79 °C: FT-IR (thin film, NaCl, CH<sub>2</sub>Cl<sub>2</sub>, cm) 3006.5, 2954.4, 2850.3, 1616.1, 754.0, 514.9; <sup>1</sup>H NMR (300 MHz, CDCl<sub>3</sub>); δ 2.57 (s, 3H), 2.83 (s, 3H), 7.43 (app s, 1H), 7.66 (ddd, *J* = 7.2, 7.2, 1.2 Hz, 1H), 7.80 (ddd, *J* = 1.2, 1.2, 6.9 Hz, 1H), 8.01 (dd, *J* = 0.7, 8.1 Hz, 1H), 8.21 (s, 1H), 8.58 (d, *J* = 8.3 Hz, 1H), 9.23 (s, 1H); <sup>13</sup>C NMR (75 MHz, CDCl<sub>3</sub>) δ 18.6, 21.9, 119.7, 122.0, 123.8, 126.1, 127.1, 128.7, 130.7, 131.4, 132.6, 136.5, 137.1, 141.1, 151.1; HRMS (EI) calcd for C<sub>15</sub>H<sub>13</sub>N 207.1046, found 207.1048; LRMS (EI) *m/z* 207 (M<sup>+</sup>, 100), 192 (42), 102 (16).

### *N*-(2-Iodo-4,6-dimethylphenyl)pivalamide (76):

2-Iodo-4,6-dimethylaniline **54** (1.067 g, 4.32 mmol), pivaloyl chloride (0.64 mL, 5.2 mmol) and pyridine (2 mL) were dissolved in CH<sub>2</sub>Cl<sub>2</sub> (100 mL) and the resulting mixture was stirred under argon for 18 h at room temp, at which point reaction was not complete by TLC.

Another 0.5 equiv of pivaloyl chloride was added and reaction was stirred for two days. Reaction mixture was diluted with CH<sub>2</sub>Cl<sub>2</sub> (100 mL) and washed with NaHCO<sub>3</sub> solution (1 x 25 mL) and water (1 x 25 mL). Organic layer was dried over MgSO<sub>4</sub>, concentrated, and purified via flash chromatography eluting with pentane/EtOAc (4/1) to yield the *title compound* as a white crystalline solid (1.426 g, 99%); mp 160-163 °C: FT-IR (thin film, CH<sub>2</sub>Cl<sub>2</sub>, NaCl, cm<sup>-1</sup>) 3274.6 (bs), 2969.9, 2923.6, 1650.8, 1502.3, 744.4; <sup>1</sup>H NMR (300 MHz, CDCl<sub>3</sub>); δ 1.37 (s, 9H), 2.20 (s, 3H), 2.26 (s, 3H), 7.00 (s, 1H), 7.09 (bs, 1H), 7.50 (s, 1H); <sup>13</sup>C NMR (75 MHz, CDCl<sub>3</sub>) δ 19.3, 20.4, 27.6, 39.3, 99.1, 131.7, 134.4, 136.9, 137.0, 138.6, 176.2; HRMS (EI) calcd for C<sub>13</sub>H<sub>18</sub>NOI 331.0428, found 331.0433; LRMS (EI) *m/z* 331 (M<sup>+</sup>, 18), 246 (100), 189 (56), 119 (83), 104 (87), 77 (82), 65 (81).

***N*-Benzyl-*N*-(2-iodo-4,6-dimethylphenyl)pivalamide (77):**

*N*-(2-Iodo-4,6-dimethylphenyl)pivalamide **76** (1.379 g, 4.16 mmol) was dissolved in dry THF (75 mL) and placed under argon and cooled to 0 °C in an icebath. NaH (125 mg, 5.2 mmol) was added portionwise and the resulting mixture was stirred until bubbling had ceased. Benzyl bromide (0.55 mL, 4.6 mmol) was added dropwise and the resulting mixture was allowed to warm to rt. Reaction was not complete after 18 h, at which point NBu<sub>4</sub>I was added. After 1 day reaction mixture was diluted with CH<sub>2</sub>Cl<sub>2</sub> (50 mL) and quenched with water dropwise until bubbling ceased. Resulting biphasic mixture was washed with NH<sub>4</sub>Cl sol'n and water. Organic layer was dried over MgSO<sub>4</sub> and concentrated. The crude mixture was purified via flash chromatography eluting with hexanes/EtOAc (11/1) to afford 20% of unreacted starting material and the *title compound* as a white crystalline solid (1.342 g, 95% yield based on recovered starting material); mp 78-80 °C; FT-IR (thin film, NaCl, cm<sup>-1</sup>) 2991.1, 1633.4, 1456.0, 1184.1, 738.6, 700.0; <sup>1</sup>H NMR (300 MHz, CDCl<sub>3</sub>); δ 1.02 (s, 9H), 1.53 (s, 3H), 2.22 (s, 3H), 2.39 (d, *J* = 13.5 Hz, 1H), 5.57 (d, *J* = 13.3 Hz, 1H), 6.82 (s, 1H), 7.17 (app s, 5H), 7.55 (s, 1H); <sup>13</sup>C NMR (75 MHz, CDCl<sub>3</sub>) δ 19.2, 20.2, 29.5, 41.4, 55.3, 102.5, 127.3, 127.9, 130.3, 131.5, 136.9, 138.1,

138.7, 139.1, 141.3, 177.5; HRMS (ESI) calcd for C<sub>20</sub>H<sub>24</sub>NOINa 444.0800, found 444.0809; LRMS (ESI) *m/z* 444 ([M+Na]<sup>+</sup>, 100), 413 (12).

***N*-Pivaloyl-2,4-dimethyl-5(6*H*)-phenanthridine(78):**

*N*-benzyl-iodoanilide **35** (320 mg, 0.76 mmol) was dissolved in benzene (75 mL, 10 mM) and pyridine (0.3 mL) was added in one portion. Tris(trimethylsilyl)silane (0.28 mL, 0.91 mmol) was added in one portion and the mixture was left open to the atmosphere with stirring at rt. The reaction was complete by TLC after 2 hours. The reaction mixture was concentrated and purified via flash chromatography eluting with pentane/EtOAc (5/1) to yield the *title compound* as a white solid (150 mg, 67%); mp 144-148 °C; FT-IR (thin film, NaCl, cm<sup>-1</sup>) 2977.6, 2958.3, 2921.6, 1637.3, 1359.6, 1166.7, 1133.9, 744.4; <sup>1</sup>H NMR (300 MHz, CDCl<sub>3</sub>); δ 1.53 (s, 9H), 2.30 (s, 3H), 2.53 (s, 3H), 4.47 (d, *J* = 15.2 Hz, 1H), 5.37 (d, 15.2 Hz, 1H), 7.17 (s, 1H), 7.40 (m, 2H), 7.50 (app dd, *J* = 7.2, 7.2 Hz, 1H), 7.58 (s, 1H), 7.94 (d, *J* = 7.8 Hz, 1H); <sup>13</sup>C NMR (75 MHz, CDCl<sub>3</sub>) δ 18.4, 21.2, 28.7, 39.3, 49.7, 122.3, 123.9, 124.9, 127.2, 128.1, 129.8, 130.9, 133.3, 134.3, 134.6, 135.5, 135.8; HRMS (EI) calcd for C<sub>20</sub>H<sub>23</sub>NO 293.1784 found 293.1780; LRMS (EI) *m/z* 293 (M<sup>+</sup>, 23), 208 (75), 192 (8), 165 (7), 85 (7).

## 5.0 APPLICATION OF FLUOROUS TECHNOLOGY TO AMIDE BOND SYNTHESIS

### 5.1 Introduction

The synthesis of amide bonds is one of the most common practices in organic chemistry, and is the backbone of peptide chemistry.<sup>90</sup> The amide bond plays a key role in biology; it is stable and can act as a hydrogen bond donor and acceptor. An in-depth analysis of the Comprehensive Medicinal Chemistry database revealed that the amide functional group exists in more than 25% of known drugs.<sup>91</sup> Accordingly, the construction of amide bonds is a popular point of diversity in the preparation of small molecule libraries and analogues.

#### 5.1.1 Carbodiimide-mediated amide bond synthesis

The typical synthetic approach to amide bond formation requires activation of the parent carboxylic acid followed by nucleophilic attack of the amine. Carbodiimides represent a widely popular class of reagents employed for achieving the coupling reaction, with the most popular being DIC (diisopropylcarbodiimide) and DCC (dicyclohexylcarbodiimide) (**Figure 29**).<sup>92</sup> An example of the carbodiimide-mediated pathway is outlined in **Scheme 20**.<sup>91</sup>



**Figure 29.** Dicyclohexylcarbodiimide (79) and diisopropylcarbodiimide (80)



the realm of high-throughput synthesis.<sup>96</sup> But the PS reagent suffers from the requirement of stoichiometric excess, the use of additives (such as HOBT), and high temperatures to reach complete conversion and acceptable yields.

### 5.1.2 Light-fluorous reagents

Fluorous technology<sup>97-106</sup> is an emerging area that is gaining popularity for what it lends to chemical synthesis -- minimization of reaction workup and isolation of the pure desired product. Any compound that qualifies as “light-fluorous” can be easily separated from organic, or “non-fluorous,” compounds by means of fluorous solid-phase extraction (F-SPE) or reverse F-SPE.<sup>107-109</sup>

Reverse F-SPE is a relatively new purification method where fluorous compounds are separated from organic compounds by means of filtration through regular silica gel, as depicted in **Figure 30**.<sup>108b</sup> A reaction mixture containing fluorous and non-fluorous components is loaded onto a plug of silica gel, and then first eluted with a fluorophilic solvent system to collect the

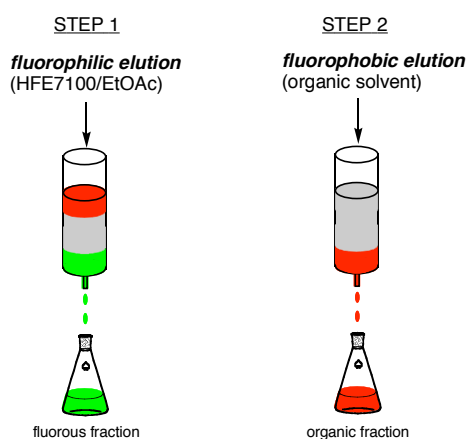


**Figure 30. Pictorial representation of reverse F-SPE over standard silica gel**

fluorous compound(s). The solvent system of choice usually consists of HFE-7100 (perfluorobutyl methyl ether) mixed with ethyl acetate or another organic solvent. Subsequently,

the organic fraction is collected by elution with a non-fluorous solvent system. Reverse F-SPE is especially attractive as a purification method when the fluorous reaction components are reagents or byproducts, since they can be eliminated in the first step, and the desired organic product can then be purified by standard flash chromatography. Furthermore, the optimum solvent system can be determined simply by conducting TLC experiments with standard TLC plates.

When conducting reverse F-SPE, perfluoroalkyl alkyl ethers (e.g. HFE-7100) are preferred over fluorocarbons for several reasons: (1) fluorocarbons have poor eluting power, and (2) fluorocarbons have poor miscibility with most organic solvents.

Use of a fluorous carbodiimide to mediate amide bond coupling was envisioned useful for the development of an efficient, solution phase protocol where the fluorous urea byproduct can be easily separated from the desired amide product.

## 5.2 Discovery and synthesis of a fluorinated carbodiimide

The main idea for synthesizing a fluorinated carbodiimide starts with imagining a molecule that is comprised of two regions: (1) a fluorous region, and (2) a carbodiimide region. Ideally, the fluorous analog will be just as chemically effective as its organic counterpart. In other words, the fluorous region of the reagent will not interfere with the reactivity of the carbodiimide functionality.

Initial attempts at synthesizing a highly fluorinated carbodiimide were successful (**Figure 31**), but reaction and separation problems arose when used in coupling reactions. The first-generation fluorous analogs of DCC and DIC, **84** and **85**, both give rise to ureas which gelled the reaction solvent. The more heavily fluorinated, second-generation diimide **86** has limited solubility in DCM and other suitable solvents.

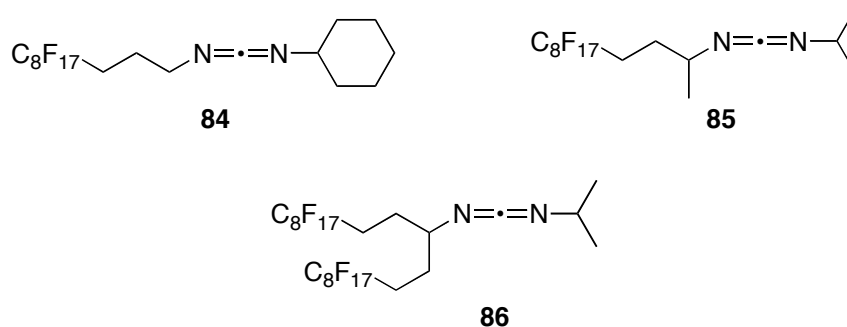


**Figure 31. First and second generation fluororous carbodiimides**

The third-generation DIC analog **87** (referred to as FDIC throughout this chapter), where the fluororous chains are installed via an ether moiety, is a colorless oil which is soluble and stable in DCM, CHCl<sub>3</sub>, Et<sub>2</sub>O, DMF, FC-72, and HFE-7100. It was found to be mostly insoluble in toluene. Furthermore, the corresponding urea (**95**) does not gel in any of the aforementioned solvents. Fluorous urea **95** is highly soluble in DCM, MeOH, THF, and HFE-7100. It is quite insoluble in FC-72, and has only limited solubility in diethyl ether, DMF, and toluene.

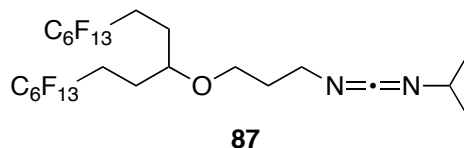
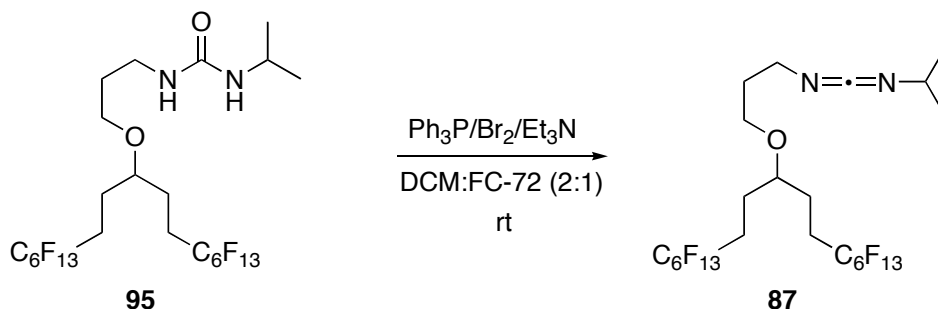


**Figure 32. Fluorous DIC analog (FDIC)**

FDIC was synthesized from the corresponding urea **95** in conjunction with FTI (Fluorous Technologies, Inc.) (**Scheme 21**). Treatment of the fluorinated octyl iodide **88** with *t*-BuLi in the presence of ethyl formate gave secondary alcohol **89** in 93% yield. Alkylation of **89** with allyl bromide provided allyl ether **90** in 92% yield. Hydroboration with 9-BBN and subsequent oxidation provided primary alcohol **91** in 67% yield. Reaction of **91** with triphenylphosphine in the presence of *N*-bromosuccinimide resulted in 92% yield of primary bromide **92**. Nucleophilic displacement of the bromine atom in **92** with the potassium salt of phthalimide and subsequent cleavage with hydrazine afforded the requisite primary amine **94** in 87% yield over the two steps. The target urea **95** was obtained in 85% by treatment of **94** with isopropyl isocyanate.



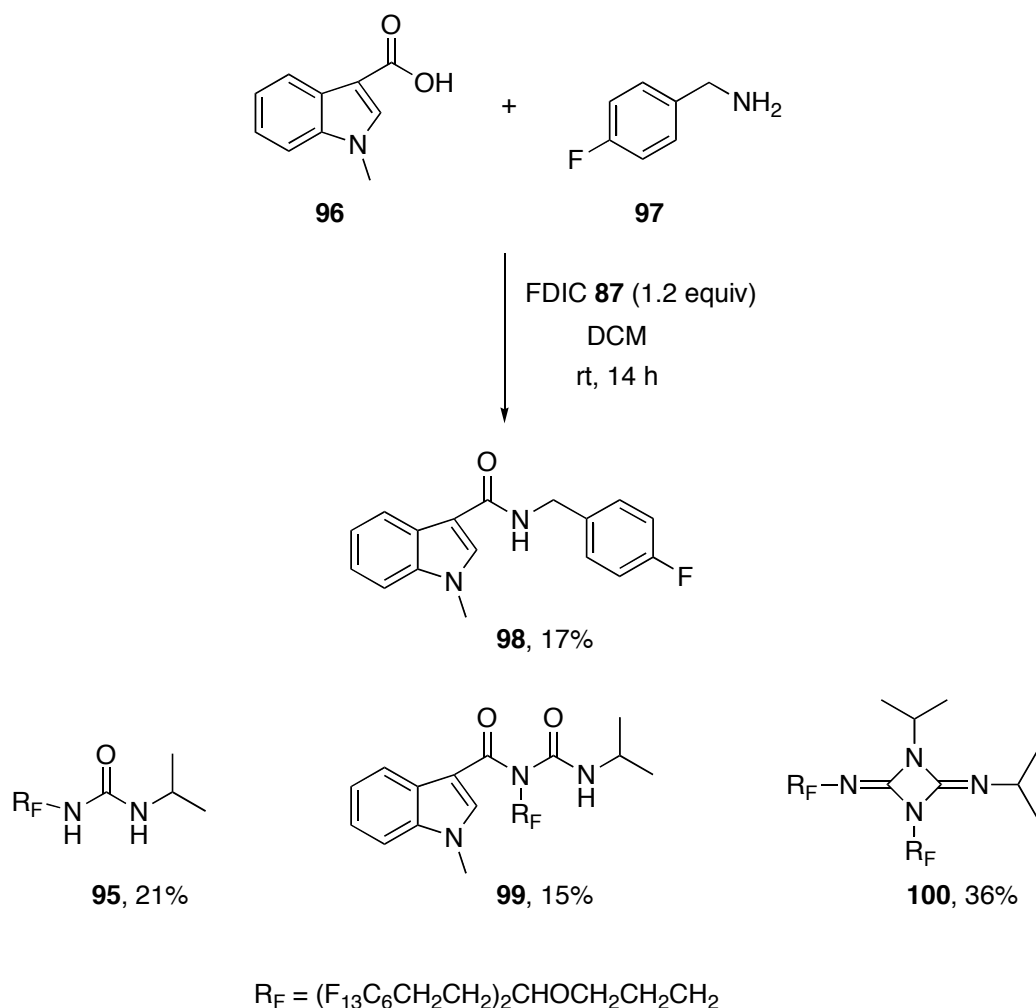


**Scheme 22.** Synthesis of FDIC **87** from fluorous urea **95**

### 5.3 Model studies with FDIC

The effectiveness of the fluorous carbodiimide in a coupling reaction was determined. This work was performed in collaboration with Dr. Carlos Pozos. FDIC **87** (1.2 equiv, 0.36 mmol) was reacted with *N*-methylindole-3-carboxylic acid **96** (1.0 equiv, 0.30 mmol) in the presence of fluorobenzyl amine **97** (1.0 equiv, 0.30 mmol), using DCM as the solvent (**Scheme 23**). After 14 h, TLC analysis of the reaction revealed four new spots: three non-polar and one polar. After separation via column chromatography, the expected amide product **98** (most polar spot) was isolated in only 17% yield, along with three less polar fluorous byproducts. These byproducts were the expected urea **95** (21%), the rearranged *N*-acyl urea **99** (15%), and a third compound **100**, believed to be the product of carbodiimide 2+2 cyclization with itself ( $^1\text{H}$ NMR and MS), in 36% yield based on FDIC.

The 2+2 cyclization of carbodiimides is a known reaction.<sup>110</sup> The  $^1\text{H}$  NMR spectrum of 2+2 product **100** show two isopropyl resonances, along with two resonances corresponding to the perfluorohexylethyl side chains. However, the LRMS of compound **100** is identical to the LRMS of FDIC. This data is consistent with the published results Hartke and Rossbach, who reported the MS spectrum of carbodiimide 2+2 products resembles that of the parent carbodiimide.<sup>110</sup>

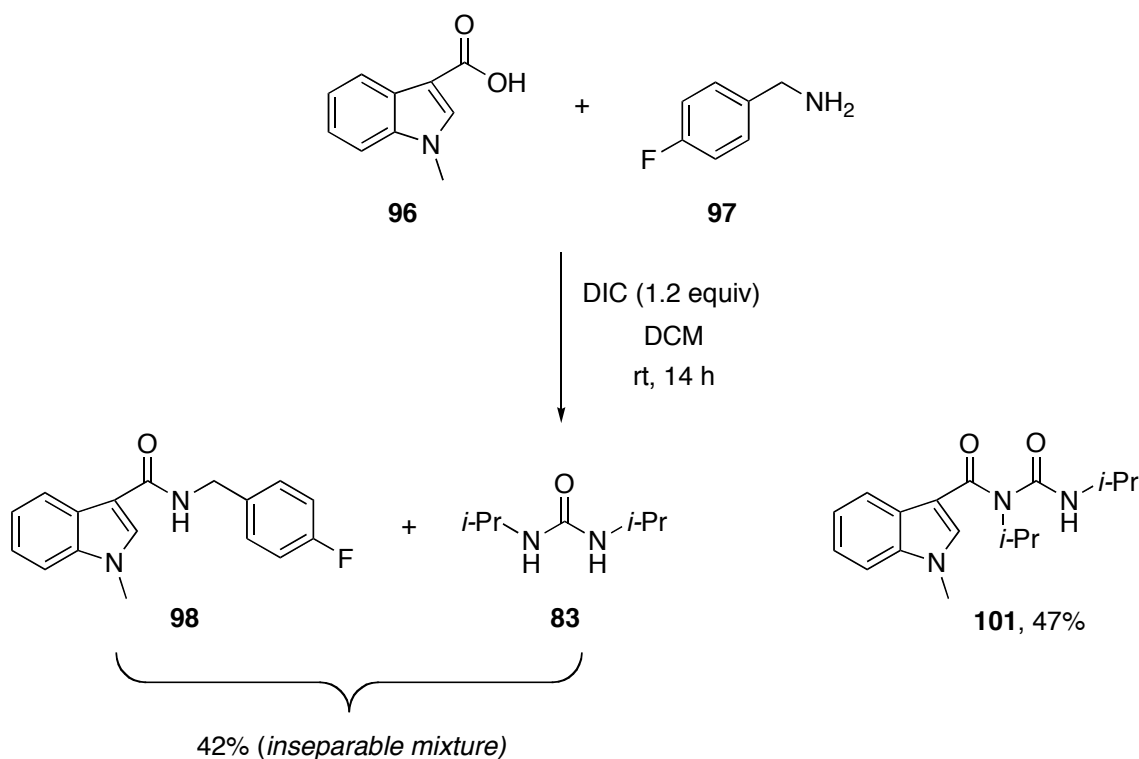


**Scheme 23. FDIC-mediated synthesis of amide 98**

The presence of byproducts **99** and **100** are due to the nature of the carboxylic acid used. If the reaction of FDIC with the carboxylic acid is slow, the amount of 2+2 product **100** increases. When the reaction of the amine with the *O*-acyl urea ester is slow, the amount of *N*-acyl urea **99** increases. Subsequent reactions with other acids gave much improved results (discussed later), which leads us to conclude that the nature of indolecarboxylic acid **96** is the reason why byproducts **99** and **100** were formed. Furthermore, Daryl Sauer and coworkers have reported that 3-indolecarboxylic acid is a poor substrate for carbodiimide coupling unless microwave conditions are used.<sup>94</sup>

While the separation of fluorous urea **89** from amide **92** was easily accomplished with column chromatography, the same cannot be said for the case where DIC was used (**Scheme 24**). As a control experiment, DIC (1.2 equiv) was reacted with indole carboxylic acid **96** (1 equiv) and fluorobenzyl amine **97** (1 equiv). The desired benzyl amide **98** and diisopropyl urea **95** were isolated in a 1:1 ratio as an inseparable mixture, in 42% yield (by weight of the mixture). The rearranged *N*-acyl urea byproduct **101** was isolated in 47% yield.

This result is comparable to when FDIC was used: the *N*-acyl urea byproduct was formed



**Scheme 24. DIC-mediated synthesis of amide 98**

in both reactions due to the poor reactivity of the indole carboxylic acid substrate. The only real difference is that the fluorous urea **95**, because of its homogenous behavior on silica gel, was completely separated from the amide product.

An additional coupling experiment was performed to ensure FDIC was not responsible for the poor yield described in the previous experiment. Cbz-glycine (0.8 mmol) and

phenethylamine (0.8 mmol) was reacted with FDIC (0.95 mmol) in DCM (2 mL), and the reaction mixture was stirred for 3 hours. After column chromatography on silica gel, the expected amide product **102** was isolated in 93% yield and analytical purity by  $^1\text{H}$  NMR. The formation of a *N*-acyl byproduct or 2+2 carbodiimide cyclization product was not observed. The yield of amide **102** is comparable to the yield obtained when DIC was used (95%), although in this case the product was contaminated with about 20 mol% of the DIC urea.

Based on the results of the control experiments, it is reasonable to conclude that the FDIC reagent can be as effective as DIC to synthesize amides from the corresponding carboxylic acid and amine. However, it is clear the FDIC urea is more easily separated from the desired amide product than is the DIC urea.

#### 5.4 Optimization of a high-throughput purification strategy

While the separation of fluoruous urea **95** with column chromatography is much more easily achieved than the non-fluorous diisopropyl urea, the real power of using a fluoruous carbodiimide is not realized unless a high-throughput SPE strategy is applied. There are two logical approaches to developing the SPE strategy for purifying FDIC mediated coupling reactions: SPE over fluoruous silica gel (standard F-SPE), or SPE over normal silica with fluoruous eluants (reverse F-SPE).

As a model for optimizing a standard F-SPE purification protocol, Cbz-glycine phenethylamide **102** was mixed with FDIC in a 1:1 molar ratio. The mixture was loaded onto a 2 g fluoruous SPE cartridge, which was subsequently eluted with MeCN/H<sub>2</sub>O (9:1). The organic fractions were concentrated and amide **102** was recovered, but as a 4:1 mixture with fluoruous urea **95** ( $^1\text{H}$  NMR). Subsequent attempts at standard F-SPE always resulted in premature elution

of fluorous urea **95** during the organic wash. This result suggests the urea functionality is sufficiently hydrophilic to compete with the inherent hydrophobic nature of the fluorous domain.

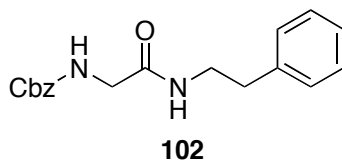


**Figure 33. Model amide employed for F-SPE optimization experiments**

Efforts were then focused on optimizing a SPE purification strategy using regular silica gel. The idea was to find an appropriate solvent system that would allow for selective elution of the fluorous material first, using fluorophilic solvents, followed by elution of the amide product. This requires a solvent system where the amide  $R_f = 0$ , or nearly zero, while the  $R_f$  of the fluorous urea is maximized.

To identify suitable solvents for reverse F-SPE, the chromatographic retention factors of amide **102** and fluorous urea **95** were compared via TLC analysis, using a variety of potential solvent systems. Selected results are compiled in **Table 7**. The highest retention factors for

**Table 7. Standard silica gel TLC retention factors for amide 102 and fluorous urea 95**

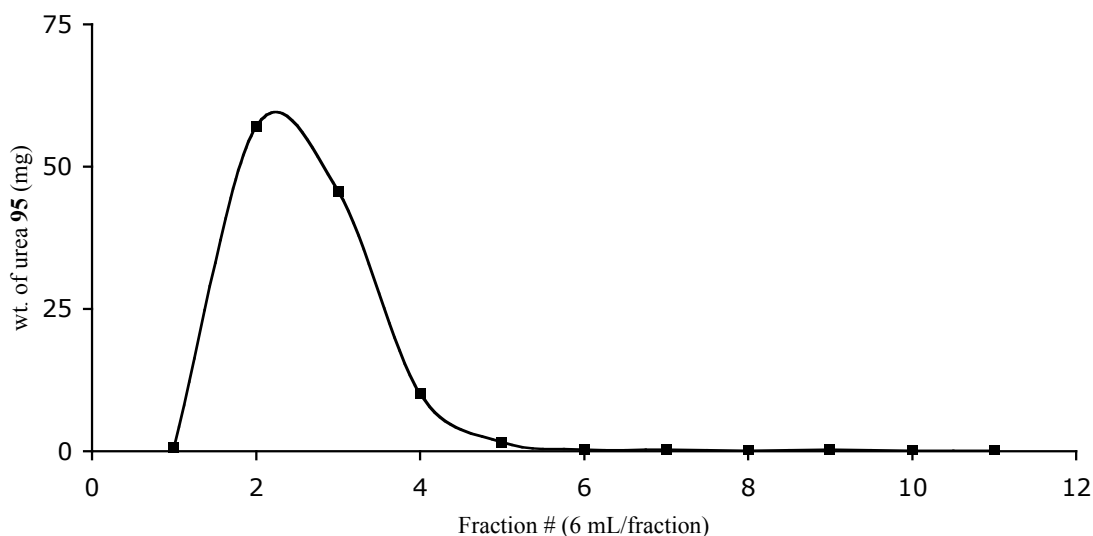
entry	solvent system	$R_f$ <b>95</b>	$R_f$ <b>102</b>
1	Hexane/EtOAc 3:1	0.38	0.21
2	HFE-7100	0.09 <sup>a</sup>	0
3	HFE-7100/MeOH 3:1	0.54	0.14 <sup>a</sup>
4	HFE-7100/EtOAc 3:1	0.48	0
5	HFE-7100/THF 3:1	0.53	0.11 <sup>a</sup>
6	HFE-7100/MeOH/EtOAc 6:1:1	0.51	0.11 <sup>a</sup>
7	HFE-7100/Et <sub>2</sub> O 3:1	0.08 <sup>a</sup>	0

<sup>a</sup> streaking observed from baseline to  $R_f$

fluorous urea **95** were observed when HFE-7100 was used as a cosolvent with MeOH, EtOAc, or THF (entries 3-6), but not when used alone. The retention factor of the model amide was minimized in entries 2,4, and 7. According to the TLC experiment, the solvent system in entry 4 is the best choice for SPE over regular silica gel.

According to the TLC analysis, the ideal solvent system is HFE-7100/EtOAc 3:1 (entry 4). The  $R_f$  of urea **95** in this case is almost 0.5, whereas the  $R_f$  of the amide is zero.

To determine the volume of solvent required to completely elute fluorous urea **95** from a SPE cartridge comprised of regular  $\text{SiO}_2$ , a model SPE was performed on a pure sample of urea. Fluorous urea **95** (117 mg, 0.14 mmol) was dissolved in THF (0.4 mL) and loaded onto  $\text{SiO}_2$  (2.5 g) in a 5 mL plastic syringe barrel. The cartridge was subsequently flushed with HFE7100/EtOAc (3/1) on a vacuum manifold until 11 fractions were collected (6 mL/fraction). Each fraction was concentrated and the amount of urea per fraction was determined by weight. The plot of mg of urea **95** versus fraction number is shown in **Figure 35**. Over 99% of the urea was accounted for in the first four fractions.



117 mg of urea **95** was dissolved in THF (0.3 mL) and loaded onto  $\text{SiO}_2$  (2.5 g), and eluted with HFE-7100/EtOAc 3:1 until 11 fractions were collected. The weight of urea **95** was measured for each fraction.

**Figure 34. Weight of fluorous urea **95** per fraction collected from SPE over standard silica gel**

About 24 mL of fluorophilic elution was necessary to eliminate the fluorous urea **95** from the SiO<sub>2</sub> cartridge.

To test the reverse F-SPE protocol, a model reaction mixture consisting of a 1:1 molar ratio of urea **95** and phenethylamide **102** was dissolved in THF (0.4 mL) and loaded onto 2.5 g of SiO<sub>2</sub> in a 5 mL plastic syringe barrel. The cartridge was eluted with HFE-7100/EtOAc 3/1 (25 mL) and then with EtOAc (18 mL). In this manner, phenylethyl amide **102** was recovered from the EtOAc fractions in 93% yield and 98% purity (<sup>1</sup>H NMR), contaminated with about 2 mol% of the fluorous urea based on integration values in the <sup>1</sup>H NMR spectrum.

### 5.5 FDIC-mediated synthesis of a small amide library

To further examine amide formation mediated by FDIC, a 3 x 5 matrix of reactions was conducted. The carboxylic acids (**103a-c**) and amines (**104a-e**) used for this exercise are shown in **Figure 35**.

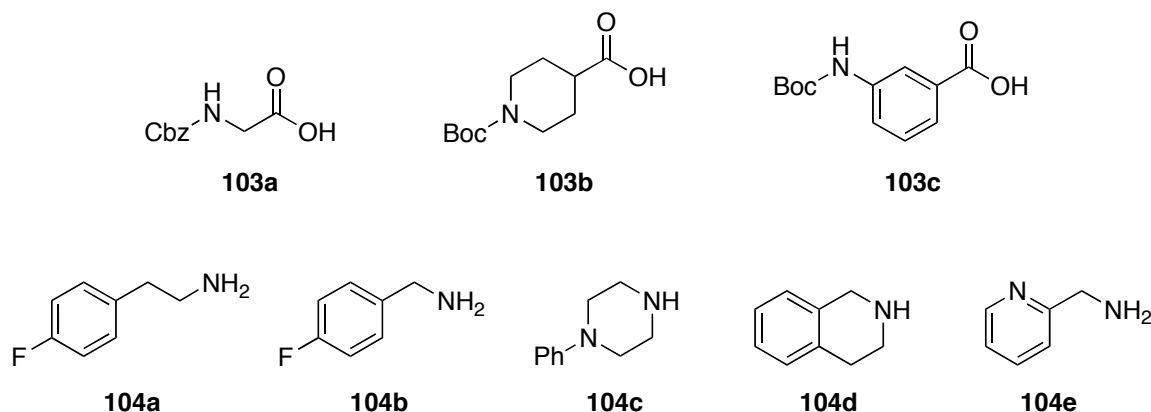


**Figure 35.** Carboxylic acids and amines used for 3x5 matrix of amide syntheses

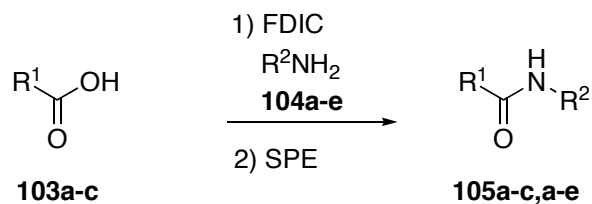
Each reaction was carried out on the same scale, and the reaction conditions (solvent, temp, etc.) were identical throughout. The general procedure is as follows: A 5 mL round bottom flask was

charged with FDIC (0.14 mmol) dissolved in DCM (2 mL). Amine **104** (0.12 mmol) was added and the resulting mixture was cooled to 0 °C under argon. After 15 minutes, carboxylic acid **103** (0.11 mmol) was added, and the reaction was warmed to rt. After stirring for 3 h, the reaction mixture was concentrated by rotary evaporation. The crude product was dissolved in a minimal amount of THF (0.4 mL) and loaded onto a 2 g SiO<sub>2</sub> cartridge. The cartridge was first washed with HFE7100/EtOAc (3:1, 36 mL) to collect the fluororous material, and subsequently washed with EtOAc (18 mL). The EtOAc fractions were evaporated in a high-speed vacuum apparatus to collect the amide product **105**.

The yields and purities of the amide products formed in the 3 x 5 library are summarized in **Table 8**. The structures of the amide products are shown in **Figure 36**. Yields were 70% or higher except for the cases where tetrahydroisoquinoline (**104d**) was used as the amine (57-61%, entries 4,9 and 14). The yields for **105ca** and **105cb** were also quite low (entries 11 and 12, respectively), but this was due to difficulties during the SPE separation. The polarity of these amides are surprisingly lower than the other 13 entries, and were obtained in only 80% purity via the SPE procedure, because they co-eluted with fluororous urea **95**. When the reactions in entries 11 and 12 were repeated and purified by flash chromatography eluting with HFE7100/EtOAc (2/1), the purities of **105ca** and **105cb** were greater than 99%. Even during flash chromatography these two amides partially co-eluted with the fluororous urea, accounting for the low yield, as the impure fractions were not kept.

The H NMR and F NMR spectra for amide **105ab** is shown in **Figure 37** and **Figure 38**, respectively, and are representative of the spectra obtained for the other amides reported in **Table 8** (Appendix C). For the amide products that contain a fluorine atom, the purity was determined by comparison of the resonance peak areas in the <sup>19</sup>F NMR spectrum. For all other amides, the purities were determined by <sup>1</sup>H NMR spectrum, by comparing the resonance peak area of the isopropyl protons from urea **95** to the peak area of a resonance of a proton from the amide.

**Table 8. 3x5 amide coupling reactions mediated by FDIC**



entry <sup>a</sup>	acid	amine	amide	yield (%)	purity (%)
1	<b>103a</b>	<b>104a</b>	<b>105aa</b>	87	95 <sup>b</sup>
2	<b>103a</b>	<b>104b</b>	<b>105ab</b>	71	99 <sup>b</sup>
3	<b>103a</b>	<b>104c</b>	<b>105ac</b>	86	95 <sup>c</sup>
4	<b>103a</b>	<b>104d</b>	<b>105ad</b>	58	95 <sup>c</sup>
5	<b>103a</b>	<b>104e</b>	<b>105ae</b>	87	99 <sup>c</sup>
6	<b>103b</b>	<b>104a</b>	<b>105ba</b>	86	98 <sup>b</sup>
7	<b>103b</b>	<b>104b</b>	<b>105bb</b>	73	98 <sup>b</sup>
8	<b>103b</b>	<b>104c</b>	<b>105bc</b>	73	95 <sup>c</sup>
9	<b>103b</b>	<b>104d</b>	<b>105bd</b>	61	95 <sup>c</sup>
10	<b>103b</b>	<b>104e</b>	<b>105be</b>	70	99 <sup>c</sup>
11	<b>103c</b>	<b>104a</b>	<b>105ca</b>	68(57)	85 <sup>b</sup> (99) <sup>b,d</sup>
12	<b>103c</b>	<b>104b</b>	<b>105cb</b>	62(45)	80 <sup>b</sup> (96) <sup>b,d</sup>
13	<b>103c</b>	<b>104c</b>	<b>105cc</b>	75	97 <sup>c</sup>
14	<b>103c</b>	<b>104d</b>	<b>105cd</b>	57	95 <sup>c</sup>
15	<b>103c</b>	<b>104e</b>	<b>105ce</b>	74	97 <sup>c</sup>

<sup>a</sup> Typical procedure: FDIC (0.14 mmol) and amine **104** were dissolved in DCM (2 mL) under argon at 0 °C. Acid **103** was added and the resulting mixture was stirred at rt for 3 h.

<sup>b</sup> Measured by <sup>19</sup>F NMR

<sup>c</sup> Measured by <sup>1</sup>H NMR

<sup>d</sup> Purified by SiO<sub>2</sub> flash chromatography

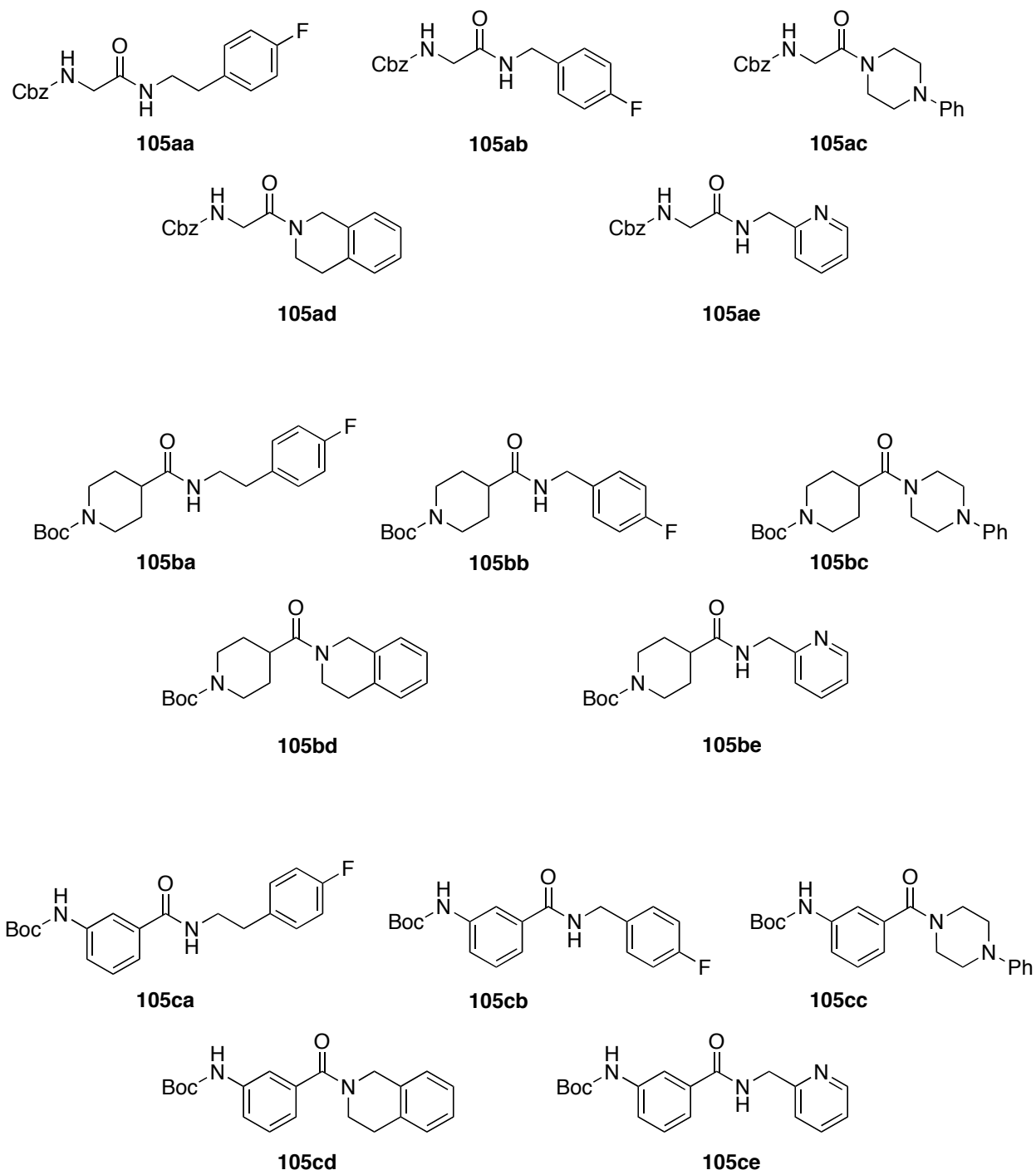


Figure 36. Amide products from 3x5 matrix of coupling reactions

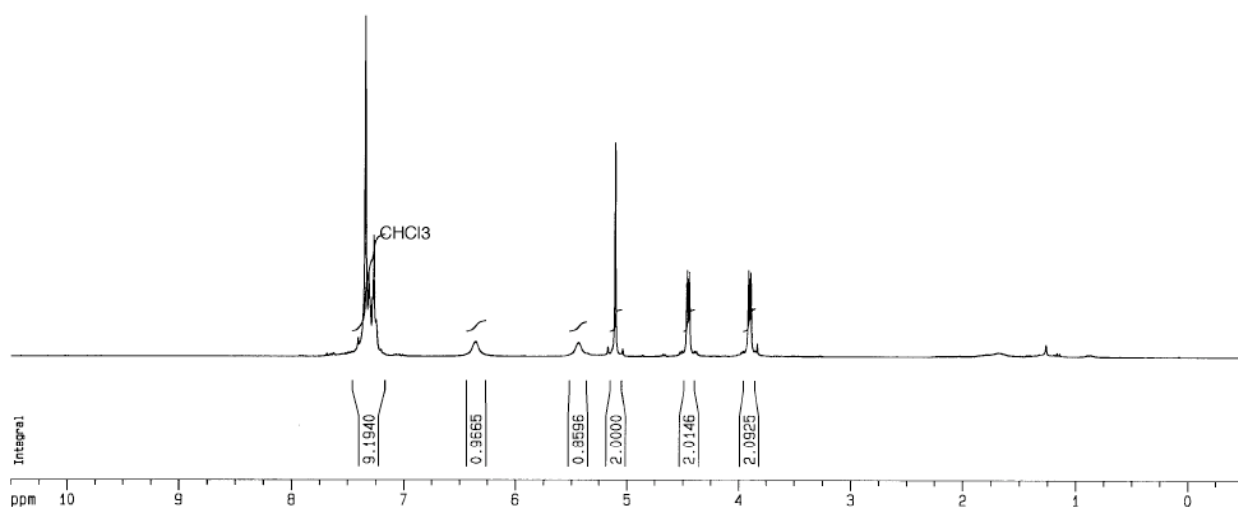


Figure 37.  $^1\text{H}$  NMR of fluorobenzyl amide 105ab

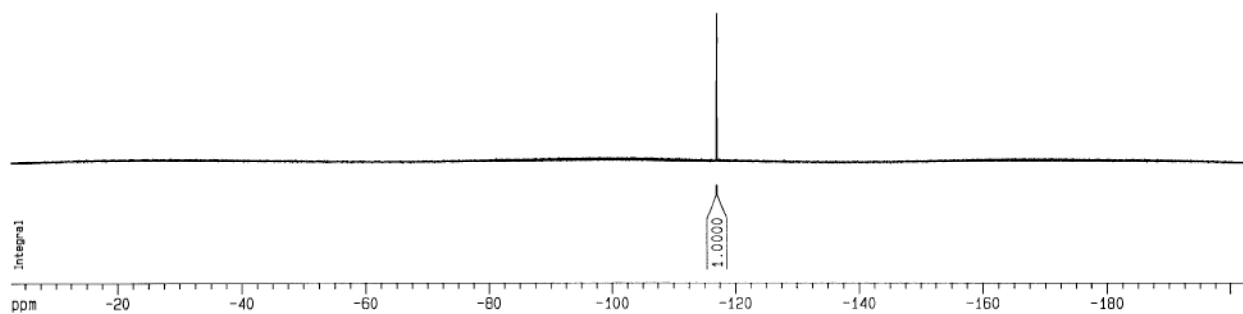


Figure 38.  $^{19}\text{F}$  NMR of fluorobenzyl amide 105ab

## 5.6 Conclusion

A fluorous carbodiimide (FDIC, **87**) was synthesized and applied to high-throughput amide forming reactions. This is part of an ongoing effort to apply fluorous technology as the solution to reactions that are traditionally problematic at the separation and purification stage.

The FDIC reagent can be as effective as DIC to promote amide bond formation, and is compatible with carboxylic acids and amines possessing a variety of functional groups. The

formation of undesired byproducts only occurs in cases where the rate of the desired coupling reaction is sluggish, regardless of whether FDIC or DIC is used.

The reverse F-SPE high-throughput purification protocol affords amide products in high purity without the use of column chromatography in the majority of the reactions we investigated. For the F-SPE protocol to be effective, the  $R_f$  of the amide product needs to be 0.05 or lower in the solvent system employed to eliminate the fluorous urea from the cartridge. In the case where the amide product is very non-polar, traditional chromatography is necessary to achieve high purity, which remains an elusive accomplishment when non-fluorous DIC is employed. FDIC, coupled with the reverse F-SPE protocol, is an attractive solution-phase alternative to PS carbodiimides and is expected to grow into a valuable tool in the realm of high-throughput amide bond synthesis.

## 5.7 Experimental

Compound **91** was synthesized, characterized, and graciously provided for this study by Fluorous Technologies, Inc.

### **3-Bromo-1-bis(perfluorohexylethyl)methoxypropane (92):**

Primary alcohol **91** (11.2 g, 14.3 mmol) was dissolved in dry dichloromethane (50 mL) in an oven-dried 200 mL pear-shaped flask and placed under argon. Triphenylphosphine (4.50 g, 17.2 mmol) was added in one portion, then *N*-bromosuccinimide (3.06 g, 17.2 mmol) was added in small portions over a 5 min period, at which point the reaction flask became warm to the touch. The reaction vessel was placed in an ice bath and allowed to stirred for about 5 min. Distilled water (50 mL) was added and the mixture became violet in color. The reaction mixture was stirred vigorously until it became reddish brown in color (5 min), at which point Et<sub>2</sub>O (150 mL) was added. The organic layer was separated and washed successively with 3% H<sub>2</sub>O<sub>2</sub> (50 mL),

H<sub>2</sub>O (50 mL), saturated Na<sub>2</sub>S<sub>2</sub>O<sub>3</sub> (50 mL), saturated NaHCO<sub>3</sub> (50 mL) and saturated brine solution (50 mL). The organic layer was dried over MgSO<sub>4</sub> and concentrated to yield crude product as a pink powder. The crude product was dissolved in hexanes (200 mL), brought to reflux, cooled to rt, and subjected to gravity filtration. The filtrate was loaded onto a thin pad of SiO<sub>2</sub>, which was eluted with hexanes (200 mL) and hexanes/Et<sub>2</sub>O (10:1, 200 mL). The resulting filtrate was concentrated via rotary evaporation to yield the *title compound* as a colorless oil (11.07 g, 92%); <sup>1</sup>H NMR (300 MHz, CDCl<sub>3</sub>) δ 1.81 (m, 4H), δ 2.09 (tt, *J* = 6.0, 6.0 Hz, 2H), δ 2.20 (m, 4H), δ 3.47 (quin, *J* = 4.6 Hz, 1H), δ 3.51 (t, *J* = 6.3 Hz, 2H), δ 3.58 (t, *J* = 5.7 Hz, 2H); <sup>13</sup>C NMR (75 MHz, CDCl<sub>3</sub>); δ 24.1, 26.6 (t, *J* = 22.1 Hz), 30.0, 32.6, 66.1, 76.6.

**2-(3-(bis(Perfluorohexylethyl)methoxy)propyl)isoindoline-1,3-dione (93):**

Primary bromide **92** (10.84 g, 12.8 mmol) was dissolved in dry DMF (50 mL) in a 250 mL round-bottom flask. Potassium phthalimide (4.76 g, 25.7 mmol) was added, the rxn vessel was sealed with a rubber septum and electrical tape. The resulting mixture was heated to 85 °C in an oil bath with stirring for 16 h. The mixture was cooled to rt, transferred to a 2 L separatory funnel, and diluted with Et<sub>2</sub>O (500 mL), H<sub>2</sub>O (300 mL), and 1 M NaOH (100 mL). The Et<sub>2</sub>O layer was collected and the aqueous layer was extracted once more with Et<sub>2</sub>O (200 mL). The Et<sub>2</sub>O layers were combined and washed with 0.4 N NaOH (2x300 mL) and saturated Na<sub>2</sub>S<sub>2</sub>O<sub>3</sub> (50 mL). The Et<sub>2</sub>O layer was dried over MgSO<sub>4</sub> and concentrated via rotary evaporation to yield the crude product as a yellow oil. The crude was purified via column chromatography eluting with hexanes/EtOAc (9:1) to provide the *title compound* as a yellow oil (10.94 g, 94%); <sup>1</sup>H NMR (300 MHz, CDCl<sub>3</sub>); δ 1.73 (m, 4H), δ 1.98 (tt, *J* = 6.3, 6.3 Hz, 2H), δ 2.19 (m, 4H), δ 3.43 (quin, *J* = 4.3 Hz, 1H), δ 3.47 (t, *J* = 5.8 Hz, 2H), δ 3.78 (t, *J* = 6.6 Hz, 2H), δ 7.69 (dd, *J* = 5.4, 3.1 Hz, 2H), δ 7.82 (dd, *J* = 5.5, 3.1 Hz, 2H); <sup>13</sup>C NMR (75 MHz, CDCl<sub>3</sub>); δ 23.9, 26.4 (t, *J* = 22.4 Hz), 29.0, 35.3, 76.7, 123.1, 132.2, 133.9, 168.4.

### **3-bis(Perfluorohexylethyl)methoxypropan-1-amine (94):**

Alkyl phthalimide **93** (10.67 g, 11.7 mmol) was dissolved in EtOH (90 mL) in a 200 mL pear-shaped flask and the vessel was flushed with argon. Hydrazine hydrate (51% hydrazine, 5.7 mL, 117.0 mmol) was added in one portion. The flask was fitted with a reflux condenser and the mixture was refluxed at 78 °C with stirring. A significant amount of white insoluble material was evident after heating for 18 hrs. After 2 d, the mixture was allowed to cool to rt before adding 2 N NaOH (100 mL). The resulting mixture was stirred at rt until the white solid had completely dissolved, and then subsequently extracted with Et<sub>2</sub>O. The ether layer was washed with 1 M NaOH (2x100 mL), H<sub>2</sub>O (2x100 mL), brine (100 mL), dried over MgSO<sub>4</sub> and filtered. The resulting ether layer was concentrated via rotary evaporation and dried under vacuum to provide the *title compound* as a clear oil (8.53 g, 93%); <sup>1</sup>H NMR (300 MHz, CDCl<sub>3</sub>); δ 1.35 (bs, 2H), δ 1.72 (tt, *J* = 6.6, 6.6 Hz, 2H), δ 1.82 (m, 4H), δ 2.16 (m, 4H), δ 2.81 (t, *J* = 6.9 Hz, 2H), δ 3.44 (quin, *J* = 5.0 Hz, 1H), δ 3.51 (t, *J* = 6.2 Hz, 2H).

### **1-(3-bis(Perfluorohexylethyl)methoxy)propyl)-3-isopropylurea (95):**

Primary amine **94** (8.46 g, 10.8 mmol) was dissolved in dry dichloromethane (70 mL) in a 250 mL round-bottom flask and placed under argon. Isopropyl isocyanate (1.15 mL, 11.7 mmol) was added dropwise over 5 min, and the resulting mixture was stirred at rt for 30 min. The reaction mixture was concentrated via rotary evaporation and dissolved in Et<sub>2</sub>O and 1 M HCl (100 mL) and stirred for 2 h. The ether layer was extracted and washed with 1 M HCl (50 mL), H<sub>2</sub>O (100 mL), and saturated brine (100 mL). The resulting ether layer was dried over MgSO<sub>4</sub>, filtered and concentrated via rotary evaporation to yield the crude product as an orange solid (9.56 g). The crude product was purified by flash chromatography eluting with pentane/ether (1:1) to yield the *title compound* as a pale yellow solid (8.01 g, 85%); IR (thin film, CH<sub>2</sub>Cl<sub>2</sub>, KCl, cm<sup>-1</sup>) 3308.3, 2971.0, 1634.1, 1568.4, 1512.3, 1456.1, 1367.1, 1318.8, 1027.2, 731.4, 707.8, 697.8, 653.4; <sup>1</sup>H NMR (300 MHz, CDCl<sub>3</sub>) δ 1.14 (d, *J* = 6.4 Hz, 6H), δ 1.78 (tt, *J* = 6.0, 6.0 Hz, 2H), δ 1.79 (m, 4H), δ 2.16 (m, 4H), δ 3.27 (dt, *J* = 6.7, 6.7 Hz, 2H), δ 3.46 (quin, *J* = 5.8 Hz, 1H), δ 3.51 (t, *J* =

6.0 Hz, 2H),  $\delta$  3.81 (dsept,  $J = 6.5, 1.2$  Hz, 1H),  $\delta$  4.14 (d,  $J = 7.7$  Hz, 1H),  $\delta$  4.49 (t,  $J = 5.3$  Hz, 1H);  $^{13}\text{C}$  NMR (75 MHz,  $\text{CDCl}_3$ );  $\delta$  23.3, 24.0, 26.5 (t, 22.5 Hz), 30.6, 37.9, 42.1, 67.2, 76.5, 157.8;  $^{19}\text{F}$  NMR (282.3 MHz,  $\text{CDCl}_3$ );  $\delta$  -126.5, -123.7, -123.3, -122.3, -114.6, -81.2; HRMS (EI) calcd for  $\text{C}_{24}\text{H}_{25}\text{N}_2\text{O}_2\text{F}_{26}$  867.1501, found 867.1509; LRMS (EI)  $m/z$  889 (6), 867 ( $\text{M}^+$ , 100), 782 (25).

### **3-bis(Perfluorohexylethyl)methoxy-*N*-((isopropylimino)methylene)propan-1-amine**

#### **(87, FDIC):**

Fluorous urea **95** (1.00 g, 1.15 mmol) and triphenylphosphine (908 mg, 3.46 mmol) were dissolved in dry dichloromethane (20 mL) and FC-72 (10 mL) in a flame dried 50 mL round-bottom flask with stirring. The resulting biphasic mixture was placed under argon and cooled to 0 °C in an ice bath. Bromine (0.18 mL, 3.46 mmol) was added dropwise via syringe until a yellow color persisted in the DCM layer, followed by the subsequent dropwise addition of triethylamine (0.31 mL, 2.31 mmol). The resulting mixture was allowed to stir at 0 °C for 15 min, then warmed to rt and stirred for an additional 12 h, at which time a dark red color was observed in the DCM layer. The reaction mixture was filtered, the FC-72 layer was separated, and the DCM layer was further extracted with FC-72 (2x20 mL). The FC-72 layers were combined and concentrated via rotary evaporation to a volume of about 10 mL, and subsequently filtered through a small plug of celite. The filtrate was concentrated via rotary evaporation and dried under vacuum to afford the *title compound* as a clear oil (906 mg, 93%), and was used without further purification; IR (neat, KCl,  $\text{cm}^{-1}$ ) 2973.5, 2126.2, 1317.3, 1239.4, 1145.1, 731.1, 707.8, 697.4;  $^1\text{H}$  NMR (300 MHz,  $\text{CDCl}_3$ )  $\delta$  1.21 (d,  $J = 6.4$  Hz, 6H),  $\delta$  1.81 (tt,  $J = 6.1, 6.1$  Hz, 2H),  $\delta$  1.79 (m, 4H),  $\delta$  2.15 (m, 4H),  $\delta$  3.33 (t,  $J = 6.6$  Hz, 2H),  $\delta$  3.45 (quin,  $J = 5.2$  Hz, 1H),  $\delta$  3.52 (t,  $J = 6.1$  Hz, 2H),  $\delta$  3.54 (sept,  $J = 6.4$  Hz, 1H);  $^{13}\text{C}$  NMR (75 Mhz,  $\text{CDCl}_3$ )  $\delta$  24.1, 24.6, 26.6 (t,  $J = 22.3$  Hz), 31.6, 43.7, 49.0, 66.0, 76.6, 140.1;  $^{19}\text{F}$  NMR (470.47 Hz,  $\text{CDCl}_3$ )  $\delta$  -78.8, -112.2, -119.9, -120.8, -121.3, -124.1; HRMS (EI) calcd for  $\text{C}_{24}\text{H}_{23}\text{N}_2\text{OF}_{26}$  849.1395, found 849.1320; LRMS (EI)  $m/z$  1697 (12), 849 ( $\text{M}^{++}$ , 100), 807 (20).

***N*-(4-Fluorobenzyl)-1-methylindole-3-carboxamide (98):**

FDIC **87** (309 mg, 0.36 mmol) and 4-fluorobenzylamine **97** (34  $\mu$ L, 0.30 mmol) were added to a 10 mL flame-dried round bottom flask. 1-Methylindole-3-carboxylic acid **96** (52.5 mg, 0.30 mmol) in dry dichloromethane (10 mL) was added and the resulting mixture was stirred under argon for 3 h. The rxn mixture was concentrated via rotary evaporation and purified by flash chromatography eluting with hexanes ether (5/1) to yield the *title compound* as a white solid (14 mg, 17%,  $R_f$  = 0.29), alongside **99** (42 mg, 15%,  $R_f$  = 0.87), **100** (109 mg, 36% based on FDIC,  $R_f$  = 0.75) and **95** (61 mg, 21%,  $R_f$  = 0.53);  $^1\text{H}$  NMR (300 MHz,  $\text{CDCl}_3$ )  $\delta$  3.79 (s, 3H),  $\delta$  4.65 (d,  $J$  = 5.6 Hz, 2H),  $\delta$  6.32 (bs, 1H),  $\delta$  7.02 (t,  $J$  = 8.7, 2H), 7.30 (m, 5H),  $\delta$  7.67 (s, 1H),  $\delta$  7.94 (dd,  $J$  = 7.3, 1.7 Hz, 1H).

**1-(3-bis(Perfluorohexylethyl)methoxy)propyl-3-isopropyl-1-(1-methylindole-3-carbonyl)urea (99):**

Colorless oil;  $^1\text{H}$  NMR (300 MHz,  $\text{CDCl}_3$ )  $\delta$  1.18 (d,  $J$  = 6.5 Hz, 6H),  $\delta$  1.68 (m, 4H),  $\delta$  1.91 (tt,  $J$  = 6.8 Hz, 2H),  $\delta$  2.00 (m, 4H),  $\delta$  3.20 (quin,  $J$  = 6.0 Hz, 1H),  $\delta$  3.40 (t, 6.1 Hz, 2H),  $\delta$  3.83 (s, 3H),  $\delta$  4.02 (dsept,  $J$  = 6.8, 6.8 Hz, 1H),  $\delta$  4.14 (t,  $J$  = 6.9 Hz, 2H),  $\delta$  7.26 (app ddd,  $J$  = 7.1, 7.1, 1.6 Hz, 2H),  $\delta$  7.32 (app dd,  $J$  = 6.7 1.3 Hz, 1H),  $\delta$  7.35 (app ddd,  $J$  = 7.1, 7.1, 1.2 Hz, 2H),  $\delta$  7.85 (app dd,  $J$  = 7.4, 1.6 Hz, 1H),  $\delta$  8.57 (bd,  $J$  = 7.3 Hz, 1H).

**(*Z*)-3-bis(Perfluorohexylethyl)methoxy-*N*-(1-(3-bis(perfluorohexylethyl)methoxy)propyl)-3-isopropyl-4-(isopropylimino)-1,3-diazetidino-2-ylidene)propan-1-amine (100):**

Colorless oil;  $^1\text{H}$  NMR (300 MHz,  $\text{CDCl}_3$ )  $\delta$  1.16 (app d,  $J$  = 5,7 Hz, 6H),  $\delta$  1.28 (app d,  $J$  = 6.6 Hz, 6H),  $\delta$  1.81 (bm, 12H),  $\delta$  2.17 (bm, 8H),  $\delta$  3.48 (m, 10 H),  $\delta$  3.75 (m, 2H); LRMS (EI)  $m/z$  1697 ( $\text{M}^+$ , 25), 1573 (15), 1571 (52), 850 (35), 849 (100), 807 (5).

**General procedure for the synthesis of amides 105a-c,a-e: Synthesis of benzyl 2-(4-fluorophenethylamino)-2-oxoethylcarbamate (105aa):**

A 5 mL round-bottom flask was charged with FDIC **87** (86 mg, 0.10 mmol) dissolved in DCM (2 mL). Amine **104a** (11  $\mu$ L, 0.083 mmol) was added and the resulting mixture was cooled to 0 °C under argon. After 15 min, carboxylic acid **103a** (17 mg, 0.083 mmol) was added, and the reaction was warmed to rt. After stirring for 3 h, the rxn mixture was concentrated via rotary evaporation. The crude material was dissolved in THF (0.4 mL) and loaded onto a 2 g SiO<sub>2</sub> cartridge. The cartridge was first washed under vacuum manifold with HFE7100 (3/1, 36 mL), and subsequently washed with EtOAc (12 mL). The EtOAc fractions were evaporated in a high-speed vacuum apparatus to provide the *title compound* as a white solid (24 mg, 87%); <sup>1</sup>H NMR (300 MHz, CDCl<sub>3</sub>)  $\delta$  2.77 (app t,  $J$  = 6.4 Hz, 2H),  $\delta$  3.46 (app dt,  $J$  = 6.6, 6.4 Hz, 2H),  $\delta$  3.80 (d,  $J$  = 5.6 Hz, 2H),  $\delta$  5.11 (s, 2H),  $\delta$  5.41 (bs, 1H),  $\delta$  6.09 (bs, 1H),  $\delta$  7.00 (app t,  $J$  = 8.6 Hz, 2H),  $\delta$  7.10 (m, 2H),  $\delta$  7.35 (app s, 5H).

**Benzyl 2-(4-fluorobenzylamino)-2-oxoethylcarbamate (105ab):**

Using carboxylic acid **103a** and amine **104b**, the *title compound* was provided in 71% yield; <sup>1</sup>H NMR (300 MHz, CDCl<sub>3</sub>)  $\delta$  3.90 (d,  $J$  = 5.7 Hz, 2H),  $\delta$  4.45 (d,  $J$  = 5.7 Hz, 2H),  $\delta$  5.11 (s, 2H),  $\delta$  5.44 (bs, 1H),  $\delta$  6.35 (bs, 1H),  $\delta$  7.31 (m, 9H).

**Benzyl 2-oxo-2-(4-phenylpiperazin-1-yl)ethylcarbamate (105ac):**

Using carboxylic acid **103a** and amine **104c**, the *title compound* was provided in 86% yield; <sup>1</sup>H NMR (300 MHz, CDCl<sub>3</sub>)  $\delta$  3.15 (app dd,  $J$  = 5.1, 5.1 Hz, 2H),  $\delta$  3.19 (app dd,  $J$  = 5.1, 5.1 Hz, 2H),  $\delta$  3.55 (dd,  $J$  = 5.1, 5.1 Hz, 2H),  $\delta$  3.79 (dd,  $J$  = 5.0, 5.0 Hz, 2H),  $\delta$  4.07 (d,  $J$  = 4.6 Hz, 2H),  $\delta$  5.84 (bs, 1H),  $\delta$  6.92 (m, 3H),  $\delta$  7.31 (m, 7H).

**Benzyl 2-(3,4-dihydroisoquinolin-2(1H)-yl)-2-oxoethylcarbamate (105ad):**

Using carboxylic acid **103a** and amine **104d** the *title compound* was isolated in 58% yield;  $^1\text{H}$  NMR (300 MHz,  $\text{CDCl}_3$ )  $\delta$  2.79 (t,  $J = 6.0$  Hz, 1H),  $\delta$  2.84 (t,  $J = 5.8$  Hz, 1H),  $\delta$  3.54 (t,  $J = 5.9$  Hz, 1H),  $\delta$  3.77 (t,  $J = 5.9$  Hz, 1H),  $\delta$  4.04 (t,  $J = 4.7$  Hz, 2H),  $\delta$  4.47 (s, 1H),  $\delta$  4.67 (s, 1H),  $\delta$  5.06 (s, 2H),  $\delta$  5.80 (bs, 1H),  $\delta$  7.18 (m, 9H).

**Benzyl 2-oxo-2-(pyridin-2-ylmethylamino)ethylcarbamate (105ae):**

Using carboxylic acid **103a** and amine **104e** the *title compound* was isolated in 87% yield;  $^1\text{H}$  NMR (300 MHz,  $\text{CDCl}_3$ )  $\delta$  3.90 (d,  $J = 5.8$  Hz, 2H),  $\delta$  4.46 (d,  $J = 5.9$  Hz, 2H),  $\delta$  5.10 (s, 2H),  $\delta$  5.55 (bs, 1H),  $\delta$  6.73 (bs, 1H),  $\delta$  7.32 (m, 6H),  $\delta$  7.63 (d,  $J = 7.7$  Hz, 1H),  $\delta$  8.52 (app s, 2H).

***tert*-Butyl 4-((4-fluorophenethyl)carbamoyl)piperidine-1-carboxylate (105ba):**

Using carboxylic acid **103b** and amine **104a** the *title compound* was isolated in 86% yield;  $^1\text{H}$  NMR (300 MHz,  $\text{CDCl}_3$ )  $\delta$  1.45 (s, 9H),  $\delta$  1.57 (app dddd,  $J = 11.9, 11.9, 11.9, 4.2$  Hz, 2H),  $\delta$  1.74 (app dd,  $J = 12.9, 2.5$  Hz, 2H),  $\delta$  2.16 (tt,  $J = 11.6, 3.8$  Hz, 1H),  $\delta$  2.71 (bt,  $J = 11.5$  Hz, 2H),  $\delta$  2.79 (t,  $J = 6.9$  Hz, 2H),  $\delta$  3.49 (dt,  $J = 6.8, 6.8$  Hz, 2H),  $\delta$  4.16 (bs, 2H),  $\delta$  5.61 (bs, 1H),  $\delta$  7.00 (t,  $J = 8.7$  Hz, 2H),  $\delta$  7.13 (d,  $J = 8.5, 5.5$  Hz, 2H).

***tert*-Butyl 4-((4-fluorobenzyl)carbamoyl)piperidine-1-carboxylate (105bb):**

Using carboxylic acid **103b** and amine **104b** the *title compound* was isolated in 73% yield;  $^1\text{H}$  NMR (300 MHz,  $\text{CDCl}_3$ )  $\delta$  1.38 (s, 9H),  $\delta$  1.58 (app dddd,  $J = 11.9, 11.9, 11.9, 4.4$  Hz, 2H),  $\delta$  1.76 (app dddd,  $J = 2.5, 2.5, 2.5, 13.0$  Hz, 2H),  $\delta$  2.18 (app tt,  $J = 11.6, 3.8$  Hz, 1H),  $\delta$  2.66 (app bt,  $J = 11.9$  Hz, 2H),  $\delta$  4.09 (bs, 2H),  $\delta$  4.34 (d,  $J = 5.7$  Hz, 2H),  $\delta$  5.70 (bs, 1H),  $\delta$  6.94 (t,  $J = 8.7$  Hz, 2H),  $\delta$  7.15 (m, 2H).

***tert*-Butyl 4-(1-phenylpiperazine-4-carbonyl)piperidine-1-carboxylate (105bc):**

Using carboxylic acid **103b** and amine **104c** the *title compound* was isolated in 73% yield; <sup>1</sup>H NMR (300 MHz, CDCl<sub>3</sub>) δ 1.39 (s, 9H), δ 1.66 (m, 4H), δ 2.60 (tt, *J* = 10.2, 4.9 Hz, 1H), δ 2.71 (t, *J* = 12.3 Hz, 2H), δ 3.10 (m, 4H), δ 3.66 (m, 4H), δ 4.10 (m, 2H), δ 6.85 (m, 3H), δ 7.22 (dd, *J* = 8.7, 7.1 Hz, 2H).

***tert*-Butyl 4-(1,2,3,4-tetrahydroisoquinoline-2-carbonyl)piperidine-1-carboxylate (105bd):**

Using carboxylic acid **103b** and amine **104d** the *title compound* was isolated in 61% yield; <sup>1</sup>H NMR (300 MHz, CDCl<sub>3</sub>) δ 1.39 (s, 9H), δ 1.66 (m, 4H), δ 2.75 (m, 5H), δ 3.67 (t, *J* = 5.9 Hz, 1H), δ 3.77 (bs, 1H), δ 4.09 (m, 2H), δ 4.60 (s, 1H), δ 4.66 (s, 1H), δ 7.13 (m, 4H).

***tert*-Butyl 3-((4-fluorophenethyl)carbamoyl)phenylcarbamate (105ca):**

Using carboxylic acid **103c** and amine **104a** the *title compound* was isolated in 57% yield after flash chromatography (HFE7100/EtOAc 2:1); <sup>1</sup>H NMR (300 MHz, CDCl<sub>3</sub>) δ 1.53 (s, 9H), δ 2.90 (t, *J* = 7.0 Hz, 2H), δ 3.67 (dt, *J* = 6.9, 6.9 Hz, 2H), δ 6.15 (bs, 1H), δ 6.56 (bs, 1H), δ 7.02 (app t, *J* = 8.7 Hz, 2H), δ 7.20 (dd, *J* = 8.6, 5.4 Hz, 2H), δ 7.34 (m, 2H), δ 7.45 (ddd, *J* = 7.3, 2.0, 2.0 Hz, 1H), δ 7.78 (app dd, *J* = 1.7, 1.7 Hz, 1H).

***tert*-Butyl 3-((4-fluorobenzyl)carbamoyl)phenylcarbamate (105cb):**

Using carboxylic acid **103c** and amine **104b** the *title compound* was isolated in 45% yield after flash chromatography (HFE7100/EtOAc 2:1); <sup>1</sup>H NMR (300 MHz, CDCl<sub>3</sub>) δ 1.52 (s, 9H), δ 4.61 (d, *J* = 5.8 Hz, 2H), δ 6.42 (bs, 1H), δ 6.56 (bs, 1H), δ 7.03 (app t, *J* = 8.6 Hz, 2H), δ 7.33 (m, 3H), δ 7.47 (m, 2H), δ 7.84 (dd, *J* = 1.8, 1.8 Hz, 1H).

***tert*-Butyl 3-(1-phenylpiperazine-4-carbonyl)phenylcarbamate (105cc):**

Using carboxylic acid **103c** and amine **104c** the *title compound* was isolated in 75% yield; <sup>1</sup>H NMR (300 MHz, CDCl<sub>3</sub>) δ 1.52 (s, 9H), δ 3.15 (bs, 2H), δ 3.24 (bs, 2H), 3.61 (bs, 2H), δ 3.92

(bs, 2H),  $\delta$  6.63 (bs, 1H),  $\delta$  6.92 (m, 3H),  $\delta$  7.08 (ddd,  $J = 7.5, 1.2, 1.2$  Hz, 1H),  $\delta$  7.31 (m, 3H),  $\delta$  7.45 (m, 2H).

***tert*-Butyl 3-(1,2,3,4-tetrahydroisoquinoline-2-carbonyl)phenylcarbamate (105cd):**

Using carboxylic acid **103c** and amine **104d** the *title compound* was isolated in 57% yield as a white solid;  $^1\text{H}$  NMR (300 MHz,  $\text{CDCl}_3$ )  $\delta$  1.45 (s, 9H),  $\delta$  2.83 (bm, 2H),  $\delta$  3.55 (bs, 1H),  $\delta$  3.90 (bs, 1H),  $\delta$  4.51 (bs, 1H),  $\delta$  4.81 (bs, 1H),  $\delta$  6.47 (bs, 1H),  $\delta$  7.13 (m, 8H).

***tert*-Butyl 3-((pyridin-2-ylmethyl)carbamoyl)phenylcarbamate (105ce):**

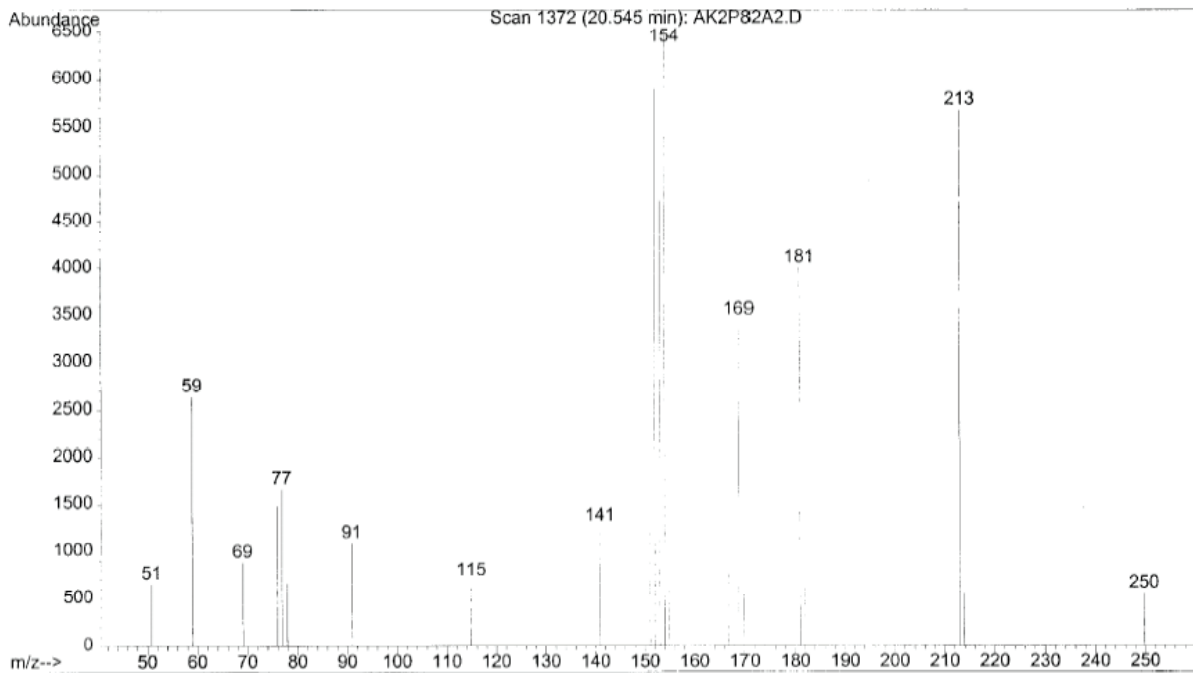
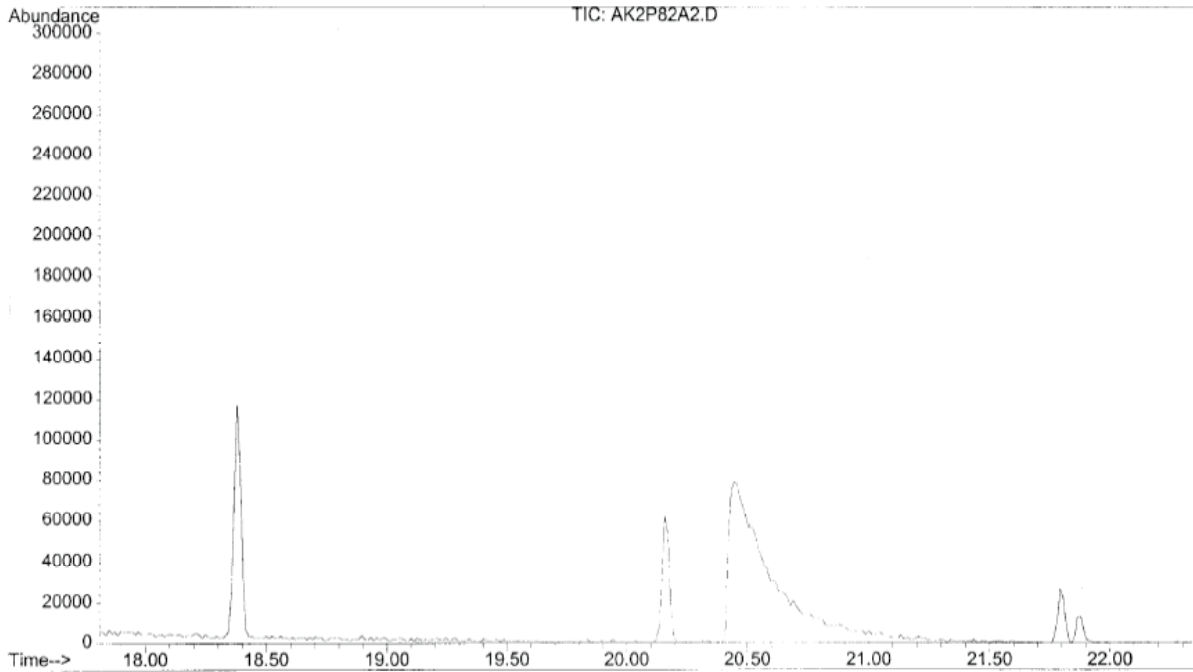
Using carboxylic acid **103c** and amine **104e** the *title compound* was isolated in 74% yield;  $^1\text{H}$  NMR (300 MHz,  $\text{CDCl}_3$ )  $\delta$  1.51 (s, 9H),  $\delta$  4.65 (d,  $J = 6.0$  Hz, 2H),  $\delta$  6.64 (bs, 1H),  $\delta$  6.72 (bs, 1H),  $\delta$  7.32 (m, 2H),  $\delta$  7.48 (m, 2H),  $\delta$  7.71 (app d,  $J = 7.8$  Hz, 1H),  $\delta$  7.88 (app dd,  $J = 1.7, 1.7$  Hz, 1H),  $\delta$  8.54 (app d,  $J = 3.8$  Hz, 1H),  $\delta$  8.60 (bs, 1H).

## **APPENDIX A**

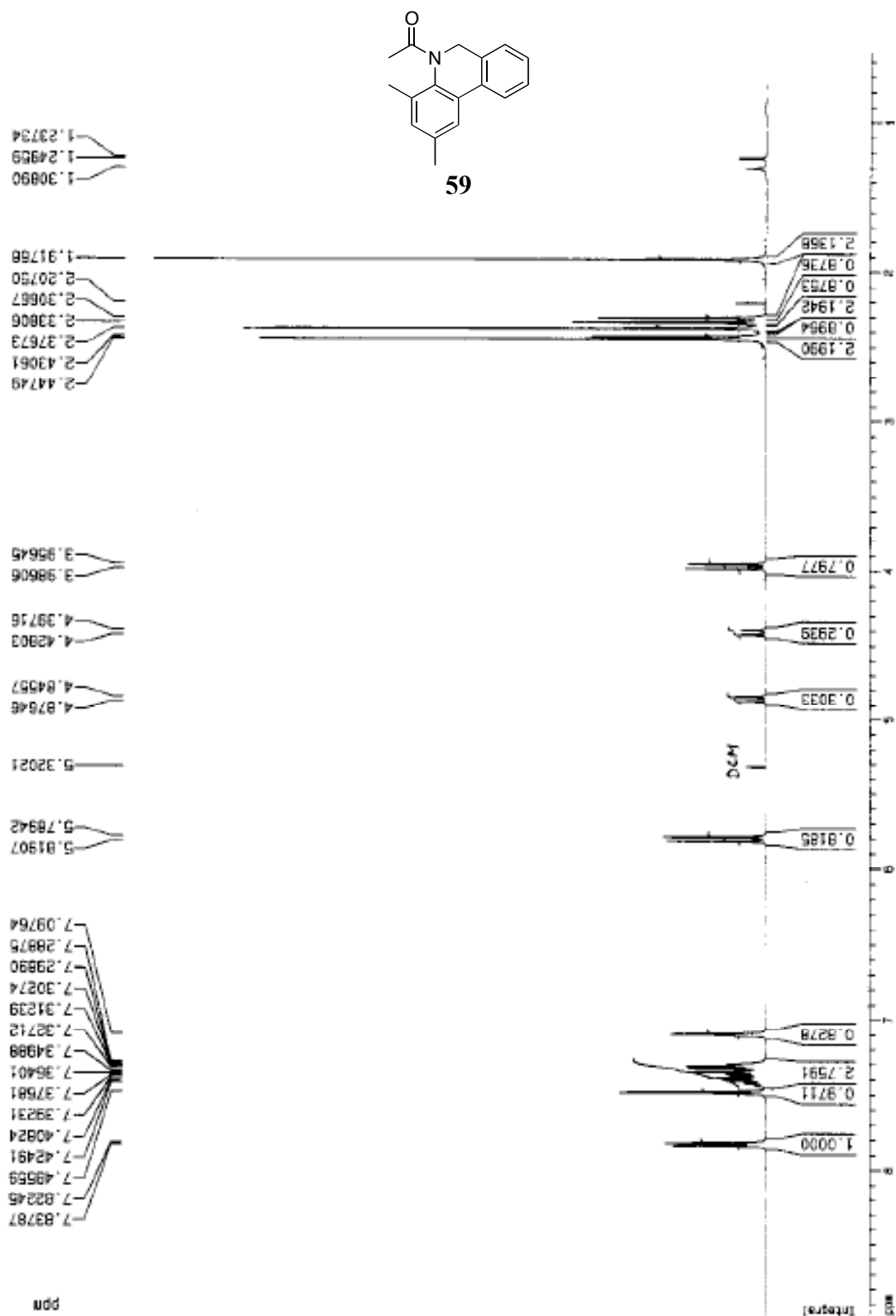
### **CHAPTER 2 SUPPORTING DATA**

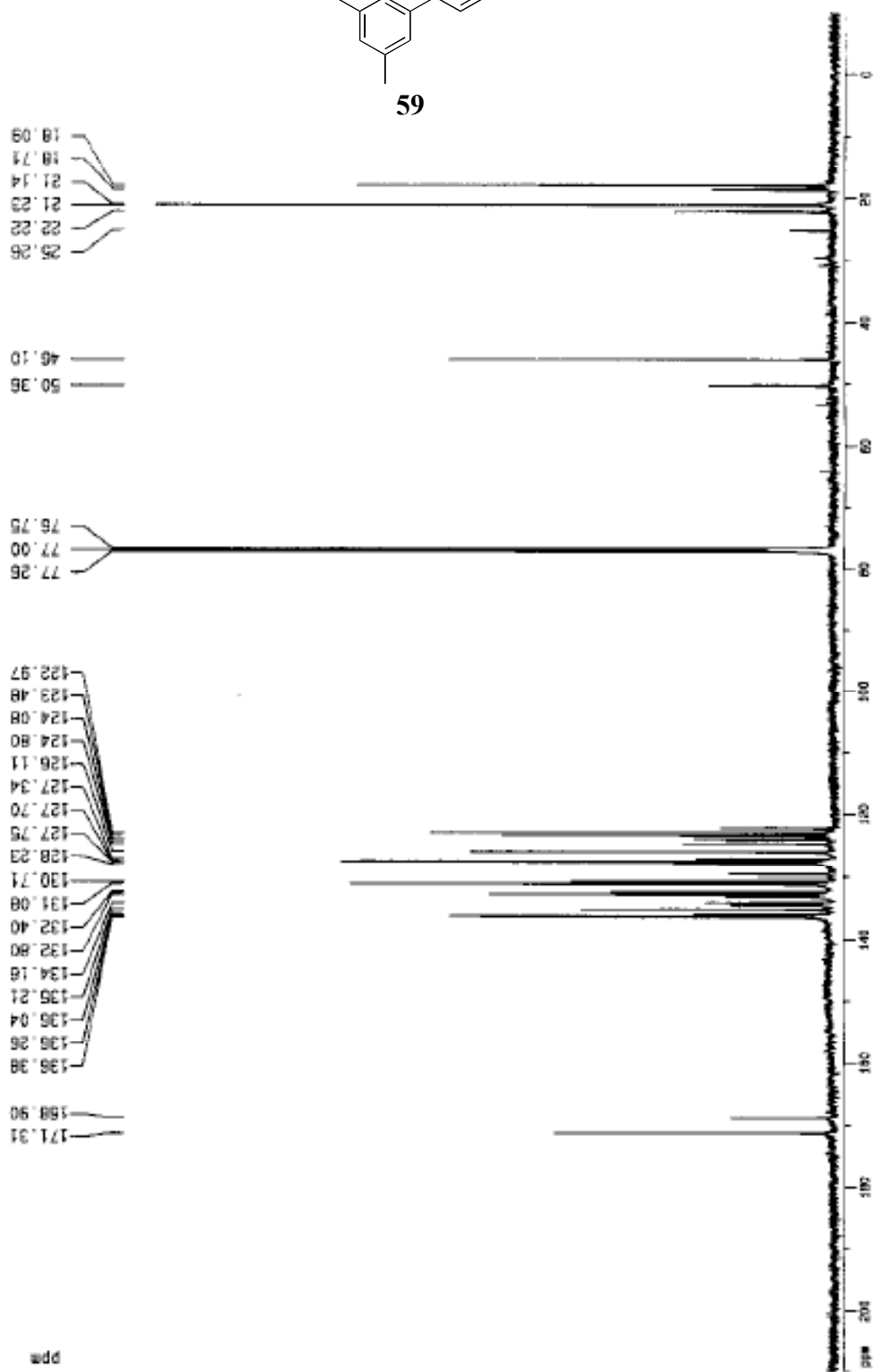
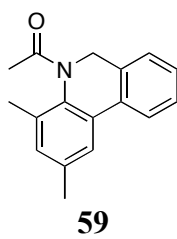
#### **A.1 GC-MS OF CONTROL REACTION SIDE PRODUCTS (TABLE 2)**

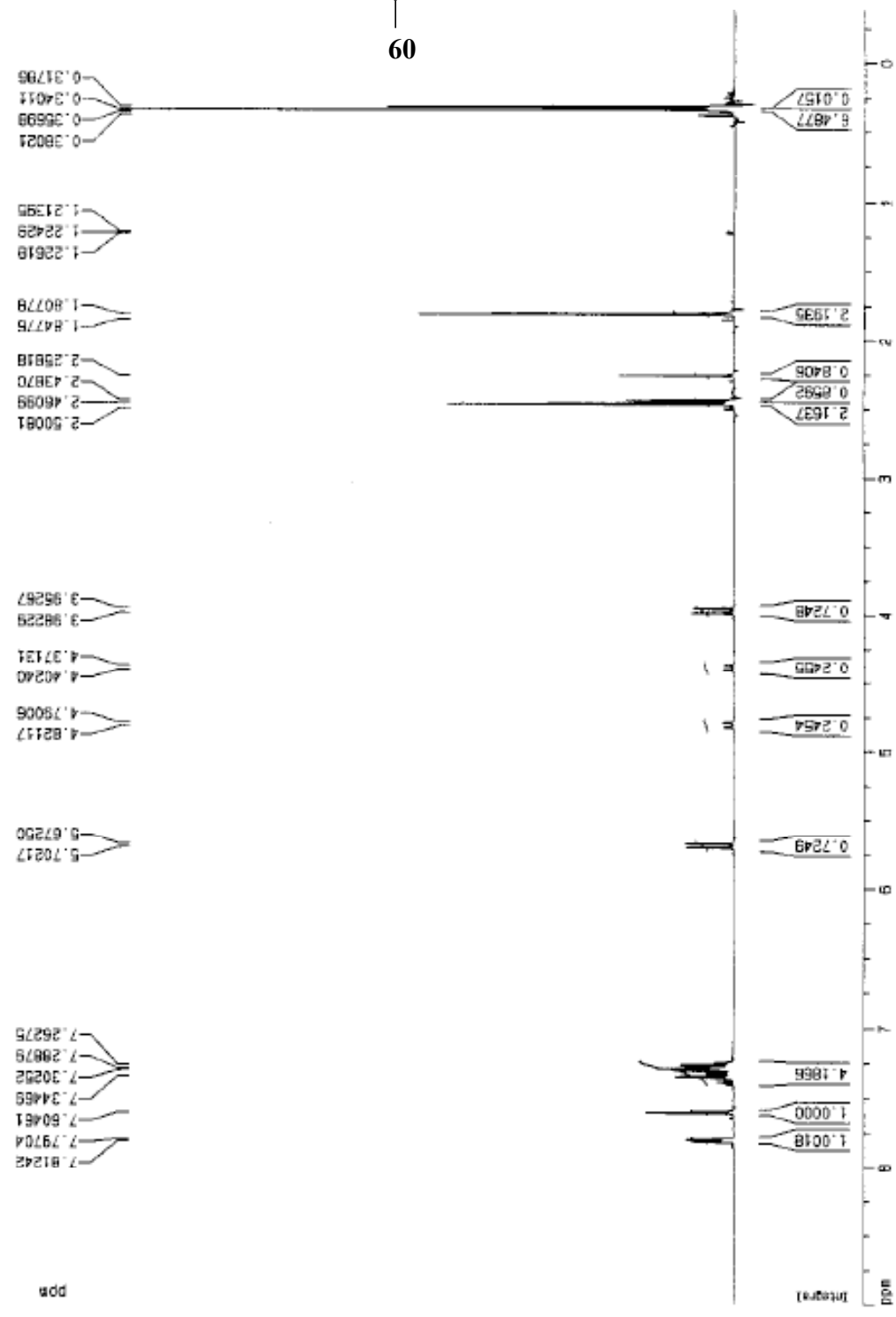
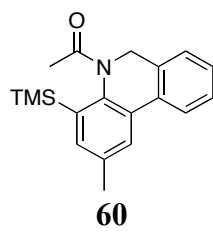
File : C:\HPCHEM\1\DATA\AK2P82A2.D  
Operator : Raghu  
Acquired : 13 Feb 2004 3:11 pm using AcqMethod TANGI  
Instrument : GC/MS Ins  
Sample Name: ak2p82a2  
Misc Info :  
Vial Number: 100

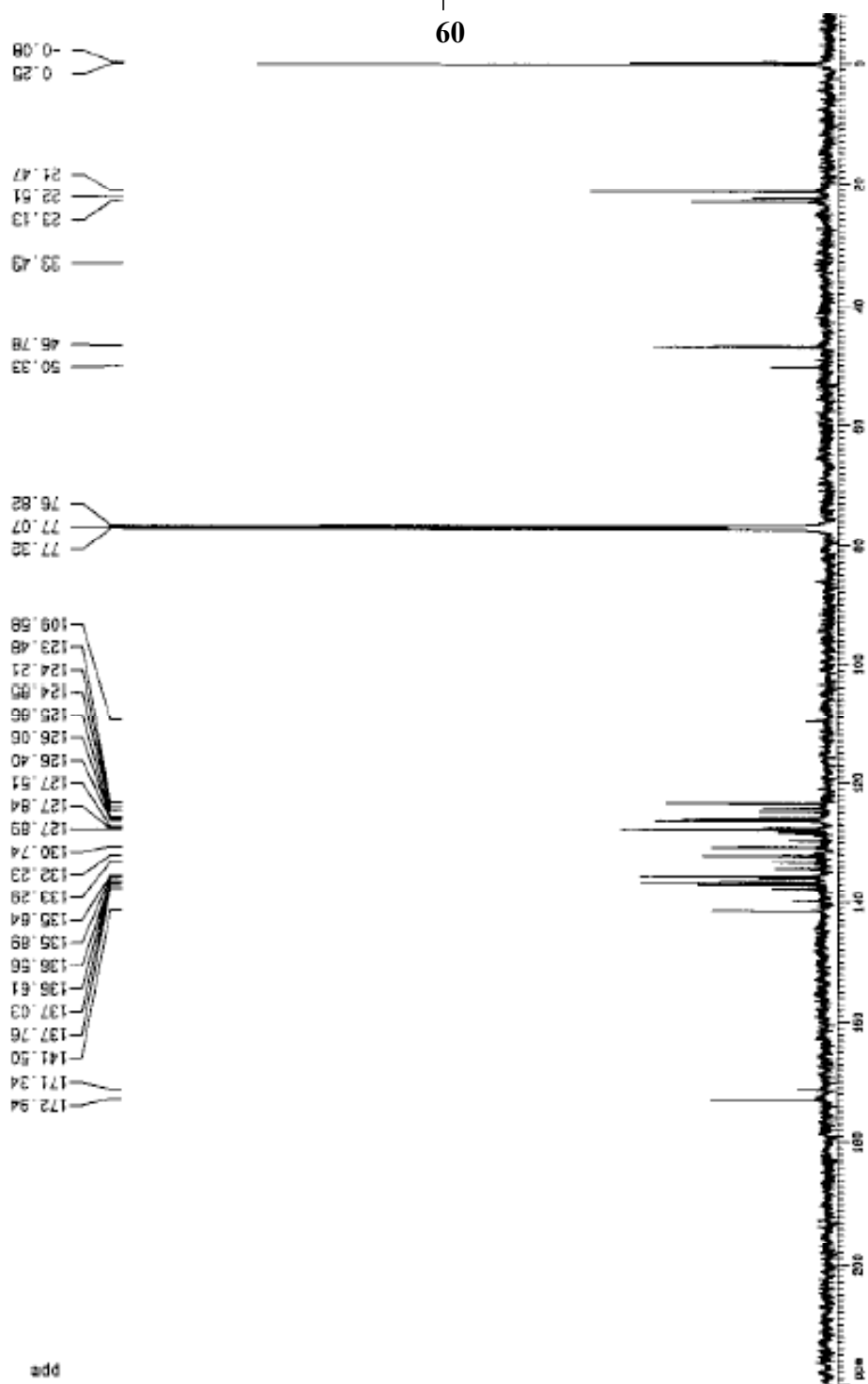
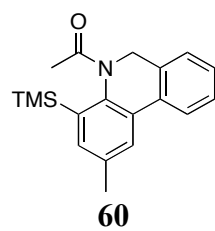


## A.2 $^1\text{H}$ NMR AND $^{13}\text{C}$ NMR

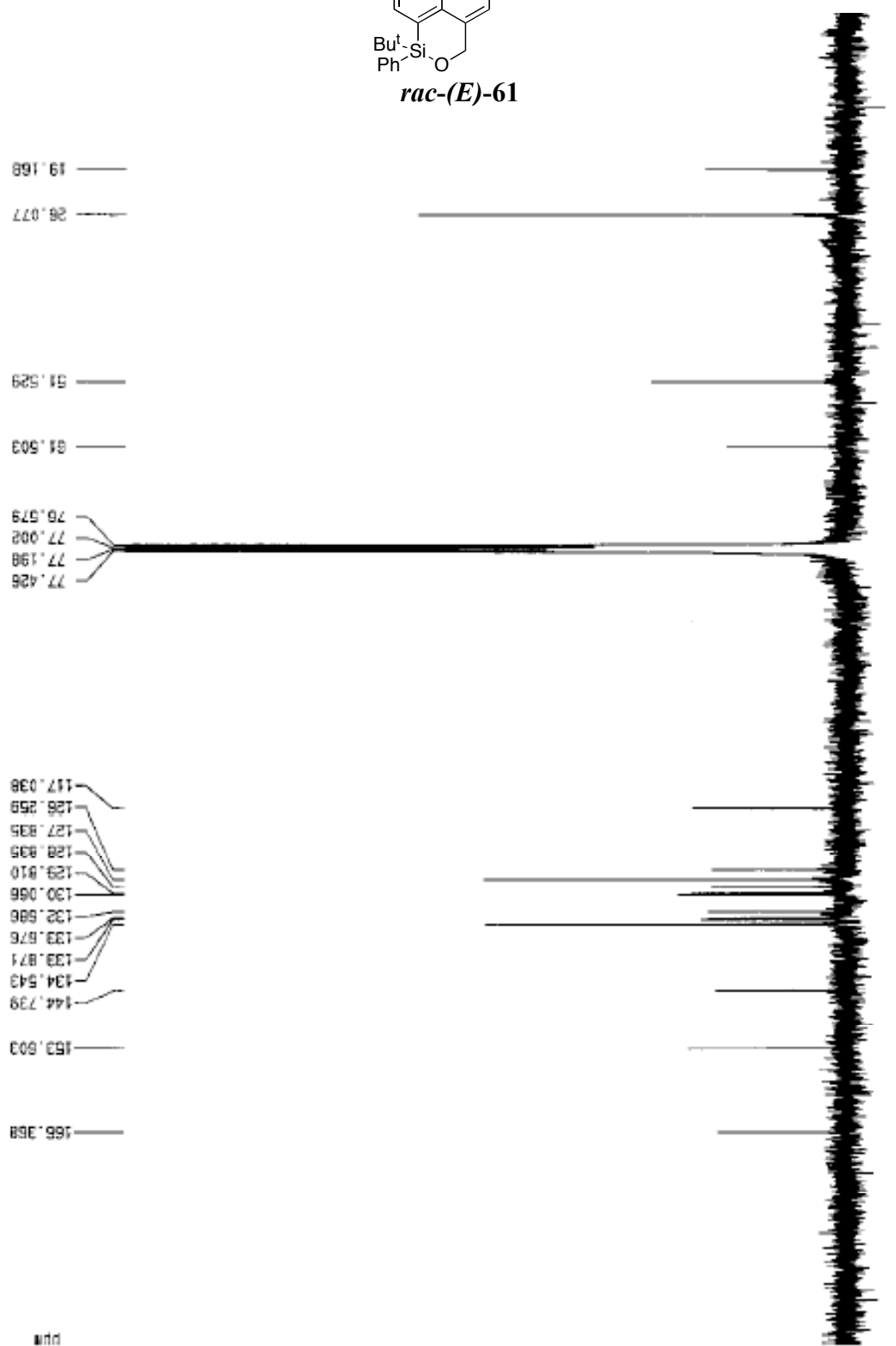
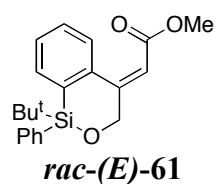








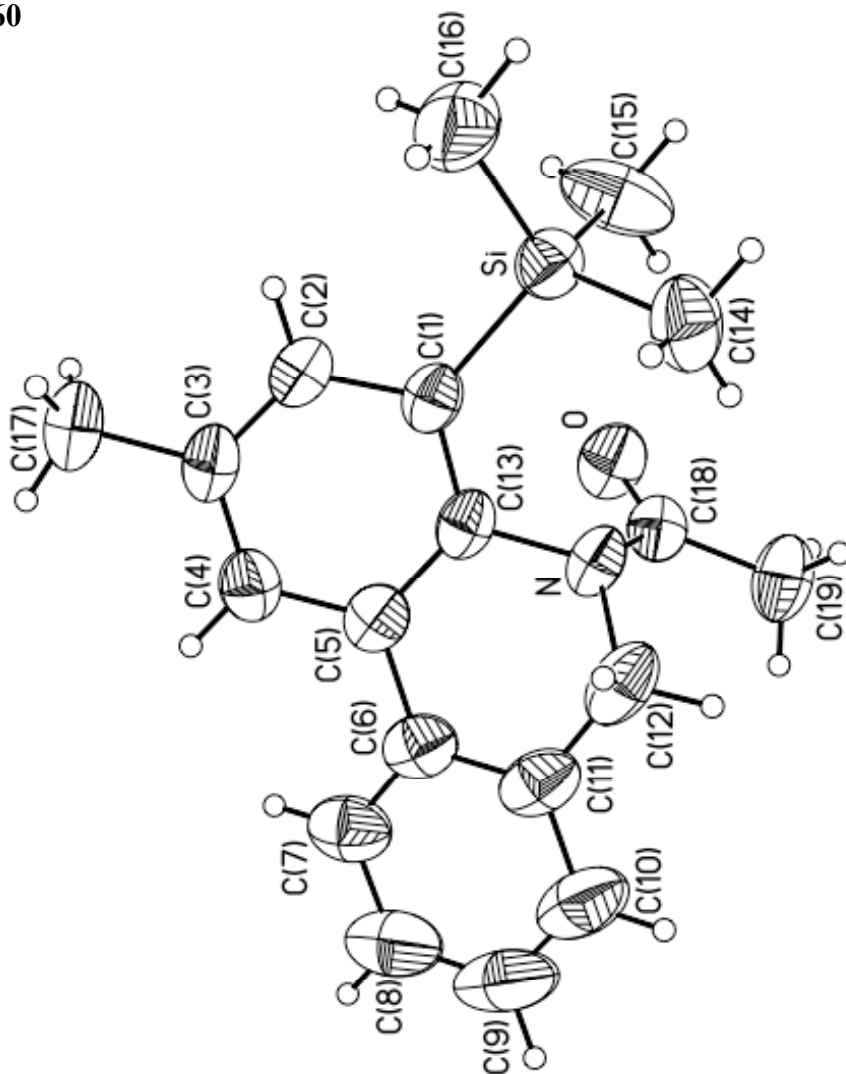
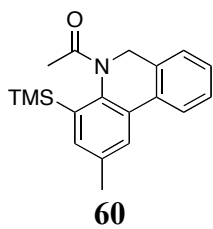




## **APPENDIX B**

### **CHAPTER 4 SUPPORTING DATA**

#### **B.1 X-RAY DATA FOR DIHYDROPHENANTHRIDINE 60**



data\_kell420s

```
_audit_creation_method          SHELXL-97
_chemical_name_systematic
;
?
;
_chemical_name_common           ?
_chemical_melting_point         ?
_chemical_formula_moiety        ?
_chemical_formula_sum
'C19 H23 N O Si'
_chemical_formula_weight        309.47
```

```
loop_
  _atom_type_symbol
  _atom_type_description
  _atom_type_scatter_dispersion_real
  _atom_type_scatter_dispersion_imag
  _atom_type_scatter_source
'C'  'C'    0.0033  0.0016
'International Tables Vol C Tables 4.2.6.8 and 6.1.1.4'
'H'  'H'    0.0000  0.0000
'International Tables Vol C Tables 4.2.6.8 and 6.1.1.4'
'N'  'N'    0.0061  0.0033
'International Tables Vol C Tables 4.2.6.8 and 6.1.1.4'
'O'  'O'    0.0106  0.0060
'International Tables Vol C Tables 4.2.6.8 and 6.1.1.4'
'Si' 'Si'   0.0817  0.0704
'International Tables Vol C Tables 4.2.6.8 and 6.1.1.4'
```

```
_symmetry_cell_setting          Monoclinic
_symmetry_space_group_name_H-M  P2(1)/c
```

```
loop_
  _symmetry_equiv_pos_as_xyz
'x, y, z'
'-x, y+1/2, -z+1/2'
'-x, -y, -z'
'x, -y-1/2, z-1/2'
```

```
_cell_length_a                  10.3479(7)
_cell_length_b                   9.2770(6)
_cell_length_c                   18.5040(12)
_cell_angle_alpha                 90.00
_cell_angle_beta                  98.7890(10)
_cell_angle_gamma                 90.00
_cell_volume                      1755.5(2)
```

_cell_formula_units_Z	4
_cell_measurement_temperature	295(2)
_cell_measurement_reflms_used	5609
_cell_measurement_theta_min	2.20
_cell_measurement_theta_max	27.38
_exptl_crystal_description	?
_exptl_crystal_colour	?
_exptl_crystal_size_max	0.29
_exptl_crystal_size_mid	0.24
_exptl_crystal_size_min	0.24
_exptl_crystal_density_meas	0
_exptl_crystal_density_diffn	1.171
_exptl_crystal_density_method	'not measured'
_exptl_crystal_F_000	664
_exptl_absorpt_coefficient_mu	0.136
_exptl_absorpt_correction_type	none
_exptl_absorpt_correction_T_min	0.9617
_exptl_absorpt_correction_T_max	0.9682
_exptl_absorpt_process_details	?
_exptl_special_details	
;	
?	
;	
_diffn_ambient_temperature	295(2)
_diffn_radiation_wavelength	0.71073
_diffn_radiation_type	MoK\alpha
_diffn_radiation_source	'fine-focus sealed tube'
_diffn_radiation_monochromator	graphite
_diffn_measurement_device_type	'CCD area detector'
_diffn_measurement_method	'phi and omega scans'
_diffn_detector_area_resol_mean	?
_diffn_standards_number	?
_diffn_standards_interval_count	?
_diffn_standards_interval_time	?
_diffn_standards_decay_%	?
_diffn_reflms_number	16633
_diffn_reflms_av_R_equivalents	0.0405
_diffn_reflms_av_sigmaI/netI	0.0390
_diffn_reflms_limit_h_min	-13
_diffn_reflms_limit_h_max	13
_diffn_reflms_limit_k_min	-12
_diffn_reflms_limit_k_max	12
_diffn_reflms_limit_l_min	-24
_diffn_reflms_limit_l_max	24
_diffn_reflms_theta_min	1.99

```

_diffn_refl_theta_max      27.50
_refl_number_total        4022
_refl_number_gt           3123
_refl_threshold_expression >2sigma(I)

_computing_data_collection 'Bruker SMART'
_computing_cell_refinement 'Bruker SMART'
_computing_data_reduction  'Bruker SAINT'
_computing_structure_solution 'SHELXS-97 (Sheldrick, 1990)'
_computing_structure_refinement 'SHELXL-97 (Sheldrick, 1997)'
_computing_molecular_graphics 'Bruker SHELXTL'
_computing_publication_material 'Bruker SHELXTL'

```

```
_refine_special_details
```

```

;
Refinement of F2 against ALL reflections. The weighted R-factor wR and goodness of fit S are based on F2, conventional R-factors R are based on F, with F set to zero for negative F2. The threshold expression of F2 > 2sigma(F2) is used only for calculating R-factors(gt) etc. and is not relevant to the choice of reflections for refinement. R-factors based on F2 are statistically about twice as large as those based on F, and R-factors based on ALL data will be even larger.

```

```

;
_refine_ls_structure_factor_coef Fsqd
_refine_ls_matrix_type full
_refine_ls_weighting_scheme calc
_refine_ls_weighting_details
'calc w=1/[\s^2^(Fo^2^)+(0.0699P)^2^+0.3979P] where
P=(Fo^2^+2Fc^2^)/3'
_atom_sites_solution_primary direct
_atom_sites_solution_secondary difmap
_atom_sites_solution_hydrogens geom
_refine_ls_hydrogen_treatment mixed
_refine_ls_extinction_method none
_refine_ls_extinction_coef ?
_refine_ls_number_reflns 4022
_refine_ls_number_parameters 199
_refine_ls_number_restraints 0
_refine_ls_R_factor_all 0.0899
_refine_ls_R_factor_gt 0.0702
_refine_ls_wR_factor_ref 0.1728

```



H14A H 0.8268 0.9835 0.2548 0.115 Uiso 1 1 calc R . .  
 H14B H 0.6847 0.9517 0.2151 0.115 Uiso 1 1 calc R . .  
 H14C H 0.7868 1.0247 0.1723 0.115 Uiso 1 1 calc R . .  
 C15 C 0.8222(4) 0.6440(4) 0.25716(18) 0.0986(12) Uani 1 1 d . .  
 .  
 H15A H 0.8749 0.6784 0.3010 0.148 Uiso 1 1 calc R . .  
 H15B H 0.8550 0.5525 0.2438 0.148 Uiso 1 1 calc R . .  
 H15C H 0.7334 0.6332 0.2655 0.148 Uiso 1 1 calc R . .  
 C16 C 1.0015(3) 0.7884(4) 0.1669(2) 0.0942(11) Uani 1 1 d . . .  
 H16A H 1.0552 0.8171 0.2116 0.141 Uiso 1 1 calc R . .  
 H16B H 1.0085 0.8585 0.1296 0.141 Uiso 1 1 calc R . .  
 H16C H 1.0301 0.6962 0.1518 0.141 Uiso 1 1 calc R . .  
 C17 C 0.7998(3) 0.5386(4) -0.08279(16) 0.0785(9) Uani 1 1 d . .  
 .  
 H17A H 0.7413 0.5215 -0.1275 0.118 Uiso 1 1 calc R . .  
 H17B H 0.8319 0.4482 -0.0621 0.118 Uiso 1 1 calc R . .  
 H17C H 0.8719 0.5965 -0.0927 0.118 Uiso 1 1 calc R . .  
 C18 C 0.4847(2) 0.7199(2) 0.17900(12) 0.0470(5) Uani 1 1 d . . .  
 C19 C 0.3935(3) 0.7828(3) 0.22651(16) 0.0665(7) Uani 1 1 d . . .  
 H19A H 0.3777 0.7130 0.2625 0.100 Uiso 1 1 calc R . .  
 H19B H 0.3123 0.8080 0.1968 0.100 Uiso 1 1 calc R . .  
 H19C H 0.4323 0.8674 0.2506 0.100 Uiso 1 1 calc R . .

loop\_

\_atom\_site\_aniso\_label  
 \_atom\_site\_aniso\_U\_11  
 \_atom\_site\_aniso\_U\_22  
 \_atom\_site\_aniso\_U\_33  
 \_atom\_site\_aniso\_U\_23  
 \_atom\_site\_aniso\_U\_13  
 \_atom\_site\_aniso\_U\_12  
 Si 0.0510(4) 0.0475(4) 0.0587(4) -0.0042(3) 0.0098(3) -0.0017(3)  
 O 0.0777(12) 0.0528(10) 0.0670(11) 0.0135(8) 0.0249(9) 0.0106(9)  
  
 N 0.0523(11) 0.0384(9) 0.0585(11) 0.0014(8) 0.0237(9) 0.0056(8)  
  
 C1 0.0519(13) 0.0399(11) 0.0526(13) 0.0004(9) 0.0172(10)  
 0.0028(9)  
  
 C2 0.0476(12) 0.0504(13) 0.0596(14) -0.0026(10) 0.0188(11)  
 0.0039(10)  
  
 C3 0.0642(15) 0.0522(13) 0.0519(13) -0.0016(10) 0.0255(12)  
 0.0033(11)  
  
 C4 0.0652(16) 0.0518(13) 0.0465(13) 0.0006(10) 0.0140(11) -  
 0.0008(11)

C5 0.0533(13) 0.0406(11) 0.0535(13) 0.0104(10) 0.0167(11)  
 0.0017(10)  
 C6 0.0533(13) 0.0492(13) 0.0614(14) 0.0204(11) 0.0134(11)  
 0.0022(10)  
 C7 0.0599(16) 0.0708(17) 0.0689(17) 0.0241(14) 0.0049(13) -  
 0.0052(13)  
 C8 0.0648(19) 0.102(3) 0.090(2) 0.033(2) -0.0030(17) -0.0007(18)  
 C9 0.0583(19) 0.124(3) 0.115(3) 0.047(3) 0.007(2) 0.023(2)  
 C10 0.0707(19) 0.082(2) 0.103(2) 0.0339(19) 0.0271(19)  
 0.0295(17)  
 C11 0.0577(15) 0.0516(14) 0.0769(17) 0.0253(13) 0.0208(13)  
 0.0108(11)  
 C12 0.0706(17) 0.0415(12) 0.0851(19) 0.0095(12) 0.0354(15)  
 0.0140(11)  
 C13 0.0521(13) 0.0339(10) 0.0518(12) 0.0029(9) 0.0201(10)  
 0.0029(9)  
 C14 0.099(2) 0.0612(17) 0.0706(18) -0.0182(14) 0.0172(16)  
 0.0015(15)  
 C15 0.103(3) 0.088(2) 0.091(2) 0.0324(18) -0.032(2) -0.022(2)  
 C16 0.0583(18) 0.116(3) 0.110(3) -0.043(2) 0.0197(17) -  
 0.0200(17)  
 C17 0.084(2) 0.094(2) 0.0644(17) -0.0148(15) 0.0331(15)  
 0.0100(17)  
 C18 0.0480(12) 0.0446(12) 0.0500(12) -0.0041(10) 0.0120(10) -  
 0.0059(10)  
 C19 0.0738(18) 0.0599(15) 0.0745(17) -0.0094(13) 0.0394(14) -  
 0.0095(13)

\_geom\_special\_details

;

All esds (except the esd in the dihedral angle between two l.s.  
 planes) are estimated using the full covariance matrix. The  
 cell esds are taken into account individually in the estimation  
 of esds in distances, angles and torsion angles; correlations  
 between esds in cell parameters are only used when they are

defined by crystal symmetry. An approximate (isotropic) treatment of cell esds is used for estimating esds involving l.s. planes.

;

```
loop_
  _geom_bond_atom_site_label_1
  _geom_bond_atom_site_label_2
  _geom_bond_distance
  _geom_bond_site_symmetry_2
  _geom_bond_publ_flag
Si C14 1.854(3) . ?
Si C16 1.855(3) . ?
Si C15 1.857(3) . ?
Si C1 1.883(2) . ?
O C18 1.209(3) . ?
N C18 1.372(3) . ?
N C13 1.442(3) . ?
N C12 1.469(3) . ?
C1 C13 1.396(3) . ?
C1 C2 1.401(3) . ?
C2 C3 1.380(3) . ?
C3 C4 1.376(4) . ?
C3 C17 1.513(3) . ?
C4 C5 1.394(3) . ?
C5 C13 1.400(3) . ?
C5 C6 1.477(3) . ?
C6 C7 1.392(4) . ?
C6 C11 1.396(4) . ?
C7 C8 1.381(4) . ?
C8 C9 1.358(5) . ?
C9 C10 1.386(5) . ?
C10 C11 1.393(4) . ?
C11 C12 1.504(4) . ?
C18 C19 1.502(3) . ?
```

```
loop_
  _geom_angle_atom_site_label_1
  _geom_angle_atom_site_label_2
  _geom_angle_atom_site_label_3
  _geom_angle
  _geom_angle_site_symmetry_1
  _geom_angle_site_symmetry_3
  _geom_angle_publ_flag
C14 Si C16 108.46(16) . . ?
C14 Si C15 109.97(17) . . ?
C16 Si C15 107.51(18) . . ?
C14 Si C1 110.02(12) . . ?
```

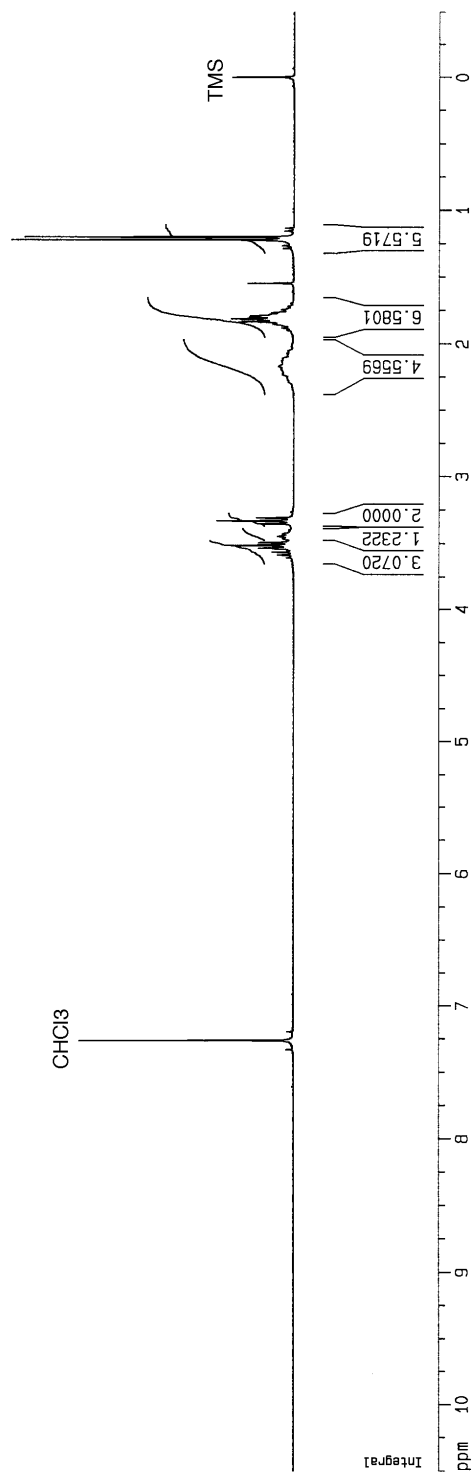
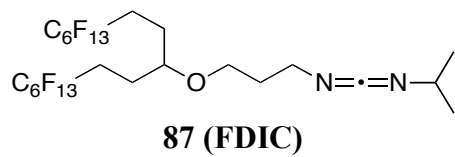
C16 Si C1 107.51(13) . . ?  
 C15 Si C1 113.21(13) . . ?  
 C18 N C13 118.57(17) . . ?  
 C18 N C12 122.02(19) . . ?  
 C13 N C12 111.29(18) . . ?  
 C13 C1 C2 115.5(2) . . ?  
 C13 C1 Si 125.16(17) . . ?  
 C2 C1 Si 119.25(18) . . ?  
 C3 C2 C1 123.7(2) . . ?  
 C4 C3 C2 118.4(2) . . ?  
 C4 C3 C17 120.9(2) . . ?  
 C2 C3 C17 120.7(2) . . ?  
 C3 C4 C5 121.3(2) . . ?  
 C4 C5 C13 118.1(2) . . ?  
 C4 C5 C6 122.9(2) . . ?  
 C13 C5 C6 119.0(2) . . ?  
 C7 C6 C11 119.2(2) . . ?  
 C7 C6 C5 122.7(2) . . ?  
 C11 C6 C5 118.0(2) . . ?  
 C8 C7 C6 120.1(3) . . ?  
 C9 C8 C7 120.6(3) . . ?  
 C8 C9 C10 120.7(3) . . ?  
 C9 C10 C11 119.6(3) . . ?  
 C10 C11 C6 119.8(3) . . ?  
 C10 C11 C12 122.8(3) . . ?  
 C6 C11 C12 117.4(2) . . ?  
 N C12 C11 109.1(2) . . ?  
 C1 C13 C5 122.8(2) . . ?  
 C1 C13 N 120.7(2) . . ?  
 C5 C13 N 116.5(2) . . ?  
 O C18 N 121.1(2) . . ?  
 O C18 C19 121.5(2) . . ?  
 N C18 C19 117.4(2) . . ?

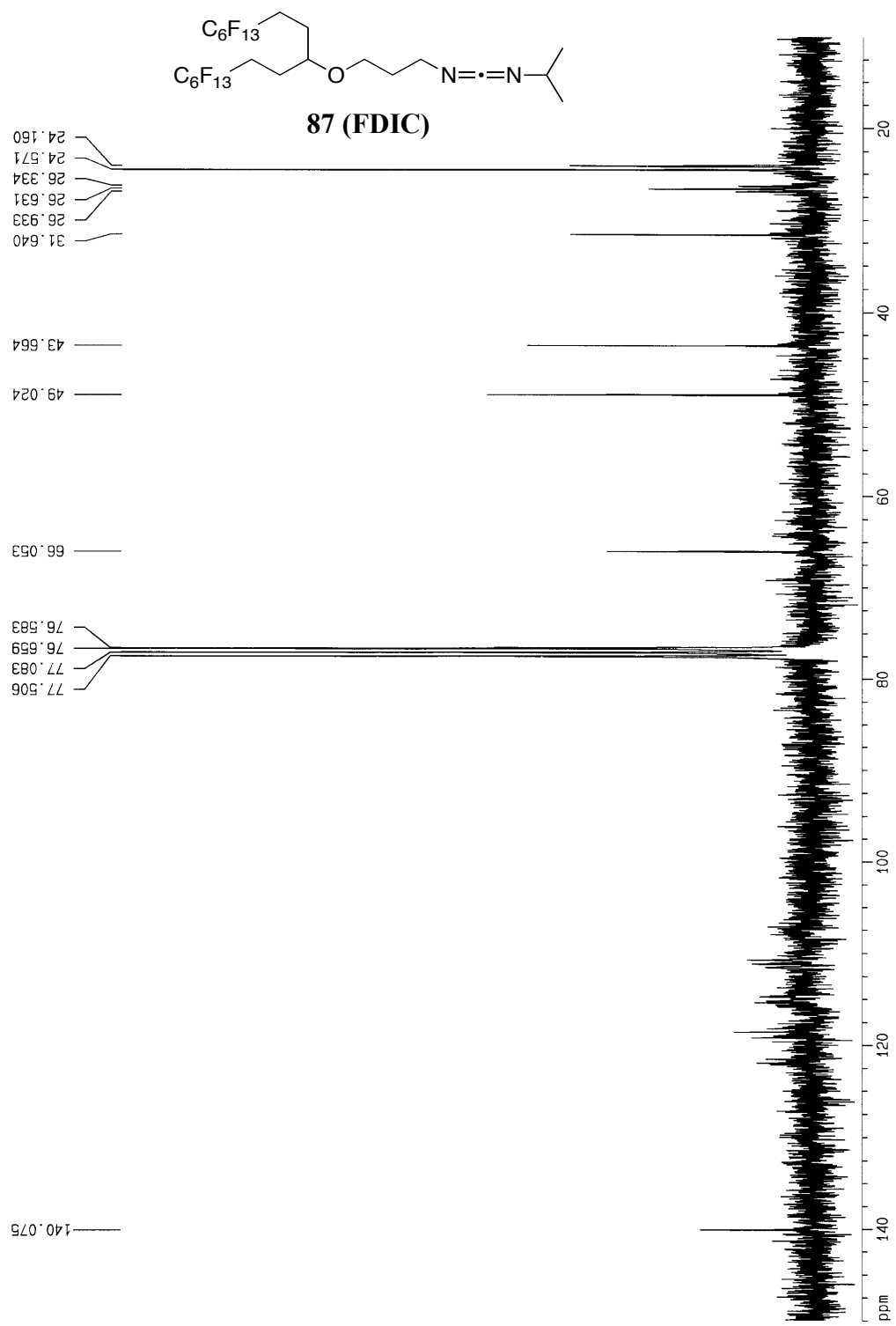
_diffraction_measured_fraction_theta_max	0.999
_diffraction_reflns_theta_full	27.50
_diffraction_measured_fraction_theta_full	0.999
_refine_diff_density_max	0.288
_refine_diff_density_min	-0.180
_refine_diff_density_rms	0.048

## **APPENDIX C**

### **CHAPTER 5 SUPPORTING DATA**

#### **C.1 SELECTED NMR SPECTRA**



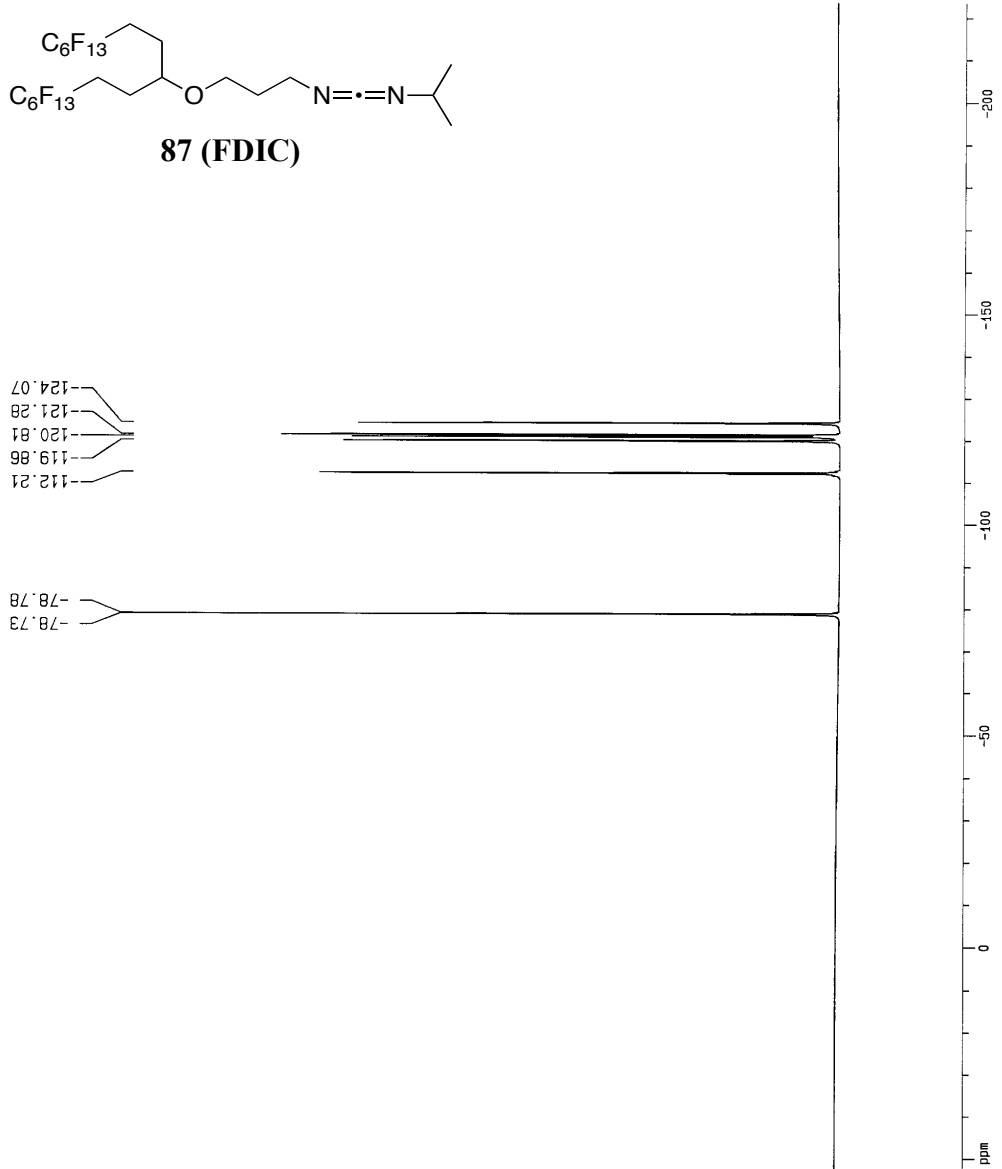
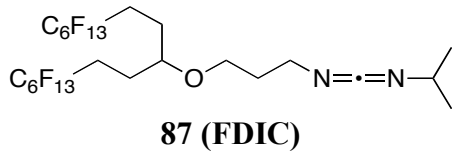


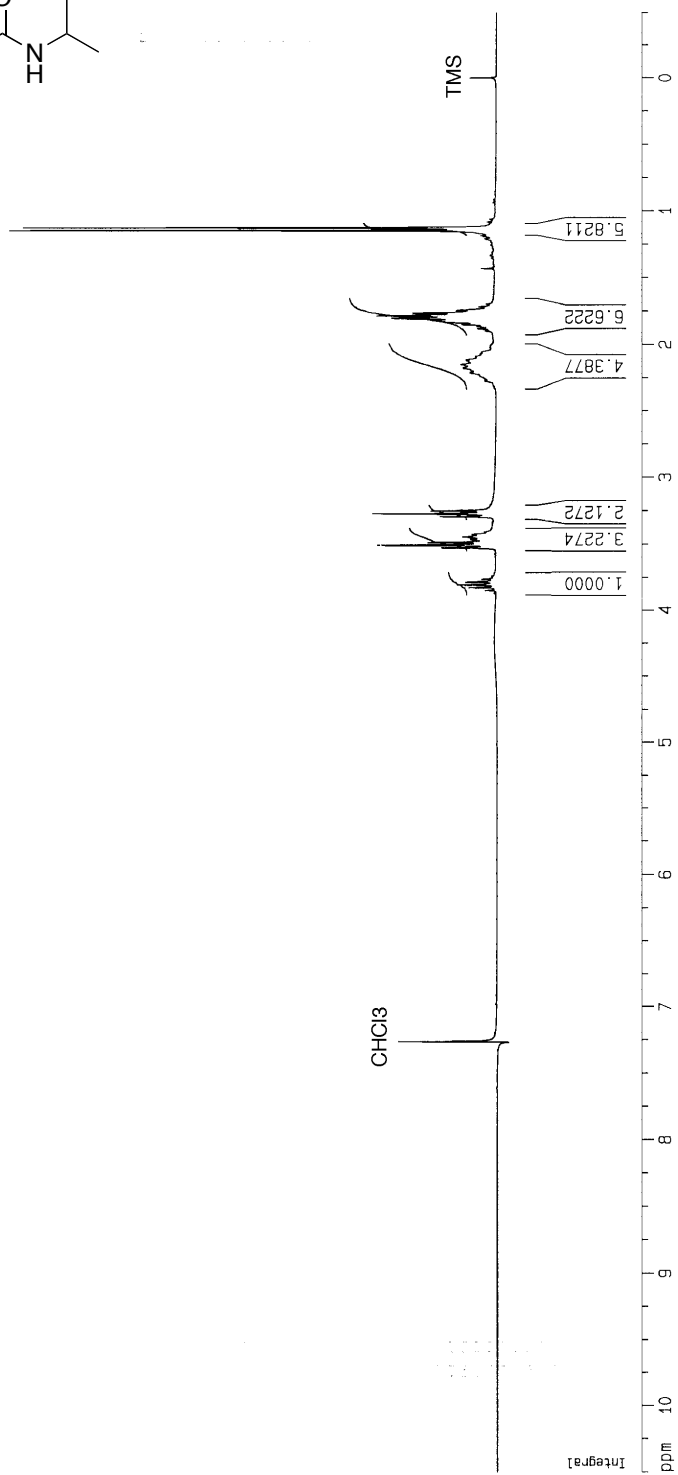
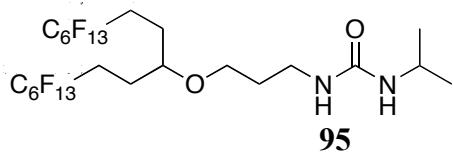
Current Data Parameters  
 NAME CP-FDCC  
 EXPNO 1  
 PROCNO 1

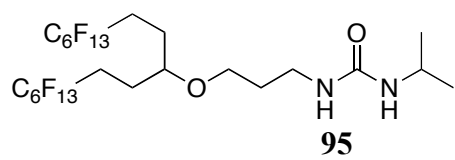
F2 - Acquisition Parameters  
 Date\_ 500000  
 Time 11.06  
 INSTRUM spect  
 PROBHD 5 mm TXI 13C  
 PULPROG c13wzgcde  
 TD 65536  
 SOLVENT CDCl3  
 NS 817  
 DS 0  
 SWH 129870.133 Hz  
 FIDRES 1.981661 Hz  
 AQ 0.2523636 sec  
 RG 181  
 OW 3.850 usec  
 DE 5.50 usec  
 TE 290.0 K  
 D3 0.00100000 sec  
 PL12 50.00 dB  
 D1 1.00000000 sec  
 CPOPRG2 waltz16  
 PCPD2 100.00 usec  
 SF02 500.1330008 MHz  
 NUC2 1H  
 PL2 120.00 dB  
 P1 9.00 usec  
 DE 5.50 usec  
 SF01 470.5511749 MHz  
 NUC1 13F  
 PL1 0.00 dB

F2 - Processing parameters  
 SI 8192  
 SF 470.5914105 MHz  
 MDW EM  
 SSB 0  
 LB 8.00 Hz  
 GB 0  
 PC 1.00

1D NMR plot parameters  
 CX 20.00 cm  
 F1P 52.486 ppm  
 F1 24699.42 Hz  
 F2P -223.486 ppm  
 F2 -105170.71 Hz  
 PPMCM 13.79861 ppm/cm  
 HZCM 6493.50635 Hz/cm



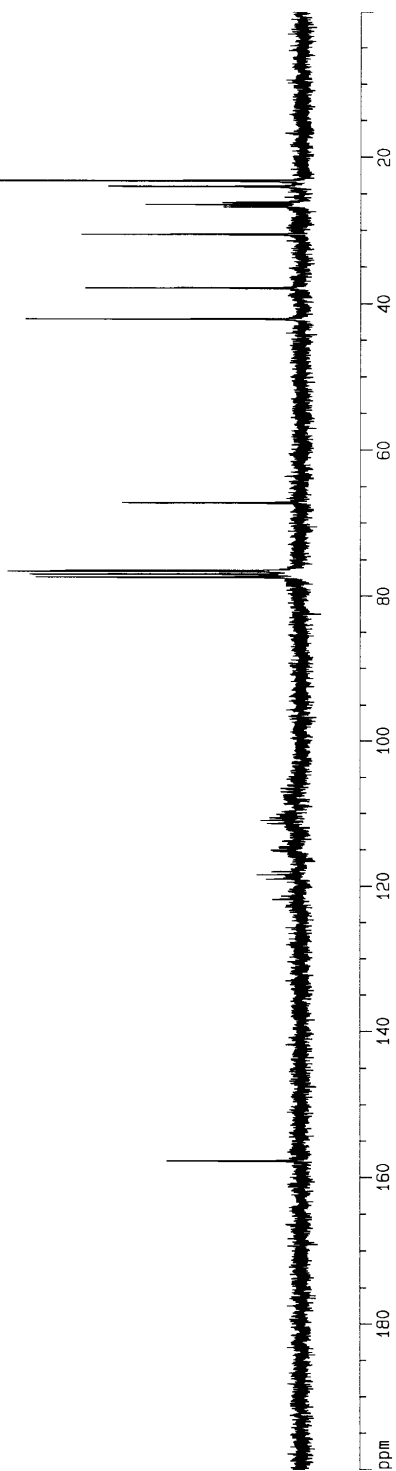


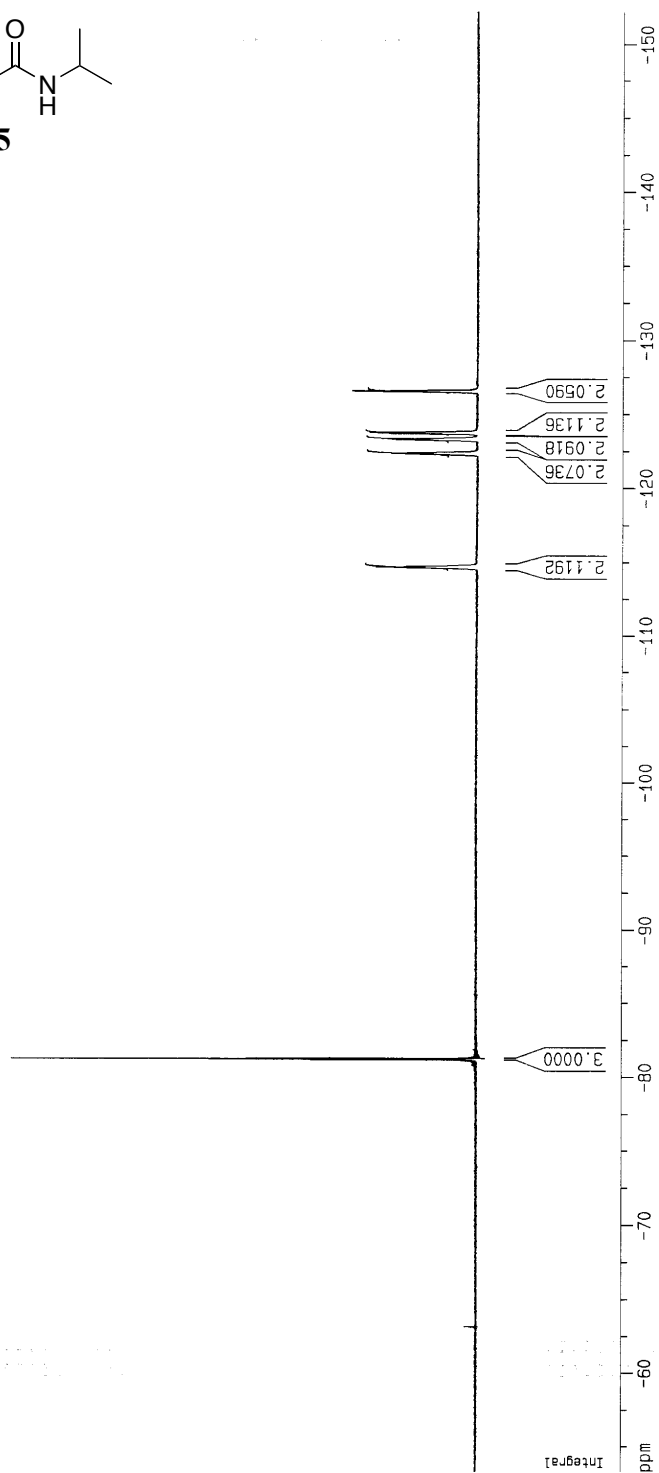
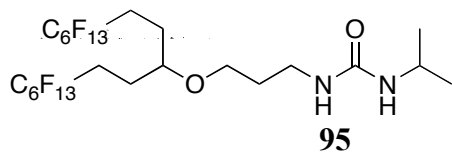


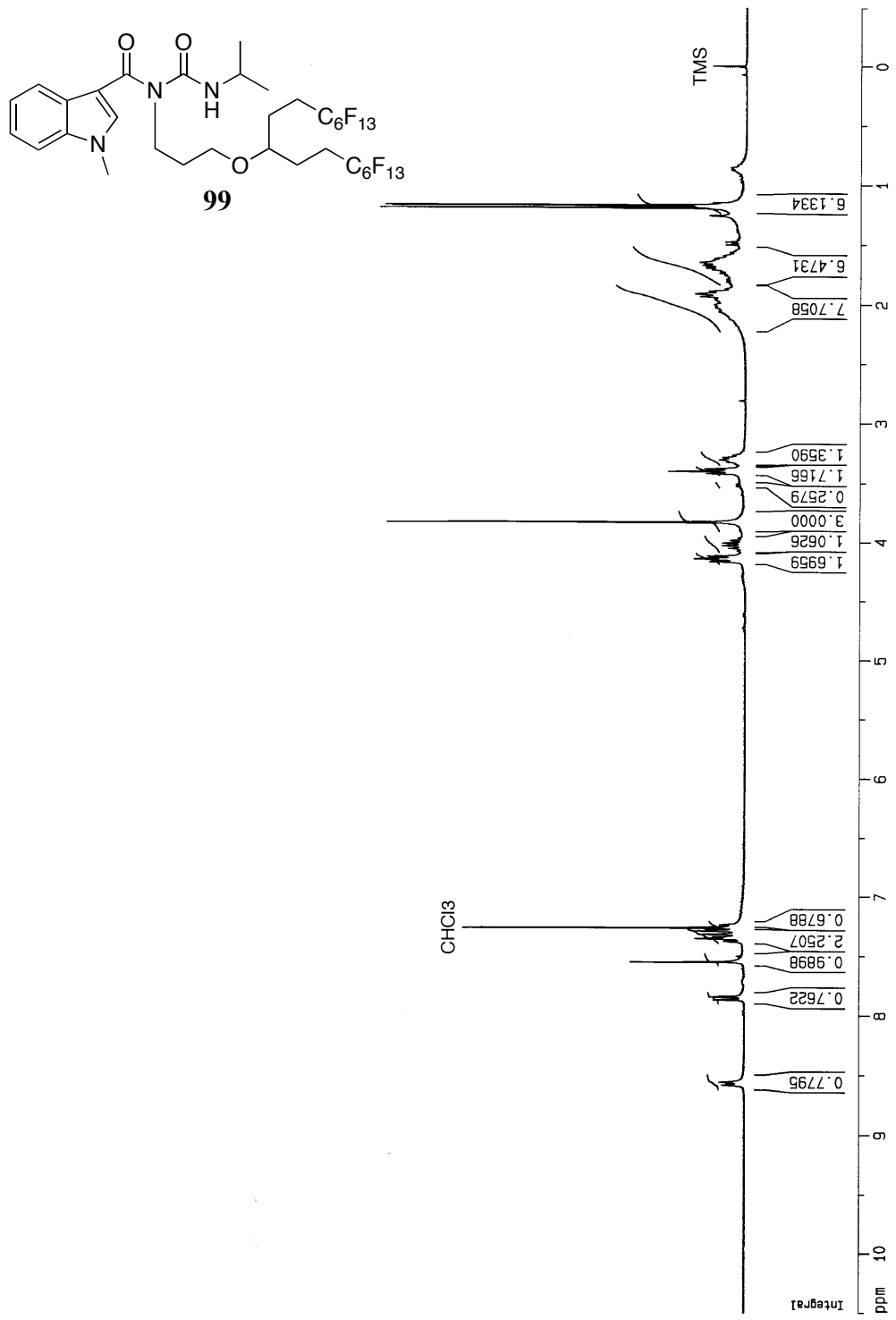
23.252  
24.000  
26.194  
26.485  
26.781  
30.589  
37.899  
42.117

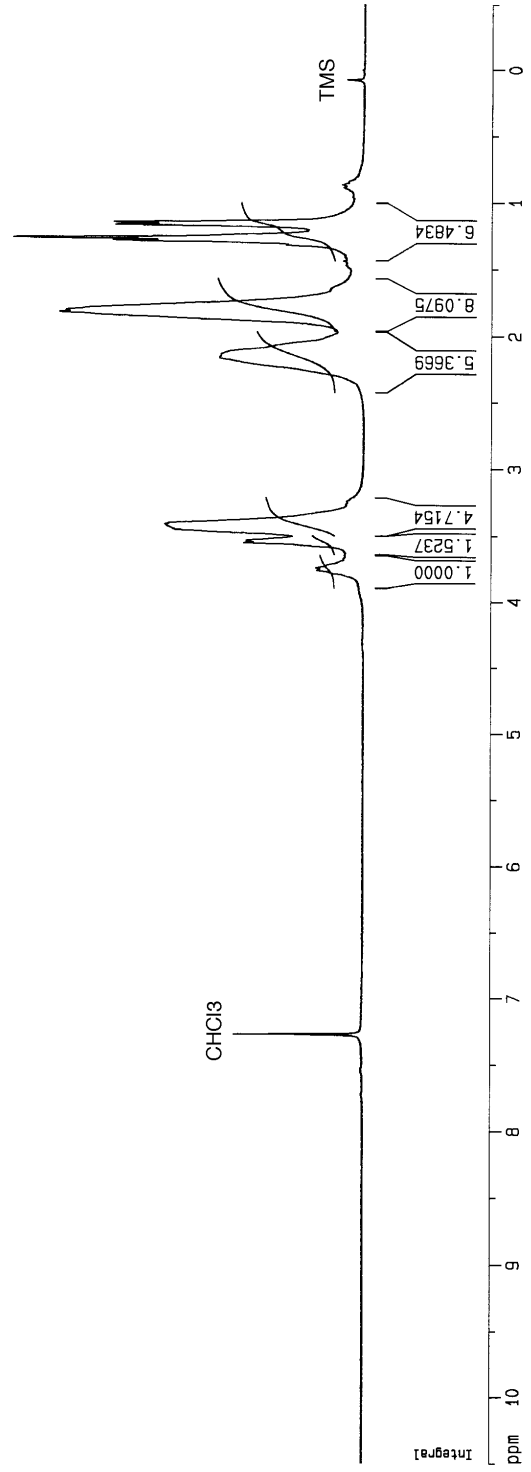
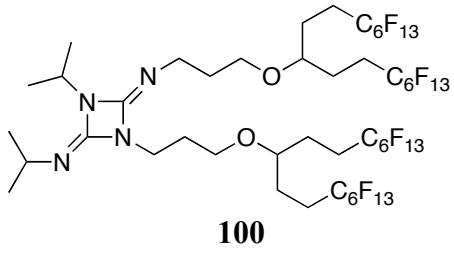
67.212  
76.506  
76.576  
77.001  
77.424

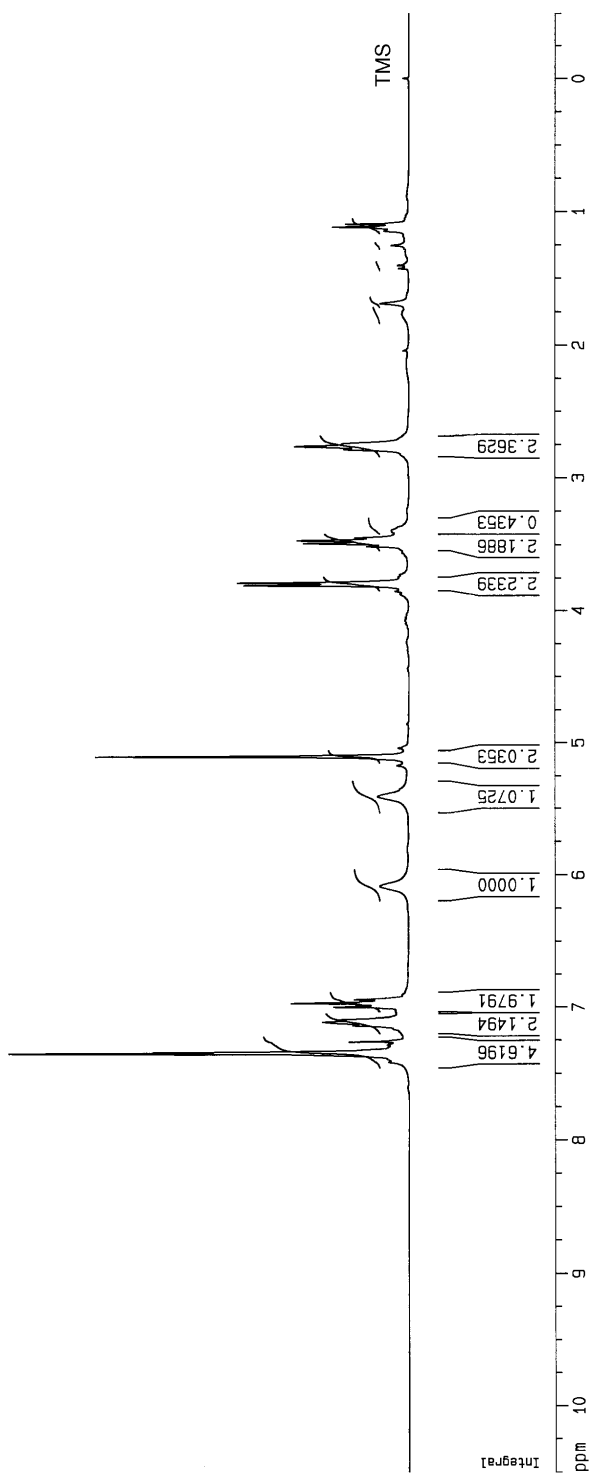
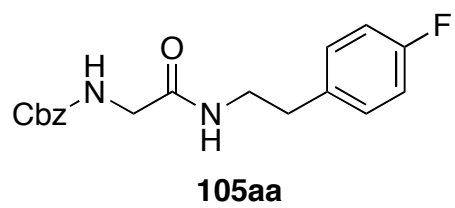
157.775

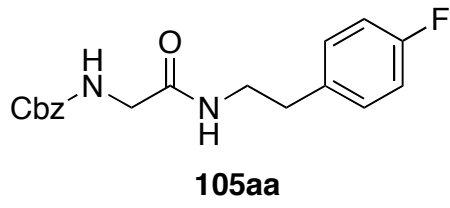








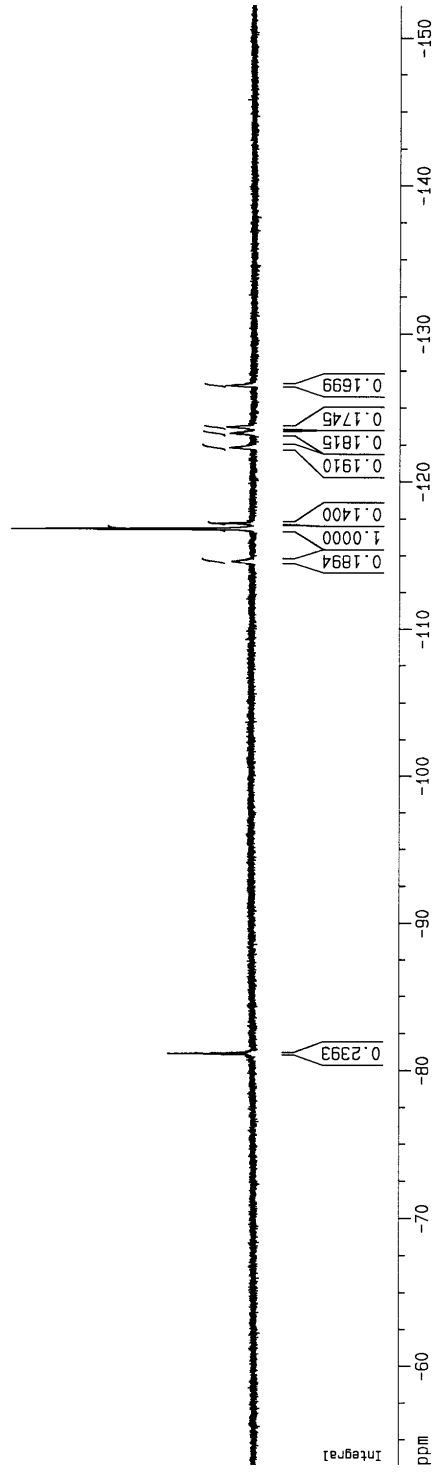


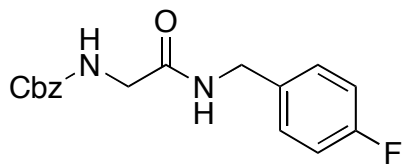


-126.51  
 -123.68  
 -123.66  
 -123.24  
 -122.29  
 -117.21  
 -117.20  
 -117.18  
 -116.81  
 -114.61

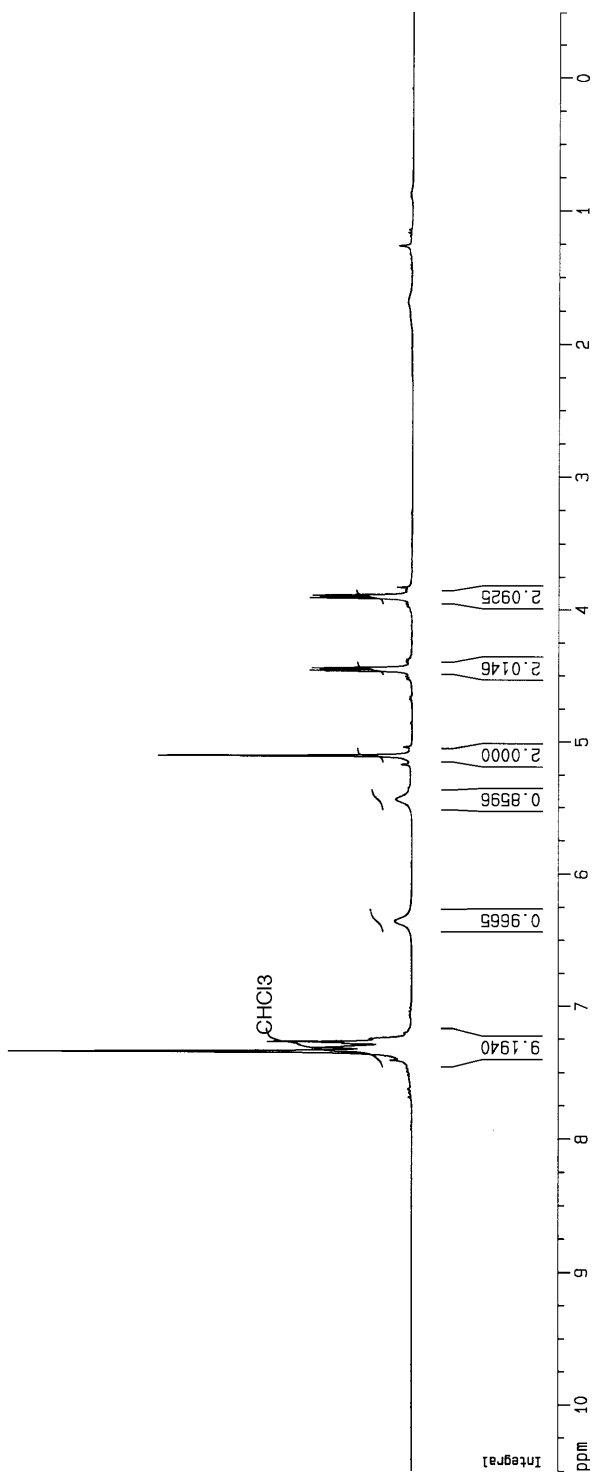
-81.18  
 -81.15  
 -81.11

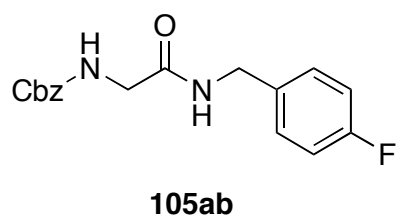
ppm



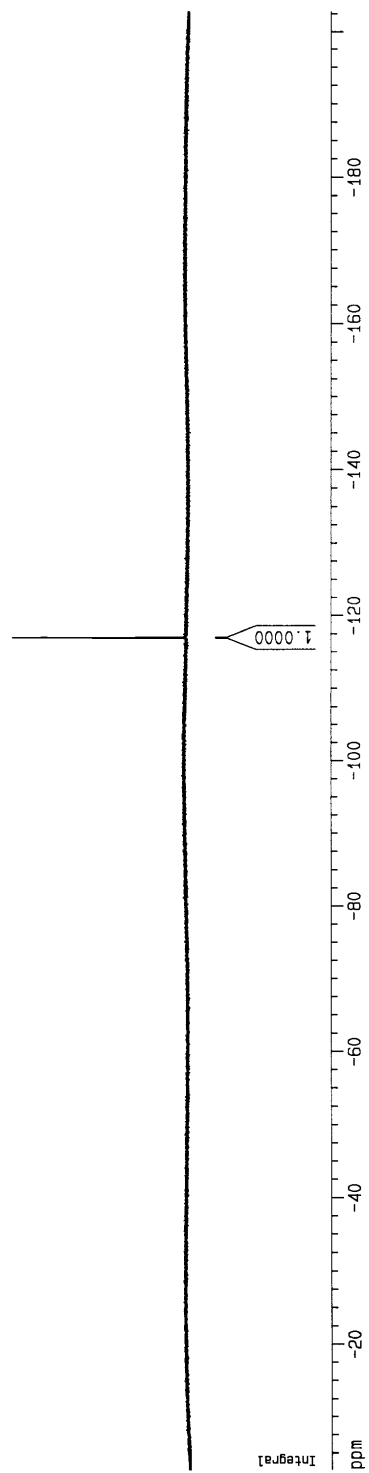


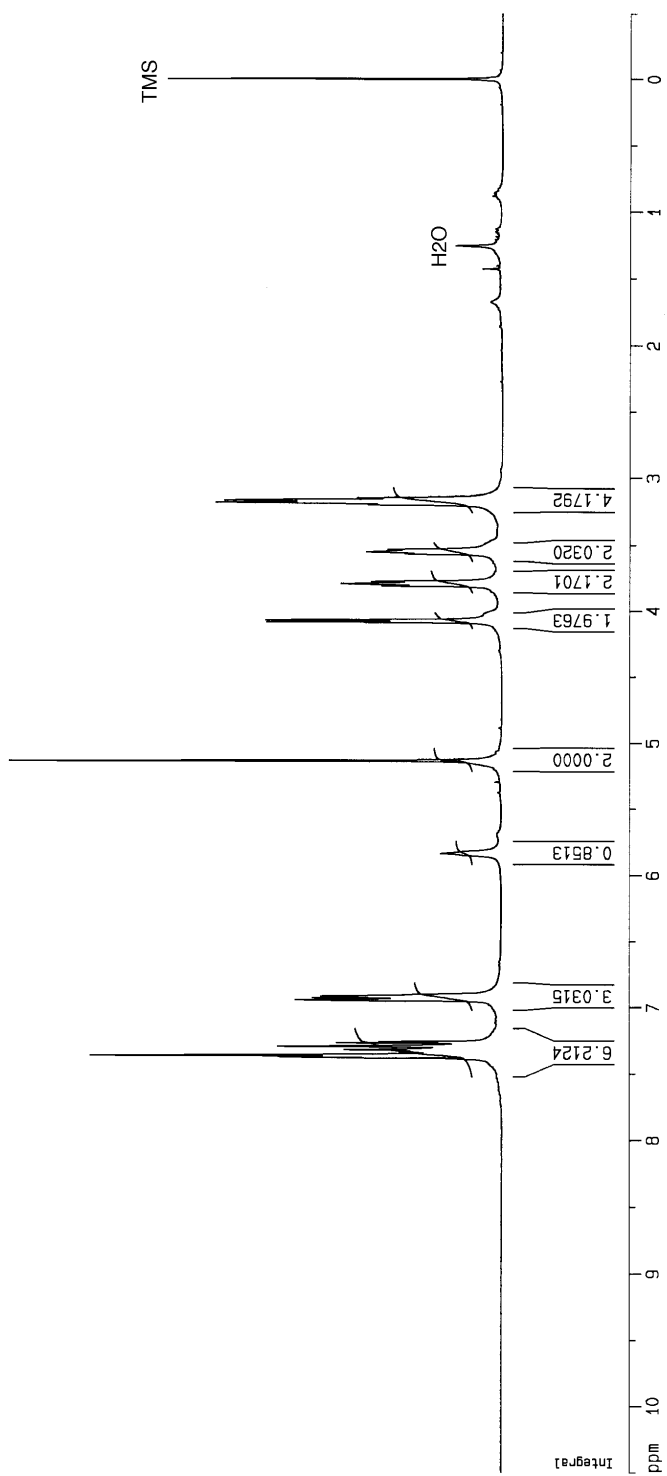
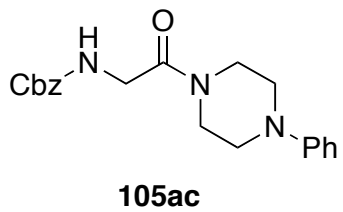
105ab

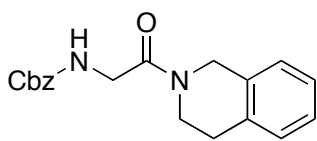




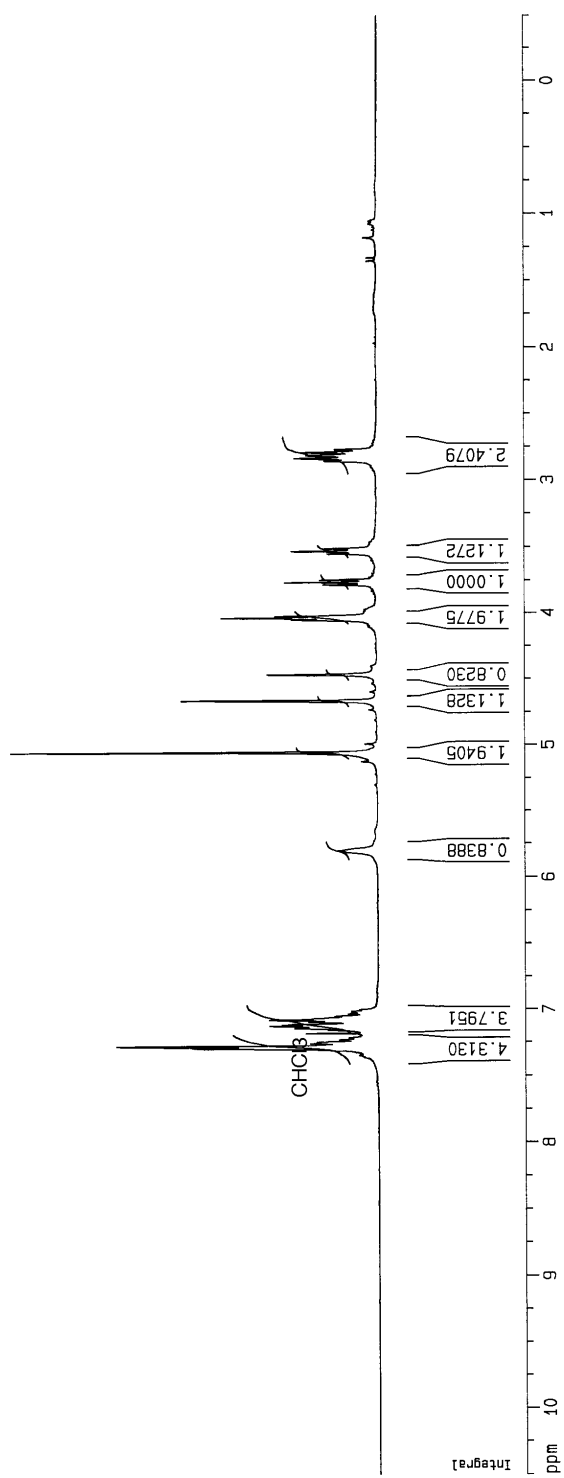
116.99  
116.97  
116.95

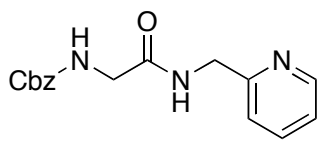




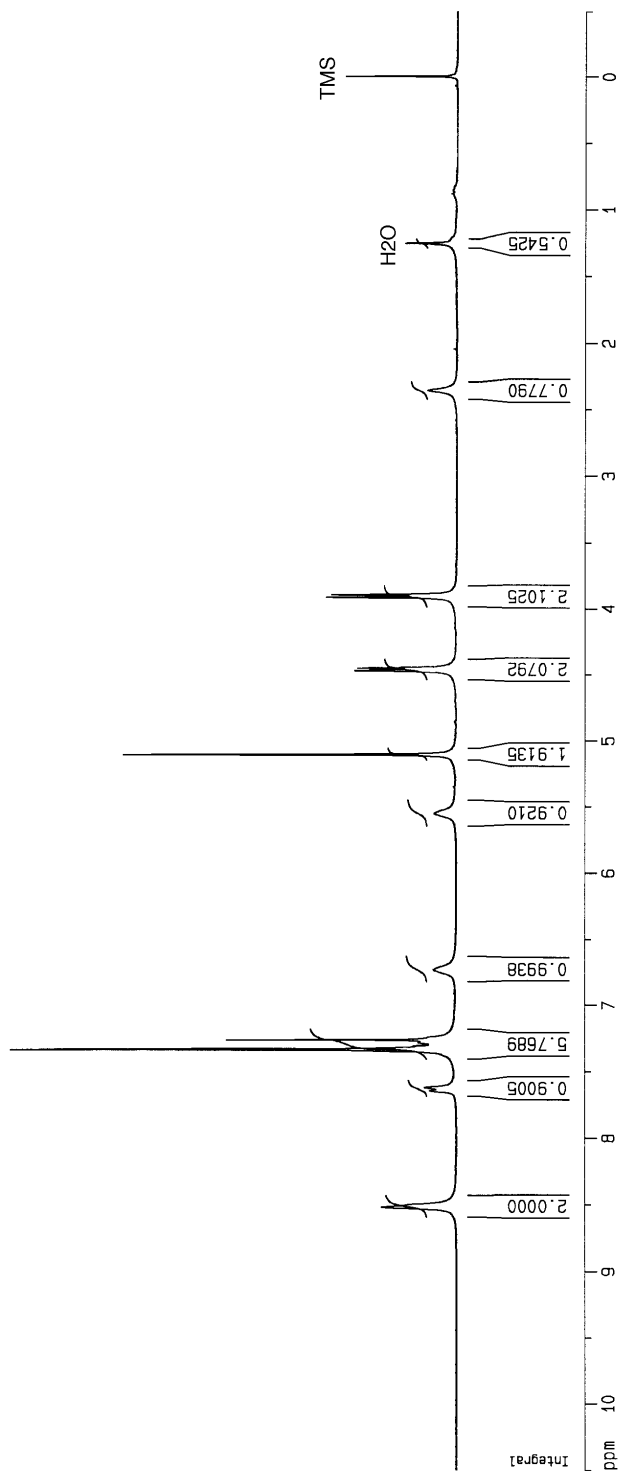


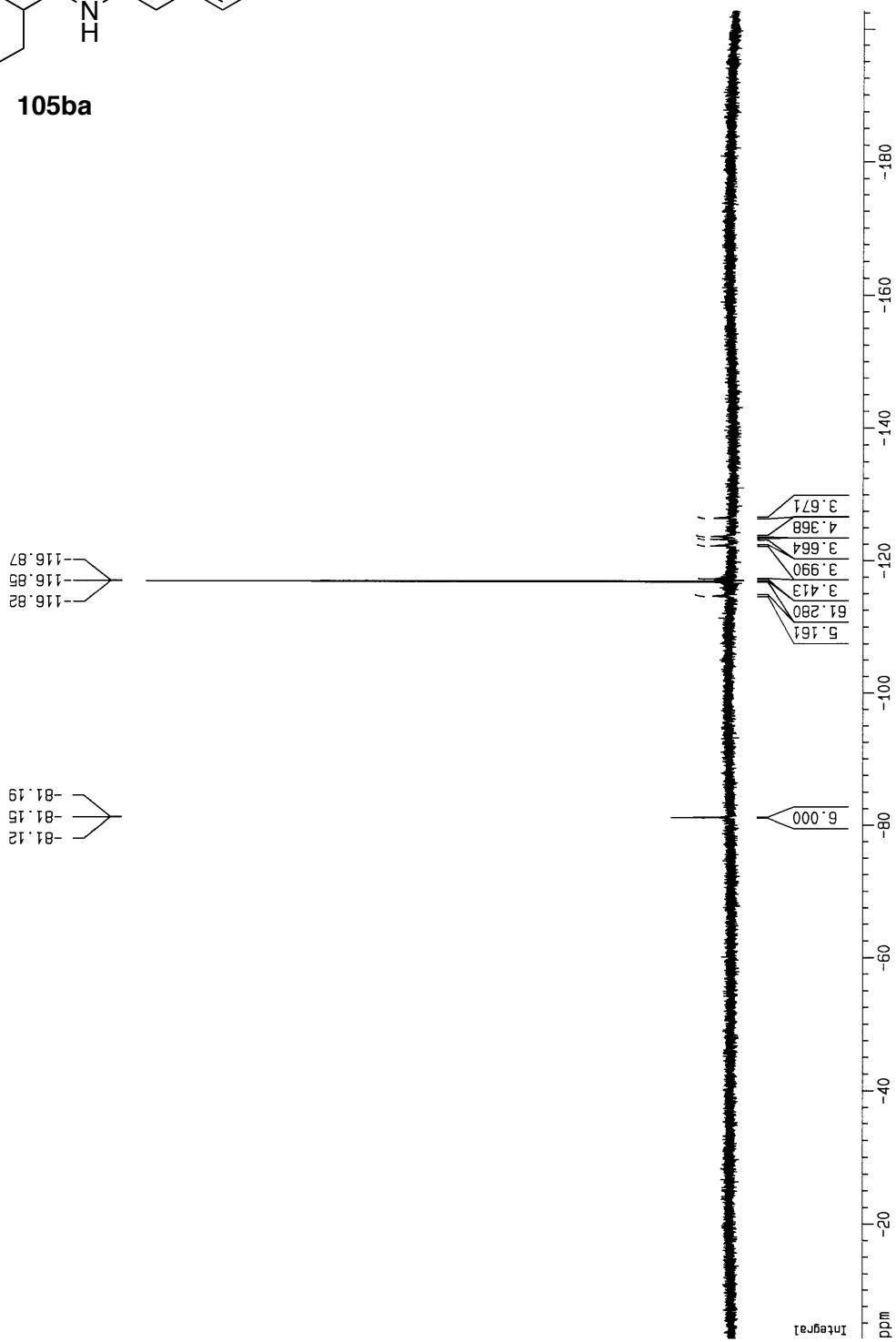
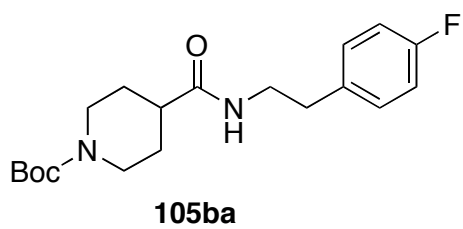
105ad

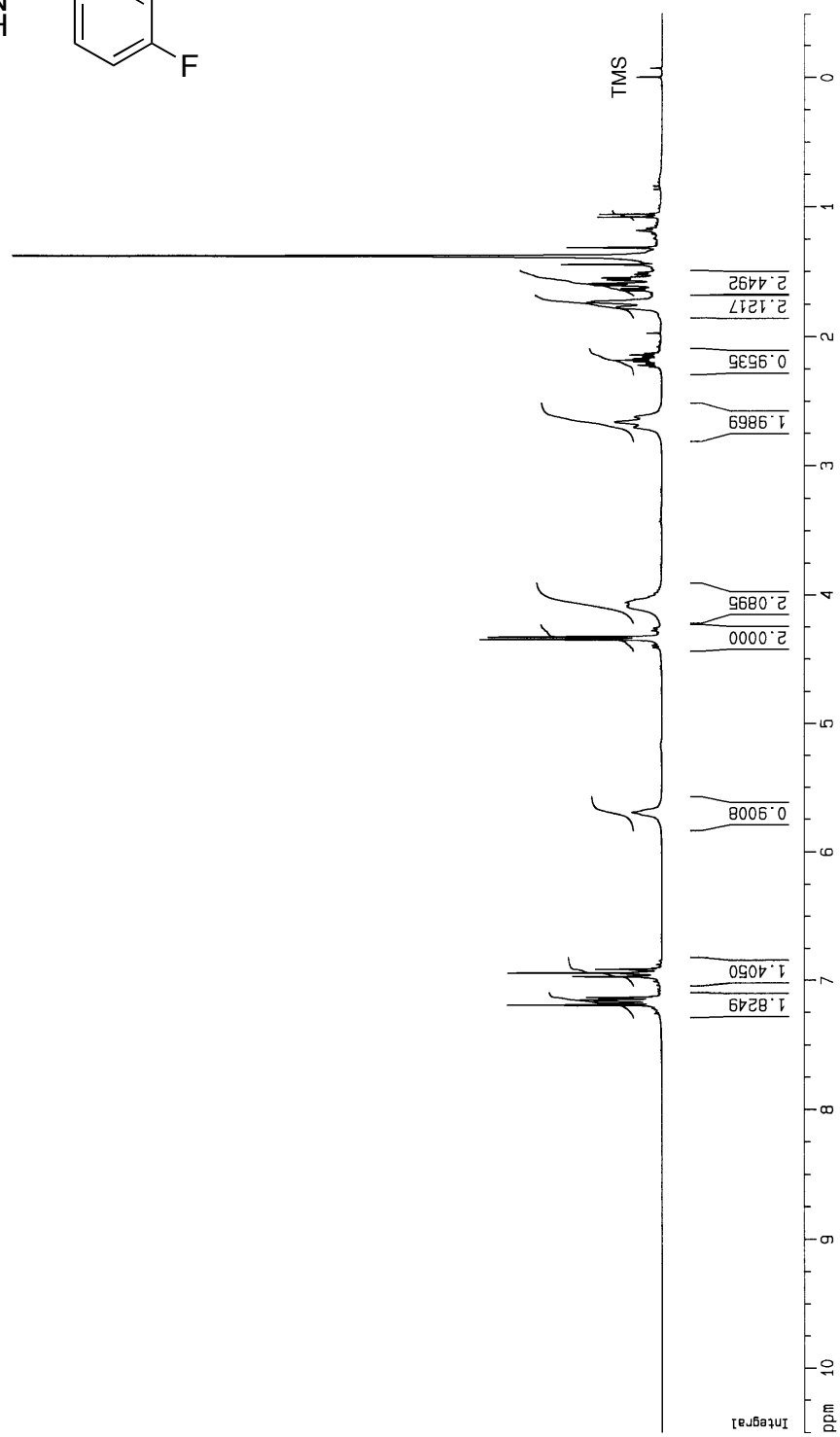
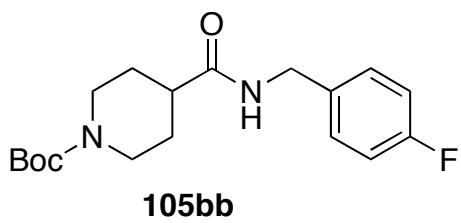


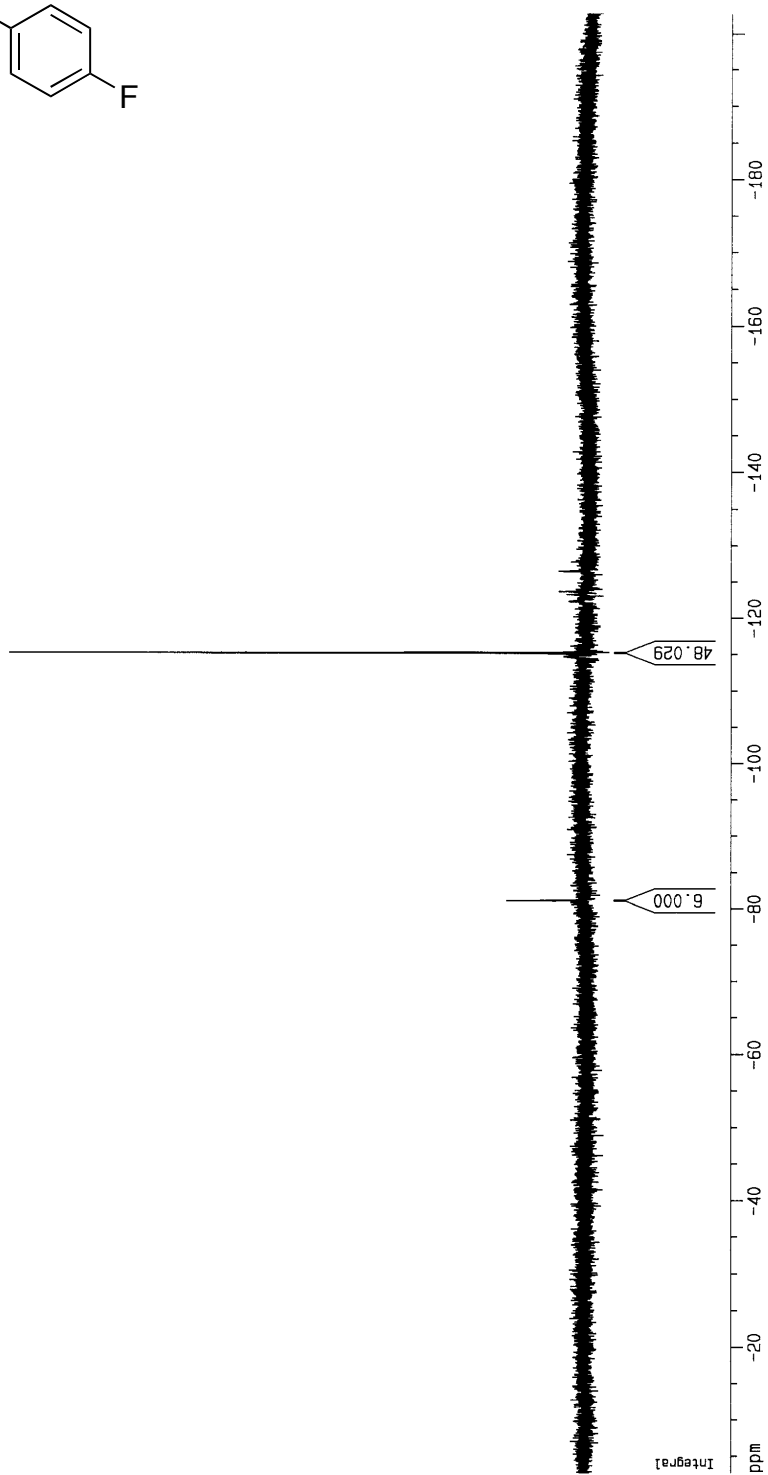
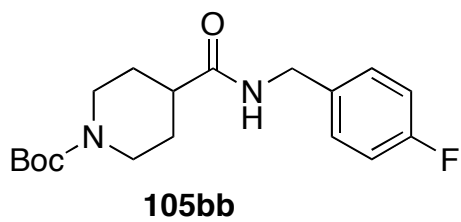


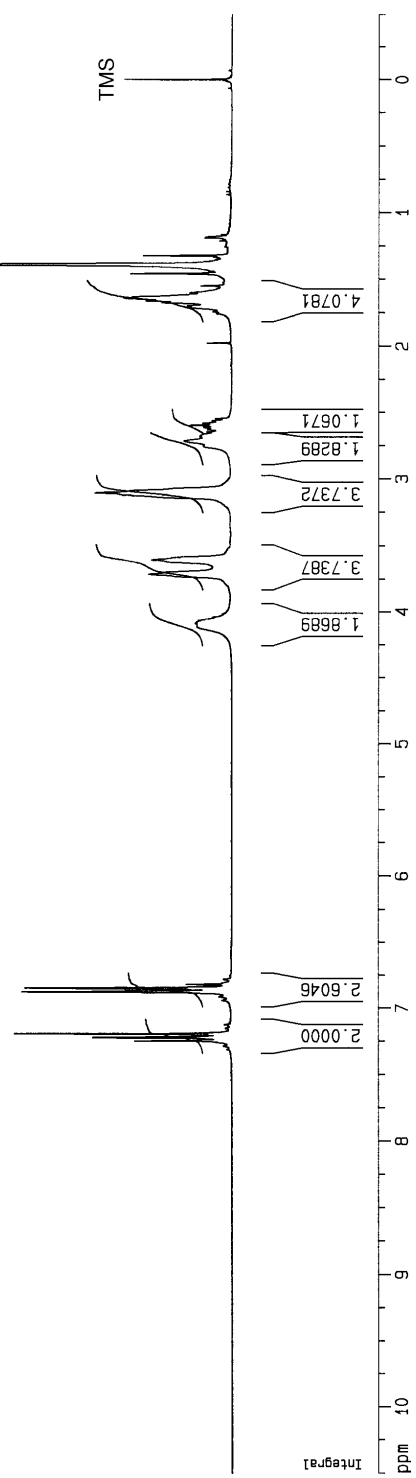
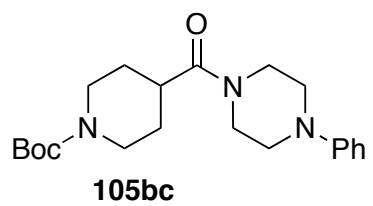
105ae

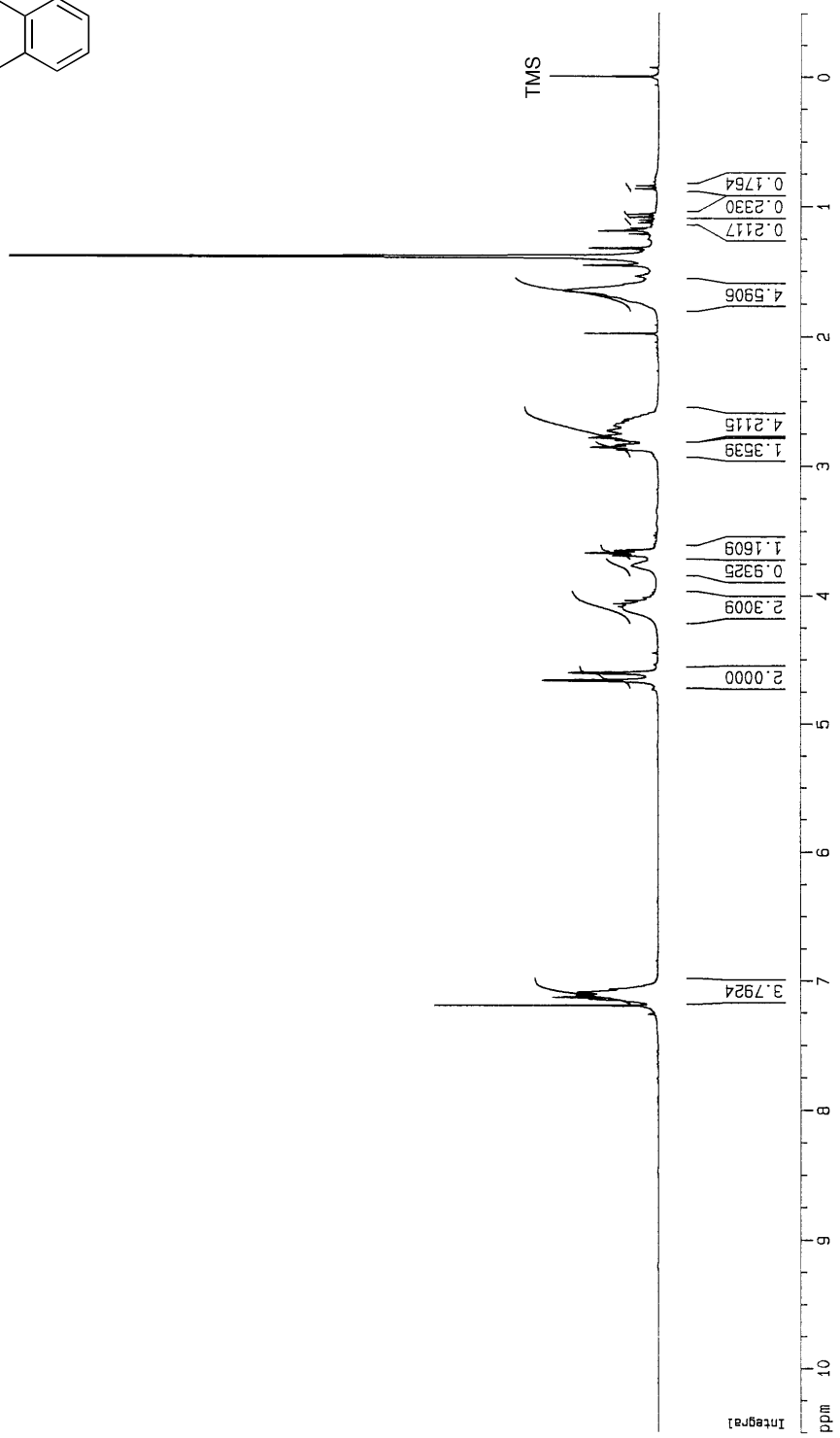
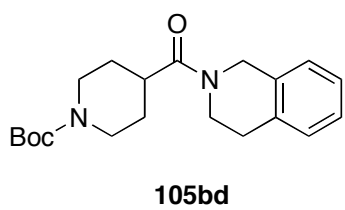


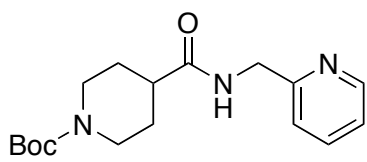




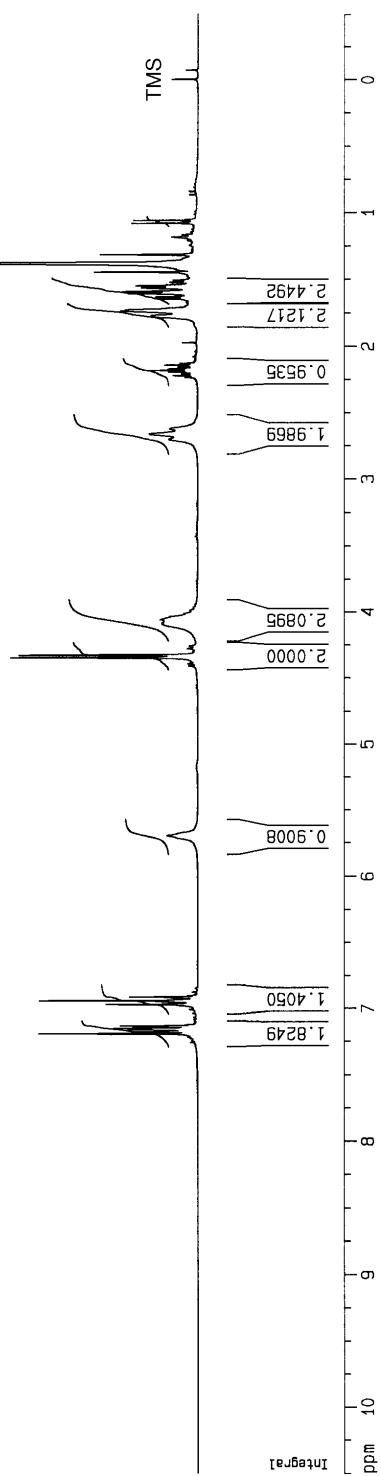


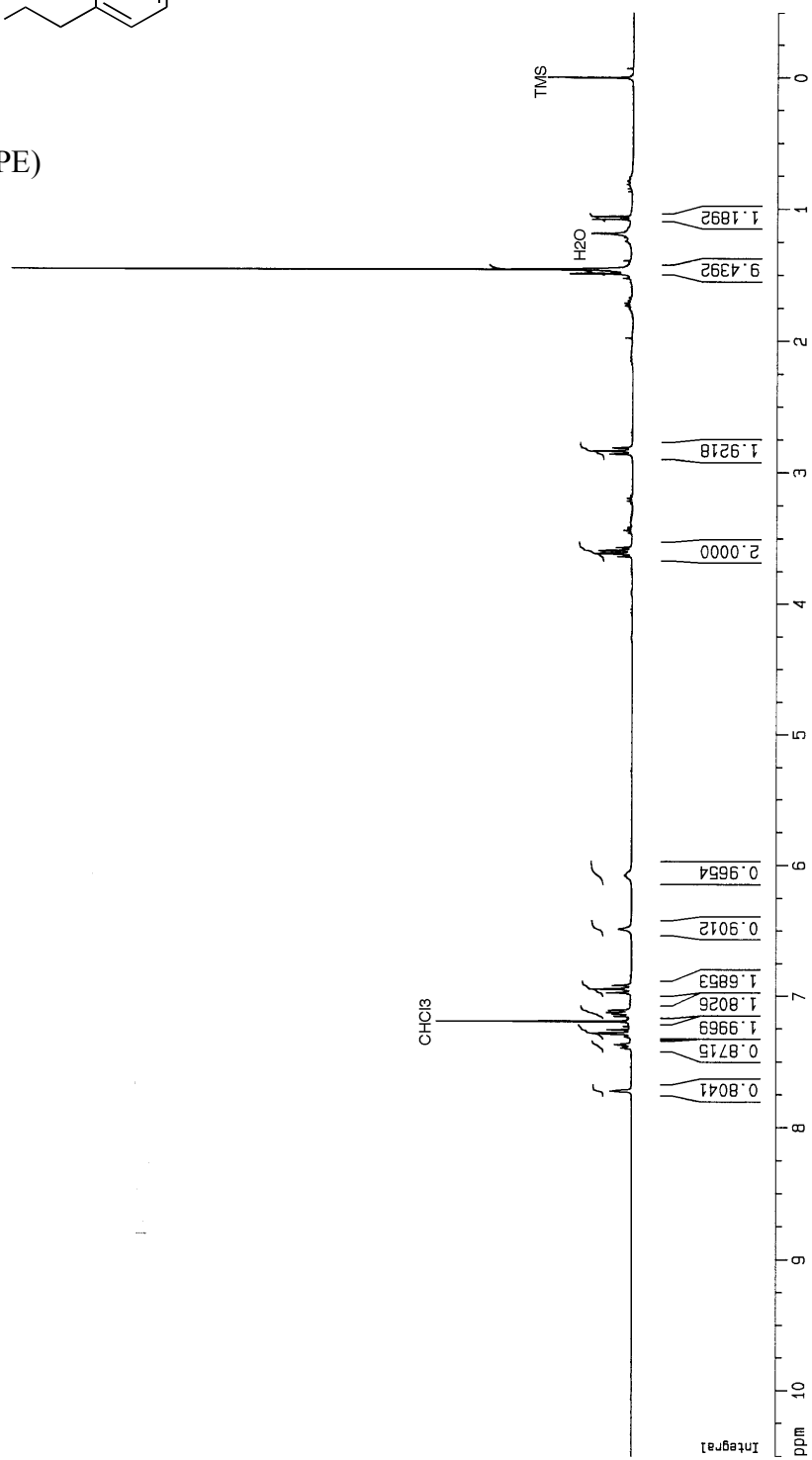
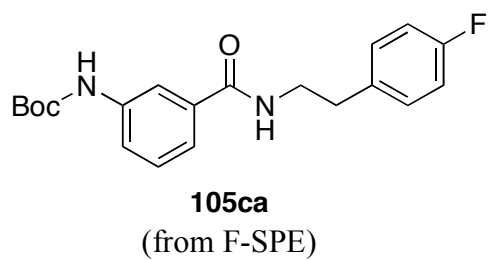


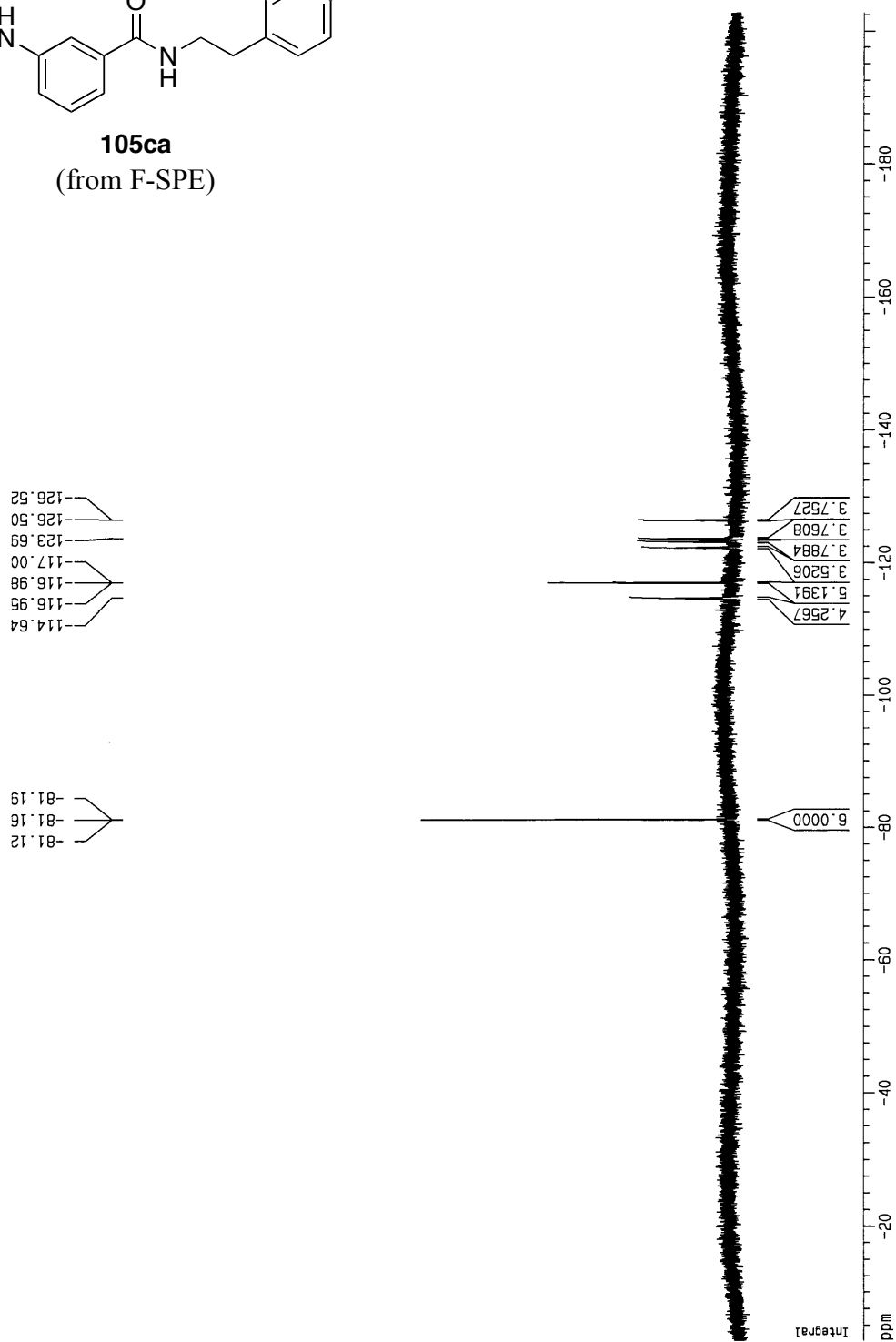
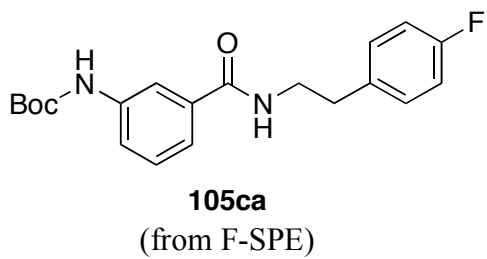


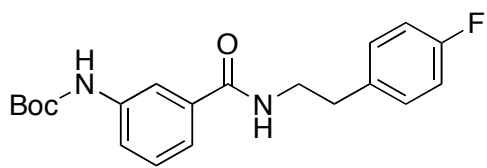


105be

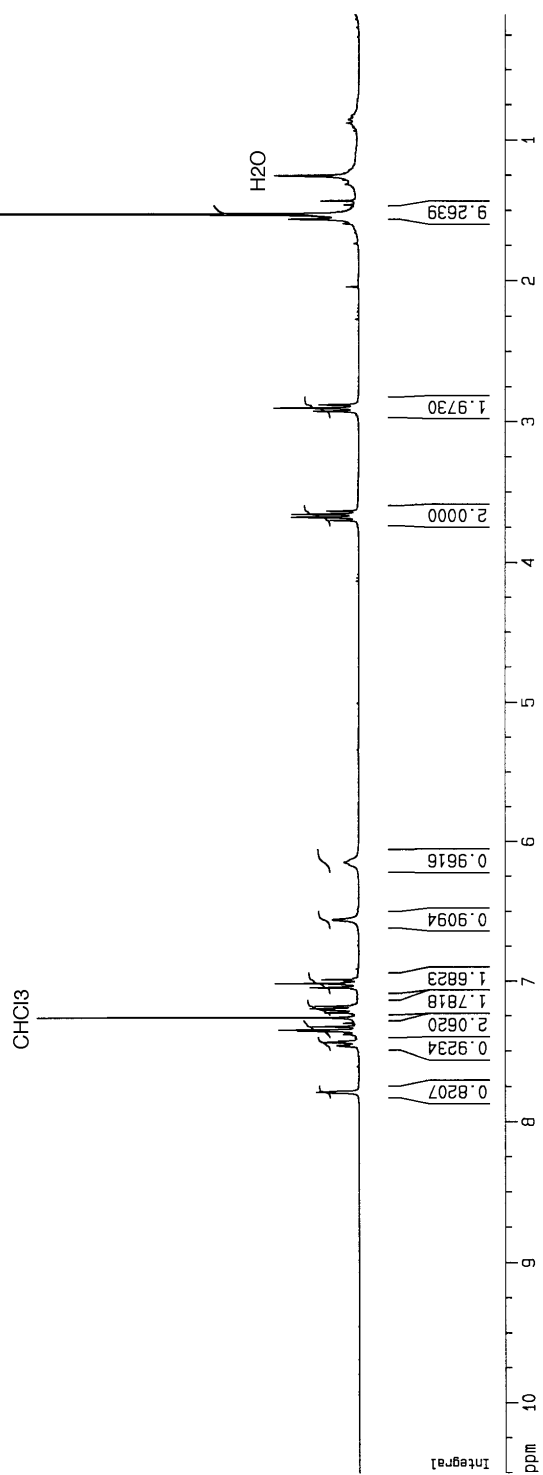


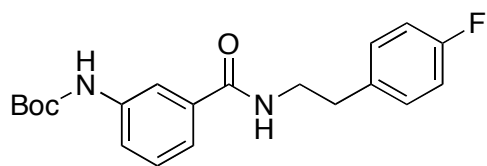




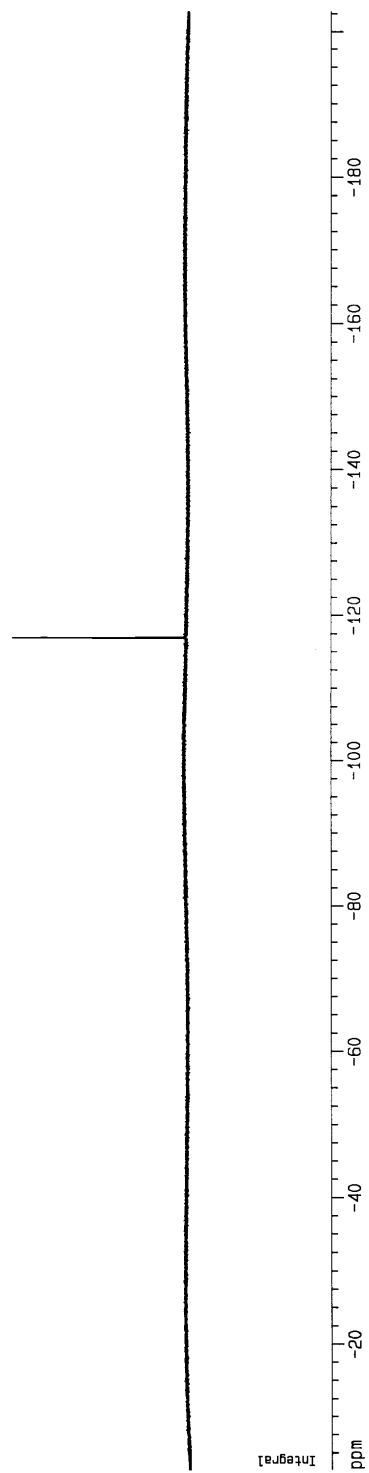


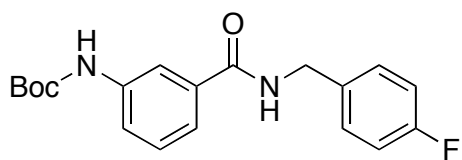
**105ca**  
(from flash column)



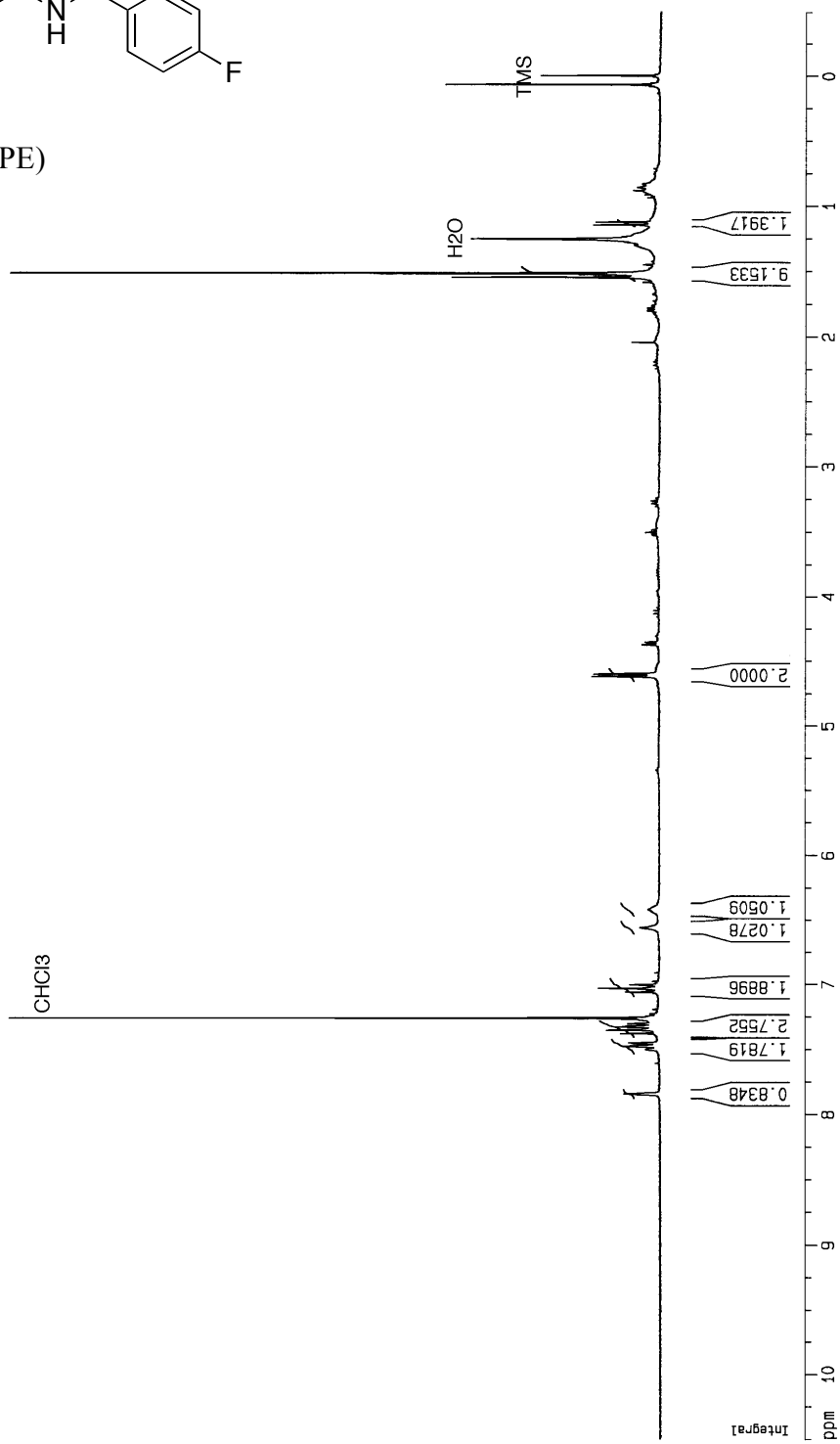


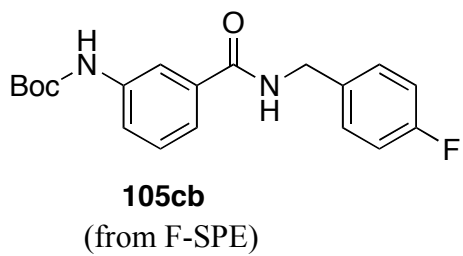
**105ca**  
(from flash column)





**105cb**  
(from F-SPE)

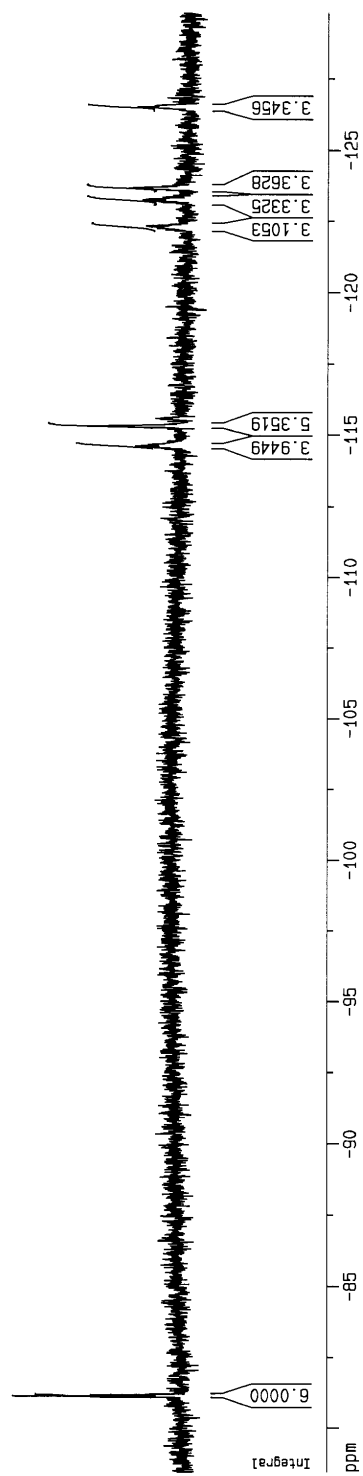


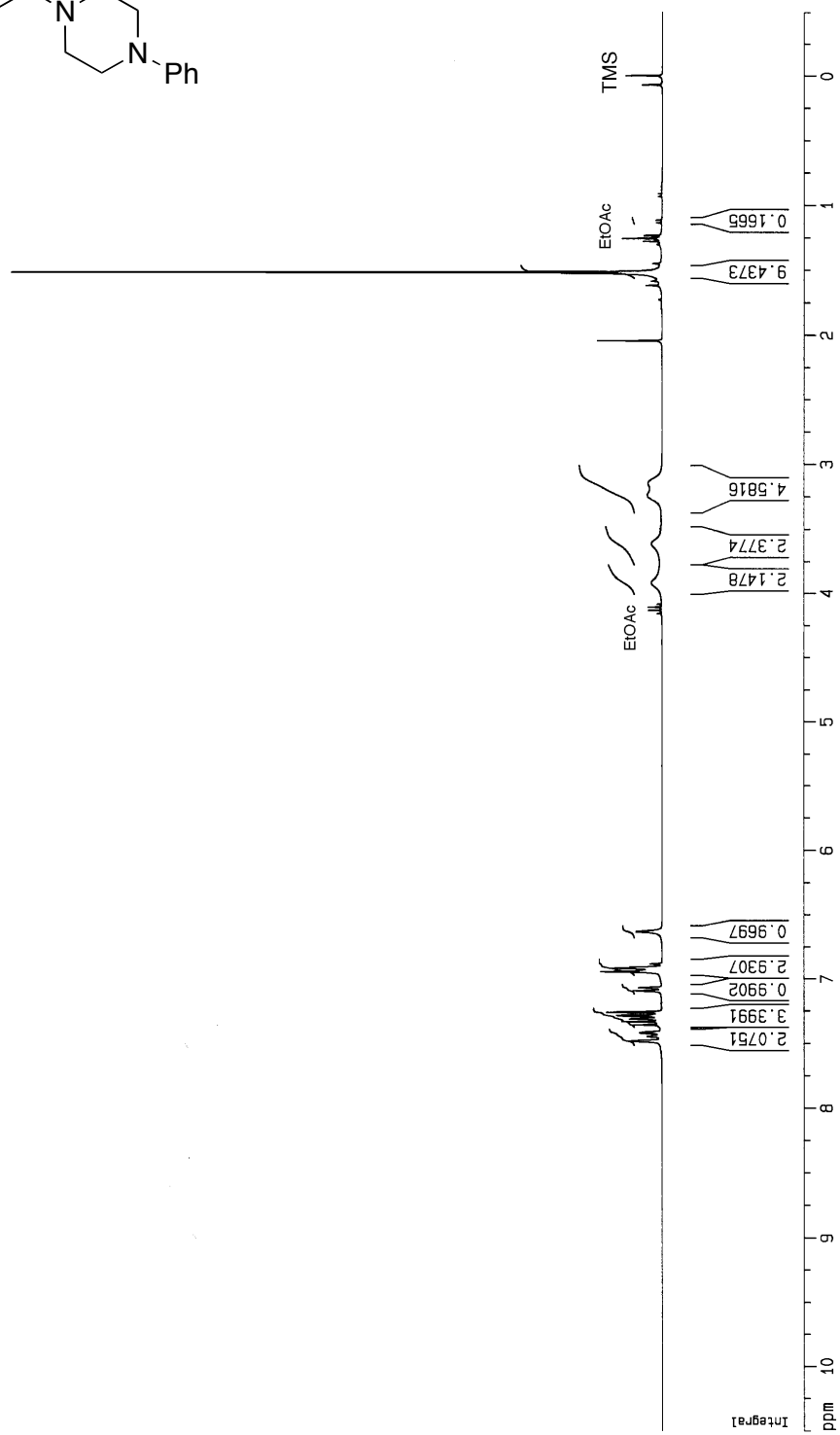
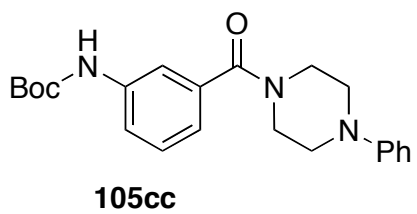


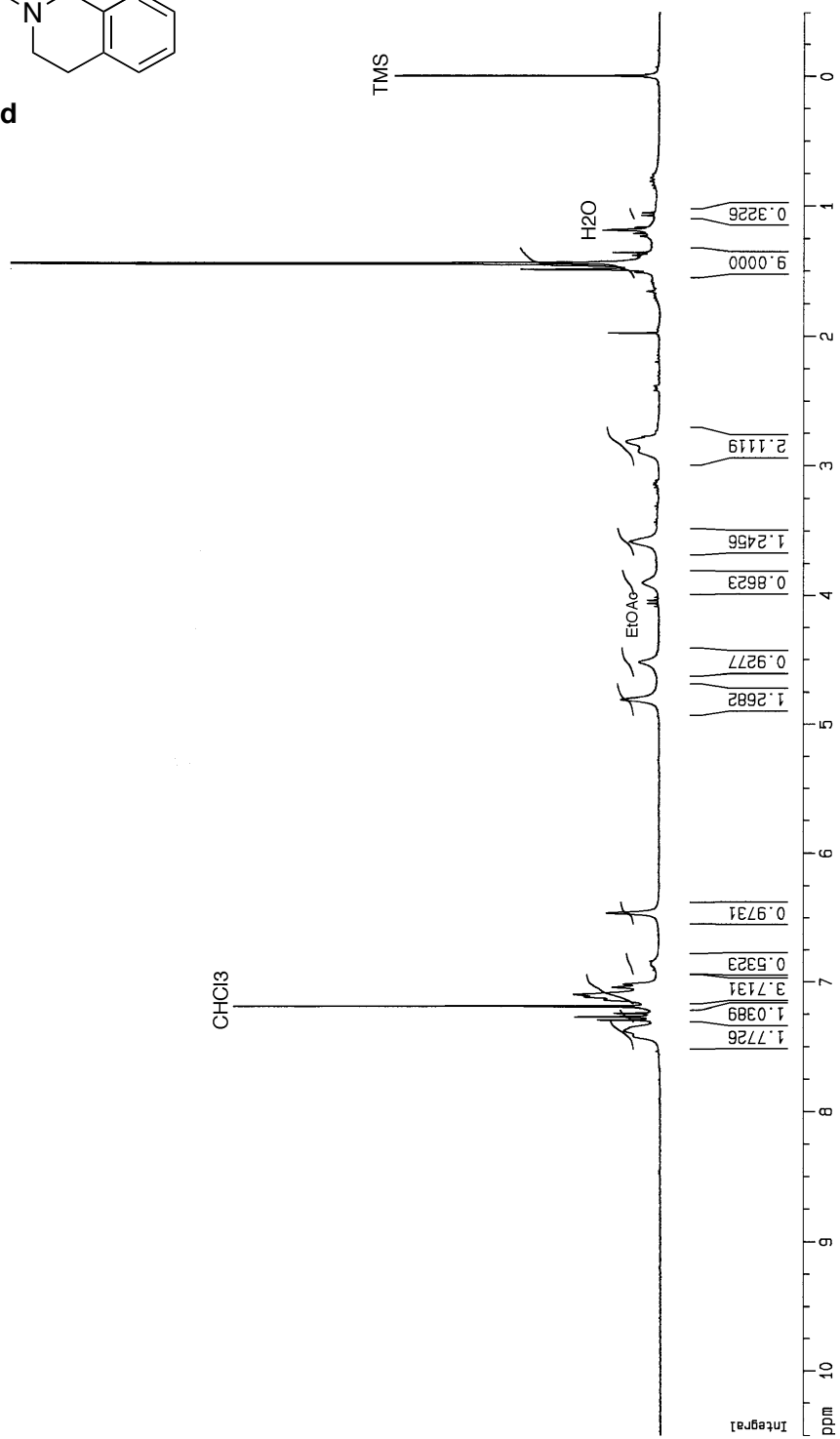
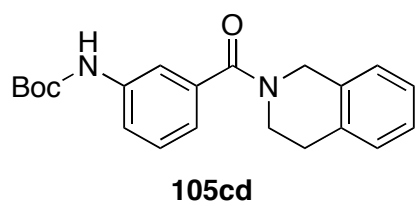
122.33  
 123.26  
 123.28  
 123.69  
 123.71  
 126.49  
 126.51  
 126.56

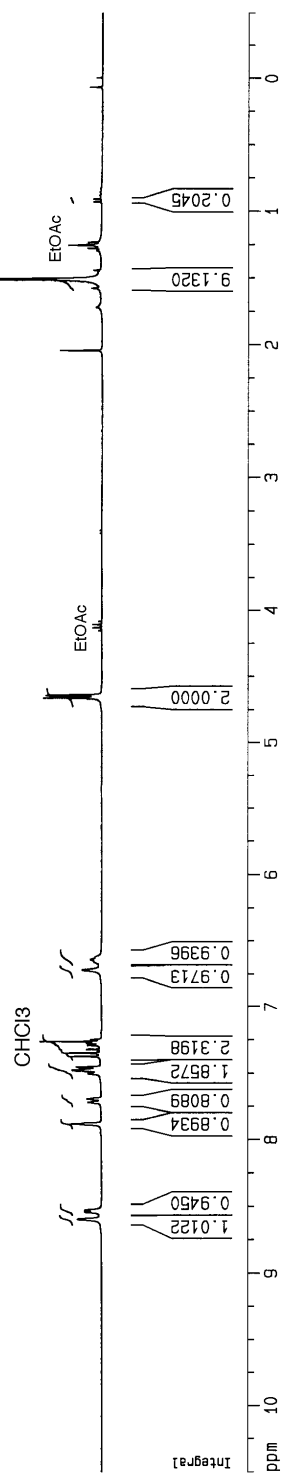
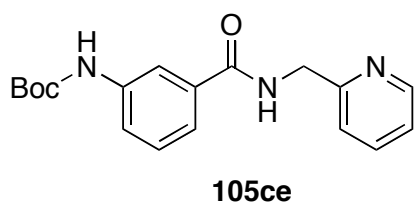
114.63  
 115.29  
 115.31  
 115.34

81.12  
 81.16  
 81.19









## BIBLIOGRAPHY

- <sup>1</sup> Studer, A.; Bossart, M. In *Radicals in Organic Synthesis*; Renaud, P., Sibi, M. P., Eds.; Wiley-VCH: Weinheim, 2001; Vol. 2, p 62-80.
- <sup>2</sup> Bowman, W. R.; Heaney, H.; Jordan, B. M. *Tetrahedron* **1991**, *47*, 10119-10128.
- <sup>3</sup> Allin, S. M.; Barton, W. R. S.; Bowman, W. R.; McNally, T. *Tetrahedron Lett.* **2002**, *43*, 4191-4193.
- <sup>4</sup> Allin, S. M.; Barton, W. R. S.; Bowman, W. R.; McNally, T. *Tetrahedron Lett.* **2001**, *42*, 7887-7890.
- <sup>5</sup> McLoughlin, P. T. F.; Clyne, M. A.; Aldabbagh, F. *Tetrahedron* **2004**, *60*, 8065-8071.
- <sup>6</sup> Curran, D. P.; Liu, H.; Josien, H.; Ko, S. *Tetrahedron* **1996**, *52*, 11385-11404.
- <sup>7</sup> Rosa, A. M.; Lobo, A. M.; Branco, P. S.; Prabhakar, S. *Tetrahedron* **1997**, *53*, 285-298.
- <sup>8</sup> Rosa, A. M.; Prabhakar, S.; Lobo, A. M. *Tetrahedron Lett.* **1990**, *31*, 1881-1884.
- <sup>9</sup> Murphy, J. A.; Sherburn, M. S. *Tetrahedron* **1991**, *47*, 4077-4088.
- <sup>10</sup> Narasimhan, N. S.; Aidhen, I. S. *Tetrahedron Lett.* **1988**, *29*, 2987-2988.
- <sup>11</sup> Jones, K.; Ho, T. C. T.; Wilkinson, J. *Tetrahedron Lett.* **1995**, *36*, 6743-6744.
- <sup>12</sup> Murphy, J. A.; Sherburn, M. S. *Tetrahedron Lett.* **1990**, *31*, 3495-3496.
- <sup>13</sup> Teichert, A.; Jantos, K.; Harms, K.; Studer, A. *Org. Lett.* **2004**, ASAP.
- <sup>14</sup> Harrowven, D. C.; Sutton, B. J.; Coulton, S. *Org. Biomol. Chem.* **2003**, *1*, 4047-4057.
- <sup>15</sup> Martinez-Barrasa, v.; Viedma, A. G.; Burgos, C.; Alvarez-Builla, J. *Org. Lett.* **2000**, *2*, 3933-3935.
- <sup>16</sup> Nunez, A.; Sanchez, A.; Burgos, C.; Alvarez-Builla, J. *Tetrahedron* **2004**, *60*, 6217-6224.
- <sup>17</sup> Osornio, Y. M.; Cruz-Almanza, R.; Jimenez-Montano, V.; Miranda, L. D. *Chem. Commun.* **2003**, 2316-2317.

- <sup>18</sup> Arai, N.; Narasaka, K. *Bull. Chem. Soc. Jpn.* **1995**, *68*, 1707-1714.
- <sup>19</sup> Curran, D. P.; Yu, H.; Lie, H. *Tetrahedron* **1994**, *50*, 7343-7366.
- <sup>20</sup> Crich, D.; Hwang, J. *J. Org. Chem.* **1998**, *63*, 2765-2770.
- <sup>21</sup> Carey, F. A.; Sundberg, R. J. *Advanced Organic Chemistry, Part B: Reactions and Synthesis*; 4th ed.; Kluwer Academic/Plenum Publishers: New York, 2001.
- <sup>22</sup> Curran, D. P. *Synthesis* **1981**, 417-439.
- <sup>23</sup> Curran, D. P. *Synthesis* **1981**, 489-513.
- <sup>24</sup> Bowman, W. R.; Heaney, H.; Jordan, B. M. *Tetrahedron* **1991**, *47*, 10119-10128.
- <sup>25</sup> Beckwith, A. L. J.; Bowry, V. W.; Bowman, W. R.; Mann, E.; Parr, J.; Storey, J. M. D. *Angew. Chem., Int. Ed.* **2004**, *43*, 95-98.
- <sup>26</sup> Kita, Y.; Matsugi, M. In *Radicals in Organic Synthesis*; Renaud, P., Sibi, M. P., Eds.; Wiley-VCH: Weinheim, New York, Chichester, Brisbane, Singapore, Toronto, 2001; Vol. 1, p 3.
- <sup>27</sup> Holt, P. F.; Hughes, B. P. *J. Chem. Soc.* **1955**, 98.
- <sup>28</sup> Engel, P. S.; Wu, W. *J. Am. Chem. Soc.* **1989**, *111*, 1830-1835.
- <sup>29</sup> Chatgililoglu, C. *Acc. Chem. Res.* **1992**, *25*, 188-194.
- <sup>30</sup> Chatgililoglu, C.; Griller, D.; Lesage, M. *J. Org. Chem.* **1988**, *53*, 3641-3642.
- <sup>31</sup> Kanabus-Kaminski, J. M.; Hawari, J. A.; Griller, D.; Chatgililoglu, C. *J. Am. Chem. Soc.* **1987**, *109*, 5267-5268.
- <sup>32</sup> Chatgililoglu, C.; Griller, D.; Lesage, M. *J. Org. Chem.* **1989**, *54*, 2492-2494.
- <sup>33</sup> Curran, D. P.; Jasperse, C. P.; Totleben, M. J. *J. Org. Chem.* **1991**, *56*, 7169-7172.
- <sup>34</sup> Chatgililoglu, C.; Newcomb, M. In *Advances in Organometallic Chemistry*; Academic Press: San Diego, 1999; Vol. 44, p 67-112.
- <sup>35</sup> Chatgililoglu, C.; Ferreri, C.; Gimisis, T. In *The Chemistry of Organic Silicon Compounds*; Rappoport, Z., Apeloig, Y., Eds.; John Wiley & Sons Ltd.: 1998; Vol. 2, p 1539-1579.
- <sup>36</sup> Chatgililoglu, C.; Guerrini, A.; Seconi, G. *J. Org. Chem.* **1992**, *57*, 2207-2208.
- <sup>37</sup> Zaborovskiy, A. B.; Lutsyk, D. S.; Prystansky, R. E.; Kopylets, V. I.; Timokhin, V. I.; Chatgililoglu, C. *J. Organomet. Chem.* **2004**, *689*, 2912-2919.
- <sup>38</sup> Maillard, B.; Ingold, K. U.; Scaiano, J. C. *J. Am. Chem. Soc.* **1983**, *105*, 5095-5099.

- <sup>39</sup> Bennasar, M.-L.; Roca, T.; Griera, R.; Bassa, M.; Bosch, J. *J. Org. Chem.* **2002**, *67*, 6268-6271.
- <sup>40</sup> Standard solutions containing 25% (1 mM), 50% (2 mM), and 100% (4 mM) theoretical yield of **44**, **45** and **46** and a fixed concentration of octadecane (0.06 mmol) were analyzed by GC to determine the response factors. The response factor for each compound did not vary when varying the concentrations and/or molar ratios of compound and internal standard.
- <sup>41</sup> The identity of the peaks in the GC chromatogram were verified by co-injection of authentic samples.
- <sup>42</sup> Bennasar, M.-L.; Roca, T.; Griera, R.; Bosch, J. *J. Org. Chem.* **2001**, *66*, 7547-7551.
- <sup>43</sup> Boger, D. L.; McKie, J. A. *J. Org. Chem.* **1995**, *60*, 1271-1275.
- <sup>44</sup> Studer, A. *Angew. Chem., Int. Ed.* **2000**, *39*, 1108-1111.
- <sup>45</sup> Studer, A. *Chem. Eur. J.* **2001**, *7*, 1159-1164.
- <sup>46</sup> Studer, A.; Amrein, S. *Synthesis* **2002**, 835-849.
- <sup>47</sup> Wetter, C.; Jantos, K.; Woithe, K.; Studer, A. *Org. Lett.* **2003**, *5*, 2899-2902.
- <sup>48</sup> Semmelhack, M. F.; Schmid, C. R.; Cortes, D. A.; Chou, C. S. *J. Am. Chem. Soc.* **1984**, *106*, 3374-3376.
- <sup>49</sup> Semmelhack, M. F.; Schmid, C. R.; Cortes, D. A. *Tetrahedron Lett.* **1986**, *27*, 1119-1122.
- <sup>50</sup> Beckwith, A. L. J.; Bowry, V. W.; Ingold, K. U. *J. Am. Chem. Soc.* **1992**, *114*, 4983-4992.
- <sup>51</sup> Carey, F. A.; Sundberg, R. J. *Advanced Organic Chemistry, Part A: Structures and Mechanisms*; Kluwer Academic/Plenum Publishers: New York, 2001.
- <sup>52</sup> Scaiano, J. C.; Stewart, L. C. *J. Am. Chem. Soc.* **1983**, *105*, 3609-3614.
- <sup>53</sup> Janzen, E. G.; Evans, C. A. *J. Am. Chem. Soc.* **1975**, *97*, 205-206.
- <sup>54</sup> Lowry, T. H.; Richardson, K. S. *Mechanism and Theory in Organic Chemistry*; 3rd ed.; Harper & Row, 1987.
- <sup>55</sup> Bartlett, P. D.; Funahashi, T. *J. Am. Chem. Soc.* **1962**, *84*, 2596-2601.
- <sup>56</sup> Dijkman, A.; Arends, I. W. C. E.; Sheldon, R. A. *Org. Biomol. Chem.* **2003**, *1*, 3232-3237.
- <sup>57</sup> Wadsworth, D. H.; Detty, M. R.; Murray, B. J.; Weidner, C. H.; Haley, N. F. *J. Org. Chem.* **1984**, *49*, 2676-2681.
- <sup>58</sup> Ingham, R. H.; Rosenberg, S. D.; Gilman, H. *Chem. Rev.* **1960**, *60*, 459-539.

- <sup>59</sup> Pagliavini, G.; Faleschini, S.; Pilloni, G.; Plazzogna, G. *J. Organomet. Chem.* **1966**, *5*, 136-146.
- <sup>60</sup> Murou, S. *Handbook of Photochemistry*; Marcel Dekker, 1973.
- <sup>61</sup> a) Hendry, D. G.; Schuetzle, D. *J. Am. Chem. Soc.* **1975**, *97*, 7123-7127. (b) Howard, J. A. In *Peroxy Radicals*; Alfassi, Z. B., Ed.; Wiley: Chichester, U. K. 1997; p 282-334. (c) Howard, J. A.; Ingold, K. U. *Can J. Chem.* **1967**, *45*, 785-792.
- <sup>62</sup> (a) Benson, S. W.; Shaw, R. *J. Am. Chem. Soc.* **1973**, *75*, 4784. (b) Howard, J. A.; Ingold, K. U. *Can. J. Chem.* **1964**, *42*, 1250.
- <sup>63</sup> a) Kranenburg, M.; Ciriano, M. V.; Cherkasov, A.; Mulder, P. *J. Phys. Chem. A* **2000**, *104*, 915-921. (b) Pan, X.-M.; Schuchmann, M. N.; von Sonntag, C. *J. Chem. Soc., Perkin Trans. 2* **1993**, 1021.
- <sup>64</sup> Chatgililoglu, C.; Timokhin, V. I.; Zaborovskiy, A. B.; Lutsyk, D. S.; Prystansky, R. E. *J. Chem. Soc., Perkin Trans. 2* **2000**, *2*, 577-581.
- <sup>65</sup> Bannasar, M. L.; Roca, T.; Ferrando, F. *J. Org. Chem.* **2005**, *70*, 9077-9080.
- <sup>66</sup> Burger, H.; Kilian, W.; Burczyk, K. *J. Organomet. Chem.* **1970**, *21*, 291-301.
- <sup>67</sup> Boo, B. H.; Kang, H. K.; Kang, S. K.; Lee, S. S. *J. Organomet. Chem.* **1992**, *436*, 1-9.
- <sup>68</sup> Bock, H.; Meuret, J.; Ruppert, K. *Journal of Organometallic Chemistry* **1993**, *44*, 19-28.
- <sup>69</sup> Percec, V.; Golding, G. M.; Smidrkal, J.; Weichold, O. *J. Org. Chem.* **2004**, *69*, 3447-3452.
- <sup>70</sup> Yanagisawa, M.; Hayamizu, K. *Magn. Reson. Chem.* **1986**, *24*, 1013-14.
- <sup>71</sup> Yanagisawa, M.; Hayamizu, K.; Yamamoto, O. *Magn. Reson. Chem.* **1987**, *25*, 184-186.
- <sup>72</sup> Li, G. Y. *J. Org. Chem.* **2002**, *67*, 3643-3650.
- <sup>73</sup> Shoji, K.; Takaaki, K.; Hiromichi, Y.; Shizuo, F.; Tsuyoshi, O. *Bull. Chem. Soc. Jpn.* **1988**, *61*, 600-602.
- <sup>74</sup> Ates, A.; Curran, D. P. *J. Am. Chem. Soc.* **2001**, *123*, 5130-5131.
- <sup>75</sup> Petit, M.; Geib, S. J.; Curran, D. P. *Tetrahedron* **2004**, *60*, 7543-7552.
- <sup>76</sup> Gunther, H. *NMR Spectroscopy: Basic Principles, Concepts, and Applications in Chemistry*; 2nd ed.; John Wiley & Sons Ltd.: Chichester, 1995.
- <sup>77</sup> Jeener, J.; Meier, B. H.; Bachmann, P.; Ernst, R. R. *J. Chem. Phys.* **1979**, *71*, 4546-4553.
- <sup>78</sup> Perrin, C. L.; Dwyer, T. *J. Chem. Rev.* **1990**, *90*, 935-967.

- <sup>79</sup> Abel, E. W.; Coston, T. P. J.; Orrell, K. G.; Sik, V.; Stephenson, D. *J. Magn. Reson.* **1986**, *70*, 34-53.
- <sup>80</sup> Bento, E. S.; Bradley, D. C.; Hawkes, G. E.; Maia, I. A.; Sales, K. D. *Magn. Reson. Chem.* **2000**, *38*, 331-335.
- <sup>81</sup> Dimitrov, V. S.; Vassilev, N. G. *Magn. Reson. Chem.* **1995**, *33*, 739-744.
- <sup>82</sup> Gibson, K. R.; Hitzel, L.; Mortishire-Smith, R. J.; Gerhard, U.; Jelley, R. A.; Reeve, A. J.; Rowley, M.; Nadin, A.; Owens, A. P. *J. Org. Chem* **2002**, *67*, 9354-9360.
- <sup>83</sup> The crystal structure was solved by Dr. Steven Geib.
- <sup>84</sup> Initially, mixing times ranging from 10 ms to 5 s were tested, and the spectra at a mixing time of 0.35 s gave the least amount of error.
- <sup>85</sup> For a detailed description of this routine, see reference 4
- <sup>86</sup> Energy barriers were determined from a single point calculation with the Eyring equation.
- <sup>87</sup> Stewart, W. E.; Siddall, T. H. *Chem. Rev.* **1970**, *70*, 517-551.
- <sup>88</sup> We missed the coalescence point of the upfield pair of resonances, so we took the coalescence temperature to be in between 343 and 353 K.
- <sup>89</sup> Li, W.-R.; Lin, Y.-S.; Hsu, N.-M. *J. Comb. Chem.* **2001**, *3*, 634-643.
- <sup>90</sup> Montalbetti, C. A. G. N.; Falque, V. *Tetrahedron* **2005**, *61*, 10827-10852.
- <sup>91</sup> Ghose, A. K.; Viswanadhan, V. N.; Wendoloski, J. J. *J. Comb. Chem.* **1999**, *1*, 55-68.
- <sup>92</sup> *Reagents for Glycoside, Nucleotide, and Peptide Synthesis*; Crich, D., Ed.; Wiley; New York, 2005.
- <sup>93</sup> Windridge, G.C.; Jorgensen, E.C. *J. Am. Chem. Soc.* **1971**, *17*, 6318-6319.
- <sup>94</sup> Sauer, D. R.; Kalvin, D.; Phelan, K. M. *Org. Lett.* **2003**, *5*, 4721-4724.
- <sup>95</sup> Lannuzel, M.; Lamothe, M.; Perez, M. *Tetrahedron Lett.* **2001**, *42*, 6703-6705.
- <sup>96</sup> Jamieson, C.; Congreve, M. S.; Emiabata-Smith, D.; Ley, S. V. *Synlett* **2000**, 1603-1607.
- <sup>97</sup> *Handbook of Fluorous Chemistry*; Gladysz, J. A., Curran, D. P., Horvath, I. T., Eds.; Wiley-VCH: Weinheim, 2004.
- <sup>98</sup> Zhang, W. *Chem. Rev.* **2004**, *104*, 2531-2556.
- <sup>99</sup> Zhang, W. *Tetrahedron* **2003**, *59*, 4475-4489.

- <sup>100</sup> Pozzi, G.; Shepperson, I. *Coord. Chem. Rev.* **2003**, *242*, 115-124.
- <sup>101</sup> Tzschucke, C. C.; Markert, C.; Baanwarth, W.; Roller, S.; Hebel, A. *Angew. Chem., Int. Ed.* **2002**, *41*, 3964-4000.
- <sup>102</sup> Yoshida, J.; Itami, K. *Chem. Rev.* **2002**, *102*, 3693-3716.
- <sup>103</sup> Dobbs, A. P.; Kimberley, M. R. *J. Fluorine Chem.* **2002**, *118*, 3-17.
- <sup>104</sup> Curran, D. P. *Synlett* **2001**, 1488-1496.
- <sup>105</sup> Curran, D. P. In *Stimulating Concepts in Chemistry*; Stoddard, F., Reinhoudt, D., Shibasaki, M., Eds.; Wiley-VCH: New York, 2000, pp 25-37.
- <sup>106</sup> Curran, D. P. *Angew. Chem., Int. Ed.* **1998**, *37*, 1175-1196.
- <sup>107</sup> Curran, D. P. *Aldrichimica Acta* **2005**, *38*, 115-121.
- <sup>108</sup> (a) Curran, D. P. Separations with Fluorous Silica Gel and Related Materials. In *Handbook of Fluorous Chemistry*; Gladysz, J. A., Curran, D. P., Horvath, I. T., Eds.; Wiley-VCH: Weinheim, 2004, pp 101-127. (b) Zhang, W.; Curran, D. P. *Tetrahedron* **2006**, *62*, 11837-11865.
- <sup>109</sup> Navigate to <http://www.fluorous.com> for detailed information on F-SPE.
- <sup>110</sup> Hartke, K.; Rossbach, F. *Angew. Chem., Int. Ed.* **1968**, *7*, 72.